



DISSERTATION RC- 143505

DEVELOPMENT OF LOW-COST BASE ISOLATION SYSTEM FOR RESIDENTIAL HOUSING IN HIGH SEISMIC ZONES

Name : YUDHA LESMANA

ID No : 03111360010007

Supervisor : Dr. Ir. Hidayat Soegihardjo M., MS

**GRADUATE DIVISION
STRUCTURAL ENGINEERING PROGRAM
DEPARTMENT OF CIVIL ENGINEERING
FACULTY OF CIVIL , ENVIRONMENTAL, AND GEO ENGINEERING
SEPULUH NOPEMBER INSTITUTE OF TECHNOLOGY
SURABAYA
2018**

**Development of Low-Cost Base Isolation System For Residential Housing In
High Seismic Zones**

by
Yudha Lesmana
03111360010007

A dissertation submitted in partial satisfaction in the requirements for the doctoral
degree in Civil Engineering in the GRADUATE DIVISION of the
SEPULUH NOPEMBER INSTITUTE OF TECHNOLOGY

Examination Date : November 2nd, 2018
Graduation Period : March 2019



Dr. Ir. Hidayat Soegihardjo M., MS
NIP: 195503251980031004

(Supervisor)



Prof. Ir. Priyo Suprobo, Msc., Ph.D
NIP. 195909111984031001

(Internal Examiner)



Ir. Handayanu, Msc., Ph.D
NIP. 196307281988031001

(Internal Examiner)



Prof. Ir. Yoyong Arfiadi, M.Eng., Ph.D
NPP. 07.88.273

(External Examiner)



I.D. A. V. Madewanthi, ST., MT., Ph.D
NIP: 19750212 199903 2 001

DEVELOPMENT OF LOW-COST BASE ISOLATION SYSTEM FOR RESIDENTIAL HOUSING IN HIGH SEISMIC ZONES

Name : Yudha Lesmana
ID No. : 03111360010007
Supervisor : Dr. Ir. Hidayat Soegihardjo M., MS

ABSTRACT

Base isolation is the most effective technique in reducing earthquake force transmitted to a building. Uncoupling a structure from earthquake effect is the main objective of using this device. The basic principal of base isolation system in reducing earthquake force is by lengthening the structure period far away from the high earthquake force period range. Therefore, the seismic demand on a structure and earthquake force transferred to a building are decreasing significantly. Generally, base isolation consists of alternating horizontal layers of rubber and reinforcement. The reinforcement serves primarily to prevent bulging effect of rubber layers under compression load. The restrain of rubber enhances the vertical stiffness of isolators due to the near-incompressibility of the rubber, resulting in a vertical stiffness that is significantly greater than the horizontal stiffness.

Currently, seismic isolation technology is applied across the world on large and expensive buildings. It is necessary to reduce the weight and cost of isolators to extend this effective yet expensive earthquake-resistant strategy to housing and commercial buildings. The isolators used in these applications are large, heavy and very expensive. A single isolator can weigh one ton or more. The primary weight in an isolator is caused by the reinforcing steel plate employed to provide the vertical stiffness of the rubber-steel composite element. In order to develop low-cost base isolation, the weight and cost of isolator must be reduced significantly. Therefore, the research purpose described in this report is to suggest that both cost and weight can be reduced by eliminating the steel reinforcing plate and replacing them with a perforated reinforcement.

In this research project, the characteristics of perforated-reinforced elastomeric isolators (PREIs) were investigated. A series of experimental test and finite element analysis (FEA) were conducted to observe PREIs behavior under compression and lateral load. The rubber material employed in the experimental test is denoted as rubber-A. The vertical tests were conducted by testing 1 specimen. A specimen was monotonically loaded to a compressive force at zero horizontal displacement. Once the compressive load was achieved, it was fluctuated over three sinusoidal cycles and then monotonically unloaded. It was carried out to investigate PREIs vertical characteristics under compression load of 80 kN. BS EN 1337-3:2005 standard was utilized as the fundamental procedure for compression test. Furthermore, in order to observe the horizontal characteristics of PREIs, horizontal test was also performed by testing 1 specimen. The horizontal test was performed under horizontal displacement control. The specimen was tested under constant vertical load of 80 kN and

moved freely in lateral using cyclic shear with three fully reversed cycles at four maximum strain levels of 5%, 10%, 20%, 50% and 100%. BS EN 15129-2009 standard was utilized as the fundamental procedure for lateral test.

The finite element analysis was also carried out to estimate the behavior of isolator and used to observe the characteristic of isolator including stress and strain. Further analysis using FE was also conducted to observe the characteristic of modified circular perforated-reinforced elastomeric isolators (MC-PREIs) in order to derive the lower horizontal stiffness by modifying loaded area of PREIs.

The experimental test and FE results indicate that producing a perforated-reinforced isolators as low-cost base isolation system for light structure is supposed to be possible. The isolators are specified as low damping natural rubber bearing since the damping ratio is below of 10%. The perforated-reinforced isolators significantly lighter and the cost will be extremely lower than conventional isolators. In addition, FE of modified circular perforated-reinforced elastomeric isolators (MC-PREIs) also indicate the possibility to reduce lateral stiffness of isolator significantly.

Keywords : base isolation, isolator, perforated-reinforced, PREIs, MC-PREIs, vertical stiffness, horizontal stiffness, low damping, low-cost base isolation, light structure.

PENGEMBANGAN TEKNOLOGI BASE ISOLATION UNTUK RUMAH TINGGAL PADA DAERAH GEMPA TINGGI

Nama : Yudha Lesmana
NRP : 03111360010007
Pembimbing : Dr. Ir. Hidayat Soegihardjo M., MS

ABSTRAK

Base isolation merupakan teknik yang paling efektif dalam mengurangi gaya gempa yang masuk pada struktur bangunan. Memisahkan pengaruh gempa dari tanah terhadap bangunan merupakan tujuan utama dari penggunaan alat ini. Prinsip dasar dari base isolation dalam mengurangi gaya gempa adalah dengan cara memperpanjang periode struktur bangunan dengan menjauhi rentang perioda energy gempa tinggi. Sehingga energy gempa yang masuk pada struktru bangunan bisa dikurangi secara signifikan. Pada umumnya base isolation terdiri dari susunan karet dan pelat baja. Pelat baja memiliki fungsi utama untuk mencegah efek menggembung pada lapisan karet saat kondisi ditekan. Dengan adanya pelat baja tersebut meningkatkan kemampuan vertical dari base isolation untuk memikul beban vertikal yang lebih besar dikarenakan juga sifat near incompressibility dari rubber tersebut sehingga menghasilkan kekakuan vertical yang jauh lebih besar bila dibandingkan dengan kekakuan horizontalnya.

Saat ini, teknologi base isolation telah diaplikasikan diseluruh dunia pada bangunan yang tinggi dan mahal. Untuk memperluas pengaplikasian teknnologi penahan gempa khusus rumah sederhana ini, dibutuhkan untuk mengurangi berat dan harga dari base isolation. Base isolation yang digunakan selama ini berukuran besar, berat dan sangat mahal. Satu unit base isolation memiliki berat kurang lebih 1 ton atau bahkan lebih. Penyebab utama yang membuat base isolation berat adalah keberadaan pelat- pelat baja yang digunakan sebagai penguat pada base isolation yang berfungsi untuk menambah kekuatan vertikal dalam memikul beban aksial. Untuk mengembangkan produk base isolation yang murah, berat dan harga dari base isolation harus mampu dikurangi secara signifikan. Oleh karena itu, maksud dari penelitian ini adalah menyarankan bahwa harga dan berat base isolation mampu dikurangi secara drastis dengan cara mengganti pelat baja dengan pelat lubang.

Dipenelitian ini, perilaku dari perforated-reinforced elastomeric isolators (PREIs) dipelajari. Sejumlah pengujian dan analisa metode elemen hingga dilakukan untuk mengamati perilaku dari PREIs dalam keadaan tekan dan juga dalam kondisi beban horizontal. Material karet yang digunakan dalam penelitian ini dinamai karet-A. Test vertikal dilakukan dengan melakukan pengujian terhadap satu benda uji dari karet-A. Benda uji dibebani secara monotonik dengan beban vertikal dalam keadaan tanpa perpindahan arah lateral. Disaat beban rencana telah tercapai, beban kemudian diberikan berupa beban sinus dengan 3 siklus dan kemudian dilepaskan secara perlahan. Hal ini dilakukan untuk mengamati perilaku dari PREIs dalam keadaan menerima

beban vertikal sebesar 80 kN. Peraturan yang digunakan dalam penelitian vertikal ini adalah BS EN 1337-3:2005. Selanjutnya, untuk memperoleh data dari perilaku horizontal PREIs, pengujian arah horizontal juga dilakukan dengan menguji 1 benda uji dari karet-A. Pengujian horizontal dilakukan dengan kontrol perpindahan. Benda uji diuji dengan beban geser bolak-balik dengan 3 siklus pada 4 regangan maksimum, yaitu 5%, 10%, 20%, 50% and 100%. Peraturan BS EN 15129-2009 digunakan sebagai dasar pengujian tes horizontal.

Metode elemen hingga juga dilakukan guna memprediksi perilaku isolator dan digunakan untuk mempelajari tegangan dan regangan yang terjadi. Analisa lanjutan dengan menggunakan metode elemen hingga juga dilakukan untuk mempelajari perilaku dari modified circular perforated-reinforced elastomeric isolators (MC-PREIs) dengan tujuan memperoleh kekakuan horizontal yang lebih kecil dengan memodifikasi luasan permukaan dari isolator.

Pengaruh dari pelat lubang terhadap perilaku isolator dalam kondisi vertikal dan lateral sedang dipelajari. Hasil dari pengujian menunjukkan bahwa isolator ini memungkinkan untuk diproduksi sebagai produk base isolation yang murah untuk struktur ringan. Base isolation ini digolongkan sebagai isolator yang memiliki nilai damping ratio tergolong rendah dikarenakan nilai dampingnya tergolong dibawah 10%. Produk base isolation ini akan sangat ringan dan harga jualnya akan sangat murah dibandingkan dengan base isolation yang ada saat ini. Selain itu, analisa metode elemen hingga dari modified circular perforated-reinforced elastomeric isolators (MC-PREIs) juga menunjukkan kemungkinan untuk mengurangi kekakuan horizontal dari isolator secara signifikan.

Kata kunci : base isolation, perforated-reinforced, PREIs, kekakuan vertikal, kekakuan horizontal, damping, base isolation murah, struktur ringan.

ACKNOWLEDGEMENT

Alhamdulillah rabil ‘alamin, the researcher expresses his highest gratitude to Allah subhanahu wa ta’ala for the blessings, love, opportunity, health, and mercy. This dissertation entitled **Development of Low-Cost Base Isolation System for Residential Housing in High Seismic Zones** is submitted as the final requirement in accomplishing doctoral degree at *Institut Teknologi Sepuluh Nopember*.

In preparing this dissertation, a lot of people have provided motivation, advices, and supports for the researcher. In this valuable opportunity, the researcher is intended to express his gratitude and appreciation to all of them. First, the researcher’s deepest appreciation goes to his beloved parents: to his mother, Zaleha, for the endless love, pray, and supports; to his father, Rustam Effendi, for the weekly phone call in order to remind me to keep going and never give up.

The researcher would like to express his sincere appreciation to his first advisor, Hidayat Soegihardjo, for his supervisions, advices, and guidance from the very early stage of this research as well as giving me extraordinary experience throughout the past few years. Finally, the researchers would like to express his love to his lovely girl, Monica Arlita Tasya, who always support and give him the greatest love.

The financial supports from Directorate General of Higher Education through the multi years *Program Hibah* are also greatly appreciated.

Finally, I would like to thank everybody who was important to the successful realization of this dissertation. This dissertation is far from perfect, but it is expected that it will be useful not only for the researcher, but also for the readers. For this reason, constructive thoughtful suggestions and critics are welcomed.

”This page is intentionally left blank”

CONTENTS

TITLE PAGE	i
APPROVAL PAGE	iii
ABSTRACT	v
ABSTRAK.....	vii
ACKNOWLEDGEMENTS.....	ix
TABLE OF CONTENTS.....	xi
LIST OF FIGURES	xvii
LIST OF TABLES	xxvii
LIST OF NOTATIONS	xxix
CHAPTER 1 INTRODUCTION	
1.1 Background of Research	1
1.2 Research Significance	4
1.3 Research Objective	6
1.4 Research Scope	7
1.5 Organization of Disseration	8
CHAPTER 2 LITERATURE REVIEW	
2.1 Introduction.....	11
2.2 Hyperelastic Material (Rubber)	14
2.2.1 Characteristic of Hyperelastic Material.....	14
2.2.2 Constitutive Model of Hyperelastic Material.....	17
2.2.3 Stress- Strain of Hyperelastic Material	23
2.2.3.1 Stress- Strain of Tension Test.....	23
2.2.3.2 Stress- Strain of Planar Test	25
2.2.3.3 Stress- Strain of Equal Biaxial Test.....	27
2.2.3.4 Stress- Strain of Volumetric Test	29
2.2.4 Incompressible Behavior.....	31
2.2.5 Hysteresis	32
2.2.6 Material Parameters form Test Data	34
2.2.7 Physical Measurements	36

2.3 Base Isolation System	39
2.3.1 The Basic Principle of Base Isolation.....	39
2.3.2 The Characteristic of Base Isolation System	40
2.3.3 Base Isolation with Rigid Reinforcement.....	43
2.3.3.1 The behavior of Isolator under Compression.....	43
2.3.3.2 The behavior of Isolator under Bending	46
2.3.4 The Buckling Behavior of Isolator	48
2.4 Perforated Plate Material	52
2.4.1 Strength of Perforated Metal	52
2.4.2 Elastic Properties of Perforated Metals (Stiffness).....	55
2.5 Isolated Structure.....	57
2.5.1 Behavior of Isolated Structure	57
2.5.2 Mathematical Modeling of Isolators.....	60
2.5.2.1 Bi-Linear Hysteretic Model of Isolator	60
2.5.2.2 Equivalent Linear Elastic-Viscous Damping	61
2.5.3 Time History Analysis	63
2.5.3.1 Ground Motion Selecting Procedure.....	63
2.5.3.2 Ground Motion Scaling Procedure.....	64
2.6 Finite Element Method (FEM)	66
2.6.1 Computational Modeling Using FEM	67
2.6.1.1 Modeling of The Geometry	67
2.6.1.2 Meshing	68
2.6.1.3 Property of Material	71
2.6.1.4 Boundary, Initial and Loading Conditions.....	71
2.6.2 Nonlinearity in Stress Analysis	72
2.6.3 Solution Algorithms (Convergence Criteria).	73

CHAPTER 3 METHODOLOGY OF RESEARCH

3.1 Introduction	77
3.2 Preliminary Design.....	79
3.3 Material Test.....	79
3.3.1 Perforated Plate.....	79
3.3.2 Rubber Material	80

3.4 Experimental Test of Base Isolation	80
3.4.1 Vertical Test	81
3.4.2 Horizontal Test	81
3.5 Finite Element Analysis (FEA)	82
3.6 Further Analysis using Finite Element	83
3.7 Conclusions and Recommendations	83
CHAPTER 4 EXPERIMENTAL PROGRAM	
4.1 Hyperelastic Material Test	85
4.1.1 Introduction	85
4.1.1.1 Testing Procedure	86
4.1.1.2 Testing in Multi Strain State	82
4.1.1.3 Loading Condition (Slow Cyclic Loading)	87
4.1.1.4 Observations	87
4.1.2 Tension Test	88
4.1.3 Planar Test	91
4.1.4 Equalbiaxial Test	94
4.1.5 Volumetric Test	97
4.2 Perforated Plate Test	100
4.2.1 Introduction	100
4.2.2 Detail of Specimens	101
4.2.3 Testing Procedure	104
4.2.4 Summary	105
4.3 Fabrication of Base	106
4.3.1 Introduction	106
4.3.2 Preparation of Material	108
4.3.3 Vulcanize Process	111
4.3.4 Summary	116
4.4 Base Isolation Test Procedure	116
4.4.1 Introduction	116
4.4.2 Experimental Setup	117
4.4.3 Testing Procedure	121
4.4.4 Summary	126

CHAPTER 5 DATA ANALYSIS

5.1 Rubber Material.....	129
5.1.1 Stress-Strain Data	129
5.1.1.1 The Stress- Strain Data Test of Uniaxial Tension.....	131
5.1.1.2 The Stress- Strain Data Test of Planar Shear.	135
5.1.1.3 The Stress- Strain Data Test of Equal Biaxial	137
5.1.1.4 The Stress- Strain Data Test of Volumetric	140
5.1.1.5 Summary	144
5.1.2 Selecting Constitutive Model	145
5.1.2.1 Modeling Uniaxial Tension Test.....	145
5.1.2.2 Modeling Planar Shear Test	148
5.1.2.3 Modeling Equal Biaxial Test	150
5.1.2.4 Modeling Volumetric Test	155
5.1.2.5 Summary	157
5.2 Perforated Plate	158
5.2.1 Strength Analysis of Perforated Plate.....	158
5.2.2 Yield Strength of Perforated Plate	170
5.2.3 Summary	180
5.3 Isolated Structure Analysis.....	181
5.3.1 Introduction.....	181
5.3.2 Structural Modeling	182
5.3.3 Modeling Approach	184
5.3.4 Ground Motion Selected.....	184
5.3.5 Ground Motion Scaling Procedure	188
5.3.6 Results	191
5.3.7 Summary.....	192
5.4 Preliminary Design of Base Isolation.....	195

CHAPTER 6 EXPERIMENTAL RESULTS

6.1 Introduction	203
6.2 Vertical Test Results	203
6.3 Horizontal Test Results	222
6.4 Summary of Experimental Test.....	235

CHAPTER 7 FINITE ELEMENT ANALYSIS

7.1 Introduction	239
7.2 Material properties	239
7.3 The contact mechanism between perforated and rubber.....	241
7.4 Finite Element Analysis of Vertical Test	242
7.4.1 Modeling geometric of isolator	242
7.4.2 Mesh condition	245
7.4.3 Loading condition	246
7.4.4 Boundary condition	248
7.4.5 Finite element result of vertical analysis.....	248
7.5 Finite Element of Horizontal Analysis.....	250
7.5.1 Modeling gemotric of isolator.....	250
7.5.2 Loading condition	253
7.5.3 Boundary condition	253
7.5.4 Finite element result of lateral analysis.....	255
7.6 Analytical method	256
7.6.1 Characteristic of PREIs using analytical.....	256
7.6.2 Bilinear model of PREIs	259
7.7 Lateral characteristic of PREIs under different vertical load.....	263
7.8 Stability under large lateral displacement	264
7.9 Summary of FE analysis	264

CHAPTER 8 FINITE ELEMENT STUDY OF MODIFIED ISOLATOR

8.1 Introduction.....	267
8.2 Geometry of FE model of MC-PREIs	268
8.3 Finite element study on vertical response of MC-PREIs.....	269
8.3.1 FE model of MC-PREIs for vertical analysis	270
8.3.2 Loading history of MC-PREIs for vertical analysis.....	271
8.3.3 Mesh condition of MC-PREIs for vertical analysis	272
8.3.4 Parametric study of MC-PREIs for vertical analysis	273
8.3.4.1 Vertical stiffness	274
8.3.4.2 Compression modulus	275
8.3.4.3 Vertical strain.....	276

8.3.4.4 Vertical stress	277
8.3.4.5 Shear stress	278
8.3.4.6 Performance reinforcement stress	281
8.4 Finite element study on lateral response of MC-PREIs	282
8.4.1 FE model of MC-PREIs for lateral analysis	282
8.4.2 Loading history of MC-PREIs for lateral analysis	284
8.4.3 Mesh condition of MC-PREIs for lateral analysis	284
8.4.4 Parametric study on MC-PREIs for lateral analysis	286
8.4.4.1 Effective lateral stiffness	286
8.4.4.2 Load-displacement relationship	287
8.4.4.3 Stress and strain in elastomer layers	288
8.4.4.4 Deform shape	292
8.4.4.5 Stress in reinforcement	293
8.5 Summary of finite element study of MC-PREIs	294
CHAPTER 9 CONCLUSIONS AND RECOMMENDATIONS	
9.1 Introduction	295
9.2 General findings	295
9.3 Vertical characteristic of PREIs under compression	296
9.4 Horizontal characteristic of PREIs under lateral load	297
9.5 Recommendations	299
REFERENCES	301
APPENDICES	311
BIOGRAPHY	317

LIST OF FIGURES

Figure 2.1 Tensile stress-strain for polymer in three physical state.....	15
Figure 2.2 Stress-strain data cycled to 20%,40%,60%,100%,150% and 200%.....	16
Figure 2.3 Shifting experimental data of hyperleastic material	17
Figure 2.4 Simple tension test frame.....	24
Figure 2.5 Idealized stress-strain state of uniaxial test	25
Figure 2.6 Planar shear specimen mounted on machine	26
Figure 2.7 Idealized stress-strain state of planar test	27
Figure 2.8 Equalbiaxial specimen mounted on machine	28
Figure 2.9 Idealized stress-strain state of equalbiaxial test.....	29
Figure 2.10 Volumetric specimen mounted on machine	30
Figure 2.11 Idealized stress-strain state of volumetric test	30
Figure 2.12 Incompressible behavior of rubber	32
Figure 2.13 Cyclic tension demonstration Mullin's effect	33
Figure 2.14 Selecting test data required for finite element program.....	35
Figure 2.15 Laser extensometer with tags on tension specimen.....	37
Figure 2.16 Laser extensometer with tags on biaxial specimen.	37
Figure 2.17 Laser Extensometer with tags on planar shear specimen.	38
Figure 2.18 Laser extensometer with tags on volumetric specimen	38
Figure 2.19 Transmission of ground motions	39
Figure 2.20 The ideal conditions of the structure acceleration and displacement.	40
Figure 2.21 Effect of seismic isolation	41
Figure 2.22 Effect of soil conditions on isolated structure response	41
Figure 2.23 Cartesian coordinate system on an arbitry shaped pad	43
Figure 2.24 Coordinate system for a circular pad of radius R.	45
Figure 2.25 Rubber pad between rigid plates in pure bending.	47
Figure 2.26 Deformation pattern for a bearing.	49
Figure 2.27 Internal forces and external loads on a deformed bearing.....	50
Figure 2.28 Boundary conditions for an isolation bearing under a vertical load ..	51
Figure 2.29 Length and width direction of perforated plate sheet.	53
Figure 2.30 Formulations percentage open area with 60” staggered formation. ...	54

Figure 2.31 Yield strength ratio depending on percentage open area	55
Figure 2.32 Effective elastic properties depending on percentage open area.	57
Figure 2.33 Mathematical model of N-story base-isolated structure.	59
Figure 2.34 Bi-linear hysteresis model of isolator.	61
Figure 2.35 Equivalent linear model of the isolator	63
Figure 2.36 Processes leading to fabrication of advanced engineering systems ...	66
Figure 2.37 Linear hexahedral element	70
Figure 2.38 Examples of non-linear problems	75
Figure 2.39 A Series of load increment over several load step	74
Figure 2.40 Convergence enhancement with recovery feature (line search)	75
Figure 2.41 Newton- Rapshon; (a). One iteration, (b). Next iteration	76
Figure 3.1 Flow chart of reserach project.....	77
Figure 4.1 Specimen of uniaxial tension test.....	88
Figure 4.2 Uniaxial tensile specimen mounted on machine	89
Figure 4.3 Loading history of uniaxial tension test	90
Figure 4.4 Stress-strain data of uniaxial tension test - specimen A.....	90
Figure 4.5 Stress-strain data of uniaxial tension test - specimen B.....	91
Figure 4.6 Stress-strain data of uniaxial tension test - specimen C.....	91
Figure 4.7 Specimen of planar shear test.....	92
Figure 4.8 Planar shear specimen mounted on machine	92
Figure 4.9 Loading history of uniaxial planar shear test	93
Figure 4.10 Stress-strain data of planar shear test - specimen A.....	93
Figure 4.11 Stress-strain data of planar shear test - specimen B.....	94
Figure 4.12 Stress-strain data of planar shear test - specimen C.....	94
Figure 4.13 Specimen of planar shear test.....	95
Figure 4.14 Equal biaxial specimen mounted on machine	95
Figure 4.15 Loading history of equal biaxial test.....	96
Figure 4.16 Stress-strain data of equal biaxial test - specimen A	96
Figure 4.17 Stress-strain data of equal biaxial test - specimen B.....	97
Figure 4.18 Stress-strain data of equal biaxial test - specimen C.....	97
Figure 4.19 Specimen of volumetric test.....	98
Figure 4.20 Volumetric specimen mounted on machine	98

Figure 4.21 Loading history of volumetric test.....	99
Figure 4.22 Stress-strain data of volumetric test - specimen A	99
Figure 4.23 Stress-strain data of volumetric test - specimen B.....	100
Figure 4.24 Stress-strain data of volumetric test - specimen C.....	100
Figure 4.25 Set of samples test for tensile test.....	102
Figure 4.26 The detail size of specimen A (mm).....	102
Figure 4.27 The detail size of plate B ₁ (mm)	103
Figure 4.28 The detail size of plate B ₂ (mm)	103
Figure 4.29 The detail size of plate B ₃ (mm)	103
Figure 4.30 The detail size of plate B ₄ (mm)	104
Figure 4.31 The specimen are mounted on the machine.....	105
Figure 4.32 Cross section of base isolation.....	107
Figure 4.33 Top view of base isolation.....	107
Figure 4.34 Heating system for producing base isolation.....	108
Figure 4.35 Preparation of the mold of base isolation	109
Figure 4.36 Preparation of perforated plate before heating process	110
Figure 4.37 Rubber compound layer for base isolation	110
Figure 4.38 Preparation of end-steel plate	110
Figure 4.39 Arrangement process of rubber and perforated plate	111
Figure 4.40 Arrangement result with 20 rubber layers and 19 perforated plate ..	112
Figure 4.41 Setup mold into heating frame.....	112
Figure 4.42 Setup rubber-perforated layers into heating frame	113
Figure 4.43 Heating process of base isolation	114
Figure 4.44 Final result of steam heating process of base isolation.....	115
Figure 4.45 Two specimens of isolator with circular shape.....	116
Figure 4.46 Schematic of test apparatus for lateral.....	118
Figure 4.47 Schematic of test apparatus for compression.....	118
Figure 4.48 The instrumentation setup for lateral test	119
Figure 4.49 The instrumentation setup for compression test	120
Figure 4.50 Loading history of horizontal test.....	122
Figure 4.51 Loading history of vertical test of 10 kN.....	123
Figure 4.52 Loading history of vertical test of 20 kN.....	123

Figure 4.53 Loading history of vertical test of 30 kN	124
Figure 4.54 Loading history of vertical test of 40 kN	124
Figure 4.55 Loading history of vertical test of 80 kN	124
Figure 4.56 Loading history of vertical test of 100 kN	124
Figure 4.57 Loading history of vertical test of 150 kN	125
Figure 4.58 Loading history of vertical test of 200 kN	125
Figure 4.59 Loading history of vertical test of 250 kN	125
Figure 4.60 A number of experimental specimens.....	126
Figure 5.1 Type of curve on experimental test data	130
Figure 5.2 Selecting curve (red line) uniaxial tension data for sample A	132
Figure 5.3 Single view for selecting curve uniaxial tension for sample A.....	132
Figure 5.4 Reduced extracted data format for uniaxial tension.....	133
Figure 5.5 Modified of selecting curve data for sample-A.....	134
Figure 5.6 Selecting curve of tension test with three data test	134
Figure 5.7 Selecting curve (green line) planar shear data for sample-A	135
Figure 5.8 Single view for selecting curve (green line) planar shear	136
Figure 5.9 Modified of selecting curve planar shear data for sample-A	136
Figure 5.10 Selecting curve of planar shear test with three data.....	137
Figure 5.11 Selecting curve (purple line) equal biaxial data for sample-A.....	138
Figure 5.12 Single view for selecting curve (purple line) equal biaxial.....	138
Figure 5.13 Modified of selecting curve equal biaxial data for sample-A	139
Figure 5.14 Number of selecting curve of equal biaxial test.....	139
Figure 5.15 Selecting curve (red line) volumetric data for sample-A	140
Figure 5.16 Single view for selecting curve (red line) volumetric data	141
Figure 5.17 Reduced extracted data format for volumetric test	142
Figure 5.18 Modified of selecting curve of volumetric test data.....	142
Figure 5.19 Number of selecting curve of volumetric test.	143
Figure 5.20 Input file form for volumetric test on ANSYS	143
Figure 5.21 Input data files of uniaxial, planar and equal data test.....	144
Figure 5.22 Input data file of volumetric test	144
Figure 5.23 FE model dimension of uniaxial tension.....	146
Figure 5.24 The deformation state of FE model under pure tension.....	147

Figure 5.25 Fitting FE of uniaxial tension model with experimental data.....	148
Figure 5.26 FE model dimension of planar shear	149
Figure 5.27 The deformation state of FE model under pure shear.....	150
Figure 5.28 Fitting FE of planar shear model with experimental data	151
Figure 5.29 FE model dimension of equal biaxial	152
Figure 5.30 The deformation state of FE model under pure radial strain	154
Figure 5.31 Fitting FE of equal biaxial model with experimental data	154
Figure 5.32 Actual dimension of volumetric specimens.....	155
Figure 5.33 The deformation state of FE volumetric model under compression	156
Figure 5.34 Fitting FE of volumetric model with experimental data.....	157
Figure 5.35 Stress – strain relationship of specimen A-1	158
Figure 5.36 Stress – strain relationship of specimen A-2	159
Figure 5.37 Stress – strain relationship of specimen A-3	159
Figure 5.38 Stress – strain relationship of specimen B1-1.....	160
Figure 5.39 Stress – strain relationship of specimen B1-2.....	161
Figure 5.40 Stress – strain relationship of specimen B1-3.....	161
Figure 5.41 Stress – strain relationship of specimen B2-1.....	162
Figure 5.42 Stress – strain relationship of specimen B2-2.....	163
Figure 5.43 Stress – strain relationship of specimen B2-3.....	163
Figure 5.44 Stress – strain relationship of specimen B3-1.....	164
Figure 5.45 Stress – strain relationship of specimen B3-2.....	165
Figure 5.46 Stress – strain relationship of specimen B3-3.....	165
Figure 5.47 Stress – strain relationship of specimen B4-1.....	166
Figure 5.48 Stress – strain relationship of specimen B4-2.....	167
Figure 5.49 Stress – strain relationship of specimen B4-3.....	167
Figure 5.50 Stress – strain relationship of specimen C1-1.....	170
Figure 5.51 Stress – strain relationship of specimen C1-2.....	171
Figure 5.52 Stress – strain relationship of specimen C1-3.....	171
Figure 5.53 Stress – strain relationship of specimen C2-1.....	172
Figure 5.54 Stress – strain relationship of specimen C2-2.....	173
Figure 5.55 Stress – strain relationship of specimen C2-3.....	173
Figure 5.56 Stress – strain relationship of specimen C3-1.....	174

Figure 5.57 Stress – strain relationship of specimen C3-2	175
Figure 5.58 Stress – strain relationship of specimen C3-3	175
Figure 5.59 Stress – strain relationship of specimen C4-1	176
Figure 5.60 Stress – strain relationship of specimen C4-2	177
Figure 5.61 Stress – strain relationship of specimen C4-3	177
Figure 5.62 Analytical models of isolated frames	182
Figure 5.63 Ground motion of Tabas - Iran (1978) in X- and Y- direction	186
Figure 5.64 Ground motion of San Fernando (1971) in X- and Y- direction.....	187
Figure 5.65 Ground motion of Northridge (1994) in X- and Y- direction	187
Figure 5.66 Ground motion of Landers (1992) in X- and Y- direction.....	187
Figure 5.67 Ground motion of Morgan Hill (1984) in X- and Y- direction.....	187
Figure 5.68 Ground motion of Loma Prieta (1989) in X- and Y- direction	188
Figure 5.69 Ground motion of Italy (1980) in X- and Y- direction	188
Figure 5.70 Unscaled response spectra of ground motion records (one storey)..	188
Figure 5.71 Unscaled response spectra of ground motion records (two storey) .	189
Figure 5.72 Scaled response spectra of ground motion records (one storey).....	190
Figure 5.73 Scaled response spectra of ground motion records (two storey).....	191
Figure 5.74 The range effective of the isolation ratio for one storey	192
Figure 5.75 The range effective of the isolation ratio for two storey	192
Figure 5.76 Plan view of isolated structure for one- and two- storey	193
Figure 5.77 Dimension of base isolation	199
Figure 6.1 Vertical characteristic of subjected to axial load of 10 kN	204
Figure 6.2 Vertical characteristic of subjected to axial load of 20 kN	206
Figure 6.3 Vertical characteristic of subjected to axial load of 30 kN	208
Figure 6.4 Vertical characteristic of subjected to axial load of 40 kN	210
Figure 6.5 Vertical characteristic of subjected to axial load of 80 kN	212
Figure 6.6 Vertical characteristic of subjected to axial load of 100 kN	214
Figure 6.7 Vertical characteristic of subjected to axial load of 150 kN	216
Figure 6.8 Vertical characteristic of subjected to axial load of 200 kN	218
Figure 6.9 Vertical characteristic of subjected to axial load of 250 kN	220
Figure 6.10 Horizontal test result of isolator in 5% shear strain (5 mm)	223
Figure 6.11 Horizontal test result of isolator in 10% shear strain (10 mm)	226

Figure 6.12 Horizontal test result of isolator in 20% shear strain (20 mm).....	228
Figure 6.13 Horizontal test result of isolator in 50% shear strain (50 mm).....	231
Figure 6.14 Horizontal test result of isolator in 100% shear strain (100 mm).....	233
Figure 6.15 Vertical test result of isolator in multi axial load	236
Figure 6.16 Horizontal test result of isolator in multi shear strain	237
Figure 7.1 The geometric of isolator in finite element software.....	243
Figure 7.2 Preview of modeling the rubber in the holes of perforated plate	244
Figure 7.3 Finite element models for vertical analysis	244
Figure 7.4 Mesh condition on FE models for vertical analysis.....	246
Figure 7.5 The loading condition of vertical analysis on FE program.....	247
Figure 7.6 Deformed shape of isolator under pure compression load	249
Figure 7.7 Comparison of vertical analysis between FE and experimental	249
Figure 7.8 FE model for horizontal analysis	252
Figure 7.9 Modification model of lateral analysis	252
Figure 7.10 The loading condition of lateral analysis on FE program.....	254
Figure 7.11 Deformed shape of isolator under lateral load.....	255
Figure 7.12 Comparison of lateral analysis between FE and experimental.....	256
Figure 7.13 Parameters of basic hysteresis loop	259
Figure 7.14 Bilinear model of PREIs under lateral displacement (100 mm).....	262
Figure 7.15 Bilinear model of PREIs compare to FE and experimental.....	262
Figure 7.16 Lateral characteristic of PREIs under different vertical load	263
Figure 8.1 Plan view of FE model of modified isolators	269
Figure 8.2 FE model of modified isolators in a quarter	271
Figure 8.3 The loading condition of MC-PREIs on FE program.....	272
Figure 8.4 Mesh condition of MC-PREIs model	273
Figure 8.5 Normalized vertical stiffness	274
Figure 8.6 Normalized compression modulus	275
Figure 8.7 Normalized shape factor	275
Figure 8.8 Vertical strain distribution of elastomer	277
Figure 8.9 Normalized vertical stress distribution of elastomer	278
Figure 8.10 Normalized S_{xz} shear stress contour.....	279
Figure 8.11 Normalized S_{yz} shear stress contour.....	280

Figure 8.12 Normalized Von Mises stress contours.....	281
Figure 8.13 FE model of modified isolators for lateral analysis	283
Figure 8.14 Mesh condition of MC-PREIs model for lateral analysis	285
Figure 8.15 Stiffness of the modified isolator normalized	287
Figure 8.16 Comparasion of lateral-displacement relationship.....	287
Figure 8.17 Local stress in the isolator.....	288
Figure 8.18 Contours of S_{11} in the center elastomer layer under compression ...	289
Figure 8.19 Contours of S_{11} in the center elastomer layer at $u/t_r = 0.50$	290
Figure 8.20 Contours of S_{11} in the center elastomer layer at $u/t_r = 1.00$	290
Figure 8.21 Variation of normalized stress profiles in the center elastomer.....	291
Figure 8.22 Contour of shear strain γ_{13} under different displacement.....	292
Figure 8.23 Distribution of S_{11} in the center of reinforcement layer	294

LIST OF TABLES

Table 4.1 Specimens Data of Experimental (Uniaxial Tension Test).....	106
Table 5.1 Experimental test results of plate-A.....	160
Table 5.2 Experimental test results of specimens B1	162
Table 5.3 Experimental test results of specimens B2	164
Table 5.4 Experimental test results of specimens B3	166
Table 5.5 Experimental test results of specimens B4	168
Table 5.6 Resume of experimental test results of specimens B.....	169
Table 5.7 Experimental test results of specimens C1	172
Table 5.8 Experimental test results of specimens C2	174
Table 5.9 Experimental test results of specimens C3	176
Table 5.10 Experimental test results of specimens C4	178
Table 5.11 Resume of experimental test results of specimens C.....	178
Table 5.12 The coefficient of perforated plate.....	180
Table 5.13 Material properties of perforated plate.....	180
Table 5.14 Member cross-sectional dimensions	183
Table 5.15 Horizontal stiffness of isolators	185
Table 5.16 Selected earthquake the ground motions.	186
Table 5.17 Scaling factor of ground motion	190
Table 5.18 Characteristic of isolator for one storey.....	194
Table 5.19 Characteristic of isolator for two storey.....	194
Table 5.20 Parameter design of Aceh	196
Table 6.1 Vertical stiffness of specimen subjected to axial load of 10 kN.....	205
Table 6.2 Vertical stiffness of specimen subjected to axial load of 20 kN.....	207
Table 6.3 Vertical stiffness of specimen subjected to axial load of 30 kN.....	209
Table 6.4 Vertical stiffness of specimen subjected to axial load of 40 kN.....	211
Table 6.5 Vertical stiffness of specimen subjected to axial load of 80 kN.....	213
Table 6.6 Vertical stiffness of specimen subjected to axial load of 100 kN.....	215
Table 6.7 Vertical stiffness of specimen subjected to axial load of 150 kN.....	217
Table 6.8 Vertical stiffness of specimen subjected to axial load of 200 kN.....	219
Table 6.9 Vertical stiffness of specimen subjected to axial load of 250 kN.....	221

Table 6.10 Horizontal test results in 5% shear strain	224
Table 6.11 Horizontal test results in 10% shear strain (10 mm)	227
Table 6.12 Horizontal test results in 20% shear strain (20 mm)	229
Table 6.13 Horizontal test results in 50% shear strain (50 mm)	233
Table 6.14 Horizontal test results in 100% shear strain (100 mm)	234
Table 6.15 Resume of the vertical characteristics of isolator.....	236
Table 6.16 Resume of the lateral characteristics of isolator.....	237
Table 7.1 Coefficients for material constitutive models.....	240
Table 7.2 Material properties of end-plate (Steel material).....	241
Table 7.3 Material properties of perforated plate	241
Table 7.4 Measure the quality of mesh in ANSYS	245
Table 7.5 Lateral characteristic of PREIs	263
Table 7.6 Comparison of vertical characteristic of PREIs	265
Table 7.7 Comparison of horizontal characteristic of PREIs	265
Table 8.1 Specimens geometric characteristics	269
Table 8.2 Vertical and horizontal characteristic of MC-PREIs.....	294

LIST OF NOTATIONS

A	: Loaded area of rubber bearing.
A_c	: Loaded area of perforated plate.
A_i	: Record's spectral acceleration.
\bar{A}_i	: Target spectral acceleration.
α_i	: Constant of shear behavior of rubber.
B_D	: Damping coefficient at DBE.
B_M	: Damping coefficient at MCE.
β_{eff}	: The effective viscous damping ratio.
C_{ij}	: Constant of strain energy function.
C_i	: Damping ratio of n -th story.
D	: Material constant of compressibility.
D_D	: Design displacement of isolator at DBE.
D_M	: Design displacement of isolator at MCE.
D_D'	: Minimum design displacement for dynamic analysis at DBE.
D_M'	: Minimum design displacement for dynamic analysis at MCE.
Δ	: Test displacement of isolator.
E_c	: Compression modulus of rubber - steel composite.
E_{loop}	: Energy dissipation per cycle of loading.
F^+	: Positive force at test displacement.
F^-	: Negative force at test displacement.
g	: Gravity.
ε	: Engineering strain.
h	: Total thickness of isolator.
I_i	: Invariants of green deformation tensor.
J_{el}	: Elastic volume ratio.
K	: Bulk modulus of rubber.

- K_{eff} : Effective stiffness.
- $K_{D,max}$: Maximum horizontal stiffness of isolator at DBE.
- $K_{M,max}$: Maximum horizontal stiffness of isolator at MCE.
- $K_{D,min}$: Minimum horizontal stiffness of isolator at DBE.
- $K_{M,min}$: Minimum horizontal stiffness of isolator at MCE.
- K_i : The story stiffness of n -th floor.
- K_H : Horizontal stiffness of base isolation.
- K_V : Vertical stiffness of base isolation.
- L : Deformed gauge length.
- L_0 : Initial gauge length.
- γ : Shear strain of isolator in horizontal direcion.
- m_b : Base mass of isolated structure.
- ω_{eff} : The effective isolation frequency.
- F_b : Restoring force of isolated structure.
- P_{crit} : Critical compression force of isolator.
- P_s : Shear stiffness per unit length.
- P_E : Euler buckling load.
- P_{ave} : Vertical pressure of isolator under compression.
- R : Radius of circular pad.
- σ : Engineering stress.
- S : Shape factor of base isolation.
- S_{D1} : Seismic coefficients at DBE.
- S_{M1} : Seismic coefficients at MCE.
- T_i : Period of isolated structure.
- T_{eff} : Effective isolation period.
- T_D : Target period of isolated at design basis earthquake (DBE).
- T_M : Target period of isolated at maximum capacity earthquake (MCE).

T_F	: Period of fixed structure.
t_r	: Total thickness of rubber material.
t_{sr}	: Total thickness of single rubber material.
μ_0	: Initial shear modulus.
λ	: Strech/ elongation ratio.
V	: Internal shear force.
V_b	: Base shear of isolated structure.
W	: Strain energy density function.
W_d	: Strain function to change the shape.
W_v	: Strain function to change the volume.

”This page is intentionally left blank”

CHAPTER 1

INTRODUCTION

1.1. Background of Research

In August 1909, J.A. Calantarients had submitted the patent application to the British patent office for his construction method proposing the building be built on "free join" that would allow the structure to move freely in the horizontal direction, thereby reducing the force transmitted to the building itself. The method proposed by Calantarients is known as base isolation or seismic isolation. A lot of methods have been developed over the last century to achieve the goal of uncoupling the building from damaging earthquake, such as rollers, balls, cables, rocking columns, as well as sand. The term base isolation uses the word isolation which means the state of being separated and the word base as a part that supports from beneath or serves as a foundation for an object or structure. As suggested in the literal sense, the structure (a building, bridge or piece of equipment) is separated from its foundation. Nowadays, the original terminology of base isolation is commonly replaced with seismic isolation, reflecting that in some cases, it is separated from the substructure columns. In another sense, the term seismic isolation is more accurate in case the structure is separated from the effect of the seismic or earthquake (Kelly, 2001).

The basic dilemma faced by structural engineers in providing seismic resistance is how to minimize floor acceleration and inter-story drift. Increasing the stiffness of structure leads to high floor acceleration which can damage sensitive internal equipment. Floor acceleration can be reduced by making the structure more flexible, but this leads to a large inter-story drift. The only effective way to significantly reduce inter-story drift and floor acceleration is by applying base isolation.

The concept of seismic isolation is quite simple. The system decouple the structure from horizontal movement by providing low horizontal stiffness between the structure and the foundation. It gives the isolated structure a fundamental frequency that is much lower than both fixed based frequency and predominant frequency of the ground motion. The first mode of isolated

structure involves deformation only in isolation system and the superstructure is supposed to be rigid. The isolation does not absorb the earthquake energy, but rather deflect it through the dynamic of the system to suppress possible resonance at the isolation frequency.

Base isolation is a very effective technique for reducing seismic forces by decoupling the structure motion from that of the soil. With regard to the earthquake, the insertion of a very flexible base-isolation system is generally favorable, particularly for reducing the ductility demand (Vulcano, 1998). The isolation system shifts the fundamental time period of the structure to a large value and/or dissipates the energy in damping, limits the amount of force that can be transferred to the superstructure, so that inter-story drift and floor acceleration are reduced significantly. The matching of fundamental frequencies of base-isolated structures and the predominant frequency contents of earthquakes is also consequently avoided, leading to a flexible structural system that is more suitable from earthquake resistance viewpoint (Matsagar and Jangid, 2004).

Seismic isolation has become famous within the last 20 years with the development of multilayer elastomeric bearings made by vulcanization bonding sheets of rubber to thin steel reinforcing plates. The bearings are very stiff vertically but very flexible horizontally, thereby enabling the structure to move laterally under strong ground motions. But the current base isolations applied are large, heavy and expensive. A single base isolation can weight one ton or more. The high cost of isolator production results from the labor involved in preparing the steel plates and assembling the rubber sheets and steel plates for vulcanization bonding in a mold. In order to extend this effectively, it is necessary to reduce the weight and cost of the isolators.

In order to develop low cost base isolation system, many research have been conducted to develop the low cost base isolation by eliminating the steel plates and replacing them with another material, such as fiber reinforcement (Kelly and Takhirov, 2001; Kelly and Andrea, 2012; Russo et al., 2013; Osgooei et al, 2014; 2015). The weight reduction is possible because fiber materials are available with an elastic stiffness that is of the same order as steel. The cost

saving may be possible if the use of fiber allows a simpler, less labor-intensive manufacturing process. Fiber reinforcement is made of many individual fibers grouped in strands and coiled into cords of sub-millimeter. The cords are more flexible in tension than the individual fibers; therefore, they may stretch when the isolator is loaded by the weight of a building.

In terms of connection to the isolator's top and bottom contact supports, FREIs can be classified as either bonded or unbounded. In a bonded (B)-FREI, two thick steel mounting plates are bonded to the outer rubber layers at the top and bottom of the isolator. During installation, the top and bottom mounting plates are bolted to the superstructure and substructure, respectively. In an unbounded FREI, the isolator is placed between the substructure and superstructure without any bond or fastening at its contact surfaces. During an earthquake, the shear loads at the contact surfaces of an unbounded isolator are transferred through friction. In a stable unbounded (SU)-FREI, the isolator's geometry can be selected so that it maintains lateral stability at extreme lateral displacements. However, the fiber-reinforced elastomeric isolators (FREIs) are more flexible in extension and have negligible flexural rigidity. Due to the low flexural rigidity of the fiber and the absence of the steel plate, FREIs exhibit a unique deformation where the upper and lower contact surfaces of isolator separate from the supports when the isolator experienced large lateral deformation. The vertical and horizontal responses of FREIs have been investigated through a number of analytical and FEA studies (Kelly, 1999; Kelly and Shakhzod, 2001; Kelly, 2002; Russo et al., 2013; Tsai and Kelly, 2002; Kelly and Konstantinidis, 2009; 2011). In addition, these solutions are based on simplified assumptions (e.g. the free surface of the rollover portion is stress-free, the fiber reinforcement is infinitely flexible, and the magnitude of the vertical load has no effect on the lateral response). One of the benefits of using fiber reinforcement instead of steel is that the bearings can be manufactured in a large rectangular sheet, and individual bearing can subsequently be cut to the required shape and size. All isolators are currently manufactured as either circular or square under a false belief that if the isolation system for a building is isotropic, it needs to be made of symmetrically shaped isolators.

Basically, the reinforcement placed on the isolator is intended to prevent the rubber to bulge sideways due to the weight of the building (Naeim and Kelly, 1999). The research aims to suggest that both the weight and cost of isolators can be reduced by eliminating the steel reinforcing plates and replacing them with perforated plates. The perforated plates are used as the strength element in numerous industrial applications, both in machine manufacturing and civil engineering. A very important characteristic of perforated plate is that the plates' perforated area which is calculated with formulas specific for each type of holes (the shape of hole and manner of holes placement on the plate).

Reinforcement is needed to provide vertical stiffness that may be obtained by using a similar volume of much lighter material such as perforated plate. Cost saving may be possible if the use of perforated plate allows a simpler, less labor-intensive manufacturing process. It is also possible that the current approach of vulcanization under pressure in a mold with steam heating can be replaced by microwave heating in an autoclave (Kelly and Takhirov, 2001).

The application of base isolation in residential buildings allows the use of perforated plate to replace the steel plate as reinforcement due to the lightweight of the structure. A certain horizontal stiffness that is relatively very small is needed in order to acquire the desired building period. It means that it also takes the type of rubber material that has a relatively small hardness in order to obtain shear modulus corresponding to the desired horizontal stiffness. The horizontal stiffness is closely related to building period, so building that originally has a small period will have a greater period and automatically, the acceleration experienced by the structure during earthquake will be reduced drastically.

1.2. Research Significance

Base isolation is well-known as the most sophisticated technology in protecting structures against extreme earthquake shaking and it has been widely used around the world for many types of building structures. The fundamental principle in preventing severe damage is by providing flexibility in the base of the structure by displacing the upper-structure as a rigid body under earthquake

impact. Furthermore, base isolation drastically extends the fundamental period of the system, taking the structure out of the dominant range of earthquake energy. This leads to a significant decrease in the earthquake force that is transferred to the structure (Vulcano, 1998; Sugihardjo et al., 2016; 2018).

Due to its many advantages, base isolation is expected to be applied to all types of structures, including low-rise residential buildings. However, the use of the isolator is still restricted too expensive and high-importance buildings only. The high cost of the manufacturing process (\$500 to \$10,000) prevents further application of the isolator (Kelly, 2001). This has encouraged many researchers to develop a low-cost base isolation, especially intended for low-rise buildings. The most general isolator, used worldwide, is the steel-reinforced elastomeric isolator (SREIs) that employs a steel plate as reinforcement to resist compression load. The existence of the steel plate on the SREI is the primary cause of the weight and high cost of base isolation.

The solution proposed by many researchers is by replacing the steel plate with an alternative material having similar performance, without reducing the safety level of the building structure. Among the research projects conducted, fiber reinforcement is the most feasible solution as an alternative material to replace the steel plate (Kelly, 1999; Kelly and Shakhzod, 2001). The fiber-reinforced elastomeric isolator (FREIs) is a new type of laminated rubber bearing developed to reduce the cost of the manufacturing process (Kelly, 1999; Kelly and Shakhzod, 2001; Kelly, 2002; Russo et al., 2013; Tsai and Kelly, 2002; Kelly and Konstantinidis, 2007; 2009; 2011). With low-cost base isolation, it is possible to economically install the isolator in residential housing and commercial buildings.

The earthquake hazard in developing countries, such as Indonesia, is significant for residential housing. The earthquake at the period of 2004 to 2018 shows that approximately 8,480 people died, accompanied by more than 400,000 residential housing heavy damage. Therefore, the low-cost base isolation is very important to reduce fatalities during an earthquake. The followings provide a summary of research needs in the area of interest:

- a. Development of new low-cost base isolation for residential housing in high seismic zones (for instance: Aceh, Yogyakarta, Manokwari, etc.).
- b. Experimental research to substantiate the new low-cost base isolation system.
- c. Assessment of the current analytical approaches validity for base isolation.
- d. Development of analytical model/procedure for perforated-reinforced elastomeric isolators (PREIs).

1.3. Research Objectives

The overall primary objective of this research project is to develop low cost base isolation system by using perforated plates as reinforcement. The experimental and FE analysis will be conducted to investigate isolator to derive certain lateral stiffness for residential housing. The specific objectives are outlined below:

- a. Investigate the characteristics of rubber material: Rubber is classified as hyperelastic material that exhibits non-linear elastic. Investigation of rubber characteristics is required to model rubber into FE Program (ANSYS). It involves 4 kinds of stress-strain data to represent rubber on ANSYS. They are uniaxial test data, planar test data, biaxial test data and volumetric test data.
- b. Investigate the characteristics of perforated plate; the existence of holes on the perforated plate affect its strength. The percentage of the perforated plate open area decreases the yield of strength and young modulus of plate. Therefore, investigation of perforated plate is required to define appropriate material properties on FE program.
- c. Investigate the vertical behavior of perforated-reinforced elastomeric isolator (PREIs) under compression load. The vertical behavior is related to the vertical stiffness of base isolation system. Investigation must be conducted in order to find out the vertical capacity of base isolation.
- d. Investigate the horizontal behavior of perforated-reinforced elastomeric isolator (PREIs) under combination loading; both lateral and compression

load. The horizontal stiffness is a valuable quantity that must be ensured since it is related to the target period of the superstructure. Certain horizontal stiffness must be achieved to yield specific fundamental period of structure.

- e. Develop an analytical model for PREIs.
- f. Evaluate the FE analysis compared to the experimental results. The finite element analysis is carried out to compare the results with experimental data. It is important to derive the optimum design of base isolation system.
- g. Produce a low-cost base isolation system for residential housing.
- h. Develop a practical design procedure of low-cost base isolation system (PREIs).

1.4. Research Scope

The scopes of the research program are as follows:

- a. Review the previous experimental and analytical research of base isolation system to determine relevant parameters for present study.
- b. Prepare and test the rubber material on axel product to establish mechanical properties of rubber material including uniaxial test, planar test, biaxial test, volumetric test and relaxation test.
- c. Prepare and test the perforated plate in order to know the yield of strength and young modulus of plate due to the effect of open area.
- d. Evaluate the test data of both rubber test and perforated test with finite element analysis. The comparison between FE and experimental data is used to derive the optimum design of material properties.
- e. Prepare the FE analysis of base isolation system. Modeling base isolation on finite element analysis prior to the experimental test is recommended to predict the behavior of specimens.
- f. Design, construct, instrumentation and test the base isolation system under axial compression and combine constant axial compression - reverse cyclic lateral loading to determine vertical stiffness and horizontal stiffness, respectively.

- g. Evaluate the test data of base isolation and investigate the effect of test variables.
- h. Evaluate the test data of base isolation with finite element analysis.
- i. Develop the analytical model for vertical stiffness and horizontal stiffness of base isolation system.
- j. Develop the design procedure for base isolation system strengthened by perforated plate.
- k. Prepare the dissertation and present the results.

1.5. Organization of Dissertation-

In this section, organization of dissertation related to the experimental test of base isolation is presented. In order to simplify the understanding of experimental test results, the dissertation is divided into seven chapters that consist of introduction, literature review, experimental program, analysis data, experimental results, finite element analysis and conclusion. The details for each chapter are as follows:

Chapter 1

This section consist of general concept of the research project. In this section, background of research, research significance, research objectives, research scopes are presented. It is expected to provide initial information for readers to understand well the general concept of the research project.

Chapter 2

In this chapter, the fundamental theory of base isolation and material properties are presented. This section provides a general concept to solve the issue of this research project. This section consists of basic principles of hyperelastic material, fundamental behavior of base isolation, characteristics of perforated plate, principal behavior of isolated structure, and theory of finite element method.

Chapter 3

In this chapter, the research methodology is presented. This section provides brief overview of the research flow. The flow chart presented on this section describes how the research is conducted with a series of experimental test and finite element analysis.

Chapter 4

In chapter 4, experimental programs are illustrated. The procedures of experimental test for all quantities of base isolation are presented including hyper elastic material test, perforated plate test, base isolation vulcanize process and base isolation test. In this section, detailed information related to experimental method to derive material properties and characteristics of base isolations are provided. It is expected to facilitate the readers to understand well how the experimental test was conducted. The results of this chapter are going to be discussed in the subsequent chapter with specific explanations.

Chapter 5

In this chapter, the analysis data of material experimental results described in chapter 4 are presented. This section provides detailed information of analytical procedure in considering the material properties obtained from the experimental test, particularly hyperelastic materials. The analysis results for each material are employed in the calculation and finite element program. In addition to material properties, fundamental characteristic of isolated structure and base isolation are also presented. The analysis results are used as the main parameter in determining the dimension of base isolation.

Chapter 6

This chapter is a particular section to discuss experimental results of base isolation subjected to compression and combination load. In other word, this section is the main part of this research project. In this chapter, the analytical procedure in investigating the characteristic of base isolation in vertical and lateral loading conditions are illustrated. The objective of this section is to

determine the vertical and horizontal stiffness of base isolation related to the experimental test. In this section, the final conclusion regarding experimental test results of vertical and horizontal test are determined. Further analysis based on the experimental test are carried out in the subsequent chapter by using finite element program.

Chapter 7

In chapter 7, finite element analysis (FEA) of base isolation is presented. Since the number of specimens employed in this project are limited, the finite element analysis (FEA) is considered extremely important to validate the experimental result and to conduct further analysis by using FE program. In this section, the experimental test of base isolation is modeled similar to the actual test in Lab. The results of FE are validated with the experimental test results to ensure that the FE modeling has a high accuracy. In addition, the FEA results are also employed for further analysis of base isolation in other condition. Additional conclusions are also presented for the characteristics of base isolation by using finite element method without conducting experimental test.

Chapter 8

Chapter 8 contains analysis of Modified Circular Perforated-Reinforced Elastomer Isolators (MC-PREIs). In this chapter, MC-PREIs is analyzed using FE program to observe the effect of modification. The introduction of modification by cutting loaded area is intended to reduce the horizontal stiffness of isolator. The FE analysis includes vertical and horizontal characteristic of MC-PREIs.

Chapter 9

Chapter 9 contains conclusions and recommendations related to the research project. This section provides the novelty of this research project and possibility for further research to develop low-cost base isolation. The recommendations are also presented to provide a general information for other researchers to continue this research project with different parameters study.

CHAPTER 2

LITERATURE REVIEW

2.1 Introduction

Over the past decades, earthquake resistant design concept of building structures have been widely based on a ductility design concept. The desired performance is to make ductile structure during major earthquake. However, this concept have proved to be unsatisfactory and far below expectation. The uncertainty of the ductility design strategy are follow :

- a. The ideal concept of "strong column weak beam" mechanism might not form in reality, because of existence of wall.
- b. Shear failure of columns due to inappropriate geometric proportions of short-column effect.
- c. Construction difficulty in grouting, typically at beam-column joints, due to complexity of steel reinforcement required by the ductility requirements.

Therefore, a number structural concept have been developed and base isolation is one of the most promising alternatives that can be applied for new structure as well as the retrofit buildings.

Many seismic construction designs and technologies have been developed over the years in attempt to mitigate the effects of earthquakes on buildings, bridges and potentially vulnerable contents. The design method using base isolation systems is a relatively recent, and evolving technology of this kind. The seismic isolation differs fundamentally from the conventional seismic design approaches in the method by which the period lengthening (detuning) and hysteretic energy-dissipating mechanisms are provided, as well as in the philosophy of how the earthquake attack is withstood. In the conventional approaches, it is accepted that considerable earthquake forces and energy will be transmitted to the structure from the ground. In the seismic isolation, however, the fundamental aim is to substantially reduce the transmission of the earthquake forces and energy into the structure. Therefore, the seismic isolation is an innovative seismic design approach aimed at protecting structures against damage

from the earthquake by limiting the earthquake attack rather than resisting it (Park et al., 2002).

Uncoupling a structure (e.g. buildings or bridges) from devastating effects of earthquakes has been one of the major concerns of scientists and engineers for a long time. Although, many efforts have been made by introducing numerous devices based on seismic isolation of structures, they are mostly intricate and a limited number of them have been applied into buildings and bridges (Dezfuli and Alam, 2013). Seismic isolation is a well-known earthquake mitigation technique, which lowers the seismic demand on a structure by shifting the natural period of vibration of the structure beyond the high energy period range of earthquakes. As a result, the seismic energy transferred to the structure is significantly reduced. The application of seismic isolation in North America has been limited almost entirely to expensive or high importance (post-disaster) structures, e.g., hospitals and emergency centers. This limited use is largely due to the high material, manufacturing and installation costs associated with conventional seismic isolators. It is expected that the use of seismic isolators can be extended to smaller structures and typical residential (normal importance) buildings if the weight and cost of the isolators are reduced (Osgooei et al. 2014; 2015).

Historically, steel plates in the form of shims have been the reinforcement of choice; however, conventional Steel-Reinforced Rubberic Isolators (SREIs) are heavy and expensive. The weight is attributed to the steel shims and thick steel end plates used to mechanically fasten the isolator to the supports. The cost is in part due to the highly labor-intensive process required to prepare the steel for bonding to the rubberic layers (Engelen, 2014). Steel reinforced rubberic isolators (SREIs), usually used for seismic isolation, consist of a number of sheets of rubberic layers alternated to thin steel plates and bonded to them. Steel plates are supposed to be rigid and consequently lateral displacements at the top and the bottom of each rubberic layer are zero, thus increasing computed vertical stiffness. Two steel plates, much thicker than others, are positioned at the top and bottom of the whole isolator; they allow the isolator to be rigidly connected, by means of other two thick steel plates, to the foundation

and to the superstructure. This kind of isolators is heavy and expensive and consequently this isolation technology is generally applied in specific cases only (emergency centers, hospitals or large-expensive buildings) (Angeli et al., 2013). The current isolators used are large, heavy and expensive thus it is necessary to reduce the weight and cost of the isolators. The primary weight in an isolators is due to the existing of steel plate as reinforcement, which provide the vertical stiffness of rubber-steel composite element. Therefore, to reduce both the weight and cost of isolators, a number of research has been carried out by replacing steel plate with alternative material, for instance, fiber as new reinforcement. The fiber reinforcement, in contrast to the steel reinforcement (which is assumed to be rigid both in extension and flexure), is assumed to be flexible in extension, but completely without flexural rigidity (Kelly and Shakhzod, 2001; Kelly and Calabrese, 2012).

Actually, in terms of strength, the use of steel plate is considerably satisfactory by providing the high vertical stiffness. In order to take the advantages of the steel strength, in this research work, perforated plate are intended to replace a steel plate as reinforcement of seismic isolator.

All the time perforated plate are only used for sound suppression, microwave and EMI/RFI radiation containment, filtration and purification of air, water and gases or in other word it only used for non structural but in this paper the perforated plate will be used as reinforcement of seismic isolator. The analysis of perforated-reinforced rubberic isolators (PREIs) is conducted by experimental and nonlinear finite element analysis.

The finite element analysis was carried out using ANSYS, a commercially available general purpose finite element program. Finite element models are evaluated using experimental data obtained from experimental test. The nearly compressible hyperelastic material constitutive mode and a linear-elastic isotropic material model was used to represent material properties of rubber and perforated plate. Hyperelastic materials such as rubber are widely used for diverse structural applications in variety of industries ranging from tire to aerospace. The most attractive property of rubbers is their ability to experience large deformation under small loads and to retain initial configuration without

considerable permanent deformation after load is removed. Their stress-strain behavior is highly non-linear and a simple modulus of elasticity is no longer sufficient. Therefore, characterization of elastic behavior of highly extensible, nonlinear materials is of great importance (Shahzad et al., 2005).

2.2 Hyperelastic Material.

2.2.1 Characteristic of Hyperelastic Material.

This section presents the issues of hyperelastic material model that used in finite element analysis to represent rubber (rubber) material. Rubber (natural and synthetic rubber) are amorphous polymers to which various ingredients are added, creating what the rubber chemist refers to as a compound. After heating and reaction (vulcanization), these materials become “rubber”. While they are elastic and rubbery, they also dissipate energy because of their viscoelastic nature. Their strength is high, especially under shear and compressive deformations.

As an engineered product, the material at some point will be subject to an external force. When a solid body is deformed, an internal reactive force called stress, acting across a unit area, tends to resist this deformation. The measure of deformation is called strain. Consider now Fig. 2.1(Gent, 2012), a tensile stress–strain diagram for three physical states of a polymer: glassy, crystalline, and rubbery. Glassy polymers are hard and brittle. The failure (rupture) point (X) is shown in Fig 2.1. Crystalline polymers go through a succession of changes: elastic deformation, yield, plastic flow, necking, strain hardening, and fracture.

Rubber is unique in being soft, highly extensible and highly elastic. The elastic behavior for these case is determined by coefficients; Young's modulus E (tension). shear modulus G (shear), bulk modulus K (compression) and poisson's ratio. For rubber, the poisson ratio (ν) is 0,499.

There are two basic mechanical properties of any material (Gent, 2012): elastic modulus (stiffness) and damping (ability to dissipate energy). Typically, some energy is lost (converted to heat) in any deformation. Viscoelastic response was originally modelled by a combination of a spring (elastic component) and dashpot (viscous response).

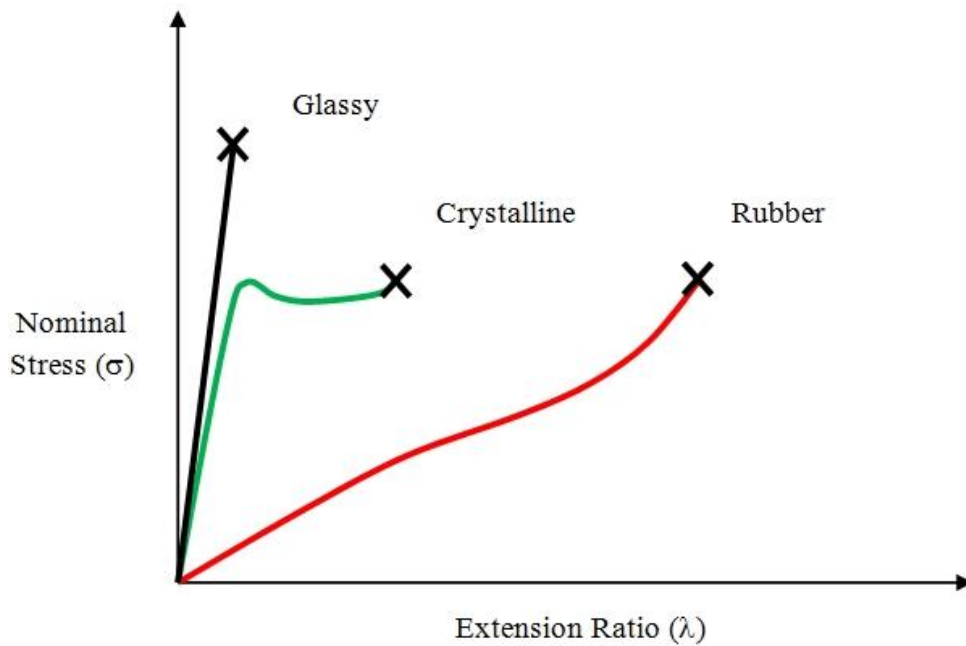


Figure 2.1 Tensile stress- strain for polymer in three physical states;
X denotes rupture.

For the spring, stress is directly proportional to strain (Hooke's law), and for the dashpot, the rate of strain is proportional to the stress applied. Of course, it is not that simple; a dashpot's resistance depends on both time and viscosity.

It is very instructive to view the stress-strain behavior for rubber. Here a tensile test is preformed (see Fig 2.2) on a natural rubber cycled to 20%, 40%, 60%, 100%, 150% and 200% strain with each cycle repeated four times. The stress-strain behavior of rubber is very different from Hooke's Law in four basic areas.

First, as the rubber is deformed into a larger strain territory for the first time, it is very stiff, but upon recycling in this same strain territory, the rubber softens dramatically. This phenomenon is often referred to as the Mullins' effect. In most applications this one time very stiff event is usually discarded where it is assumed in these applications repetitive behavior will dominate. Nonlinear elasticity has several stress and strain measures, however, it is most common to measure rubberic experimental data using stress and strain measures, whereby the stress is the current force is divided by the original area, and the strain is the

change in length divided by the original length. All test data presented and discussed herein will use stress and strain measures.

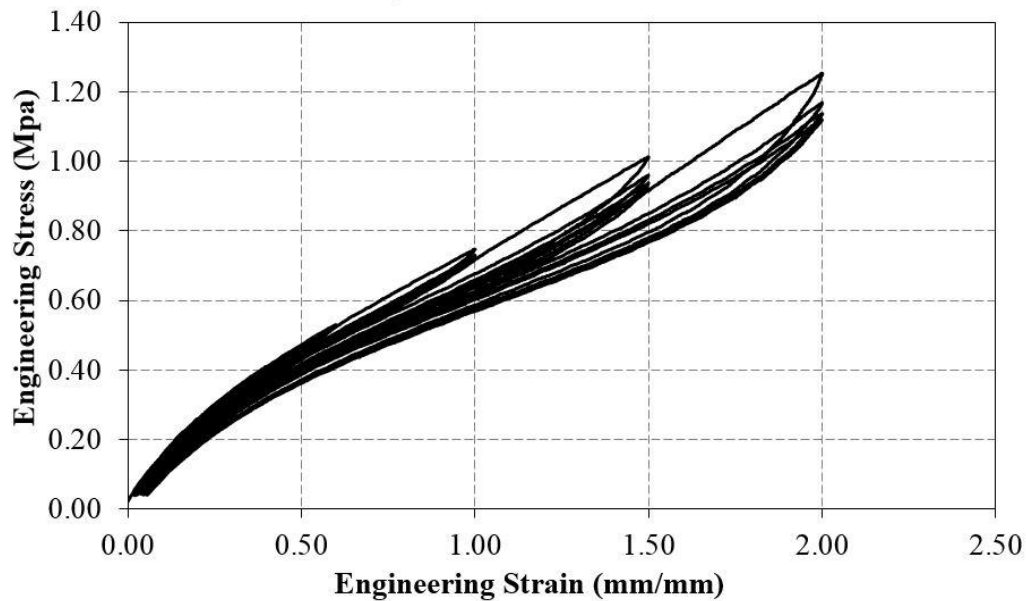


Figure 2.2 Stress- strain data cycled to 20%, 40%, 60%, 100%, 150% and 200%.

Secondly, there is always a viscoelastic effect present in rubber leading to a stable hysteresis loop when cycled over the same strain range. Hyperelastic models seek to find a simple equilibrium curve, not a hysteresis loop because viscoelastic effects may be included as we shall see later. Also discarded with the “one time” stiffness event is the shifting of the data to go through the origin, a requirement for hyperelastic materials; this will cause an apparent change in gage length and original cross sectional area. This shift ignores irreversible damage in the material when first stretched, as shown in Fig 2.3.

The third area of difference between hyperelastic laws and Hooke’s law, is the enormous difference between tension and compression of hyperelastic materials. Hooke’s law always assumes that stress is proportional to strain, whereas this is never observed for rubberic materials, hence Hooke’s law is inadequate for rubber. The incompressibility of rubber with its ratio of bulk to shear modulus over 1,000 times larger than steel, causes the larger stress magnitudes in compression as compared to tension for the same strain magnitude.

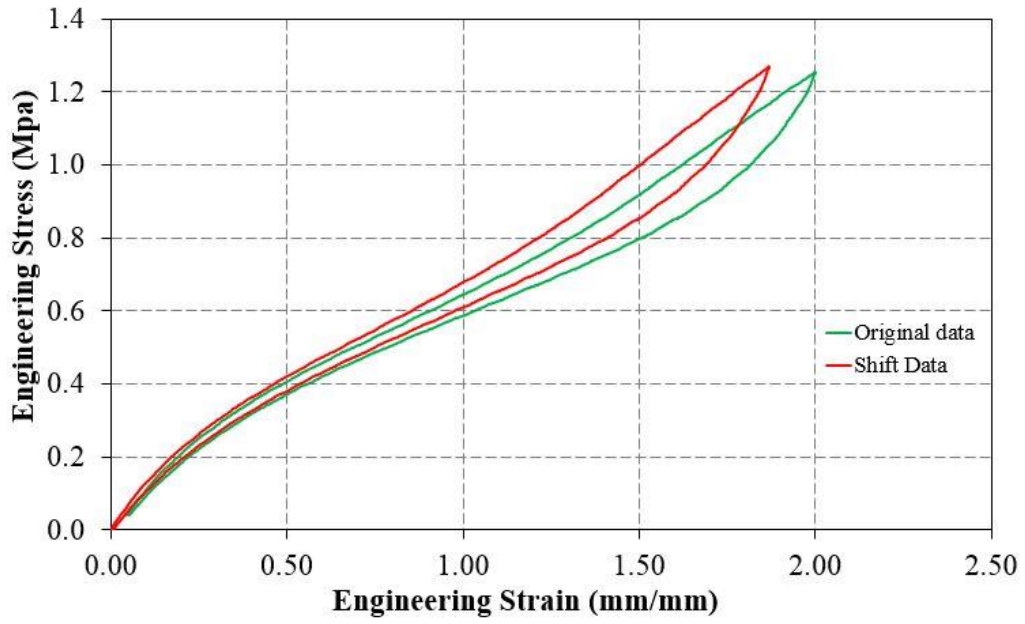


Figure 2.3 Shifting experimental data of hyperelastic material.

The final difference between hyperelastic laws (there are many) and Hooke's law is the sensitivity of the hyperelastic constants to deformation states. Any comprehensive treatment of rubber behavior should address these different strain states. For example, uniaxial, biaxial and planar shear are show here with their corresponding stress-strain responses. As the hyperelastic laws become more sophisticated with more constants to be determined experimentally, data from these three modes becomes more important to prevent spurious analytical behavior not observed experimentally. If you only have one mode, say tension, stick to the Neo-Hookean (one constant Mooney), Gent or Arruda-Boyce hyperelastic material models to be safe.

2.2.2 Constitutive Model of Hyperelastic Material

Strain is the intensity of deformation. If we pull a slender rubber rod along its length, the stretch ratio,, (or stretch) is defined as the ratio of the deformed gauge length \mathbf{L} divided by the initial length \mathbf{L}_0 , namely

$$\lambda = \frac{L}{L_0} = \frac{(L_0 + L - L_0)}{L_0} = 1 + \frac{(L - L_0)}{L_0} = 1 + \varepsilon \quad (1)$$

where is the strain. Generally, if we apply an in-plane, biaxial load to a piece of rubber, we can define three principal stretch ratios in the three respective principal directions. In large deformation analysis of nonlinear materials (such as rubber), the stretch ratios are a convenient measure of deformation and are used to define strain invariants, I_j for $j=1,3$, which are used in many strain energy functions.

Hyperelastic materials such as rubber are widely used for diverse structural applications in variety of industries ranging from tire to aerospace. The most attractive property of rubbers is their ability to experience large deformation under small loads and to retain initial configuration without considerable permanent deformation after load is removed. Their stress-strain behavior is highly non-linear and a simple modulus of elasticity is no longer sufficient. Therefore, characterization of elastic behavior of highly extensible, nonlinear materials is of great importance (Shahzad et al., 2005).

Rubberic material models are characterized by different forms of their strain energy (density) functions. Such a material is also called hyperelastic. Implicit in the use of these functions (usually denoted by W) is the assumption that the material is isotropic and elastic. If we take the derivative of W with respect to strain, we obtain the stress, the intensity of force. The commonly available strain energy functions have been represented either in terms of the strain invariants which are functions of the stretch ratios or directly in terms of the stretch ratios themselves. The constitutive behavior of hyperelastic material is obtained from strain energy function based on three strain invariants, I_1 , I_2 and I_3 , as follow :

$$W = W_d + W_v = f(I_1, I_2, I_3) \quad (2)$$

where W_d is strain function to change the shape; W_v is strain function to change volume; I_1 , I_2 and I_3 are three invariants of green deformation tensor determined in term of principal stretch ratios and given by :

$$\begin{aligned}
I_1 &= \lambda_1^2 + \lambda_2^2 + \lambda_3^2 \\
I_2 &= \lambda_1^2 \lambda_2^2 + \lambda_2^2 \lambda_3^2 + \lambda_3^2 \lambda_1^2 \\
I_3 &= \lambda_1^2 \lambda_2^2 \lambda_3^2
\end{aligned} \tag{3}$$

Basically, (Jakel, 2010) hyperelastic materials are considered as incompressible material that there is no volume change under load ; $I_3 = 1$ hence only two independent strain measures namely I_1 and I_2 remain. This implies that strain energy function of I_1 and I_2 only

$$W = \sum_{i,j=1}^{\infty} C_{i,j} (I_1 - 3)^i (I_2 - 3)^j + \sum_{k=1}^N \frac{1}{D_k} (J - 1)^{2k} \tag{4}$$

A considerable amount of literature has been published on modeling of rubber material. The choice of the model depends to its application, corresponding variables and its available data to determine material parameters. The validity of possible models should be studied and the simplest is selected with high accuracy and low materials parameters. An efficient hyperelastic model can be explained by four main qualities (Ali et al., 2010) :

- a. It should have the ability to exactly reproduce the whole ‘S’ shaped response of rubbers.
- b. The change of deformation modes must not be problematic, i.e., if the model operates sufficiently in uniaxial tension, it must also be exact in simple shear or in equibiaxial tension.
- c. The number of fitting material parameters should be small, in order to decrease the number of experimental tests for their determination.
- d. The mathematical formulation should be simple display practicable for the numerical performance of the model.

Two types of hyperelastic material models are available and each model defines the strain energy function in a different way. One is the phenomenological models which treat the problem from the viewpoint of continuum mechanics and stress-strain behavior is characterized without reference to the microscopic structure. Other one is physically motivated models which consider the material

response from the viewpoint of microstructure. A brief review about the hyperelastic models available in ANSYS exploited during this study is given below.

Polynomial model: The polynomial model offered here in the compressible form, based on the 1st and the 2nd invariant of the deviatoric Cauchy-Green tensor:

$$W = \sum_{i,j=1}^{\infty} C_{i,j} (I_1 - 3)^i (I_2 - 3)^j + \sum_{i=1}^N \frac{1}{D} (J_{el} - 1)^{2i} \quad (5)$$

where W is strain energy density function (strain/ unit of reference volume). J_{el} is elastic volume ratio, I_1 and I_2 are 1st and 2nd invariants of deviatoric strain and C_{ij} and D_i are material constant, while N is a positive determining number of terms in strain energy function ($N = 1,2,3$). C_{ij} describes shear behavior of material, D_i introduce compressibility and is set equal to zero for fully incompressible material. This model is usually utilized un modeling stress- strain behavior of filled rubber, with 4-5 terms (Forno et al., 1999).

Ogden model: This model proposes the strain energy function based on the principal stretches fo incompressible materials that is assumed $\lambda_1^2 \lambda_2^2 \lambda_3^2 = 1$. The principal stretches are directly measurable quantities and it is one obvious advantage of using them. The relation of Ogden strain energy potential is given by:

$$W = \sum_{i=1}^N \frac{2\mu_i}{\alpha_i} (\lambda_1^{\alpha_i} + \lambda_2^{\alpha_i} + \lambda_3^{\alpha_i} - 3) + \sum_{i=1}^N \frac{1}{D} (J_{el} - 1)^{2i} \quad (6)$$

where :

J = $\lambda_1 \lambda_2 \lambda_3$; the jacobian determinant

λ = The principal stretches

J_{el} = The elastic volume ratio

The constants μ_i and α_i describe the shear behavior of the material and D_i the compressibility. Calculation of invariant derivatives of Ogden's energy

function is more used and computationally intensive than that of polynomial form (Forno et al., 1999). Ogden model can be more accurate in fitting, when data from multiple experimental test are available (Korochkina et al., 2005).

Mooney-Rivlin model : Strain energy potential is proposed :

$$W = \sum_{i,j=1}^{\infty} C_{i,j} (I_1 - 3)^i (I_2 - 3)^j + \sum_{i=1}^N \frac{1}{D_i} (J_{el} - 1)^{2i} \quad (7)$$

where C_{ij} are material parameter and $C_{00} = 0$. By setting $N = 1$ in polynomial model or $N = 2$, $\alpha_1 = 2$ and $\alpha_2 = -2$ in Ogden model, Mooney-Rivlin model is obtained as (Seibert and Schoche 2000)

$$W = C_{10}(I_1 - 3) + C_{01}(I_2 - 3) + \frac{1}{D_1}(J - 1)^2 \quad (8)$$

Most favorite ones of constitutive models are Mooney-Rivlin and Ogden models; disadvantage is that material parameters (not physically-based) must be obtained by experiments Fitting method can be complicated if number of parameters is large (Bol and Reese, 2003).

Neo-Hookean model : This model is the simplest hyperelastic model for rubberic materials when material data is insufficient. The reduced polynomial model change to Neo-Hookean model :

$$W = C_{10}(I_1 - 3) + \frac{1}{D_1}(J_{el} - 1)^2 \quad (9)$$

This model is offered only in term of first deviatoric invariant (Timbrell et al., 2003). Moreover, this model is simples hyperelastic model and used for rubberic material when material data insufficient. This model is significant because of statistical theory of rubber elasticity appears at strain energy function.

Yeoh model : The Yeoh model strain energy function is presented as following when $N = 3$ in the reduced Polynomial model

$$W = \sum_{i=1}^3 C_{i,j} (I_1 - 3)^i + \sum_{i=1}^3 \frac{1}{D} (J_{el} - 1)^{2i} \quad (10)$$

The initial shear modulus and bulk modulus are given by :

$$\mu_0 = 2C_{10}, K_0 = \frac{2}{D_1} \quad (11)$$

This model is applicable for a much wider range of deformation and able to predict the stress-strain behavior in different deformation modes from data gained in one simple deformation mode such as uniaxial extension.

Arruda and Boyce Model : Physical models are based on an explanation of a molecular chains network. Strain energy is assumed to be equal to the sum of strain energies of individual chains oriented in space randomly (Ghosh et al., 2003). This model is as follow

$$W = \mu \sum_{i=1}^5 \frac{C_i}{\lambda^{2i-2}} (I_1^i - 3) + \frac{1}{D} \left[\frac{J_{el}^2 - 1}{2} - \ln(J_{el}) \right] \quad (12)$$

where $C_1 = \frac{1}{2}$, $C_2 = \frac{1}{20}$, $C_3 = \frac{11}{1050}$, $C_4 = \frac{19}{7000}$, $C_5 = \frac{519}{673750}$, μ is initial shear modulus and λ_m locking stretch, at which upturn of stress- strain curve would rise significantly. D is double the inverse bulk modulus at small strain as $D = \frac{2}{K}$; and

D is set to zero for incompressible material (Seibert and Schoche, 2000).

This model, in the range of smaller strain, helps to make accurate solutions with neglecting second variant of left Cauchy-Green tensor. With increasing locking stretch parameter, a sufficient accuracy in both small and large strain is obtained.

2.2.3 Stress-Strain of Hyperelastic Material.

The primary objective of the testing material is to determine and to satisfy the input requirements of mathematical material models into non-linear

finite element analysis software. The testing of rubber for the purpose of defining material models is often misunderstood. The appropriate experiments are not yet clearly defined by national or international standards organizations. This difficulty derives from the complex mathematical models that are required to define the nonlinear and the nearly incompressible attributes of rubber (Miller, 2000). Most of these models are referred to as hyperelastic material models. However, most models share common test data input requirements. In general, stress and strain data sets developed by stretching the rubber in several modes of deformation are required and “fitted” to sufficiently define the variables in the material models.. Appropriate experimental loading sequences and realistic strain levels are needed to capture the rubber behavior that applies in the analysis. The basic strain state are simple tension, pure shear and equal biaxial extension. For slightly compressible situations where an rubber is highly constrained, a volumetric compression test may be needed to determine the bulk behavior. The following tests are:

2.2.3.1 Simple Tension Testing.

Simple tension test are very popular for rubber (Fig 2.4). There are several standards for the testing of rubber in tension. However, the experimental requirements for analysis are somewhat different than most standardized test method. The most significant requirement is that in order to achieve a state of pure tensile strain, the specimen must be much longer in the direction of stretching than in the width and thickness dimensions.

The objective is to create an experiment where there is no lateral constraint to specimen thinning. The specimen needs to be at least 10 times longer than the width or thickness. The material is cut from sheets and is typically a dog bone-shape specimen with an effective length of 50 mm. Typically, ASTM D412 die D is used. The length in this case refers to the specimen length between the instrument clamps. In the process of gripping, specimen clamps create an

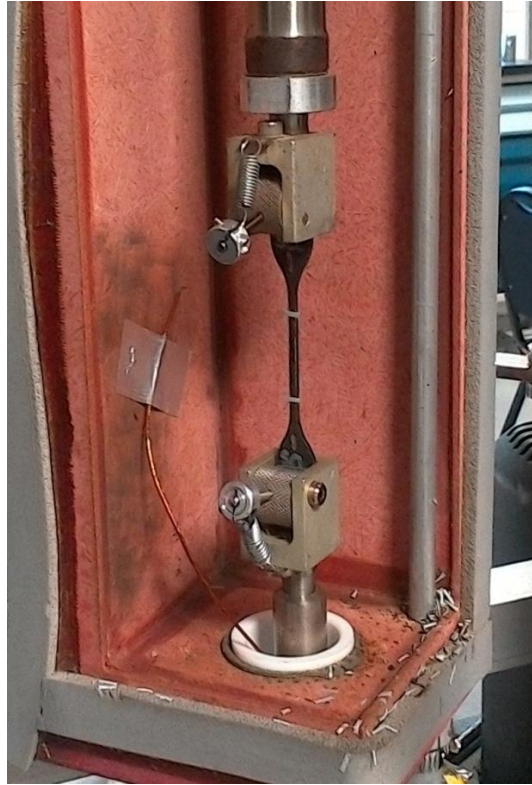


Figure 2.4 Simple tension test frame.

indeterminate state of stress and strain in the region surrounding the clamp. Therefore, the specimen straining must be measured on the specimen, but away from the clamp in a region where a pure tension strain state is occurring. A non-contacting strain measuring device such as a video extensometer or laser extensometer is required to achieve this.

An Instron servo-hydraulic or electromechanical test instrument is used to provide the loading. The instrument is fitted with a strain gage load cell to measure force for the calculation of stress. A laser strain measuring device is used to measure strain in a strain gradient free region of the test specimen.

The stress/strain state for uniaxial tension test could be idealized as shown Fig 2.5. The red arrow, σ_1 , exhibits the tensile force that deform the specimen to the strain level ε_1 . The stresses (red) or strain (blue) where no arrow is shown are zero. The uniaxial stretch ratio can be expressed as

$$\lambda_1 = \frac{1}{\lambda_2^2} = \frac{1}{\lambda_3^2} \quad (13)$$

where σ_1 and ε_1 are stress and strain in stretching direction, respectively. The strain ε_2 and ε_3 describe no lateral constraint to the specimen thinning.

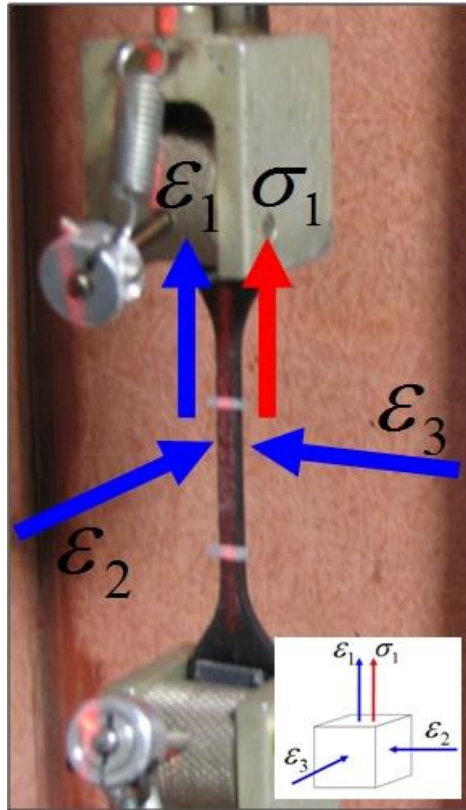


Figure 2.5 Idealized stress/ strain state of uniaxial test.

2.2.3.2 Planar Tension Testing (Pure Shear)

Pure shear experiment (Fig 2.6) used for analysis is not what most of us would expect. The experiment appears to be nothing more than a very wide tensile test. However, because the material is nearly incompressible, a state of pure shear exists in the specimen at a 45 degree angle to the stretching direction. The most significant aspect of the specimen is that it is much shorter in the direction of stretching than the width. The objective is to create an experiment where the specimen is perfectly constrained in the lateral direction such that all specimen thinning occurs in the thickness direction. The specimen must be at least 10 times wider than the length in the stretching direction. The material is cut

from sheets and is about 150 mm wide and 15 mm tall. The nature of the test, as mentioned, is such that the width must be at least 10 times as much as the gauge length.

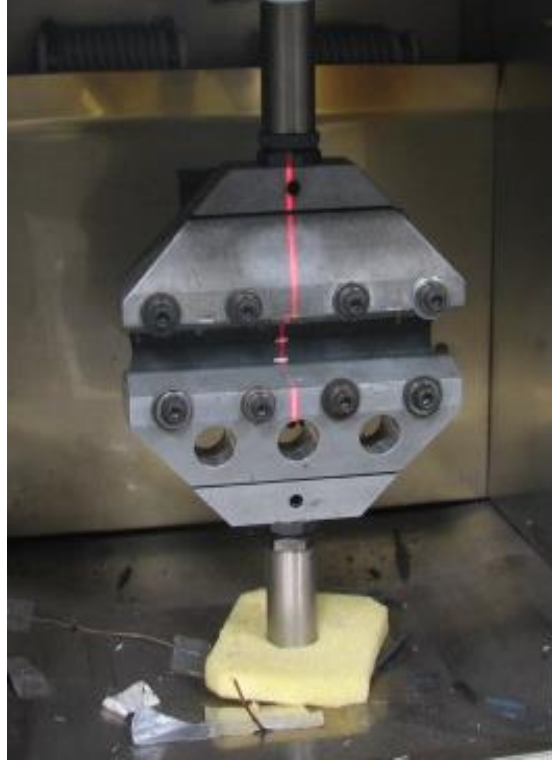


Figure 2.6 Planar shear specimen mounted on machine.

The red arrow, σ_1 , exhibits the tensile force that deform the specimen to the strain level ε_1 . As shown in Fig 2.7, the stresses (red) or strain (blue) where no arrow is shown are zero. The planar stretch ratio can be expressed as

$$\lambda_1 = \frac{1}{\lambda_2}; \lambda_3 = 1 \quad (12)$$

where σ_1 and ε_1 are stress and strain in stretching direction, respectively. The stress σ_3 and no strain ε_3 describe perfectly constrained in lateral direction such that all specimen thinning occurs in the thickness direction.

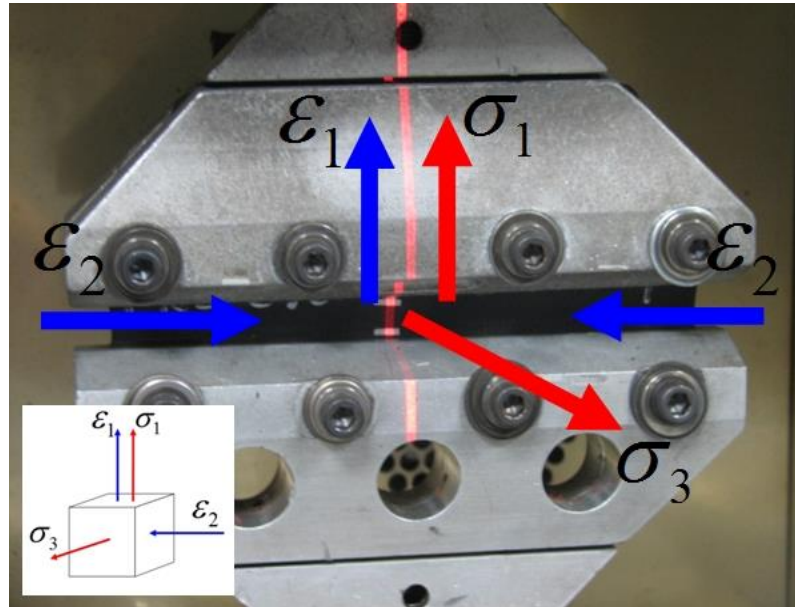


Figure 2.7 Idealized stress/strain state of planar test.

The aim is to create an experiment with perfect lateral constrain to specimen thinning. A non-contacting strain measuring device must be used to measure strain where the pure strain state is occurring, away from the clamp edges. A non-contacting strain measuring device such as a video extensometer or laser extensometer is required to achieve this. An instron servo hydraulic or electromechanical test instrument is used to provide the loading. The instrument is fitted with a strain gage load cell to measure force for the calculation of stress. A laser strain measuring device is used to measure strain in a strain gradient free region of the test specimen.

2.2.3.3 Equalbiaxial Testing.

For incompressible or nearly incompressible materials, equalbiaxial extension of a specimen creates a state of strain equivalent to pure compression (Fig 2.8). Although the actual experiment is more complex than the simple compression experiment, a pure state of strain can be achieved which will result in a more accurate material model. The equalbiaxial strain state may be achieved by radial stretching a circular disc. Once again, a non-contacting strain measuring device must be used such that strain is measured away from the clamp edges. The material is cut from sheets and is 75 mm in diameter, with an effective area of 50

mm in diameter. the effective gauge length of specimen is 25 mm in radial direction. An Instron servo-hydraulic or electromechanical test instrument is used to provide the loading. The instrument is fitted with a strain gage load cell to measure force for the calculation of stress. A laser strain measuring device is used to measure strain in a strain gradient free region of the test specimen .

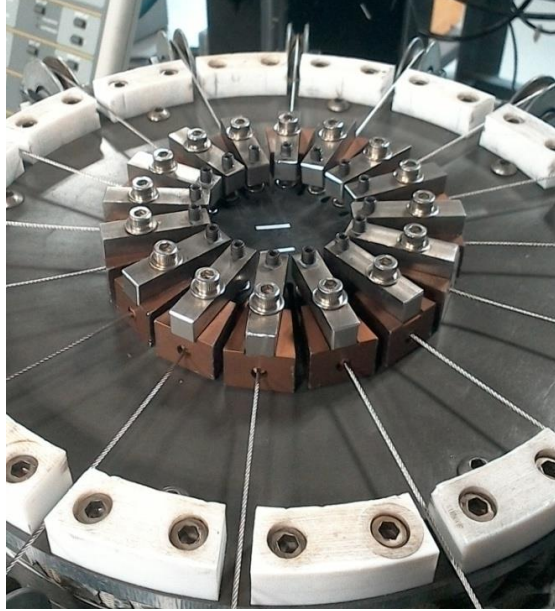


Figure 2.8 Equalbiaxial specimen mounted on machine.

The stress/strain state for equalbiaxial test could be idealized as shown in Fig 2.9. The red arrow, σ_1 and σ_2 , exhibits the tensile force that deform the specimen to the strain level ε_1 and ε_2 in radial direction. The stresses (red) or strain (blue) where no arrow is shown are zero. The radial stretch ratio can be expressed as

$$\lambda_1 = \lambda_2 = \frac{1}{\sqrt{\lambda_3}} \quad (13)$$

where σ_1 and σ_2 are stress in stretching radial direction. The strain $\varepsilon_1, \varepsilon_2, \varepsilon_3$ describe a state of strain equivalent to pure compression. Although the actual experiment is more complex than a simple compression experiment, a pure state of strain can be achieved which will result in a more accurate material model.

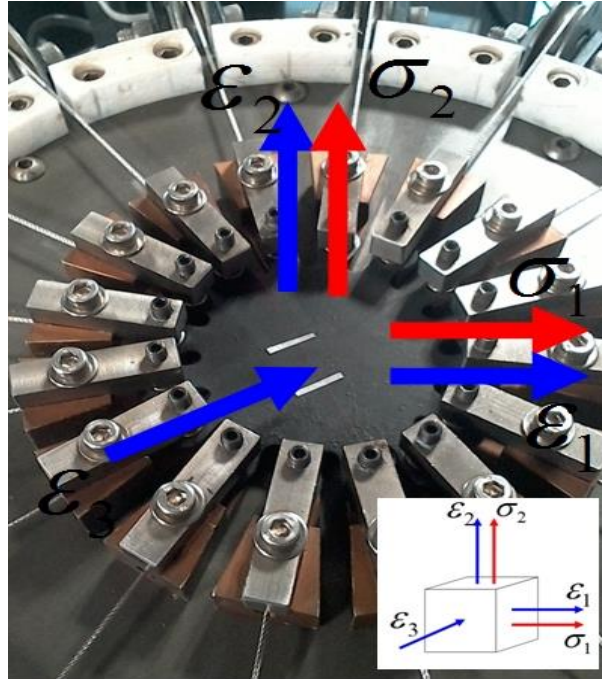


Figure 2.9. Idealized stress/strain state of equalbiaxial test.

2.2.3.4 Volumetric Compression Testing.

The volumetric compression experiment is performed to measure the relationship between hydrostatic and volume change in a dense rubber. It is also referred to as constrained compression. Circular disk of an rubber are stacked in a cylindrical void in a steel fixture and compressed on one end such that material reacts against the bottom and sides of the cylinder. The assumption is made that the dense rubber behaves similar to a fluid in that the reaction force in all directions are essentially equal. The volume change and required pressure to compress the material are measured and the initial slope of the pressure-volume curve is taken to be the bulk modulus. The test specimens are cut from sheets or slabs and are 6,35 mm in diameter. Typically, 5 disk, 1-2 mm thick each, are stacked (Figure 2.10).

An Instron servo-hydraulic or electromechanical test instrument is used to provide the loading. The instrument is fitted with a strain gage load cell to measure force for the calculation of stress. A laser strain measuring device is used to measure strain at the fixture-specimen interface. The stress/strain state for volumetric test could be idealized (as shown in Fig 2.11).

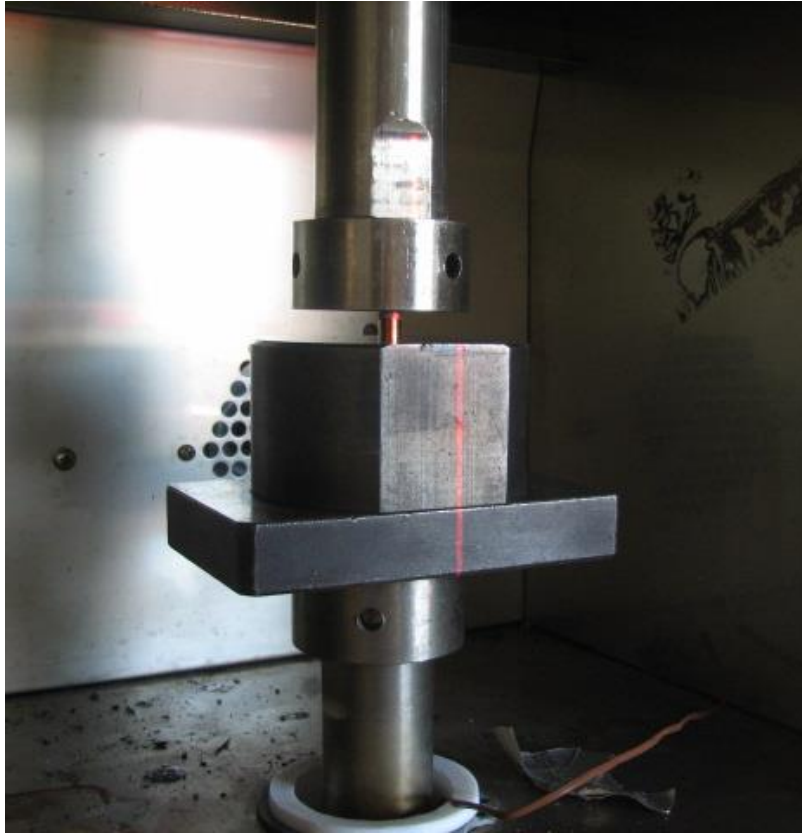


Figure 2.10 Volumetric specimen mounted on machine.

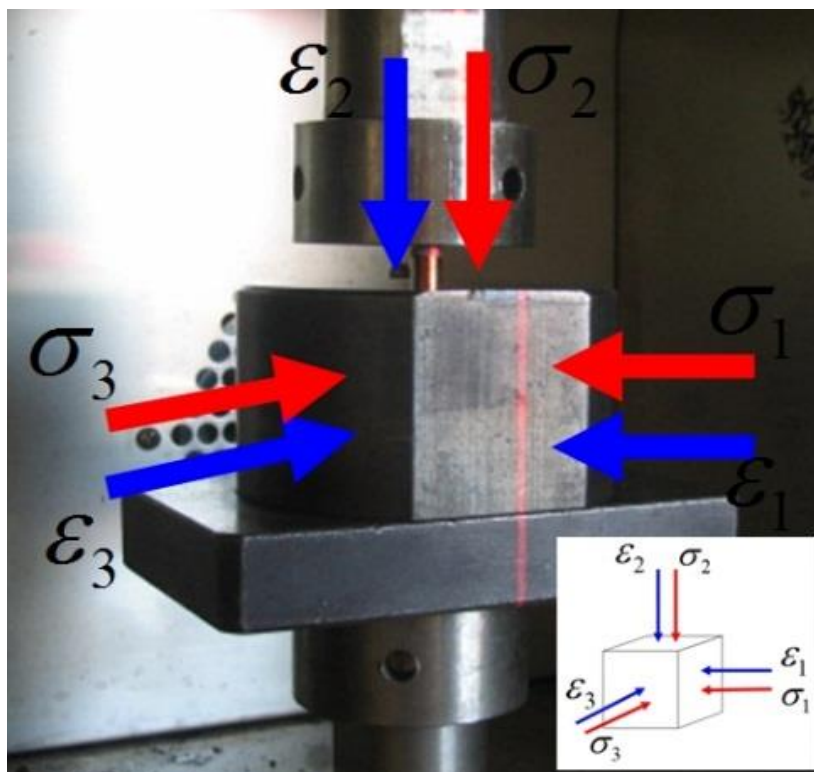


Figure 2.11 Idealized stress/ strain state of volumetric Test.

The red arrow, σ_1 , σ_2 and σ_3 , exhibits the hydrostatic pressure that deform the specimen to the strain level ε_1 , ε_2 and ε_3 in all direction. The stresses (red) or strain (blue) where no arrow is shown are zero. The volume ratio ratio can be expressed as

$$\lambda_1 = \lambda_2 = \lambda_3 = J^{1/3} \leq 1 \quad (14)$$

where σ_1 , σ_2 and σ_3 are hydrostatic pressure. The strain ε_1 , ε_2 , ε_3 describe that it is constrained in a very stiff fixture.

2.2.4 Incompressible Behavior.

Exact (or total) incompressibility literally means the material exhibits zero volumetric change (isochoric) under hydrostatic pressure. The pressure in the material is not related to the strain in the material; it is an indeterminate quantity as far as the stress-strain relationship is concerned. Poisson's ratio is exactly one-half, while the bulk modulus is infinite. Mathematically, the incompressibility of the material can be represented by $I_3 = 1$; $\lambda_1 \lambda_2 \lambda_3 = 1$, and $\det F = 1$, where F is the deformation gradient. Incompressibility was first considered in FEA by (Herrmann, 1965). Analytical difficulties arise when it is combined with nonlinearities such as large displacements, large strains, and contact. “Near incompressibility” means that Poisson's ratio (ν) is not exactly one-half; for example, 0.49. Perfect incompressibility is an idealization to make modeling more amenable for obtaining closed form solutions. In the real world, natural as well as filled rubbers are slightly compressible, thereby, facilitating development of algorithms with greater numerical stability. Special formulation for lower-order triangular and tetrahedral elements satisfying the LBB condition or simply the Babuska-Brezzi stability condition effectively handles analysis of incompressible materials (Liu et al., 1998).

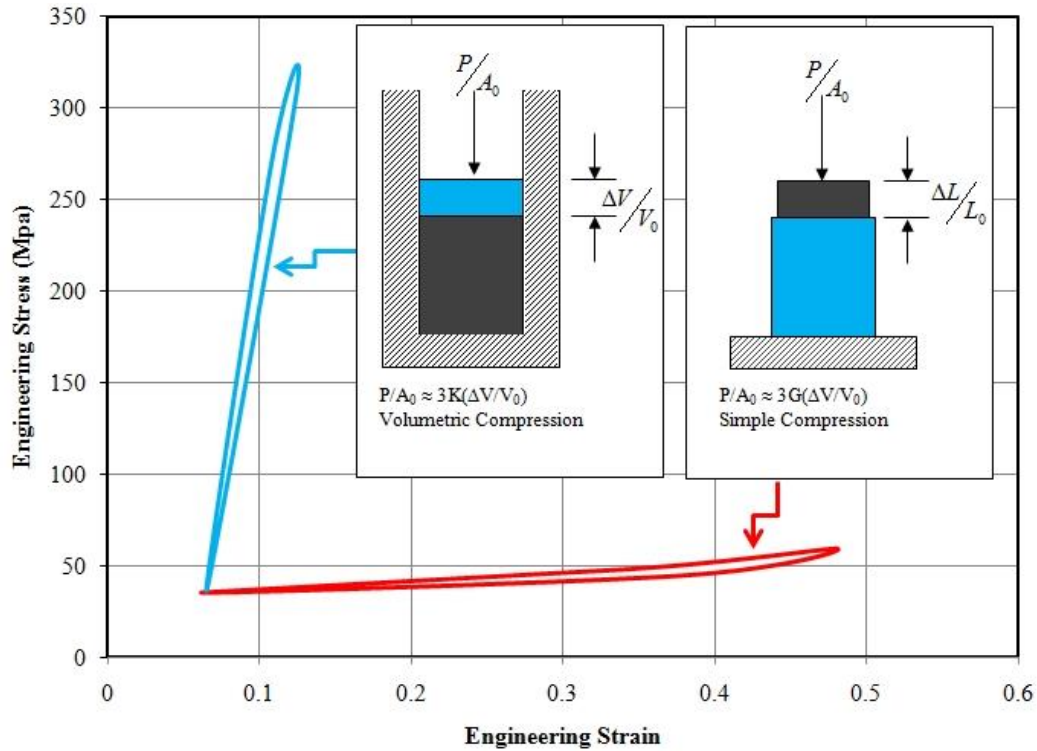


Figure 2.12 Incompressible behavior of rubber.

2.2.5 Hysteresis.

Under cyclic loading, rubber dissipates energy—due to hysteresis effects. The steady-state response is quite different from the initial response. Filled rubber experiences so-called stress-induced softening (sometimes referred to as damage), a phenomenon caused by a breakdown of crosslinks and a progressive detachment of rubber molecules from the surfaces of reinforcing fillers. This stress softening, which is known as the Mullins effect, occurs in the filled rubbers. This phenomenon probably reflects a breakdown of weak bonds between rubber molecules and filler particles, and at very small strains, between filler particles themselves incurred during previous loading (Ashkezari et al., 2008).

In a filled rubber with carbon black filler particles, the carbon black particles tend to form a loose reticulated structure because of their surface activity or mutual interactions. They are also interlaced by the network of rubber chain molecules which are crosslinked during vulcanization. The breakdown of these aggregates, and of the matrix/filler interfacial bonds due to loading, gives rise to hysteresis.

Although rubber will stiffen under load in certain situations, here we will only discuss the more common case of rubber softening.

Modification and reformation of rubber network structures in the initial loading stages can show a lower stiffness and changes in damping characteristics. This strain-induced stress softening in carbon black-filled rubbers is called the Mullins' effect although such a phenomenon has been observed in unfilled rubbers also. It manifests itself as history-dependent stiffness. The uniaxial stress-strain curve remains insensitive at strains above the previous achieved maximum, but experiences a substantial softening below this maximum strain. The larger the previously attained maximum, the larger the subsequent loss of stiffness.

In a cyclic test (as shown in Fig 1.3), the material is loaded in tension to a strain state labeled "1" along path "a". If the material is again loaded, the stress-strain curve now follows path "b" to point "1" and not path "a". If additional loading is applied, path "a" is followed to a point labeled "2". Upon unloading, path "c" is followed, thereby resulting in an even greater loss of stiffness in the material.

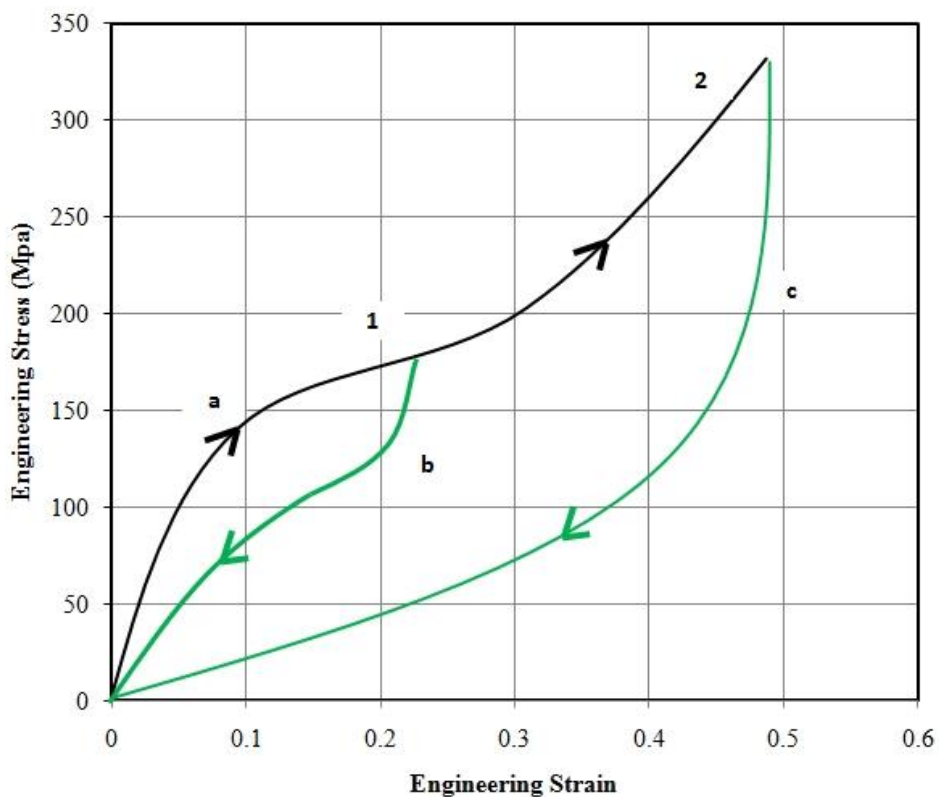


Figure 2.13 Cyclic tension demonstration Mullin's effect.

Features contributing to the stress-softening behavior include the modification and reformation of rubber network structures involve chemical effects, micro-structural damage, multi-chain damage, and micro-void formation. These mechanisms are considerably enhanced by strain amplification caused by rigid particles in filled rubbers.

2.2.6 Material Parameters from Test Data

Successful modeling and design of rubber components hinges on the selection of an appropriate strain energy function, and accurate determination of material constants in the function. For time-independent nonlinear elasticity, the fitting procedure may be carried out for polynomial representations of incompressible materials, the generalized Ogden model for slightly compressible materials, and the Foam model for compressible materials. Six different types of experiments are supported: uniaxial tension, uniaxial compression, equibiaxial, planar shear, simple shear, and volumetric tests. The significance of (non-equivalent) multiple tests for material modeling cannot be overemphasized. In general, a combination of uniaxial tension/compression and simple shear is required in the very least. Data from equibiaxial tension or planar shear may also be needed depending on the deformation modes of the structure. Volumetric data must be included for materials undergoing large compressible deformations, for example, foams.

After selecting appropriate test data for the application and adjusting the data to become comply with hyperelastic assumptions , typical behavior of many elastomeric materials have stress-strain curves as shown Fig 2.14. The importance of performing multiple mode tests is to assure that hyperelastic model predicts the correct behavior of other modes. The curve-fitting shows how other (non-measured) modes would behave. More sophisticated hyperelastic materials seeking more constants require more modes to be tested. From a mathematical point of view, determining the material constants for an incompressible material is relatively easy, since they follow from the least squares method in a straight forward fashion. However, the material constants may turn out to be negative and therefore physically not meaningful.

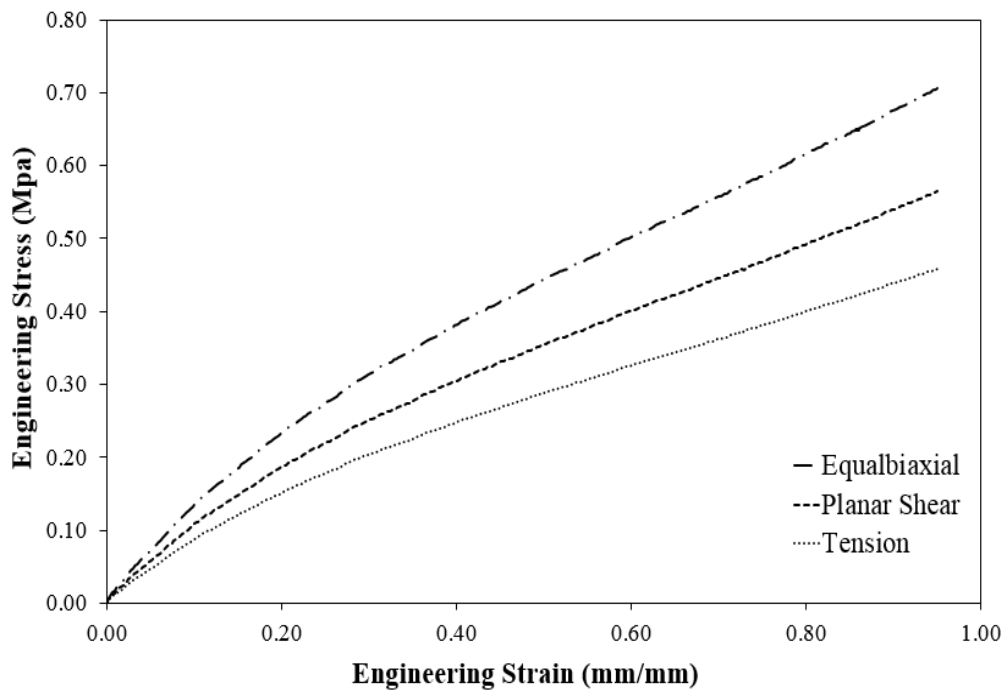


Figure 2.14 Selecting test data required for finite element program.

The phenomenon is a numerical serendipity and not a fundamental material behavior. In this case, a constrained optimization process can be invoked, based on sequential linear programming.

The stress strain response of a typical test are shown at the right as taken from the laboratory equipment. In its raw form, the data is not ready for fitting to a hyperelastic material model. It needs to be adjusted. The raw data is adjusted as shown by isolating a stable upload cycle. In doing this hysteresis is ignored. This cycle needs to be shifted such that the curve passes through the origin. Remember hyperelastic models must be elastic and have their stress vanish to zero when the strain is zero. This shift changes the apparent gauge length and original cross sectional area.

There is nothing special about using the upload curve, the entire stable hysteresis cycle can be entered for the curve fit once shifted to zero stress for zero strain. Fitting a single cycle gives an average single equilibrium curve to represent the hysteresis of that cycle. Also one may enter more data points in important strain regions than other regions. The curve fit will give a closer fit where there are more points. Many elastomeric materials have this basic shape of the three modes,

with uniaxial, planar shear and biaxial having increasing stress for the same strain, respectively.

2.2.7 Physical Measurements.

Basic physical measurements (as shown in Fig 2.15- Fig 2.18) discussed here are limited to force, length, temperature and time. Force is usually measured by a load cell. The load cell actually measures changes in resistance of strain gages placed in a bridge on a metal shape that deforms slightly as the specimen is loaded. The change of resistance is calibrated to report force. The load cell can be seen at the top of the specimen in the right top figure. The output from the load cell enters the data acquisition system in the computer along with the initial specimen area. The recorded force is divided by the initial specimen area automatically by the data acquisition system. Length or position is best measured by a non-contacting device such as a video extensometer as shown in the middle right figure. The video extensometer senses differences in color between two marks on the specimen. The length between these two marks is continuously recorded by the data acquisition system. Another non-contacting technique is the use of a laser extensometer. The laser sends out a planar light which is reflected back from reflector tags attached to the specimen as shown in the bottom right figure. At the start of the test, the initial gage length is entered into the data acquisition system, and as the test progresses the change in gage length is recorded by the data acquisition system. Time is recorded by the data acquisition system that synchronizes the force and length measurements. The data recorded can be output in ascii files that contain the stress, strain and time that are later used for the hyperelastic material model fitting. In the following tests, the material, temperature, strain range, strain rates, and preconditioning should be determined by the application to be modeled.



Figure 2.15 Laser extensometer with tags on tension specimen.

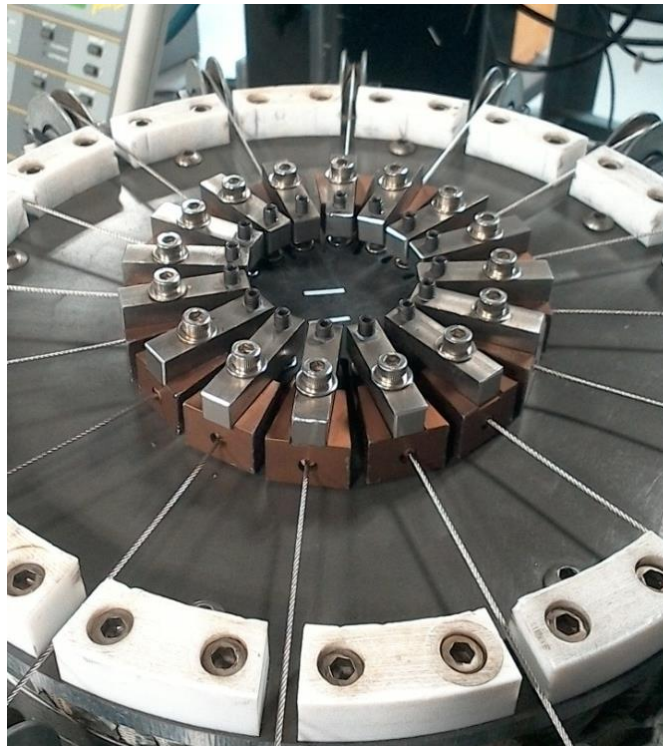


Figure 2.16 Laser extensometer with tags on biaxial specimen.

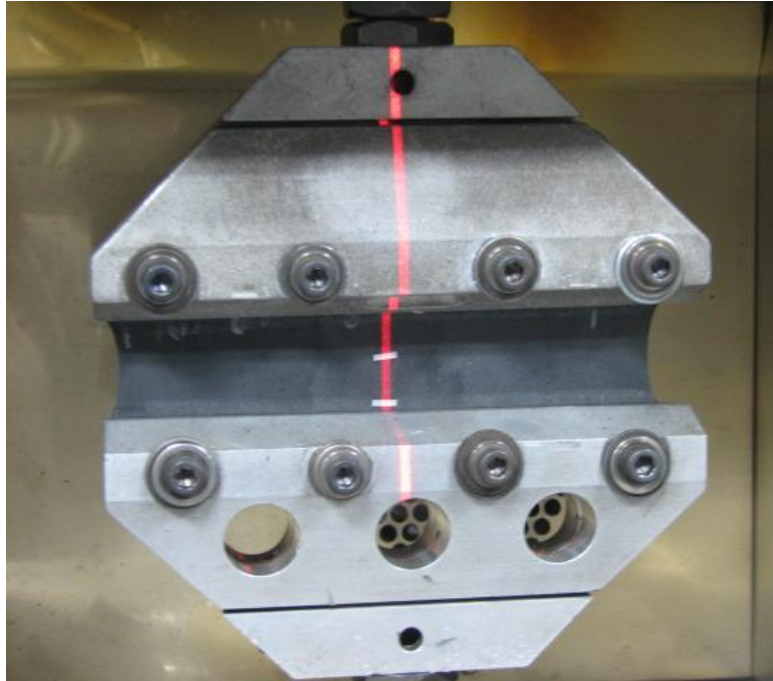


Figure 2.17 Laser Extensometer with tags on planar shear specimen.



Figure 2.18 Laser extensometer with tags on volumetric specimen.

2.3. Base Isolation System

2.3.1 The Basic Principle of Base Isolation

The basic principle of base isolation is to lengthen the period of the superstructure to be longer than previous state (fixed based). It means that it is possible to reduce the acceleration of the building by increasing the building's period and decoupling the movement of the structure with ground acceleration without transmitting these force into the building. In an ideal system this separation would be total but in the reality it should be some device between the structure and the ground.

Since the building with perfectly rigid (see Figure 2.19a) , the structure and ground move the same amount, both displacement and period of structure will be zero due to the acceleration induced in the building is equal to the ground acceleration. If the building with perfectly flexible (see Figure 2.19b), the acceleration induced the structure will be zero and relative the displacement between structure and ground is equal to the ground displacement. The structure will not move but the ground will.

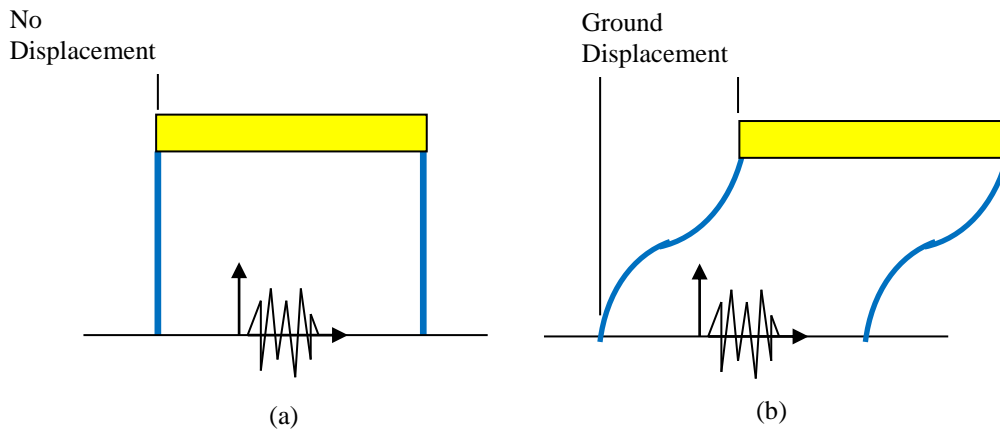


Figure 2.19 Transmission of ground motions; (a). Rigid structure, (b). Flexible structure.

In the fact, no structure which is perfectly rigid and perfectly flexible. The real state of the structure is between these two extremes conditions, as shown in Figure 2.20. The Period of the structure between zero (rigid) and infinity (flexible), the maximum accelerations and displacement relative to the ground are

a function of the earthquake. The flexibility of the structure will significantly increase the period and the displacement of the building and thus reduce base shear (see Figure 2.21). The relative displacement will generally not exceed the peak ground displacement, that is the finite period displacement. The exception of this case, particularly for soft soil, (as shown in Figure 2.22)and site which are near by the fault generating the earthquake.

2.3.2 The Characteristic of Base Isolation

The general feature of base isolation is large ratio between the vertical stiffness relative to the horizontal stiffness. The stiffness is obtained by using plate, which is normally used thin steel plate as reinforcement. The steel reinforcement prevents lateral bulging of the rubber but it still allows the rubber move horizontal freely. The vertical stiffness are able to be a hundred times of the horizontal stiffness. The using of steel reinforcement makes isolator stable under vertical load.

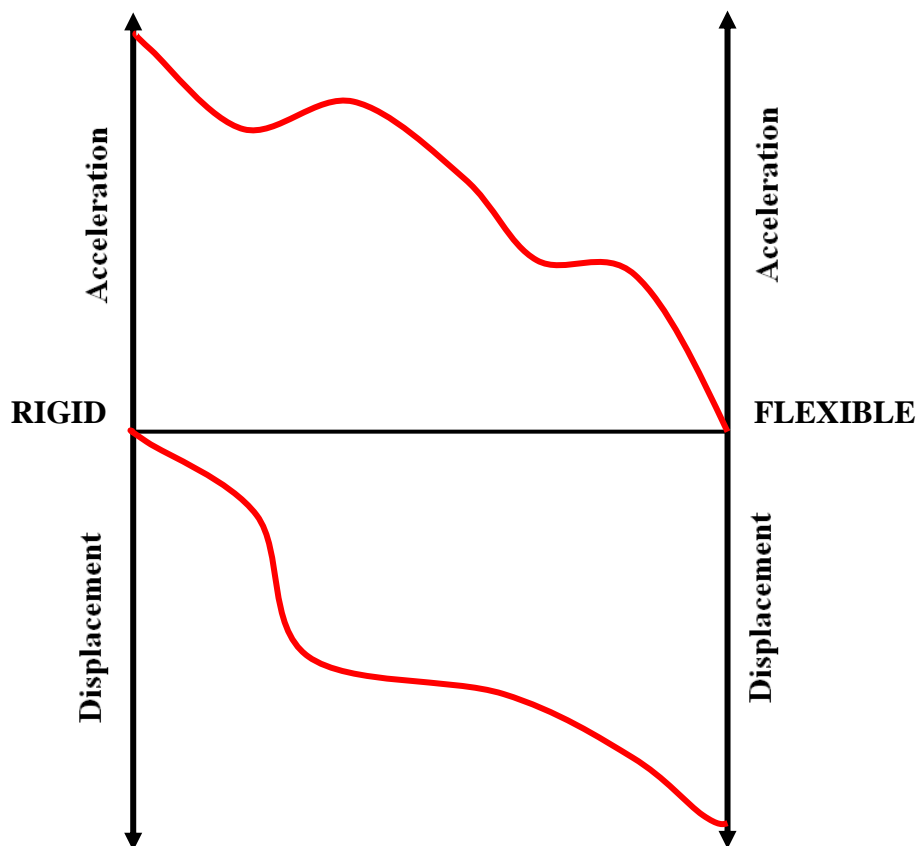


Figure 2.20 The ideal conditions of the structure acceleration and displacement.

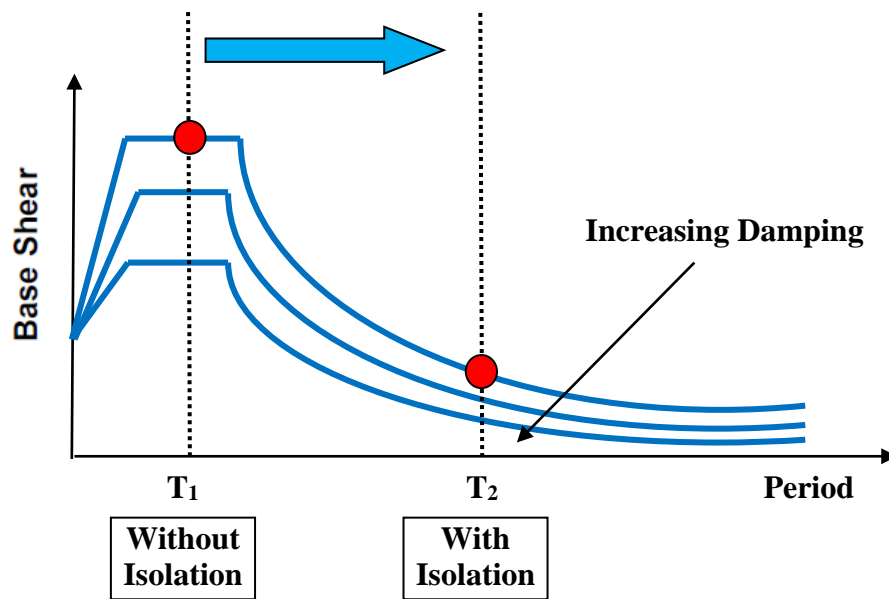


Figure 2.21 Effect of seismic isolation
(Acceleration Response Spectrum Perspective)

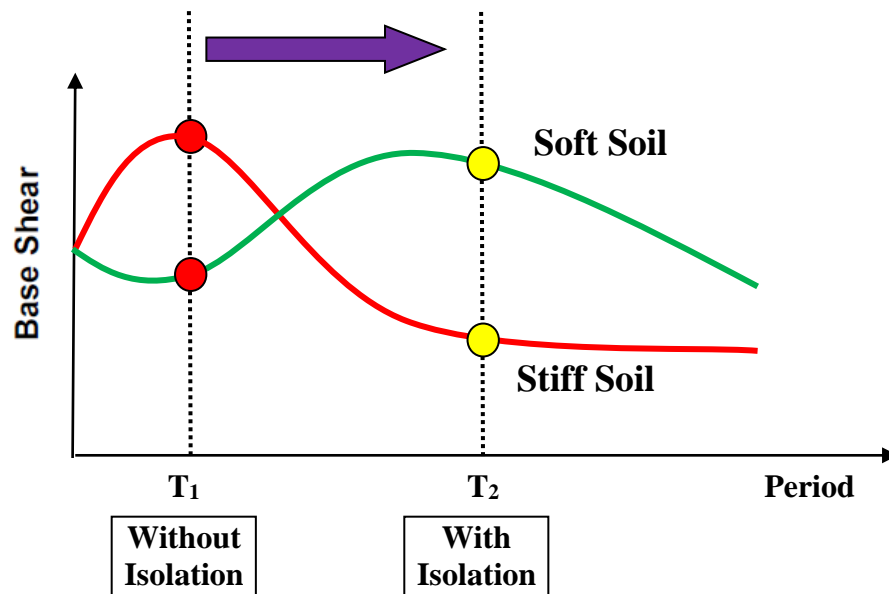


Figure 2.22 Effect of soil conditions on isolated structure response.

The general formulation of the vertical stiffness of rubber bearing is as follows :

$$K_v = \frac{E_c A}{t_r} \quad (15)$$

where A is loaded area of rubber bearing, t_r is the total thickness of the rubber bearing, E_c is compression modulus of rubber - steel composite under the vertical load. The value of E_c for single rubber layer is controlled by shape factor S. For single pad in circular form, the compression modulus E_c is given by (Naeim and Kell, 1999):

$$E_c = 6GS^2 \quad (16)$$

where S may be written as (for circular pad, radius R and thickness t) :

$$S = \frac{R}{2t} \quad (17)$$

The vertical frequency of isolation system, which is often to be crucial considering in a project, is the important design quantity for vibration of an isolator or a structure. The vertical frequency is controlled by vertical stiffness of bearing comprising the system. In order to define the vertical frequency, the engineer simply need considering the vertical stiffness of bearing due to dead load and linier analysis is adequate for analysis process.

Besides the vertical stiffness, the most important characteristic of base isolation is, of course, its horizontal stiffness; this given by :

$$K_H = \frac{GA}{t_r} \quad (18)$$

where G is the shear modulus of rubber bearing, A is the full cross-section area and t_r is the total thickness of the rubber.

2.3.3 The Base Isolation System with Rigid Reinforcement.

2.3.3.1 The Behavior of Isolator under Compression.

In order to measure approximate value of the vertical stiffness and bending rigidity , a linier elastic theory is the most common solution to solve this problem. There are two assumptions to illustrate this case by kinematic theory related to the deformation and the stress state, as follows :

(i). points on a vertical line before deformation lie on a parabola after loading.

(ii). horizontal planes remain horizontal.

The equilibrium solution by kinematic for arbitrary shape of thickness t and locate in middle surface of pad (see Figure 2.23 a & b) in coordinate system (x,y,z) , shows that the displacement (u,v,w) in the coordinate direction under compression are :

$$u(x, y, z) = u_0(x, y) \left(1 - \frac{4z^2}{t^2} \right) \quad (19)$$

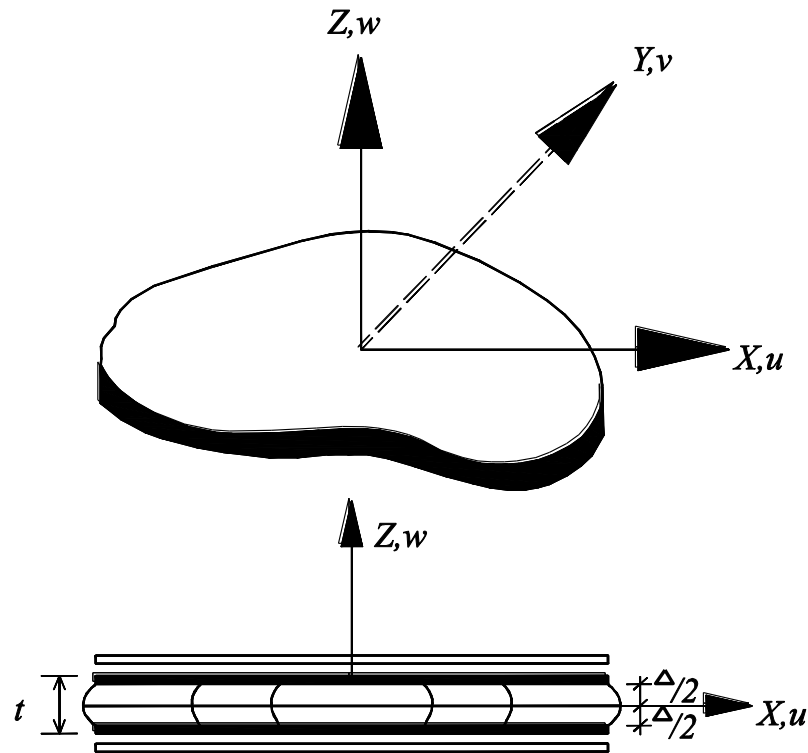


Figure. 2.23 (a) Cartesian coordinate system on an arbitry shaped pad;

(b) displacement fields of an arbitrary shaped pad.

$$v(x, y, z) = v_0(x, y) \left(1 - \frac{4z^2}{t^2} \right) \quad (20)$$

$$w(x, y, z) = w(z) \quad (21)$$

The displacement of the solution above, satisfy the requirement the rigid substrates condition that is assumed on the top and bottom surfaces of the pad. Under incompressibility assumption, it is derived three component of strain in $\varepsilon_{xx} = \partial u / \partial x, \varepsilon_{yy} = \partial v / \partial y, \varepsilon_{zz} = \partial w / \partial z$ the form :

$$\varepsilon_{xx} + \varepsilon_{yy} + \varepsilon_{zz} = 0 \quad (22)$$

The stress is assumed dominated by internal pressure P , for instance the normal stress component $\sigma_{xx}, \sigma_{yy}, \sigma_{zz}$, differ from $-p$ only by term of order $(t^2/l^2)p$ P (where L is length of x-y plane section)

$$\sigma_{xx} \approx \sigma_{yy} \approx \sigma_{zz} \approx -p \left(1 + O\left(\frac{t^2}{l^2}\right) \right) \quad (23)$$

The complete solutions of equilibrium for stresses are

$$\begin{aligned} \frac{\partial \sigma_{xx}}{\partial x} + \frac{\partial \tau_{xy}}{\partial y} + \frac{\partial \tau_{xz}}{\partial z} &= 0 \\ \frac{\partial \tau_{xy}}{\partial x} + \frac{\partial \sigma_{yy}}{\partial y} + \frac{\partial \tau_{yz}}{\partial z} &= 0 \\ \frac{\partial \tau_{xz}}{\partial x} + \frac{\partial \tau_{yz}}{\partial y} + \frac{\partial \sigma_{zz}}{\partial z} &= 0 \end{aligned} \quad (24)$$

by assumption

$$\begin{aligned}\tau_{xx,x} + \tau_{xz,z} &= 0 \\ \tau_{yy,y} + \tau_{yz,z} &= 0\end{aligned}\tag{25}$$

For circular pad with diameter, R (see Fig 2.24), the equation P becomes

$$\nabla^2 p = \frac{d^2 p}{dr^2} + \frac{1}{r} \frac{dp}{dr} = -\frac{12G\varepsilon_c}{t^2}, r = \sqrt{x^2 + y^2}\tag{26}$$

general solution for the equation is

$$p = A \ln r + B - \frac{3G\varepsilon_c}{t^2} r^2\tag{27}$$

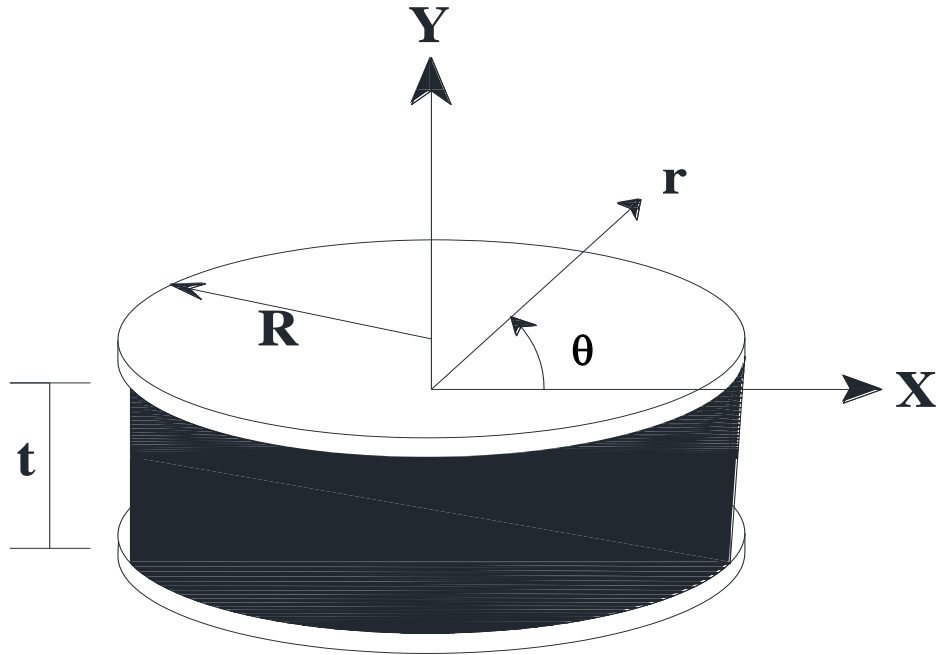


Figure 2.24 Coordinate system for a circular pad of radius R .

and due to P restricted on $r = R$, and $p = 0$ at $r = R$, the complete solution becomes

$$p = \frac{3G\varepsilon_c}{t^2} (R^2 - r^2) \quad (28)$$

and

$$p = 2\pi \int_0^R p(r) r dr = \frac{3G\varepsilon_c \pi R^4}{2t^2} \quad (29)$$

In order to illustrate the maximum of the stresses value in term of the average pressure over the plate, p_{ave} , is written as

$$p_{ave} = E_c \varepsilon_c = 6GS\varepsilon_c \quad (30)$$

Therefore

$$\frac{\sigma_{max}}{p_{ave}} = \frac{\frac{6G}{t} \frac{3+v}{8} R^2 \varepsilon_c}{6GS^2 \varepsilon_c} = \frac{3+v}{2} \frac{t}{t_f} \quad (31)$$

which can be used to define the maximum pressure needed due to yield in the shim at the center. It shows, under nominal circumstances, consideration of the stress in the shims cause of the pressure is not considered important.

2.3.3.2 The Behavior of Isolator under Bending.

The bending stiffness is one of the important property bearing that must be investigate regarding the buckling behavior of isolator. The bending stiffness is calculated using similar approximate solution such as compression stiffness. The configuration of displacement is derived in two process. In order to illustrate the deformation that occur related to the beam theory, as shown in Fig 2.25.

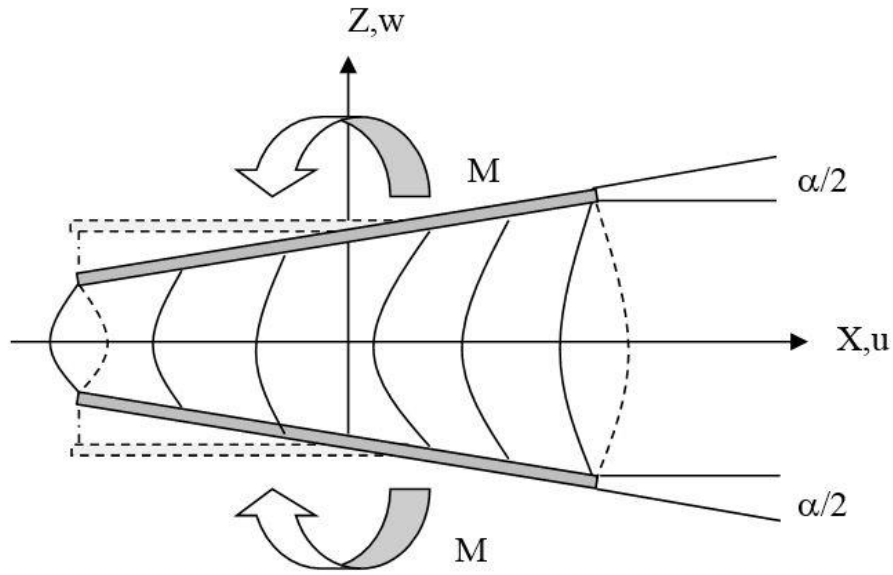


Figure 2.25 Rubber pad between rigid plates in pure bending.

The shear strain caused of the bending moment are the important quantity for designing process and they also effect the stresses can be compressive and could produce buckling of the shims.

$$u(x, y, z) = u_0(x, y) \left(1 - \frac{4z^2}{t^2} \right) - \frac{\alpha Z^2}{2t} \quad (32)$$

$$v(x, y, z) = v_0(x, y) \left(1 - \frac{4z^2}{t^2} \right) \quad (33)$$

$$w(x, y, z) = \frac{\alpha Z X}{t} \quad (34)$$

The angle between the plate (see Fig 2.30) within deformation condition is denoted by symbol (α) and the bending is about the y-axis. The radius of curvature, derived by the deformation is associated to α by

$$\frac{1}{\ell} = \frac{\alpha}{t} \quad (35)$$

The equilibrium solution is to solve for P and to calculate the bending moment (M) from

$$M = -\int_A p(x, y)xdA \quad (36)$$

Using the analogy with beam theory, where

$$M = EI \frac{1}{\ell} \quad (37)$$

The solution for the bending stiffness is written by

$$(EI)_{eff} = \frac{M}{\alpha/t} \quad (38)$$

2.3.4 The Buckling Behavior of Isolator.

The base isolation is susceptible undergoing buckling similar behavior with column, dominated by shear-low stiffness of bearing. According to the previous analysis, the deformation of single pad is able to use for buckling analysis considering bearing as composite system. This analysis treats the bearing as a beam and the deformation is assumed to be such that plane sections normal to the undeformed central axis remain plane, but not necessarily normal to the deformed axis. The deformation (see Fig 2.26), is derived by two feature : $v(x)$ is the displacement of the middle surface of the bearing, and $\psi(x)$ is the rotation of a face originally normal to the undeformed axis.

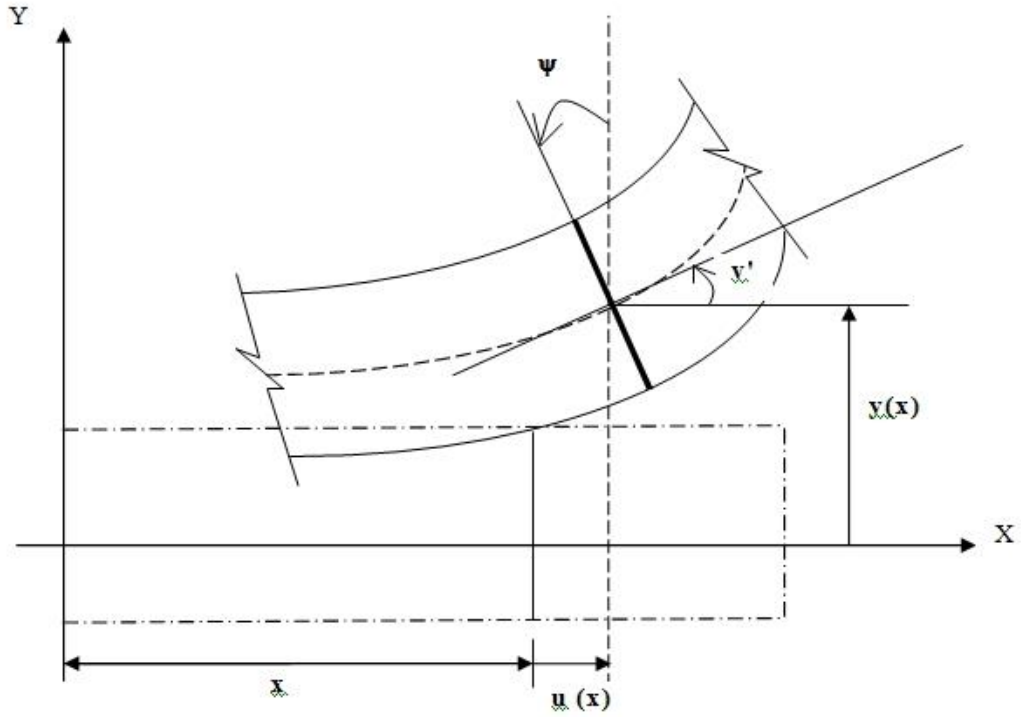


Figure 2.26 Deformation pattern for a bearing.

Figure 2.27 shows the internal and external forces on the bearing in the deformed state. The shear force, V , and the axial force, N , are shown parallel and perpendicular, respectively, to the rotated face. The end loads, including the axial load, P , are defined by a lateral reaction, H_0 , and bending moment, M_0 , which may be specified or unknown, depending on the problem M . The internal shear force, V , is associated to the shear deformation as follows

$$V = GA_s (v' - \psi) \quad (39)$$

where A_s is not cross area such as full cross area A , but $A (h/t_r)$, h is total height of isolator and t_r is total thickness of rubber. The increasing of A is necessary to obtain the fact that the steel plate does not deform in the composite system. The solutions related to bending moment and shear force are (see Fig 2.32) are given by

$$M + P(v - v_0) - M_0 - H_0 x = 0 \quad (40)$$

$$V + H_0 - P\psi = 0 \quad (43)$$

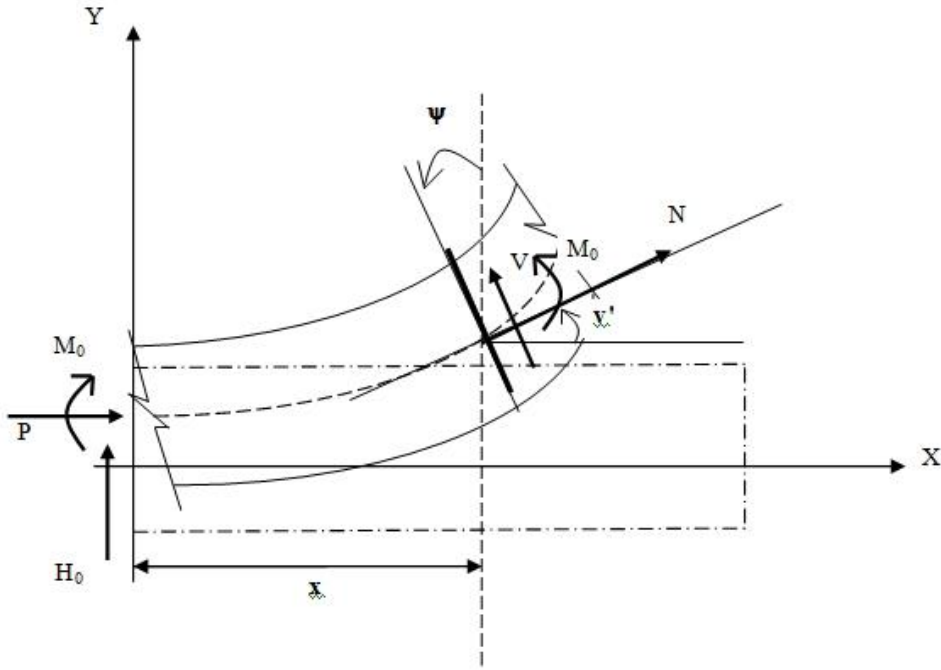


Figure 2.27 Internal forces and external loads on a deformed bearing.

Shown in Fig 2.28. The bearing is restricted against the displacement at the bottom and restricted to rotation at the top and the bottom moving horizontal freely on the top level. The arrangement of the bearing, $x = 0$ at the bottom and $x = h$ at the top level, results as follows :

$$\psi(0) = \alpha\beta B = 0 \quad (41)$$

$$\psi(h) = -\alpha\beta A \sin(\alpha h) = 0 \quad (42)$$

therefore , $\alpha h = \pi$, and general solution become

$$v(x) = \frac{1}{2} \delta \left(1 - \cos\left(\frac{\pi x}{h}\right) \right) \quad (43)$$

$$\psi(x) = \frac{1}{2} \alpha \beta \delta \sin\left(\frac{\pi x}{h}\right) \quad (44)$$

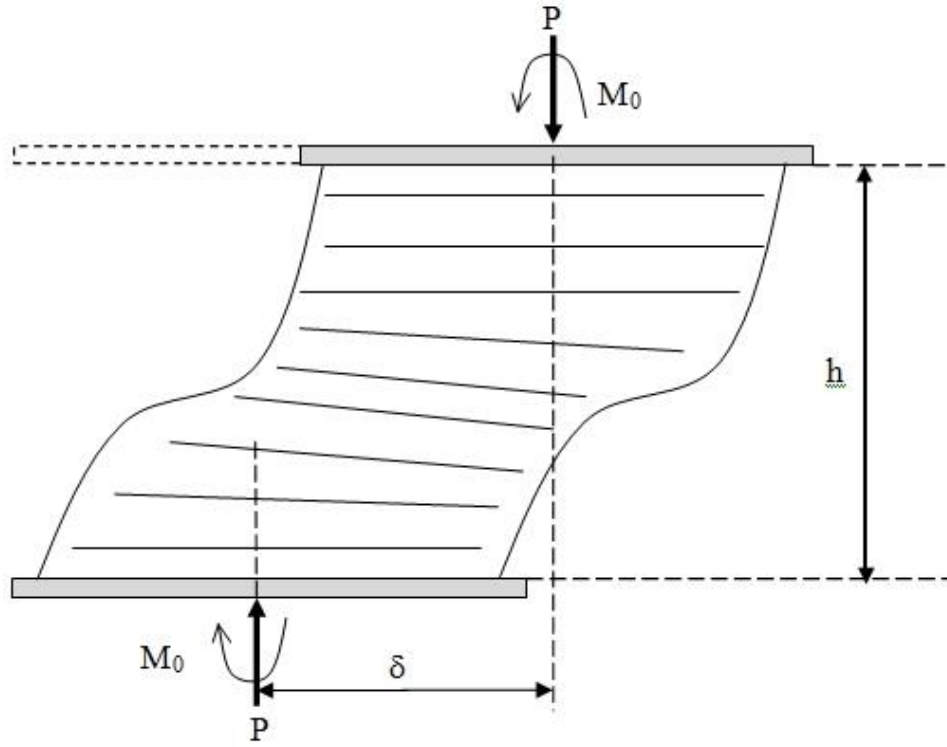


Figure 2.28 Boundary conditions for an isolation bearing under a vertical load.

and $M_0 = P\delta/2$ where $\delta = v(h)$

which the critical load, P_{crit} , is given by

$$P_{crit} = \frac{-P_s + \sqrt{P_s^2 + 4P_s P_E}}{2} \quad (45)$$

if it considers that $P_s \approx GA$

$$P_E = \frac{\pi}{h^2} \frac{1}{3} 6GS^2 I \approx GA \left(\frac{2\pi^2 S^2 I}{Ah^2} \right) \quad (46)$$

the critical load can be approximated by

$$P_{crit} = \sqrt{P_s P_E} \quad (47)$$

using this expression and recalling that

$$P_s = GA \frac{h}{t_r} \quad (48)$$

$$P_E = \frac{\pi^2}{h^2} \frac{1}{3} E_c I \frac{h}{t_r} \quad (49)$$

we have

$$P_{crit} = \sqrt{\left(GA \frac{h}{t_r} \right) \left(\frac{\pi^2}{h^2} \frac{1}{3} E_c I \frac{h}{t_r} \right)} = \frac{\sqrt{2\pi G A S_r}}{t_r} \quad (50)$$

2.4 Perforated Plate

Strength of Perforated Metal

Perforated metallic materials have a big potential to be used in construction. Stiffness, strength and elastic/plastic properties of perforated metallic materials open up good opportunities for their wide range of use in the building industry. For example they could be used as spacers for wall and floor constructions, reinforcement materials, fixtures and connectors for nodes of wooden constructions, etc.

Because of high strength, light weight, good painting abilities and easy installation, perforated materials are becoming widely used in the design of building facades. The main materials for producing perforated construction elements are the steel, aluminium and copper. Steel perforated materials have better perspectives for use as a material for cellular building structures and constructions due to their lower cost and higher strength. The weight of perforated aluminium products will be lower, but at the same time, the final products from perforated aluminium will have worse tensile strength properties compared to other materials. Harder workable materials due to their mechanical properties are

steel and different copper alloys. However, the strength of constructions is much better (Lisicins et al., 2015).

Round holes arranged in a standard 60° triangular pattern ranging from .020" to 3/4" account for more than half of the perforating industry's production. In perforating this pattern, the direction of the stagger is the short dimension or width of the sheet as illustrated. The straight row of closely-spaced holes is parallel to the long dimension or length of the sheet. This is the so-called "closed pattern." Under special order, the holes may be punched in the "open pattern." The directional properties are then reversed from those described herein (Fig 2.29).

The standard 60° staggered formation is the most popular hole arrangement because of its inherent strength and the wide range of open areas it provides. Formulas for determining percentage open area (see Fig.2.30) is given by :

$$\frac{D^2 \times 90,69}{C^2} = \% \quad (51)$$

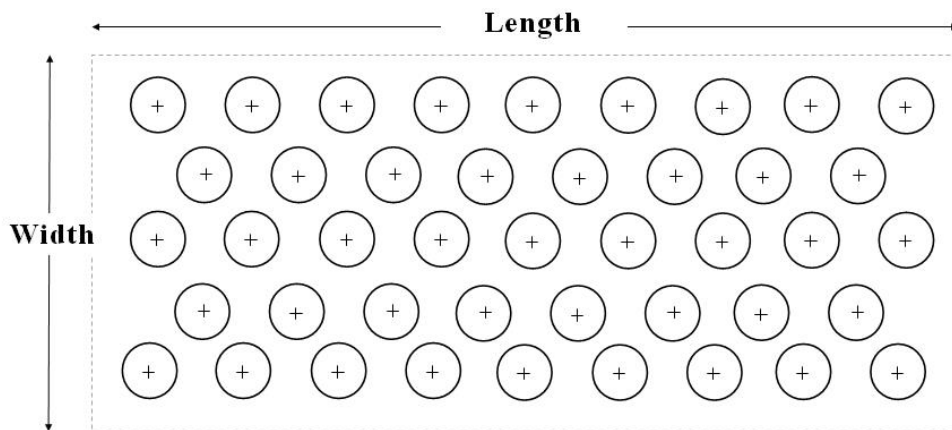


Figure 2.29 Length and width direction of perforated plate sheet.

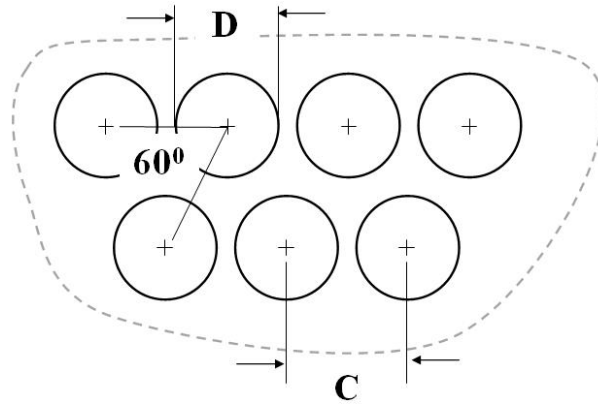


Figure 2.30. Formulations percentage open area with 60° staggered formation.

The concept of equivalent solid material is widely used for design analyses of perforated materials. As applied herein, the equivalent strength of the perforated material is used in place of the strength of the solid material (IPA, 1993). By evaluating the effect of the perforations on the yield strength of the material, the equivalent yield strength of the perforated material, (S^*), can be obtained as a function of the yield strength of the solid or unperforated material, S . Thus, the designer is able to determine safety margins for the perforated material for any geometry of application and any loading conditions. The S^*/S ratios are the same for bending and stretching of the material. Having the S^*/S ratios for the particular penetration pattern of interest, it is therefore easy for the designer to determine what thickness of perforated material will provide strength equal to that of the unperforated material. Perforated material has different strengths depending on the direction of loading. Values of S^*/S are given for the width (strongest) and the length (weakest) directions. The values for the length direction have been calculated conservatively as shown in Fig 2.31.

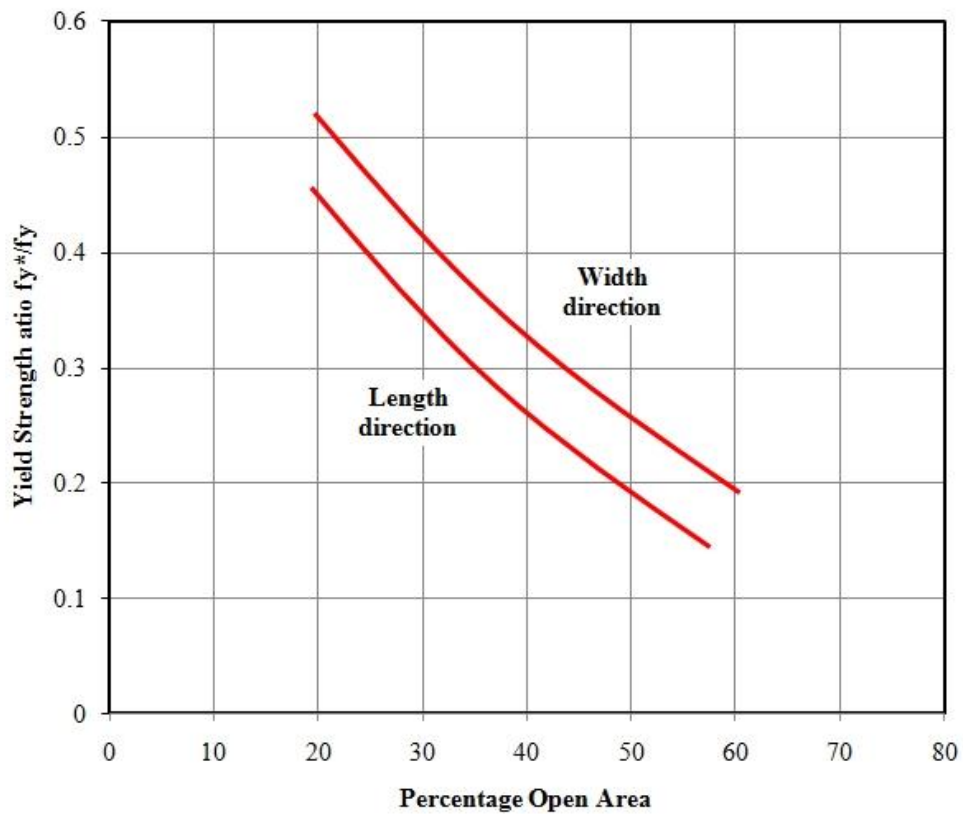


Figure 2.31 Yield strength ratio depending on percentage open area.

Elastic Properties of Perforated Metals (Stiffness).

There are many potential new applications where perforated materials could be used. In many of these uses, however, the strength and stiffness properties of the perforated sheet are very important. The following information covers the stiffness properties for the standard 60° triangular penetration pattern. Since perforated materials can potentially be used in so many applications involving different geometries, materials and loading conditions, design data are given in a very general form. The ratio of the effective elastic modulus of the perforated material, E^* , to the elastic modulus of the unperforated material, E , and the effective Poisson's ratio, $(\nu)^*$, are given material (IPA, 1993). These values are given for all the Standard IPA numbered perforations which cover round holes arranged in the standard 60° triangular pattern ranging from 0.020" to 1", and account for more than half of the perforating industry's production.

The concept of equivalent solid material is widely used for design analyses of perforated materials. As applied herein, the equivalent stiffness of the

perforated material is used in place of the stiffness of the solid material. By evaluating the effect of the perforations, the equivalent effective elastic modulus of the perforated material, E^* , is obtained as a function of the elastic modulus of the solid or unperforated material, E . In addition, the effective Poisson's ratio, $(\nu)^*$, of the perforated material is obtained (Fig. 2.32). This Poisson's Ratio may be used in cases where correction for load biaxiality is important.

The effective elastic constants presented herein are for plane stress conditions and apply to the in-plane loading of the thin perforated sheets of interest. The bending stiffness of such perforated sheets is somewhat greater. However, most loading conditions involve a combination of bending and stretching, and it is more convenient to use the same effective elastic constants for the combined loading conditions. The plane stress effective elastic constants given herein can be conservatively used for all loading conditions. Using these effective elastic properties, the designer is able to determine the deflections of the perforated sheet for any geometry of application and any loading conditions using available elastic solutions. It is therefore easy for the designer to determine what additional thickness of the perforated material will provide stiffness equal to that of unperforated material

Mechanical properties of different types of metallic materials (tapes, plates) changes during punching. Relationships shown, characterise the yield strength ratio and effective elastic properties depending on the percentage of perforation .. It is evident that the perforation reduces the yield strength ratio and effective elastic properties. The modulus of elasticity and Poisson's ratio (ν) of metallic material shows ultrarapid changes. Main methods for manufacturing of different types of cellular building constructions from perforated metallic materials are stretching, corrugation, plate shearing, cut-sheet and stretching, perforated tape twisting, method of interlacement, profiling and welding (Bogojavenskij et al., 1978; Wadley et al., 2003). The right choice of method is directly affected by the properties of raw and perforated materials.

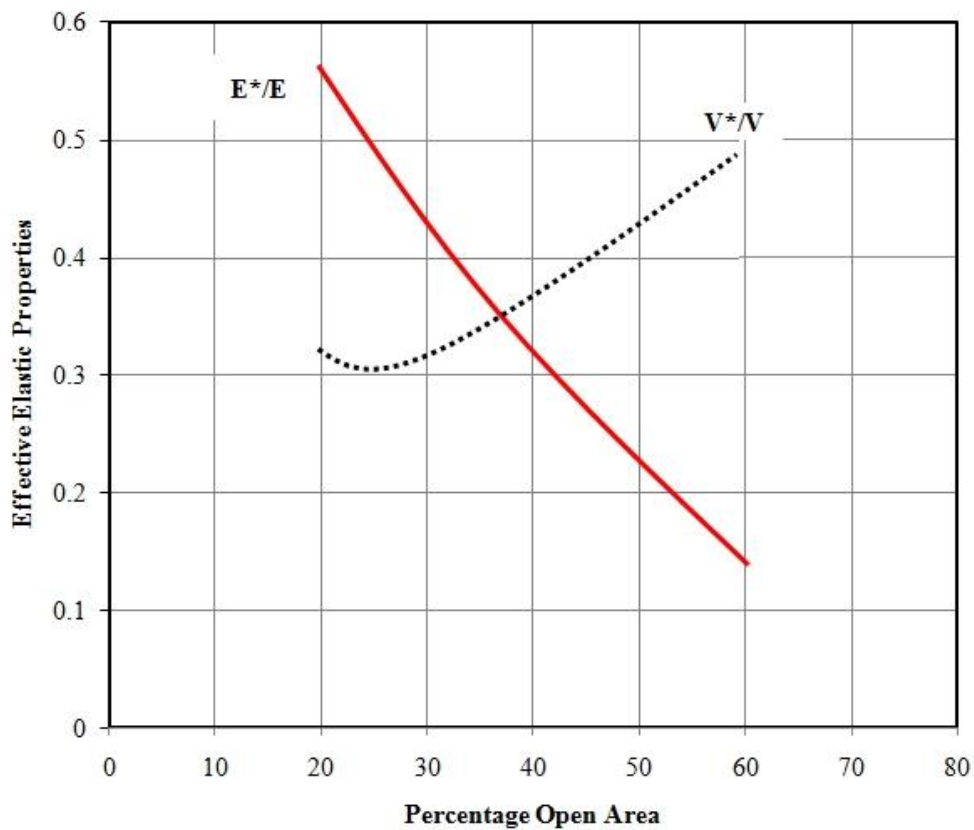


Figure 2.32 Effective elastic properties depending on percentage open area.

For example, the method of stretching requires a slightly high strength of glued locations of connected plates (enough to allow the stretching of the structure) which in the case of a thin cell wall is usually provided with modern adhesive polymers. The value of force necessary for stretching the cells steadily approaches the strength of adhesion between the plates, when the ratio of the cell wall's thickness against the cell size increases. In this case, for the production of a honeycomb structure with a higher relative density, another method of manufacturing (corrugation) or method of joining the elements (welding, soldering) is necessary.

2.5 Isolated Structure.

2.5.1 Behavior of Isolated Structure.

Numerous studies and applications in the field of seismic base isolation have demonstrated that this alternative seismic protection system is extremely effective for minimizing the damage of certain building types during seismic

action. Research on the development of natural rubber bearings for isolating buildings from earthquakes began in 1976 at the Earthquake Engineering Research Center (EERC) of the University of California at Berkeley and an approximate linear theory of isolation which can be used for the design of base isolation systems that use multilayer elastomeric isolators was proposed by Kelly (Kelly, 1998; Kelly, 1990; Konstantinidis et al., 2008). The implementation of rubber bearing and damper has provided a promising alternative for building construction in seismic areas, even for ordinary multi-storey buildings, such as offices, residential houses, and industrial buildings (Kilar and Koren, 2009). The construction of ordinary (apartment) buildings and critical facilities using seismic isolation costs 30-35% cheaper in comparison with the conventionally designed buildings (Melkumyan, 2008). The isolation reduces the fundamental frequency of the structure from its fixed base frequency and thus shifts the position of the structure in the spectrum from the peak-plateau region to lower regions. Also, it brings additional damping due to the increased damping introduced at the base level and thus further reduction in the spectral acceleration is achieved (Santhosh et al., 2013).

The implementation of the base isolators with high-damping natural rubber in developing countries has been initialized in Indonesia (Taniwangsa and Kelly, 1996). An extensive experimental program using samples of full-size bearings of a building in Indonesia was carried out to evaluate the dynamic properties of the low-cost natural rubber isolators with low shear modulus. Demonstrative buildings in Italy, Chile, China, and Indonesia have been constructed for implementing the base isolation technique to low-cost housing and studying its dynamic behavior (Taniwangsa, 1996).

The idealized mathematical model of the N-story base-isolated building considered are shown in Fig 2.33. The base-isolated building is modeled as a shear type structure mounted on isolation systems with one lateral degree-of-freedom at each floor.

Following assumptions are made for the structural system under consideration (Matsagar et al., 2004):

1. The superstructure is considered to remain within the elastic limit during the earthquake excitation. This is a reasonable assumption as the isolation attempts to reduce the earthquake response in such a way that the structure remains within the elastic range.
2. The floors are assumed rigid in its own plane and the mass is supposed to be lumped at each floor level.
3. The columns are inextensible and weightless providing the lateral stiffness.
4. The system is subjected to single horizontal component of the earthquake ground motion.
5. The effects of soil–structure interaction are not taken into consideration.

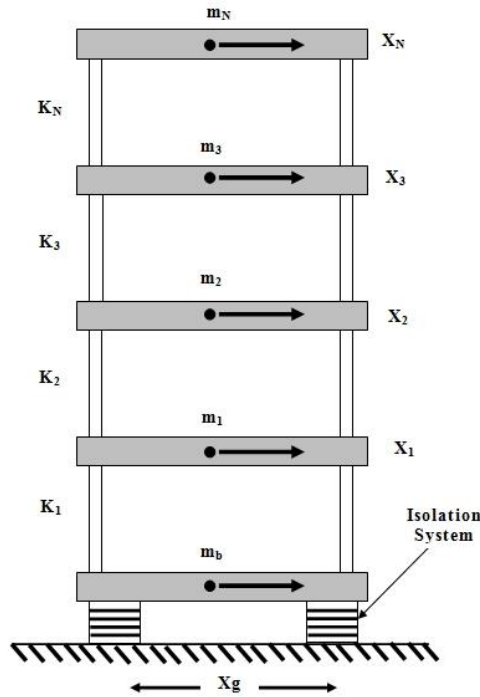


Figure 2.33 Mathematical model of N-story base-isolated structure.

For the system under consideration, the governing equations of motion are obtained by considering the equilibrium of forces at the location of each degrees of- freedom. The equations of motion for the superstructure under earthquake ground acceleration are expressed in the matrix form as

$$[M_s]\{\ddot{X}_s\} + [C_s]\{\dot{X}_s\} + [K_s]\{X_s\} = -[M_s]\{r\}(\ddot{X}_b + \ddot{X}_g) \quad (52)$$

where $[M_s]$, and $[C_s]$, $[K_s]$ are the mass, damping and stiffness matrices of the superstructure, respectively; $\{X_s\}$, $\{\dot{X}_s\}$ and $\{\ddot{X}_s\}$ are the unknown relative floor displacement, velocity and acceleration vectors, respectively; and \ddot{X}_b and \ddot{X}_g the relative acceleration of base mass and earthquake ground acceleration, respectively; and $\{r\}$ is the vector of influence coefficients.

The corresponding equation of motion for the base mass under earthquake ground acceleration is expressed by

$$m_b \ddot{x}_b + F_b - k_1 x_1 - c_1 \dot{x}_1 = -m_b \ddot{x}_g \quad (53)$$

where m_b and F_b are the base mass and restoring force developed in the base isolation system, respectively; k_1 is the story stiffness of first floor; and c_1 is the first story damping. The restoring force developed in the base isolation system, F_b depends upon the type of isolation system considered and approximate numerical models shall be used.

2.5.2 Mathematical Modeling of Isolators.

The force-deformation behavior of the isolator is modeled as (i) non-linear hysteretic represented by the bi-linear model and (ii) the code specified equivalent linear elastic-viscous damping model for the non-linear systems. A comparison of the response of the isolated structure by using the above two models will be useful in establishing the validity of the code specified equivalent linear model.

2.5.2.1 Bi-linear hysteretic model of isolator.

The non-linear force-deformation behavior of the isolation system is modeled through the bi-linear hysteresis loop characterized by three parameters namely: (i) characteristic strength, Q (ii) post-yield stiffness, k_b and (iii) yield displacement, q as shown in Fig 2.34.

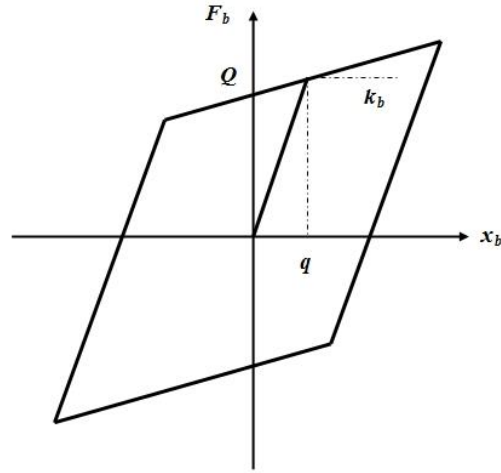


Figure 2.34 Bi-linear hysteresis model of isolator.

The bi-linear behavior is selected because this model can be used for all isolation systems used in practice. The characteristic strength, Q is related to the yield strength of the lead core in the elastomeric bearings and friction coefficient of the sliding type isolation systems. The post-yield stiffness of the isolation system, k_b is generally designed in such a way to provide the specific value of the isolation period, T_b expressed as

$$T_b = 2\pi \sqrt{\frac{M}{k_b}} \quad (54)$$

where $M = (m_b + \sum_j^N m_j)$ is the total mass of the base isolated structure; and m_j is the mass of j th floor of the super structure.

Thus, the bi-linear hysteretic model of the base isolation system can be characterized by specifying the three parameters namely T_b , Q and q . The characteristic strength, Q is normalized by the weight of the building, $W = M_g$ (where g is the gravitational acceleration).

2.5.2.2 Equivalent Linear Elastic-Viscous Damping Model of Isolators.

As per Uniform Building Code (UBC) and International Building Code (IBC), the non-linear force-deformation characteristic of the isolator can be replaced by an equivalent linear model through effective elastic stiffness and

effective viscous damping. The linear force developed in the isolation system can be expressed as

$$F_b = k_{eff} x_b + c_{eff} \dot{x}_b \quad (55)$$

where k_{eff} is the effective stiffness; $c_{eff} = 2\beta_{eff} M \omega_{eff}$ is the effective viscous damping constant; β_{eff} is the effective viscous damping ratio; $\omega_{eff} = 2\pi / T_{eff}$ is the effective isolation frequency; and $T_{eff} = 2\pi \sqrt{M / k_{eff}}$ is the effective isolation period.

The equivalent linear elastic stiffness (Naem and Kelly, 1999; Kelly and Takhirov, 2001; Matsagar et al., 2004) for each cycle of loading is calculated from experimentally obtained force-deformation curve of the isolator and expressed mathematically as

$$k_{eff} = \frac{F^+ - F^-}{\Delta^+ - \Delta^-} \quad (56)$$

where F^+ and F^- are the positive and negative forces at test displacement Δ^+ and Δ^- , respectively. Thus the is the slope of the peak-to-peak values of the hysteresis loop as shown in Fig 2.35.

The effective viscous damping of the isolator unit calculated for each cycle of loading is specified as

$$\beta_{eff} = \frac{2}{\pi} \left[\frac{E_{loop}}{k_{eff} \left(|\Delta^+| + |\Delta^-| \right)^2} \right] \quad (57)$$

where E_{loop} is the energy dissipation per cycle of loading.

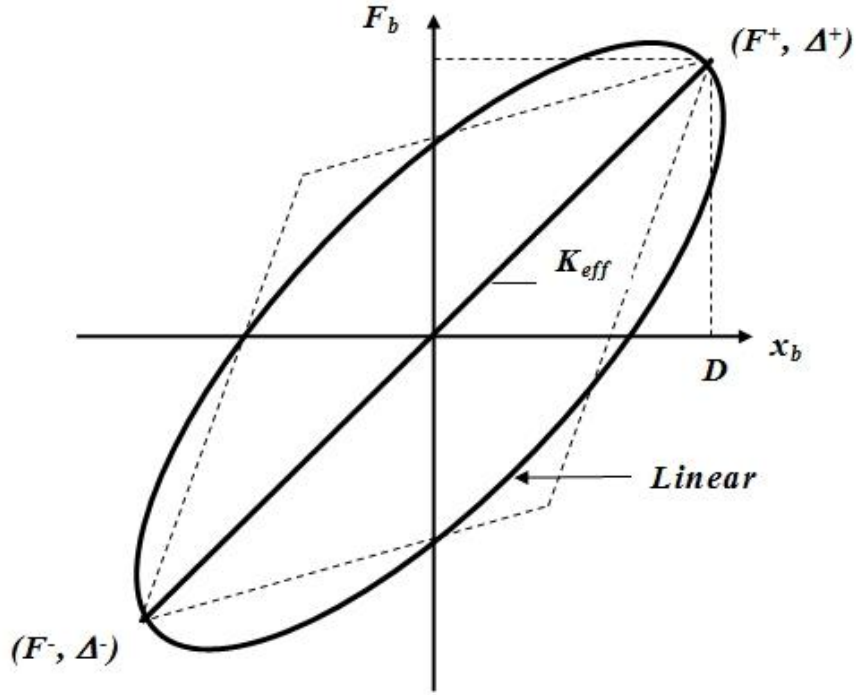


Figure 2.35 Equivalent linear model of the isolator.

at a specified design isolation displacement, D , the effective stiffness and damping ratio for a bi-linear system are expressed as

$$k_{eff} = k_b + \frac{Q}{D} \quad (58)$$

$$\beta_{eff} = \frac{4Q(D-q)}{2\pi k_{eff} D^2} \quad (59)$$

2.5.3 Time History Analysis.

2.5.3.1 Ground Motion Selecting Procedure.

In nonlinear response history analyses, the selection of acceleration records is an important step because the use of acceleration records with the same features can exaggerate or underestimate the building response (Inel et al., 2007). Appositely selecting records considering the hazard conditions for a given site helps to reduce the dispersion of EDPs and increase accuracy by achieving better estimates of the “true median”. Before scaling ground motions, one needs to

define the hazard conditions associated with a given site either through deterministic or probabilistic site-specific hazard analysis or alternatively from the USGS seismic hazard maps. Spectral shape (i.e., response spectrum normalized by PGA) defines ground motion demand characteristic on MDF systems. Therefore in selecting candidate records for nonlinear RHAs, one needs to carefully identify records whose spectral shapes are close to each other.

The parameters that need to be considered in identifying the scenario conditions are those that have the most influence on ground motion spectral shape (Kalkan and Chopra, 2010):

a. Magnitude Dependence: To derive the magnitude influence on the response spectral shape, the magnitude in the Next Generation Attenuation (NGA) database ranges from 4.9 to 7.9.

b. Distance: predominant period shifts to higher values with an increase in distance from the fault for the given earthquake. For a particular event, the predominant period shifts from approximately 0.35 second at the closest fault distance (0-20 km) to 1.2 second at the farthest fault distance (120-140 km).

c. Soil Condition: The spectral shape is also dependent on the site conditions. The predominant period of the spectra from the rock soil type is generally lower than the predominant period of the spectra from the soft soil type. The average spectral shape in V_s 30 for the rock soil type and the soft soil type ranges from 180-360 m/s and 540-720 m/s, respectively.

The best method for preventing a biased sample is the selection of a random sample. This process statically enables the spectrum of a random sample to be treated as the “true” target spectrum. Therefore, records with similar spectral shapes should be carefully identified in the selection of candidate records for nonlinear time history analysis (NLTHA).

2.5.3.2 Ground Motion Scaling Procedure.

According to ASCE 7-10 standard, ordinate of the target spectrum over the period range were $0.2T_1$ to $1.5T_1$. The target pseudo-acceleration spectrum for the buildings site was taken as the median of the 5% damped pseudo-acceleration response spectra corresponding to the average of the horizontal components of the

unscaled records, related to Indonesia earthquake code (BSN, 2012; 2013). Least Square Method, scaling technique used to match the spectrum, was proposed by (Kalkan and Chopra, 2010). Under this method, the input acceleration were multiplied by a scalar that minimizes the weighted sum of the errors between the ground motion spectra and the target spectrum. In order to obtain a minimum scale factor for each of seven records, residuals between the record's scaled spectrum and target spectrum is minimized between $0.2T_1$ and $1.5T_1$ through a method of least square whereby square of sum of residuals is expressed as

$$\lambda = \sum_{i=1}^n [\bar{A}_i - (SF \cdot A_i)]^2 \quad (60)$$

where \bar{A}_i and A_i are the target spectral acceleration and record's (unscaled) spectral acceleration, respectively. The symbol i is spectral period, and n is the number of periods (log spaced) covered between $0.2T_1$ to $1.5T_1$. The aim is to find a values of SF that minimize the error. In multivariable calculus, we learn that this requires us to find the SF such that

$$\frac{d\lambda}{dSF} \cong 0 \quad (61)$$

$$\lambda = \sum_{i=1}^n [\bar{A}_i^2 - 2\bar{A}_i \cdot A_i \cdot SF + A_i^2 SF^2] \quad (62)$$

$$\frac{d\lambda}{dSF} = \sum_{i=1}^n [2SF \cdot A_i^2 - 2\bar{A}_i A_i] = 0 \quad (63)$$

$$SF = \left(\sum_{i=1}^n \bar{A}_i A_i \right) / \left(\sum_{i=1}^n A_i^2 \right) \quad (64)$$

Note that Eq. (64) yields an optimal scaling factor to ensure that the record's scaled spectrum match closely the target spectrum between $0.2T_1$ to $1.5T_1$.

Occasionally, the average spectrum of seven scaled records may fall below the target spectrum in this period range and violates the ASCE 7-10 requirement. If this situation is encountered, each record needs to be further amplified with the same factor of the ratio of maximum difference.

2.6 Finite Element Method

The Finite Element Method (FEM) has developed into a key, indispensable technology in the modeling and simulation of advanced engineering systems in various fields like housing, transportation, communications, and so on. In building such advanced engineering systems, engineers and designers go through a sophisticated process of modeling, simulation, visualization, analysis, designing, prototyping, testing, and lastly, fabrication (see Fig.2.36).

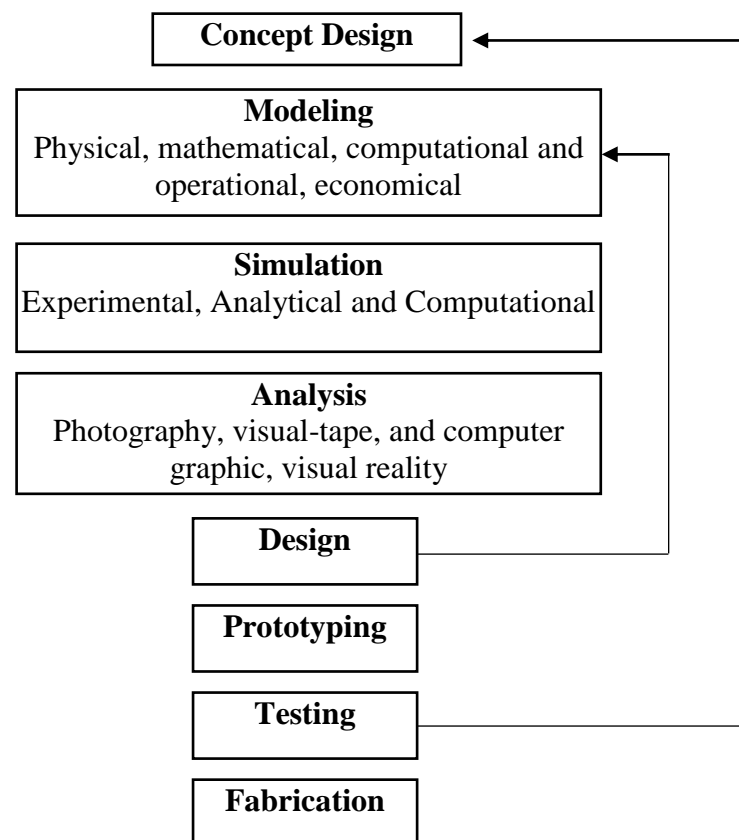


Figure 2.36 Processes leading to fabrication of advanced engineering systems.

This process is often iterative in nature, meaning that some of the procedures are repeated based on the results obtained at a current stage, so as to achieve an optimal performance at the lowest cost for the system to be built. Therefore, techniques related to modeling and simulation in a rapid and effective way play an increasingly important role, resulting in the application of the FEM being multiplied numerous times because of this (Liu and Quek, 2003).

The finite element analysis of base isolation is challenging for finite element because the problems involve amount of characteristic of isolator such as contact condition, sliding, large strain (elastomeric behavior) and near-incompressibility of the rubber. In addition, the problems need capability of robust contact and self-contact because the bearing undergoing deformation to fold over upon itself. The finite element analysis consists of two-dimensional models under the plane strain assumption and three dimensional models for the other considered element (Kelly and Calabrese, 2012).

2.6.1 Computational Modeling Using FEM.

The behavior of a phenomenon in a system depends upon the geometry or domain of the system, the property of the material or medium, and the boundary, initial and loading conditions. For an engineering system, the geometry or domain can be very complex. Further, the boundary and initial conditions can also be complicated. It is therefore, in general, very difficult to solve the governing differential equation via analytical means. In practice, most of the problems are solved using numerical methods. Among these, the methods of domain discretization championed by the FEM are the most popular, due to its practicality and versatility.

2.6.1.1 Modeling of The Geometry.

Real structures, components or domains are in general very complex, and have to be reduced to a manageable geometry. Curved parts of the geometry and its boundary can be modeled using curves and curved surfaces. However, it should be noted that the geometry is eventually represented by a collection of

elements, and the curves and curved surfaces are approximated by piecewise straight lines or flat surfaces, if linear elements are used.

Knowledge, experience and engineering judgment are very important in modeling the geometry of a system. In many cases, finely detailed geometrical features play only an aesthetic role, and have negligible effects on the performance of the engineering system. These features can be deleted, ignored or simplified, though this may not be true in some cases, where a fine geometrical change can give rise to a significant difference in the simulation results.

Depending on the software used, there are many ways to create a proper geometry in the computer for the FE mesh. Points can be created simply by keying in the coordinates. Lines and curves can be created by connecting the points or nodes. Surfaces can be created by connecting, rotating or translating the existing lines or curves; and solids can be created by connecting, rotating or translating the existing surfaces. Points, lines and curves, surfaces and solids can be translated, rotated or reflected to form new ones.

Graphic interfaces are often used to help in the creation and manipulation of the geometrical objects. There are numerous Computer Aided Design (CAD) software packages used for engineering design which can produce files containing the geometry of the designed engineering system. These files can usually be read in by modeling software packages, which can significantly save time when creating the geometry of the models. However, in many cases, complex objects read directly from a CAD file may need to be modified and simplified before performing meshing or discretization. It may be worth mentioning that there are CAD packages which incorporate modelling and simulation packages, and these are useful for the rapid prototyping of new products.

2.6.1.2 Meshing.

Meshing is performed to discretize the geometry created into small pieces called elements or cells. The rational behind this can be explained in a very straightforward and logical manner. We can expect the solution for an engineering problem to be very complex, and varies in a way that is very unpredictable using functions across the whole domain of the problem. If the problem domain can be

divided (meshed) into small elements or cells using a set of grids or nodes, the solution within an element can be approximated very easily using simple functions such as polynomials. The solutions for all of the elements thus form the solution for the whole problem domain. Proper theories are needed for discretizing the governing differential equations based on the discretized domains. The theories used are different from problem to problem, and will be covered in detail later in this book for various types of problems. But before that, we need to generate a mesh for the problem domain. Mesh generation is a very important task of the pre-process. It can be a very time consuming task to the analyst, and usually an experienced analyst will produce a more credible mesh for a complex problem. The domain has to be meshed properly into elements of specific shapes such as triangles and quadrilaterals. Information, such as element connectivity, must be created during the meshing for use later in the formation of the FEM equations. It is ideal to have an entirely automated mesh generator, but unfortunately this is currently not available in the market. A semi-automatic pre-processor is available for most commercial application software packages. There are also packages designed mainly for meshing. Such packages can generate files of a mesh, which can be read by other modeling and simulation packages.

For the three-dimensional models, the isolator is illustrated by eight-node, isoparametric, three-dimensional hexahedral elements with trilinear interpolation. The hexahedral element has eight corner nodes with isoparametric natural coordinates given by s, t and z as shown in Figure 2.37. The formulation of the stiffness matrix follow steps analogous to the isoparametric solution of the stiffness matrix for the plane element. The function use to illustrate the generals degree of freedom a_i 's is given by

$$x = a_1 + a_2s + a_3t + a_4z + a_5st + a_6tz + a_7zs + a_8stz \quad (65)$$

It expands to include the z coordinate as follows :

$$\begin{Bmatrix} x \\ y \\ z \end{Bmatrix} = \sum_{i=1}^8 \begin{Bmatrix} N_i & 0 & 0 \\ 0 & N_i & 0 \\ 0 & 0 & N_i \end{Bmatrix} \begin{Bmatrix} x_i \\ y_i \\ z_i \end{Bmatrix} \quad (65)$$

where the shape function are given by

$$N_i = \frac{(1 + ss_i) + (1 + tt_i) + (1 + zz_i)}{8} \quad (67)$$

The element stiffness matrix is given by

$$[k] = \iiint_V [B]^T [D] [B] dV \quad (68)$$

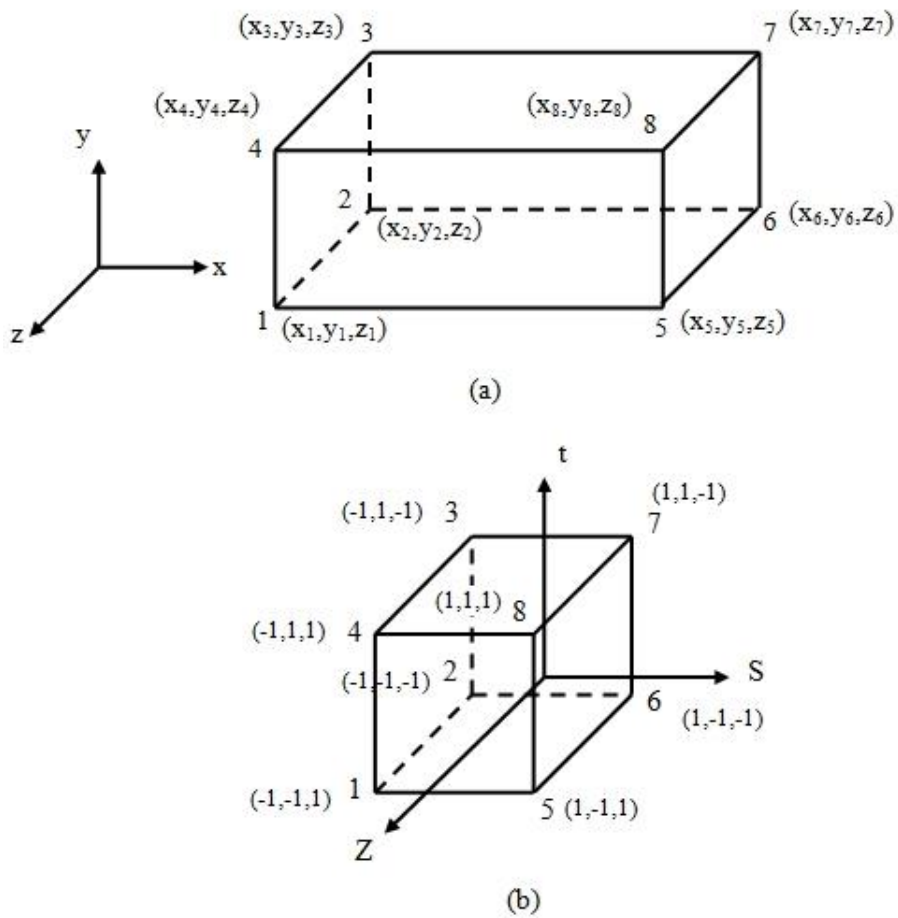


Figure 2.37 Linear hexahedral element (a). in a global-coordinate system and (b). element mapped into a cube of two unit sides.

The surface force are given by

$$\{f_s\} = \iint_s [N_s]^T \{T\} dS \quad (69)$$

The element use eight-point Gaussian integration and use the mixed formulation for incompressible analysis. Large strain theory was employed for all analyses. The kinematic of deformation is illustrated according to the update Lagrangian formulation. Next, it will utilize method of Raphson solution including both nonlinear material and nonlinear effects, since the bearing can undergo high shear strain during earthquake.

2.6.1.3 Property of Material.

Many engineering systems consist of more than one material. Property of materials can be defined either for a group of elements or each individual element, if needed. For different phenomena to be simulated, different sets of material properties are required. For example, Young's modulus and shear modulus are required for the stress analysis of solids and structures, whereas the thermal conductivity coefficient will be required for a thermal analysis. Inputting of a material's properties into a pre-processor is usually straightforward; all the analyst needs to do is key in the data on material properties and specify either to which region of the geometry or which elements the data applies. However, obtaining these properties is not always easy. There are commercially available material databases to choose from, but experiments are usually required to accurately determine the property of materials to be used in the system.

2.6.1.4 Boundary, Initial and Loading Conditions.

Boundary, initial and loading conditions play a decisive role in solving the simulation. Inputting these conditions is usually done easily using commercial pre-processors, and it is often interfaced with graphics. Users can specify these conditions either to the geometrical identities (points, lines or curves, surfaces, and solids) or to the elements or grids. Again, to accurately simulate these conditions for actual engineering systems requires experience, knowledge and proper engineering judgments.

2.6.2 Nonlinearity in Stress Analysis.

Concept of nonlinearity are introduced by explaining simple solution algorithms. In *linear* analysis, response is directly proportional to load. Linearity might be a good representation of reality or may only be the inevitable results of assumptions made for analysis purpose. In linear analysis we assume that displacement and rotations are small, support do not settle, stress is directly proportional to strain and load maintain their original direction as the structure deforms. However, any of the convenient assumptions that lead to a linear analysis may be at odds with reality. Elastic material might become plastic, or the material might not have a linear stress-strain relation at any stress level. The structure might loss the stiffness due to failure of material or buckling effect. Displacements and rotations might become large enough that equilibrium equations must be written for the deformed configuration rather than the original configuration. Large rotations lead lo pressure load to change in direction and also to change in magnitude if there is a change in the area to which they are applied. Thus, for various reasons, a problem may become nonlinear. Simple examples of nonlinear problems are illustrated in Fig. 2.38. A non linear problems appeared in Figure 2.38 (a), mean that nonlinearity arises because of significant changes in the geometry of the structure. Material nonlinearity causes the behavior in Figure 2.43 (b); material of which the beam is made has a nonlinear stress-strain relation.

Nonlinearity makes a problem more complicated because equations that represent the solution must appropriate conditions not fully known until the solution is known- the actual configuration, loading condition, state of stress and support condition. The solution cannot be derived in a single step of analysis. It must take several steps, update the tentative solution after each step and repeat until a convergence test is satisfied. The usual linear analysis is only the first step in this sequence. Nonlinear analysis can treat a great variety of problems, but in a sense it is more restrictive than linear analysis because the principle of superposition does not apply. Examples of nonlinear phenomena are as follow :

- a. Materials in which deformation depends on load rate as well as load level (creep, viscoelasticity, viscoplasticity).
- b. The case experiences large strain, as in metal-forming processes.

- c. Linkages, mechanisms and other problems that involve large rigid-body motion.
- d. Couple problems, such as fluid-structure interaction, in which fluid forces cause a structure to move, but by moving it alters the fluid forces.
- e. Nonlinear dynamic problems, such as nonlinear vibrations and projectile impact.
- f. Nonlinearity in problems other than stress analysis.

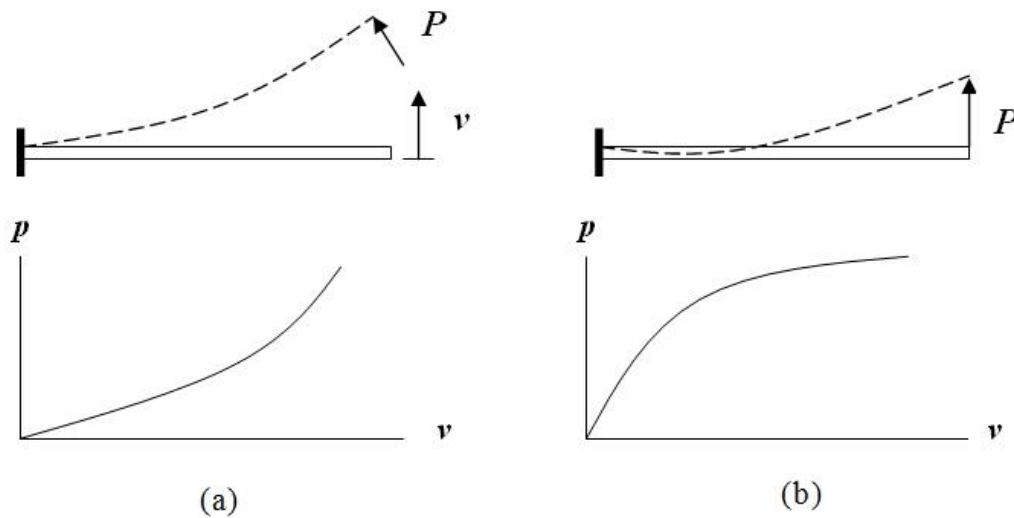


Figure 2.38 Examples of non-linear problems;

- (a). Slender elastic beam loaded by a follower force, (b) Elastic-plastic beam loaded by a fixed-direction force.

2.6.3 Solution Algorithms (Convergence Criteria).

How does the software solve a nonlinear problem? It is important to understand of solution algorithms because the analyst must make initial choices and know what to try next if a procedure fails. Many aspects of nonlinear solution methods can be discussed independently of the source of nonlinearity (Cook, 1995). Numerous finite element program employs Newton-Raphson method to solve nonlinear problems. The load is subdivided into a series of load increments that can be applied over several load steps, as shown in Fig. 2.39. A non linear analysis is organized into three levels of operation:

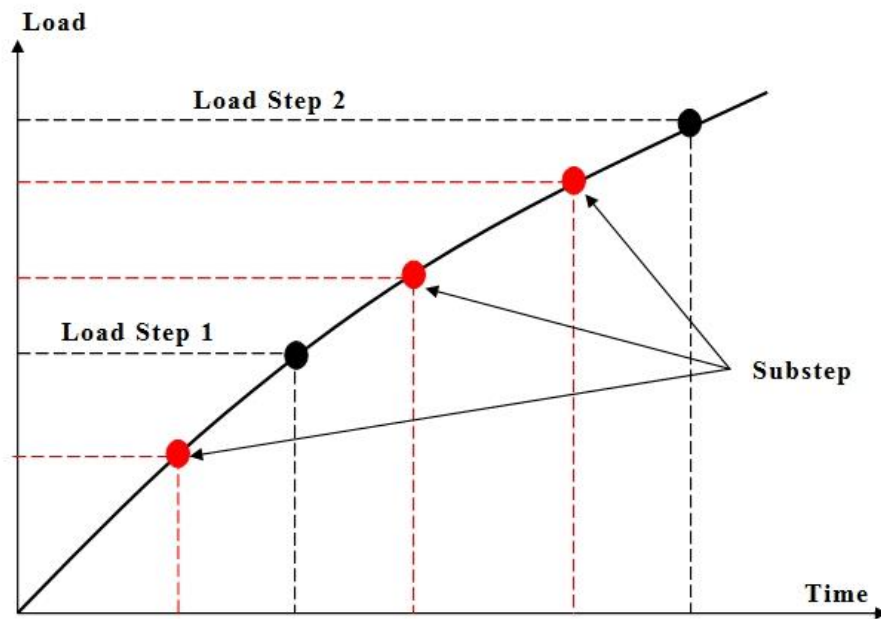


Figure 2.39 A Series of load increment over several load step.

- a. The "top" level consists of the load steps that defined explicitly over time span. Load are assumed to vary linear within load step (for static analysis).
- b. Within each load step, it can direct the program to perform several solutions (substep or time steps) to apply the load gradually.
- c. At each substep, the program will perform a number of equilibrium iterations to derived a converged solution.

A number convergence- enhancement and recovery features (such as line search, automatic load stepping and bisection) can be activated to help the problems to convergence, such as in Fig 2.40. The arc-length method cause the Newton-Raphson equilibrium iteration to converge along an arc, thereby often preventing divergence, even the slop of load versus deflection curve become zero or negative.

The program performs a linear solution using the out of balance load and check for convergence. If convergence criteria are not satisfied, the out of balance is reevaluated. The stiffness matrix is updated and new solution is derived. This iterative procedure continues until the program converges. The finite element discrization process yields a set of simultaneous equations:

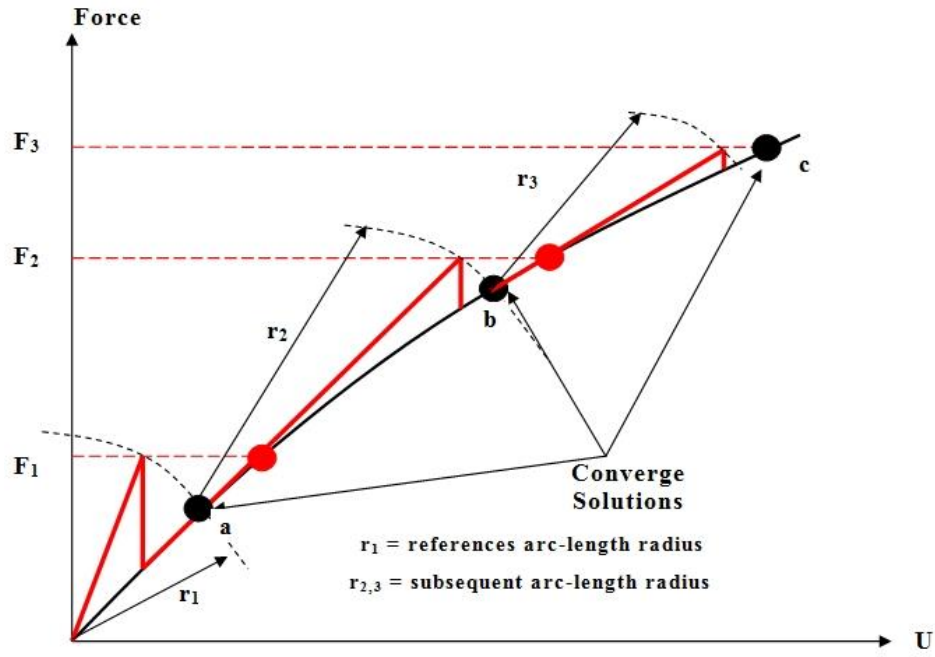


Figure 2.40. Convergence enhancement with recovery feature (line search).

$$[k] \times \{u\} = \{F^a\} \quad (70)$$

where $[k]$ is coefficient stiffness matrix, $\{u\}$ is a vector of unknown dof values and $\{F^a\}$ is vector of applied loads. The Newton-Raphson method is an iterative process of solving the nonlinear equations (see Fig 2.41).

$$[k_i^T] \times \{\Delta u_i\} = \{F^a\} - \{F_i^{nr}\} \quad (71)$$

And

$$\{u_{i+1}\} = \{u_i\} + \{\Delta u_i\} \quad (72)$$

As seen in Fig 2.41, more than one Newton-Raphson iteration is needed to achieve a converged solution. The general algorithm proceeds as follows:

- Assume $\{u_0\} = \{0\}$ is usually the converge solution from the previous time.
- Compute the update tangent matrix $[K_i^T]$ and $\{F_i^{nr}\}$ restoring load from configuration $\{u_i\}$.
- Calculated $\{u_i\}$ from Eq. 71.

- g. Add $\{\Delta u_i\}$ to $\{u_i\}$ in order to derived the next approximation $\{u_{i+1}\}$.
- h. Repeat all steps until convergence is obtained.

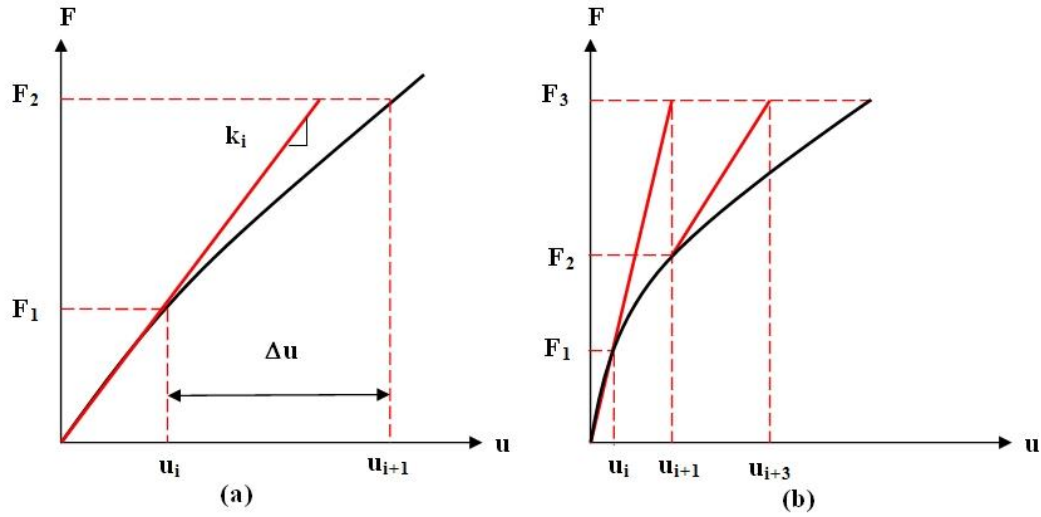


Figure 2.41 Newton- Raphson; (a). One iteration, (b). Next iteration.

CHAPTER 3

METHODOLOGY OF RESEARCH

3.1 Introduction The primary objective of this study is to develop low-cost base isolation system for residential housing by replacing thin-steel plate using perforated plate. The critical issue of developing isolator for light structure is how to provide the low lateral shear stiffness of isolator under large earthquake shaking. Therefore, the low-grade of rubber material is employed to derive lowest shear modulus (G) of rubber material. A series analysis and experimental test have been carried out to discover the optimum design of isolator. The isolator used perforated plate as reinforcement is denoted as perforated-reinforced elastomeric isolators (PREIs). The details concepts of research project are presented in Fig 3.1 as follow:

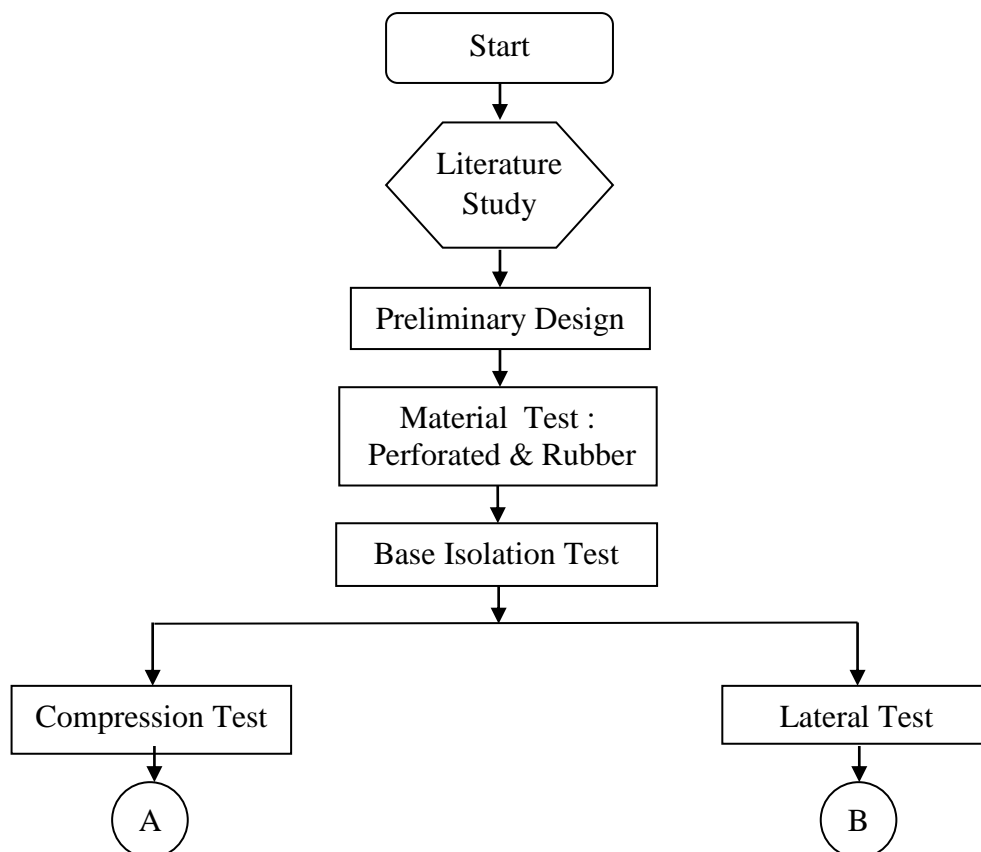


Figure 3.1 Flow chart of research project.

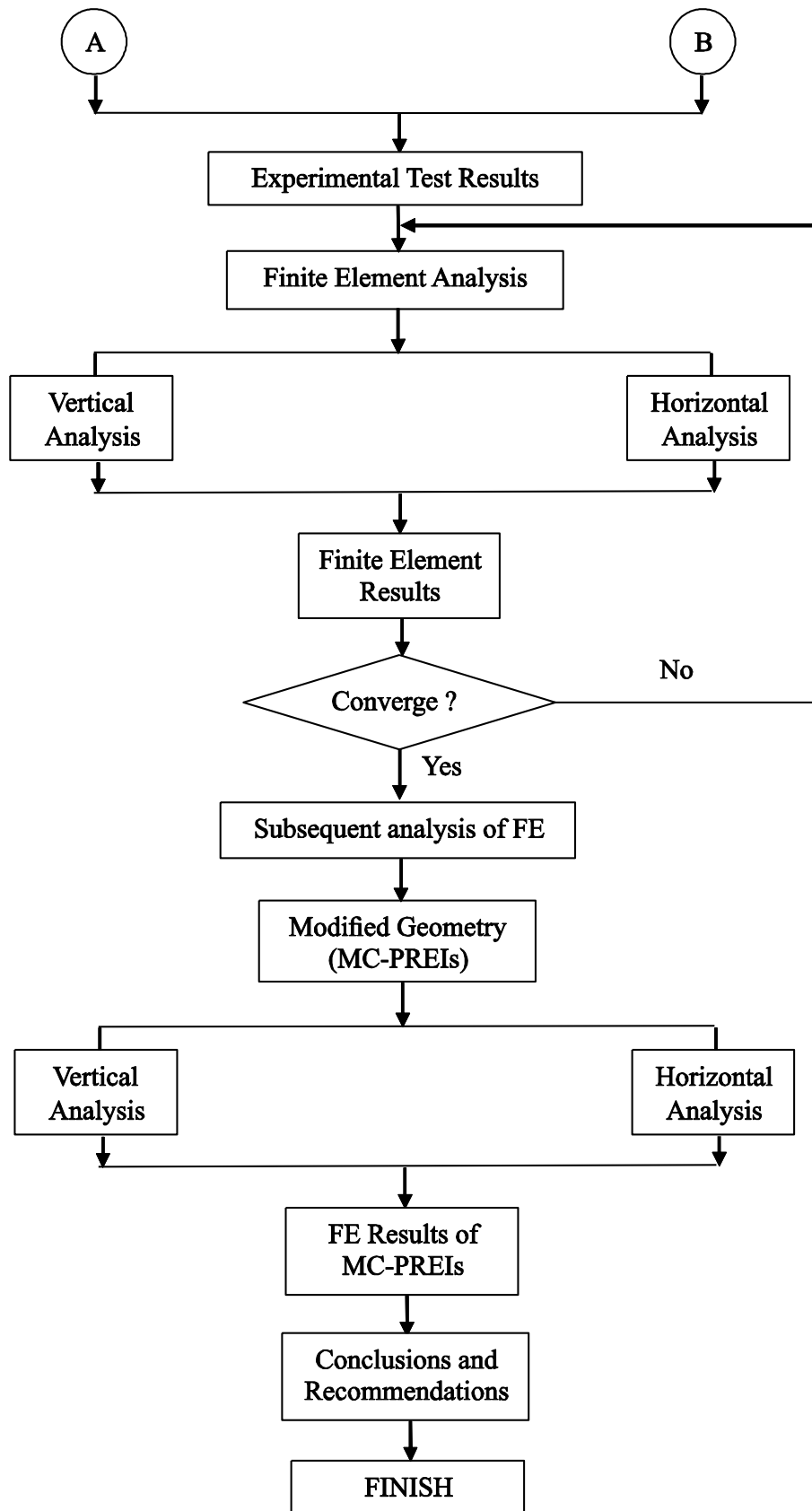


Figure 3.1 Flow chart of research project (continued).

3.2 Preliminary design

In this step, the aim of preliminary design is to estimate the appropriate dimension of isolator to provide the desired lateral stiffness for obtaining the target fundamental period of structure. The process is started by calculating the design displacement of isolator under DBE and MCE conditions. The parameters earthquake are corresponding to Aceh-Indonesia as high seismic zone with soil condition of rock. Furthermore, the design displacement is employed to predict the total rubber thickness with initial assumption of shear strain of 1.5. Prior to defining the diameter, the lateral stiffness must be determined related to both target fundamental period (2sec) and axial load (80kN). The diameter is selected 2 times than total thickness of rubber. It is conducted to satisfy the lateral stability under large displacement. Besides the isolator dimension, the parameter of isolator including vertical stiffness, horizontal stiffness and critical load are presented. It must be defined earlier to ensure the analysis and experimental process will be conform as desired.

3.3 Material test

In order to develop low-cost base isolation system, there are two primary material used in this research work. They are rubber material and perforated plate. Prior to conducting further analysis, material properties are required to model isolator in FE program. Therefore, the series experimental test were carried out to obtain the quantities of material properties. The detail test for each material is given below:

3.3.1 Perforated plate.

Commonly, perforated plate is applied within non-structural members; for instance, in the filtration of air, gases and water (IPA, 1993). These application are not required the material properties since it is not used on the structural members. Therefore, the information related to properties of material are not available in the market. In this research, the perforated plate would be employed as structural member as reinforcement on isolator. The experimental test was conducted to derive the material properties of plate. Since the

appropriate experiments for perforated plate are not yet clearly defined by nation or international standards organization, the series experimental test would be carried out to obtain the yield strength and young's modulus of plate. These quantities would be used in determining material properties on finite element program.

3.3.2 Rubber material.

The objective of the testing described herein is to define and to satisfy the input requirements of mathematical material models that exist in structural, non-linear finite element analysis software.

The testing of elastomers for the purpose of defining material models is often misunderstood. The appropriate experiments are not yet clearly defined by national or international standards organizations. This difficulty derives from the complex mathematical models that are required to define the nonlinear and the nearly incompressible attributes of elastomers. There are four type of test conducted to obtain stress-strain data of rubber material. They are tension, planar shear, equalbiaxial and volumetric test. These strain-data would be input on the FE program to represent hyperelastic material. The experimental test was conducted in Axelproduct, USA.

Most of these models are referred to as hyperelastic material models. However, most models share common test data input requirements. In general, stress and strain data sets, developed by stretching the elastomer in several modes of deformation, are required and "fitted" to sufficiently define the variables in the material models. Appropriate experimental loading sequences and realistic strain levels are needed to capture the elastomer behavior that applies in the analysis.

3.4 Experimental test of base isolation

In order to complete the study, experimental test of base isolation must be conducted to observe the real behavior of isolator under vertical and lateral conditions. Since the number of specimen of isolator was limited, the experimental test must be verified with FE result. There were two experimental test, compression test and lateral test. The tests were conducted in the R & D

Center of Settlement, Ministry of Public Works and Housing, Cileunyi, Bandung, Indonesia. The detail of the test for each material is given below:

3.4.1 Vertical test

The compression test was carried out to observe the vertical characteristic of isolator under axial load. The BS EN 1337-3: 2005 standard was used as the fundamental procedure for vertical test. In vertical test, the specimens were monotonically loaded to a compressive force at zero horizontal displacement. In order to observe the vertical characteristic of isolator, the specimen was loaded in multi vertical load started with 10 kN, 20 kN, 30kN, 40 kN, 80 kN, 100 kN, 150 kN, 200 kN and terminated by 250 kN.

The vertical load was performed using load control. Once the compressive load was achieved, it was fluctuated $\pm 1/3$ of force over three sinusoidal cycles at loading rate of 5.0 ± 0.5 Mpa/min (2.6 kN/sec) and then monotonically unloaded. The vertical load was obtained from the load cell located on the top of frame. The relative vertical displacement between the end plate of the specimen was averaged from four LVDT data (V_1, V_2, V_3 and V_4) that were located at the four corners of the end plates.

3.4.2 Horizontal test

The lateral test is conducted to observe the lateral characteristic of isolator under combination load. The horizontal test of base isolation is carried out according to BS EN 15129:2009.

The specimen is subjected to constant vertical load then sheared freely in horizontal direction. Initially, the specimen is monotonically loaded to a compressive force of 80 kN at zero horizontal displacement by hydraulic actuator. Once the compressive load is achieved, the vertical reaction frame connected with horizontal actuator is fluctuated over three sinusoidal cycles for each shear strain (i.e. 5%, 10%, 20%, 50%, and 100%) at a frequency of 0.5 Hz. After shear displacement is complete, then the specimen is monotonically unloaded. In the horizontal test, lateral displacement is performed using horizontal displacement control and vertical load is performed using vertical load control. During the

horizontal test, the specimen is characterized by the applied horizontal load and the horizontal displacement of the top frame. The imposed horizontal load is computed as shear load measured by load cell located on the horizontal actuator. The relative horizontal displacement located on the left side of frame is averaged from two LVDT data.

3.5 Finite element analysis (FEA)

In this research project, finite element was used to simulate and verify the isolator model. In addition, it was also used to observe the further analysis related to stress and strain state of isolator under different conditions. In determining material properties of hyperelastic material, stress-strain data derived experimental test were used to simulate rubber material on FE program.

Ogden model was selected as strain energy function (SEF) of rubber by conducting curve fitting process corresponding to stress-strain data test. The FEA was carried out using ANSYS, a commercially available general purpose finite element program. In modeling element both rubber and perforated plate, the brick element with 20 nodes was employed. The reduce integration was selected to represent numerical model related to element type. In addition, the contact between the rubber and reinforcement were defined as bond.

In modeling loading condition, single loading was used to represent axial load and lateral displacement. It was carried out due to the running process was very time consuming. The FE element results would be fitted with backbone of experimental data test results for both vertical test and horizontal test.

Further analysis was also performed to observe the behavior of rubber in different condition related to stress and strain state. The modification on loading area of isolator was also conducted to obtain the lower horizontal stiffness. In this case, there were 4 type of FE model used according to the inner diameter on the loaded area. The models were observed related to vertical and horizontal characteristic due to the modification. The stress-strain condition were also studied to make sure that the isolator is able to behave as desired.

3.6 Further Analysis using Finite element

An alternative method is required to enhance the lateral characteristic of PREIs by reducing the horizontal stiffness significantly. The viable method was proposed by Engelen (Engelen et al 2014; Osgooei et al 2015) by modifying the geometric of isolator to enhance the lateral response characteristic of isolator. The modifying geometric of isolator is by cutting holes in the center portion of the isolator or removing sections from the sides. It was carried out to increase the lateral response of isolator.

Therefore, to enhance the lateral response of PREIs, the modifying geometric is also conducted by removing section in the center portion of the isolator. This modified is extremely expected to reduce significantly the horizontal stiffness of PREIs under lower axial load.

In this section, the modified circular perforated-reinforced elastomeric isolators (MC-PREIs) are investigated. The primary objective of the study is to reduce horizontal stiffness of PREIs. In this case, FE analysis is employed to investigate the lateral and vertical response of MR-PREIs with an axial load. The detail of analysis of MR-PREIs using FE analysis are presented in Chapter-8.

3.7 Conclusions and Recommendations

In this chapter, the conclusion related to experimental and analysis results are presented. The details of conclusion and recommendation are illustrated in Chapter-9. In this section, a number of general finding of research project are described. In addition, the conclusions of study according to experimental test and FE analysis are also presented. The constraints in the research work are also discussed to improve the subsequent study involving experimental test and finite element analysis.

"This page is intentionally left blank"

CHAPTER 4

EXPERIMENTAL PROGRAM

4.1 Hyperelastic Material Test

4.1.1 Introduction

The objective of the test described is to determine and satisfy the mathematical material models input requirements of hyperelastic materials that exist in structural, non-linear finite element analysis software.

The test procedure of hyper elastic materials for the purpose of defining material models is often misunderstood. The appropriate experiment procedure has not yet clearly defined by the national or international standards organizations. This difficulty is obtained from the complex mathematical models required to determine the nonlinear and nearly incompressible attributes of rubber.

Most of these models are referred to as hyper elastic material models. However, most of the models require common test data input. In general, stress and strain data pairs performed by stretching the rubber in several modes of deformation area is required and "fitted" to sufficiently define the variables in the material models. Appropriate experimental loading sequences and realistic strain levels are needed to capture the rubber behavior that applies in the finite element analysis program. A typical set of stress-strain curves appropriate to be included into fitting routines are uniaxial tension test, planar shear test, equal biaxial test and volumetric test. Those experimental series are utilized to represent rubber material in FE program, ANSYS.

Each mode of deformation put the material into a particular state of strain. The primary objective of the test is to achieve the "pure" state of strain, so that the stress strain curve represents the rubber behavior is only in the desired state. The test is not failure oriented. The concern is to model behavior of the material in the working range of stress and strain. For incompressible elastomer, the basic states are simple tension, pure shear and simple compression. For experimental reasons, compression is replaced by equal biaxial extension. For slightly compressible situations or situations where an elastomer is highly

constrained, a volumetric compression test may be needed to determine the bulk behavior.

The behavior of rubber that exhibits a rate-dependent on both temperature and time, can be modeled as a viscoelastic material. When unloaded, it eventually returns to the original, unreformed state. When subjected to a constant stress, it creeps. When given a prescribed strain, the stress decreases with time; this phenomenon is called stress relaxation. Therefore, in order to capture the viscoelasticity of the rubber material, stress relaxation test was conducted.

All of the tests (uniaxial tension test, planar shear test, equal biaxial test, volumetric test and stress relaxation test) are conducted in AxelProducts, Inc. The tests details are as follows:

4.1.1.1 Testing Procedure

Although the experiments are performed separately and the strain states are different, the data from all of the individual experiments are used as a set. It means that the specimens used for each experiment must be of the same material. This may seem obvious, but if the specimens are specially molded to accommodate the differing instrument clamps for different experiments, it is possible that the material processing parameters may cause material variations from test to test. While it is reasonable to assume that variation exists in the production environment and that we can never really get the exact material properties every time, it is not acceptable to have this same variation within the data set. The data represents a “snapshot” in time. If a slight variation exists between experiments, a physically impossible material model may be developed in the analysis software. The best way to avoid this problem is to cut specimens for simple tension, pure shear and equal biaxial extension from the same slab of material.

4.1.1.2 Testing in Multi Strain State

Each mode of deformation put the material into a particular state of strain. One objective of the test is to achieve the “pure” state of strain, so that the stress strain curve represents the elastomer behavior is only in the desired state.

This test is not failure oriented. The intention is to model the behavior of the material in the working range of strain and stress.

4.1.1.3 Loading Condition (Slow Cyclic Loading)

The structural properties of elastomers change significantly during the first several times that the material experiences straining. This behavior is commonly referred to as the Mullin's effect. If an elastomer is loaded to a particular strain level followed by complete unloading to zero stress several times, the change in structural properties from cycle to cycle as measured by the stress strain function will diminish. When the stress strain function no longer changes significantly, the material may be considered to be stable for strain levels below the particular maximum strain. If the elastomer is then taken to a new higher maximum strain, the structural properties will change significantly again.

4.1.1.4 Observations

Several observations can be made regarding this behavior which are true to a varying degree for all elastomers.

- ✓ The stress strain function when an elastomer is strained for the 1st time is never to be repeated again. It is a unique event.
- ✓ The stress strain function stabilizes between 3 and 20 repetitions for most elastomers.
- ✓ The stress strain function will change significantly again if the material experiences strains greater than the previous stabilized level. In general, the stress strain function is sensitive to the maximum strain ever experienced.
- ✓ The stress strain function of the material while increasing strain is different than the stress strain function of the material while decreasing strain.
- ✓ After the initial straining, the material does not return to zero strain at zero stress. There is some degree of permanent deformation.

4.1.2 Uniaxial Tension Test

Simple tension experiments are very popular for elastomers. There are several standards for the testing of elastomers in tension. However, the experimental requirements for analysis are somewhat different from most standardized test methods. The test was performed on a dog bone-shaped specimens with an effective gauge length of 50 mm prepared according to ASTM D412 (Figure 4.1). There were 3 specimens from the same material (Sample A, Sample B and Sample C) used for testing. The specimen was divided into 3 samples to investigate the quality of material production, thus it was taken from different batch.

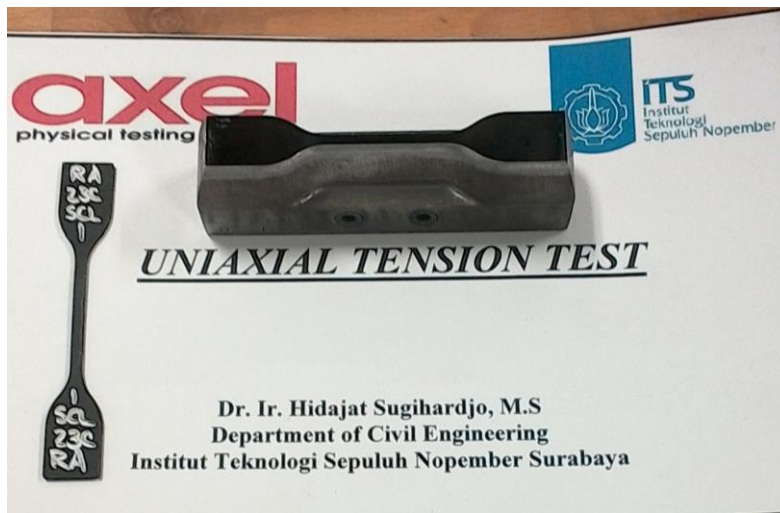


Figure 4.1 Specimen of uniaxial tension test.

The aim is to create an experiment with no lateral constraint to specimen thinning. A non-contacting strain measuring device such as a video extensometer or laser extensometer was required to achieve this. An Instron servo hydraulic or electromechanical test instrument was used to provide the loading (Figure 4.2). The instrument was fitted with a strain gauge load cell to measure the force for the stress calculation. A laser strain measuring device is used to measure strain in a strain gradient free region of the test specimen. The most significant requirement was the specimen must be much longer in the stretching direction than in the width and thickness dimensions in order to achieve a state of pure tensile strain. The specimen length needs to be at least 10 times its width or thickness. Also, there was no absolute specimen size requirement.

An Instron servo-hydraulic or electromechanical test instrument was used to provide the loading. The instrument was fitted with a strain gauge load cell to measure the force for the stress calculation. A laser strain measuring device was used to measure strain in a strain gradient free region of the test specimen.



Figure 4.2 Uniaxial tensile specimen mounted on the machine.

Loading type of the test was slow cyclic loading (SLC). In slow cyclic loading, the specimen was stretched to a selected strain level and then unloaded at the same rate to a near zero stress condition. Each time the specimen was loaded or unloaded, the segment number increased. The loading history of the test is shown in Fig 4.3. For example, the first loading segment was 0 followed by unloading segment 1, loading segment 2, unloading segment 3 and so on until the experiment is completed. The strain levels applied to the specimens were 20%, 40%, 60%, 100%, 150%, and 200%. The purpose of this loading was to investigate the softening effect of the material. Loading rate will be presented in strain per second or mm/mm/s. The loading rate applied for all tests was 0.01/s. The experiment was performed at room temperature (23°C). The results of the test are shown in Fig 4.4 - 4.6.

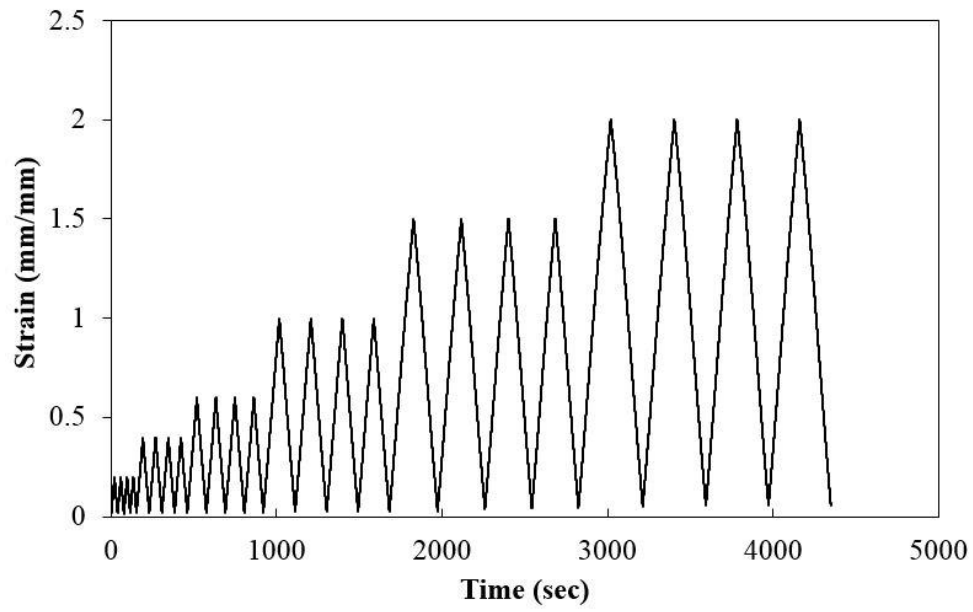


Figure 4.3 Loading history of uniaxial tension test.

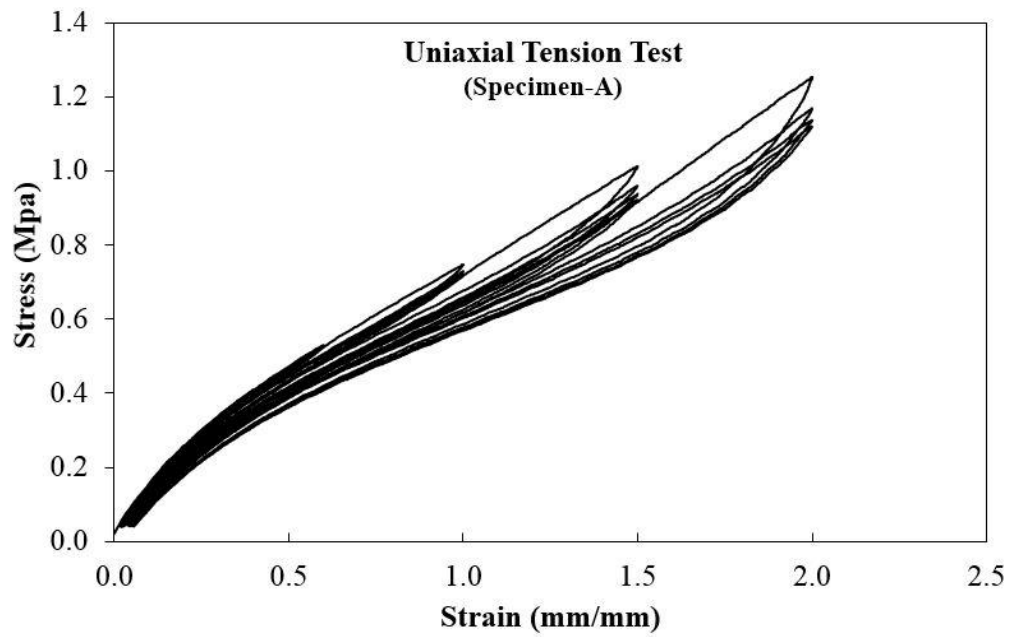


Figure 4.4 Stress-strain data of uniaxial tension test - specimen A.

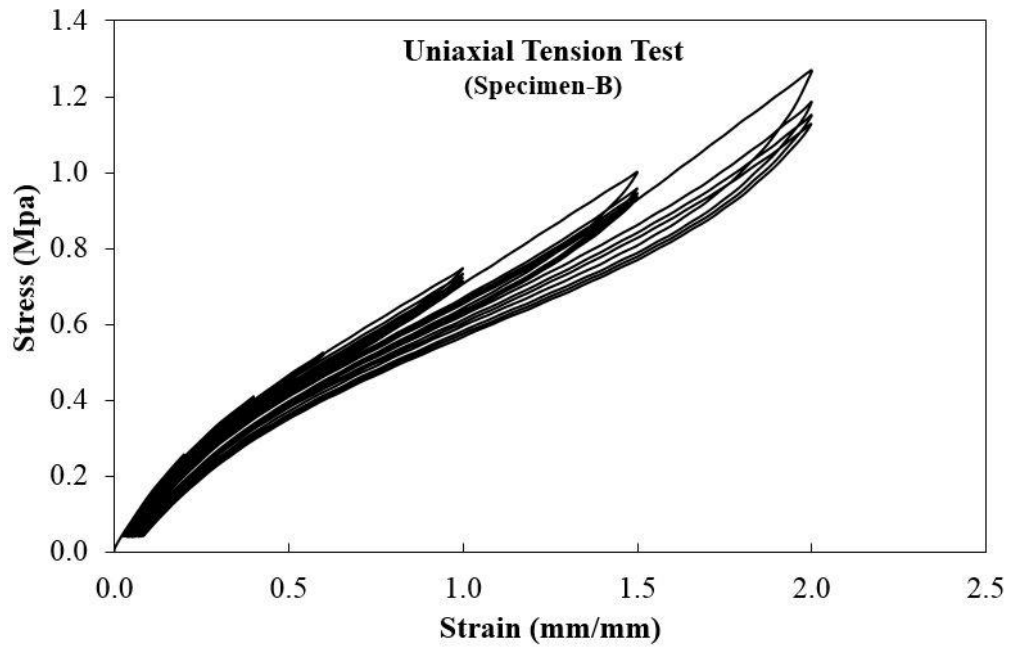


Figure 4.5 Stress-strain data of uniaxial tension test - specimen B.

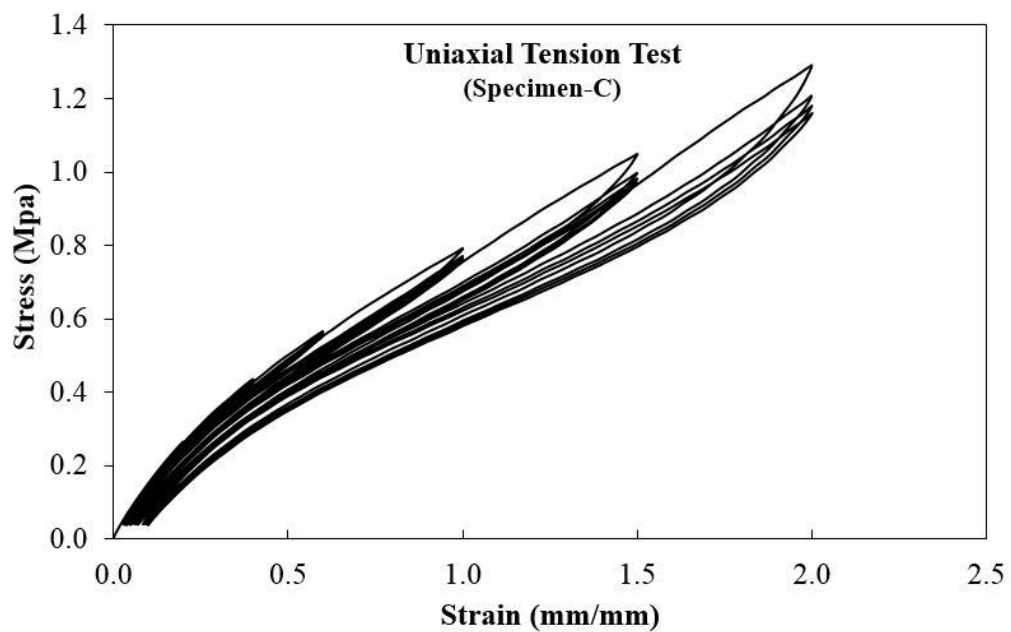


Figure 4.6 Stress-strain data of uniaxial tension test - specimen C.

4.1.3 Planar Shear Test

The pure shear experiment used for the analysis is not what most of us would expect. The experiment, at first glance, appeared to be nothing more than a very wide tensile test. However, because the material was nearly incompressible,

a state of pure shear existed in the specimen at a 45 degree angle to the stretching direction. The most significant aspect of the specimen was that it was much shorter in the direction of stretching than the width. The objective was to create an experiment where the specimen was perfectly constrained in the lateral direction so that all specimen thinning occur in the thickness direction.

The material was cut from sheets about 150 mm wide and 15 mm tall (Fig 4.7). The nature of the test, as mentioned, was conducted so that the width must be at least 10 times as much as the gauge length.

An Instron servo-hydraulic or electromechanical test instrument was used to provide the loading. The instrument was fitted with a strain gauge load cell to measure the force for the stress calculation. A laser strain measuring device was used to measure strain in a strain gradient free region of the test specimen (Fig 4.8).



Figure 4.7 Specimen of planar shear test.

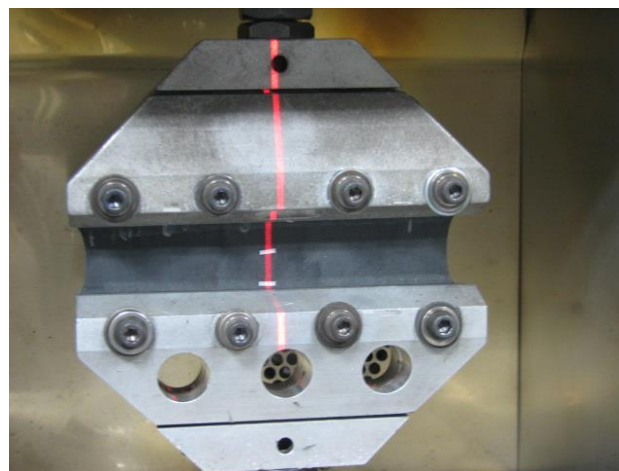


Figure 4.8 Planar shear specimen mounted on the machine.

Similar to uniaxial tension test, the loading type of planar shear test was slow cyclic loading (SLC). In slow cyclic loading, the specimen was stretched to a selected strain level and then unloaded at the same rate to a near zero stress condition. Each time the specimen was loaded or unloaded, the segment number increments. The loading history of planar shear test are shown in Fig 4.9.

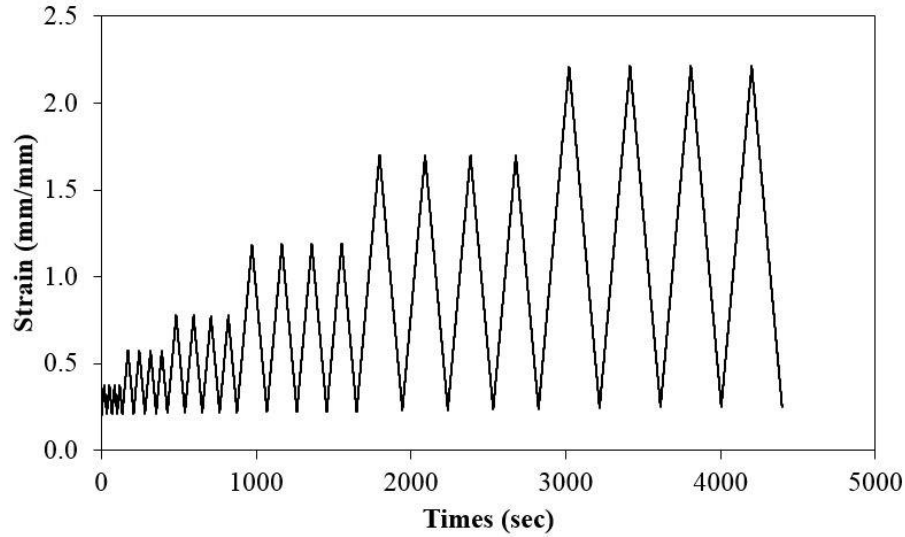


Figure 4.9 Loading history of planar shear test.

Loading rate will be presented in strain per second or mm/mm/s. The loading rate applied for planar shear tests was 0.01/s. The experiment was performed at room temperature (23°C). The results of the test are shown in Fig 4.10 - 4.12.

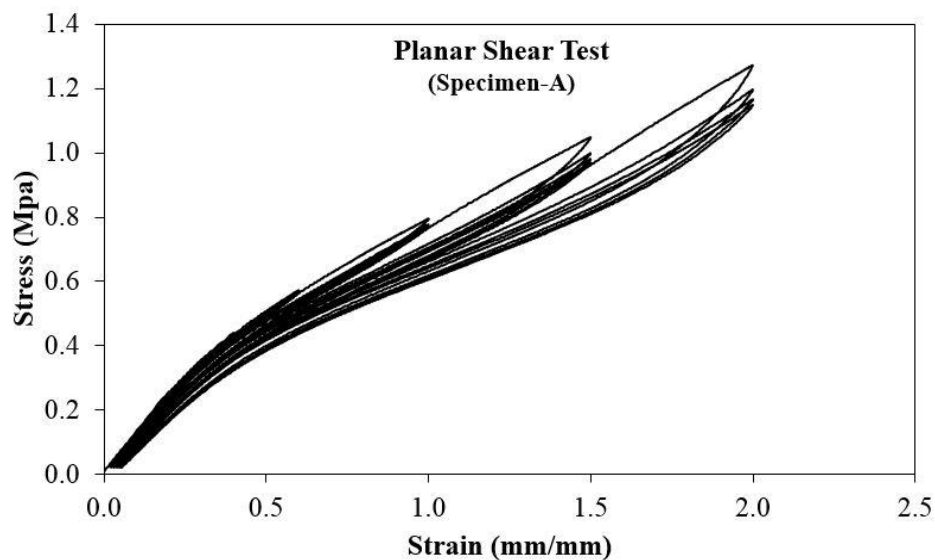


Figure 4.10 Stress-strain data of planar shear test - specimen A.

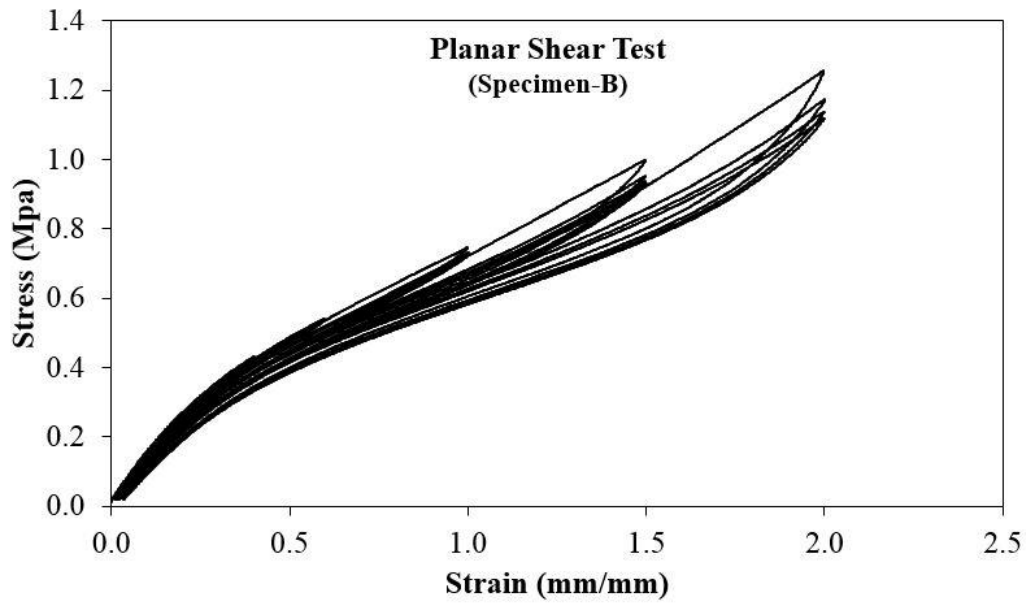


Figure 4.11 Stress-strain data of planar shear test - specimen B.

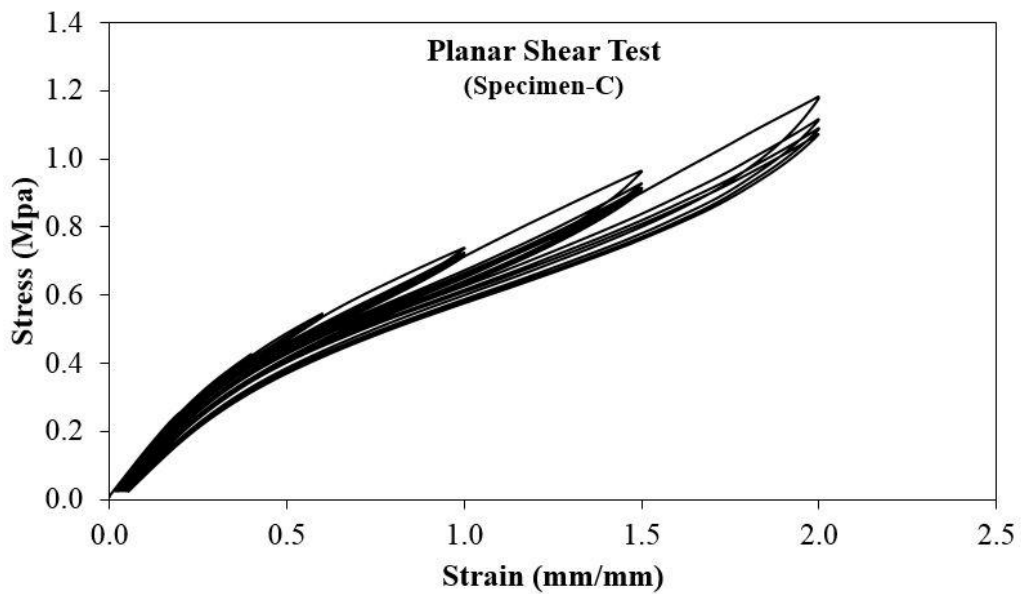


Figure 4.12 Stress-strain data of planar shear test - specimen C.

4.1.4 Equalbiaxial Test

For incompressible or nearly incompressible materials, equalbiaxial extension of a specimen creates a state of strain equivalent to pure compression. Although the actual experiment is more complex than the simple compression experiment, a pure state of strain can be achieved which will result in a more accurate material model. The equal biaxial strain state may be achieved by radial

stretching a circular disc. Once again, a non-contacting strain measuring device must be used so that the strain is measured away from the clamp edges

The material is cut from sheets and is 75 mm in diameter, with an effective area of 50 mm in diameter (Figure 4.13). The effective gauge length of specimen was 25 mm in radial direction. An Instron servo-hydraulic or electromechanical test instrument was used to provide the loading. The instrument was fitted with a strain gauge load cell to measure the force for the stress calculation. A laser strain measuring device was used to measure strain in a strain gradient free region of the test specimen (Figure 4.14).



Figure 4.13 Specimen of Equalbiaxial test.



Figure 4.14 Equalbiaxial specimen mounted on the machine.

Similar to uniaxial tension test and planar test, the loading type of equal biaxial test was slow cyclic loading (SLC). The loading history of equal biaxial test was shown in figure 4.15. The loading rate applied for equal biaxial tests was 0.01/s. The experiment was performed at room temperature (23°C). The results of the test are shown in Fig 4.16 - 4.18.

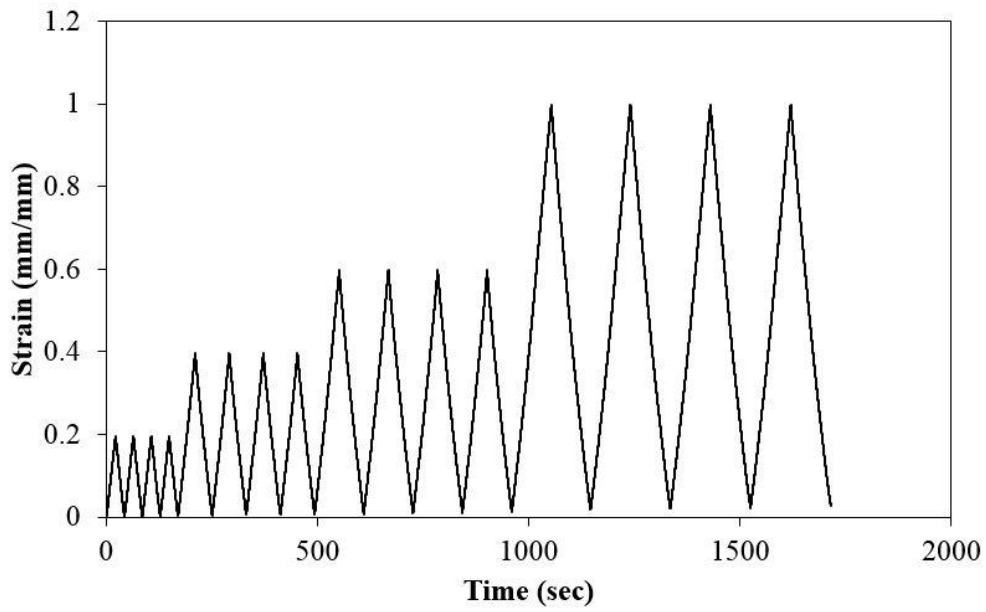


Figure 4.15 Loading history of equalbiaxial test.

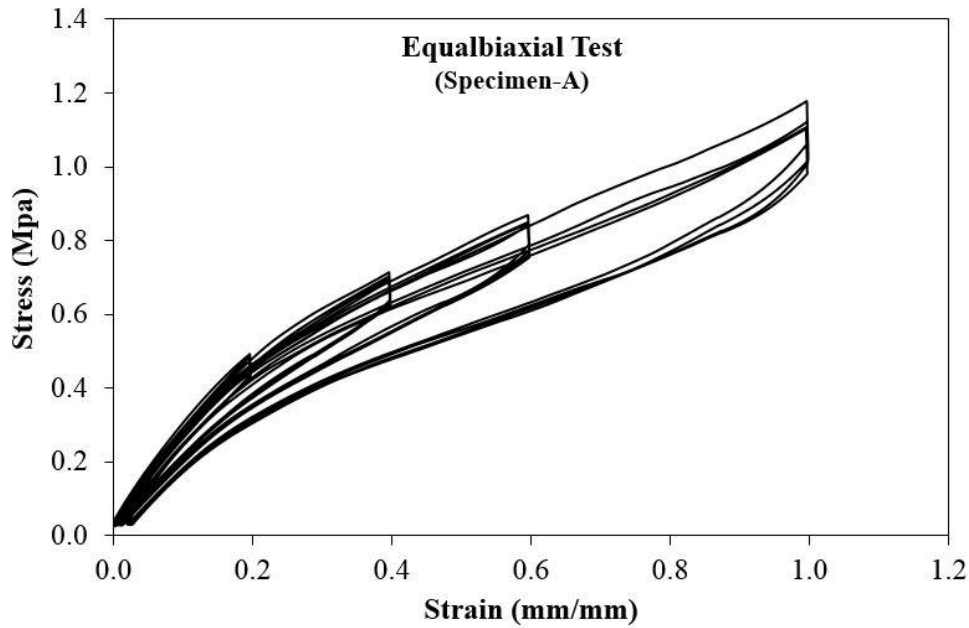


Figure 4.16 Stress-strain data of equalbiaxial test - specimen A.

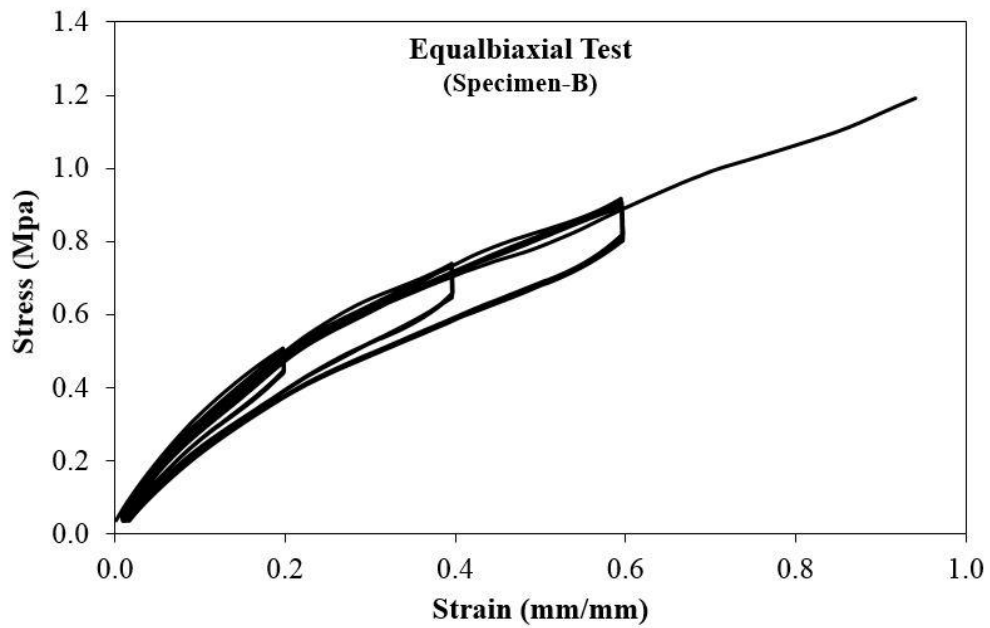


Figure 4.17 Stress-strain data of equalbiaxial test - specimen B.

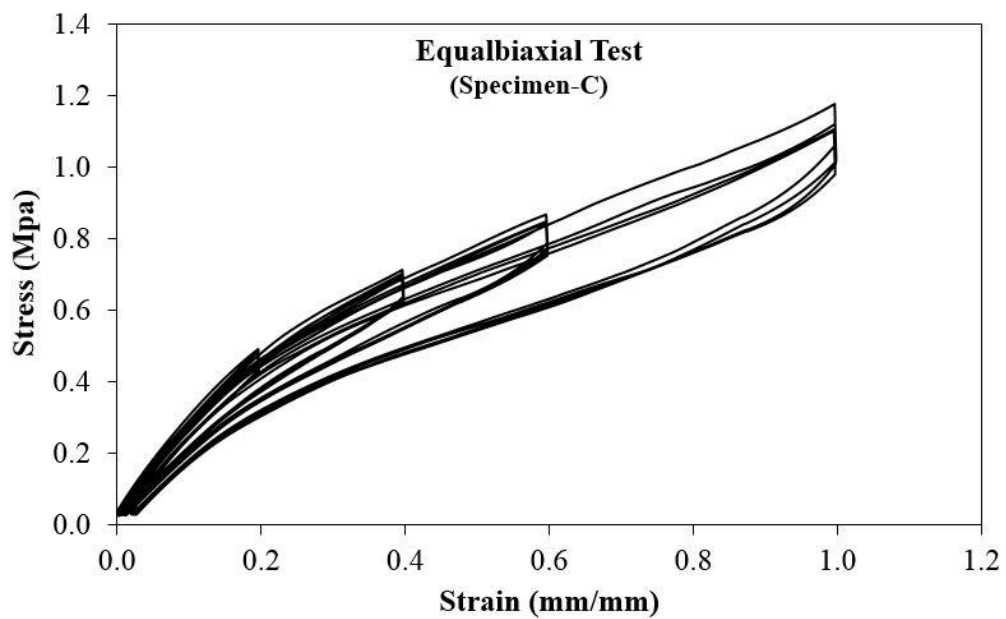


Figure 4.18 Stress-strain data of equalbiaxial test - specimen C.

4.1.5 Volumetric Test

The volumetric compression experiment was performed to measure the relationship between hydrostatic and volume change in a dense elastomer. It was also referred to as constrained compression. Circular disk of a rubber was stacked in a cylindrical void in a steel fixture and compressed on one end such that

material reacts against the bottom and sides of the cylinder. The assumption made was that the dense rubber behaves similar to a fluid, so that the reaction forces in all directions were essentially equal. The volume changed and pressure was required to compress the material measured and the initial slope of the pressure-volume curve was taken to be the bulk modulus. The test specimens were cut from sheets or slabs and were 6.35 mm in diameter. Typically, 5 disk, 1-2 mm thick each, were stacked (Figure 4.19). An Instron servo-hydraulic or electromechanical test instrument was used to provide the loading. The instrument was fitted with a strain gauge load cell to measure the force for the stress calculation. A laser strain measuring device was used to measure strain in a strain gradient free region of the test specimen (Figure 4.20).



Figure 4.19 Specimen of volumetric test.

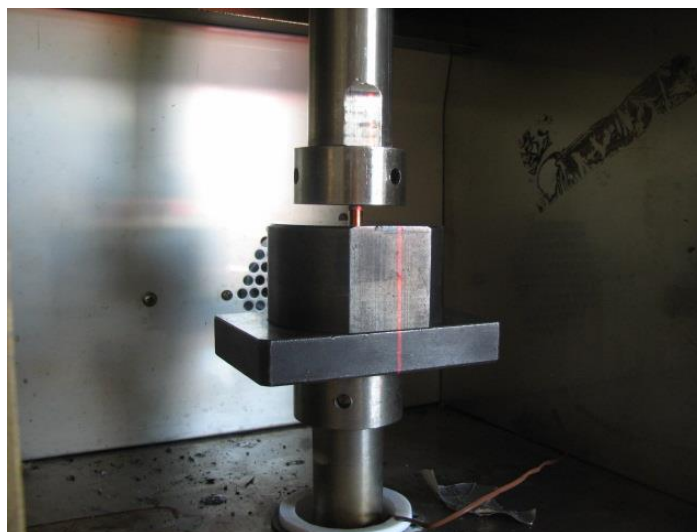


Figure 4.20 Volumetric specimen mounted on the machine.

Similar to the previous test, the loading type of equal biaxial test was slow cyclic loading (SLC). The loading history of equal biaxial test was shown in Fig 4.21. The loading rate applied for equal biaxial tests was 0.01/s. The experiment was performed at room temperature (23°C). The results of the test are shown in Fig 4.16 - 4.18.

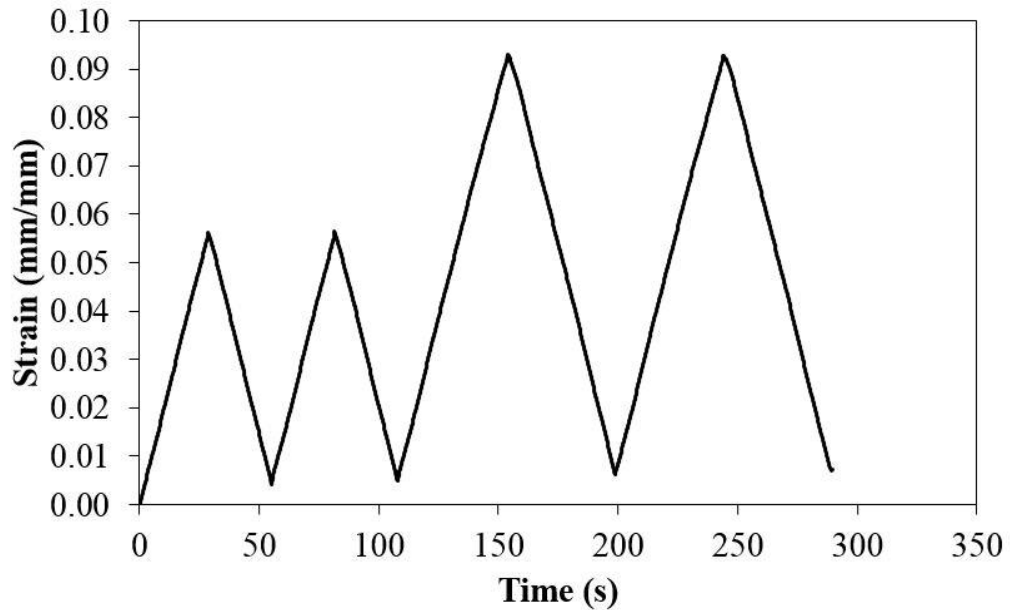


Figure 4.21 Loading history of volumetric test.

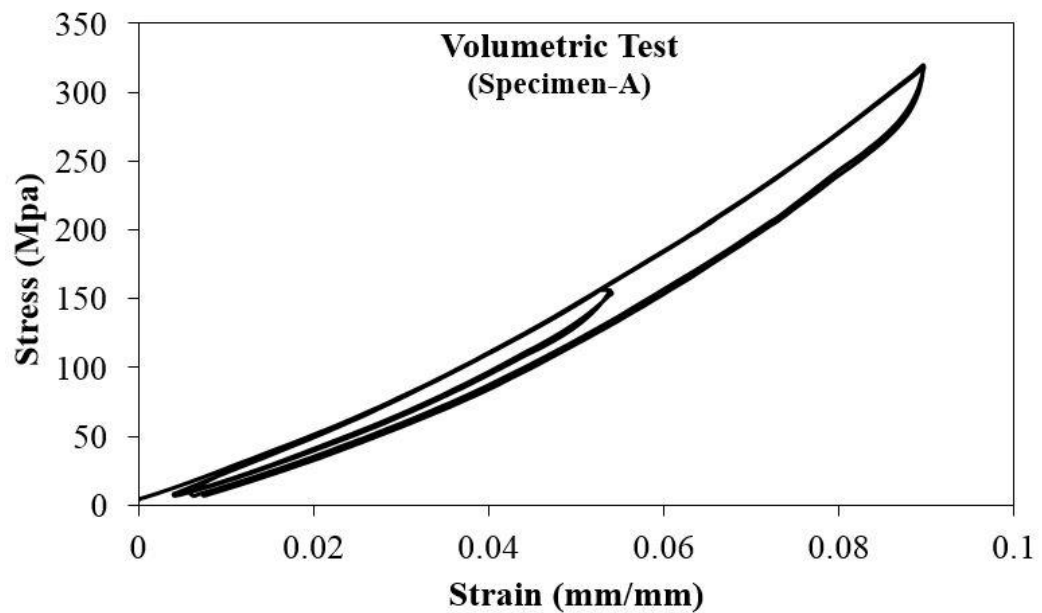


Figure 4.22 Stress-strain data of volumetric test - specimen A.

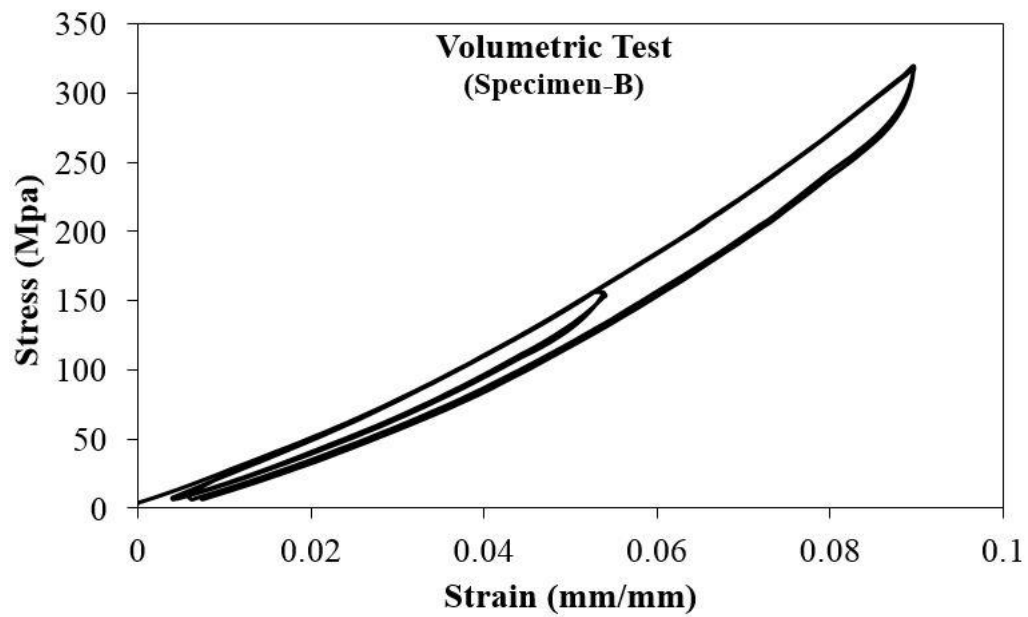


Figure 4.23 Stress-strain data of volumetric test - specimen B.

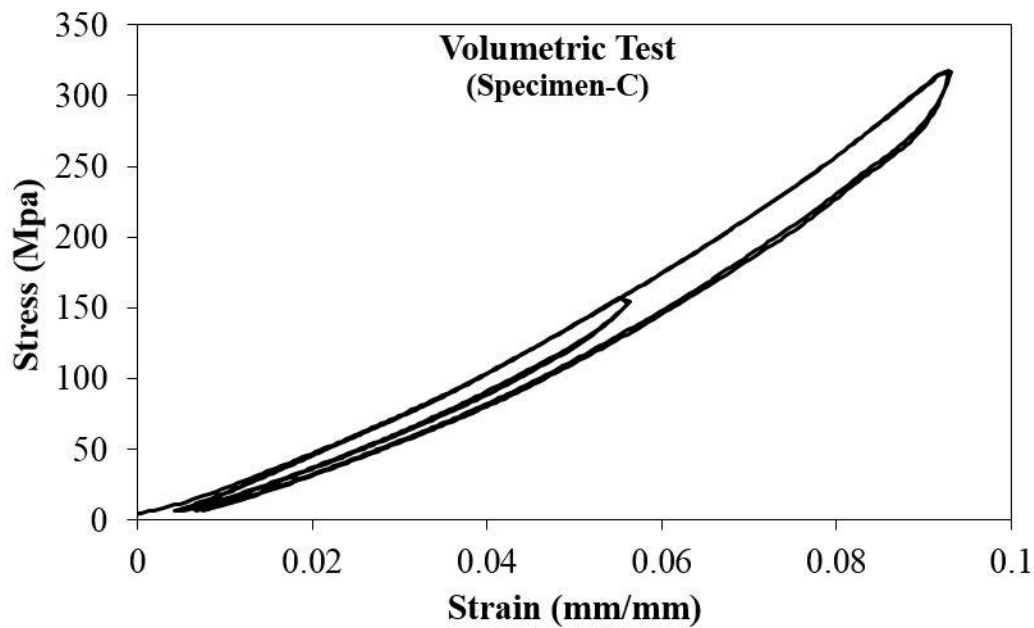


Figure 4.24 Stress-strain data of volumetric test - specimen C.

4.2 PERFORATED PLATE TEST

4.2.1 Introduction

A series of experimental program was carried out in order to define the appropriate method in determining the yield stress of perforated plate. The existing holes on the plate caused the common standard test procedure for plate

inappropriate for perforated. The testing procedure of perforated plate to derive tensile strength is often misunderstood. The appropriate experiments are not yet clearly determined by the national or international standards organizations. Therefore, the researchers intend to present an approach method to derive the yield stress of perforated plate. The concept of equivalent solid material was used for designing the analysis of perforated materials by evaluating the effect of perforation on the yield strength of materials.

In order to achieve the test objectives, two phases of experimental program were conducted. The first phase focused on the investigation to discover an appropriate method test standard procedure for determining the material characteristics of perforated plate, for instance; yield stress (f_y) and Young's modulus (E). In the first phase, the full plate would be formed similar to the perforated plate geometry. It was conducted to find out the equivalent relationship between strength of perforated material and strength of unperforated plate. The results obtained in the first phase would be compared to the previous research that had been conducted by O'Donnell (IPA, 1993). In the second phase, the perforated plate material would be performed according to the first phase results. The material properties of perforated material would be obtained with the standard procedure discovered in the first phase.

The kind of test that will be presented here is the uniaxial tension test. Generally, the procedure is not different from the typical tension test, but there is a bit of difference in the specimens shape based on the existing holes on the plate. All test specimens were instrumented such that the force resistance and deformations could be measured. Details of test specimens, test set up and instrumentation are described in this chapter.

4.2.2 Detail of Specimens

In the present investigation, perforated plate with circular holes in a standard is staggered in 60° pattern with the percentage of open area 51%, were used as samples to define the yield strength of the material. There were 3 types of plate that would be used in the experimental program as shown in Fig 4.25. The specimens of plate (A and B) were used in the first phase to discover a proper test

method for the perforated plate and would not be used for specimens of base isolation. In other word, they were only used to observe the equivalent concept relationship between solid materials and perforated materials. The specimens of Plate C were material that will be used for the base isolation as reinforcement. It would be utilized in the second phase to derive material properties based on the first phase result.

The specimens A were parts of the solid or unperforated plate used for tension test. It would be used to determine the yield strength of the solid plate (denoted S). The thickness of all specimens (A, B, and C) were similar, approximately 1.0 mm. The detailed size of specimens A are shown in Fig.4.26.

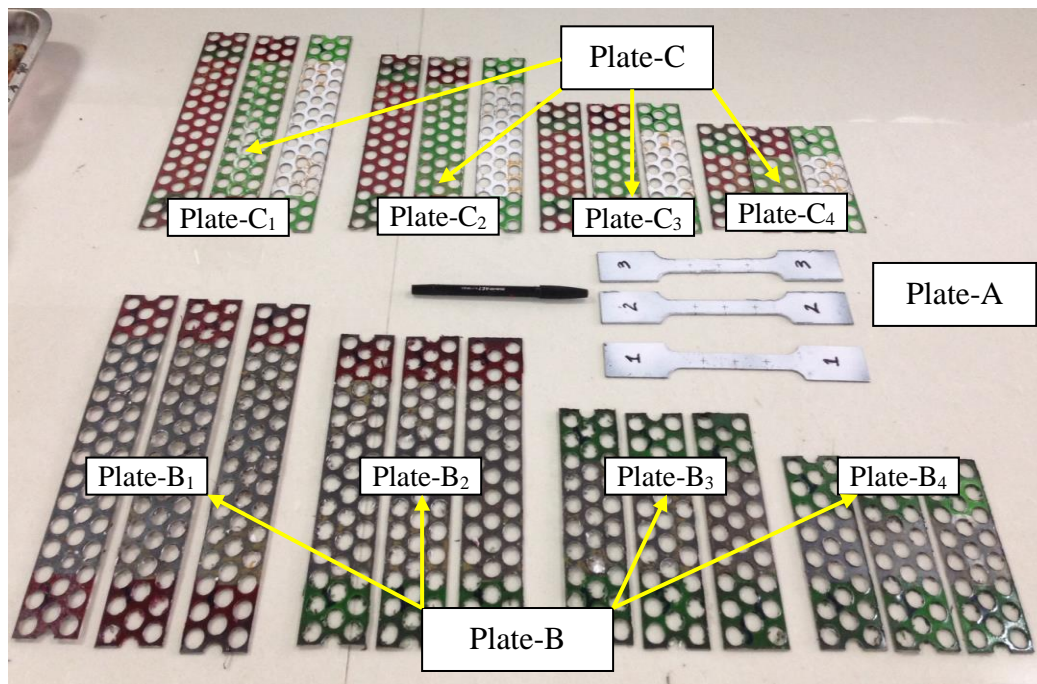


Figure 4.25 Set of samples test for tensile test.

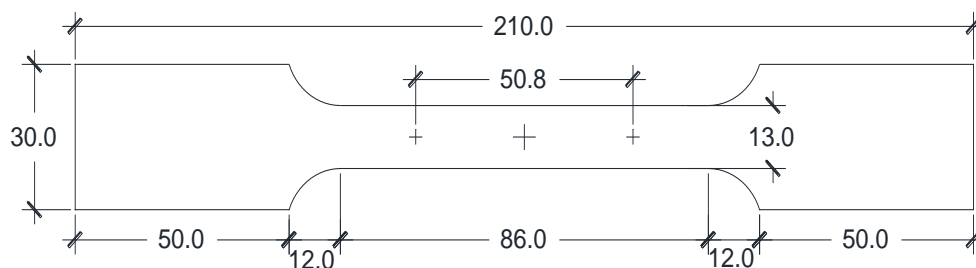


Figure 4.26 The detail size of specimens A (in mm).

The second material was Specimens B. Unlike the specimens A, a set of specimens B were designed similar to perforated plate in a geometry. The perforation process was conducted on the solid plate (specimens B) to create similar geometry such as perforated plate (specimens C). It should be remembered that specimens A and specimens B are from the same material. The specimens B were categorized as 4 types according to the length to width ratio. They were denoted plate B₁, B₂, B₃, and B₄ with approximate ratio (length to width) 4:1, 3:1, 2:1, and 1:1, respectively. The detailed size of specimens A are shown in Fig. 4.27 to Fig. 4.30.

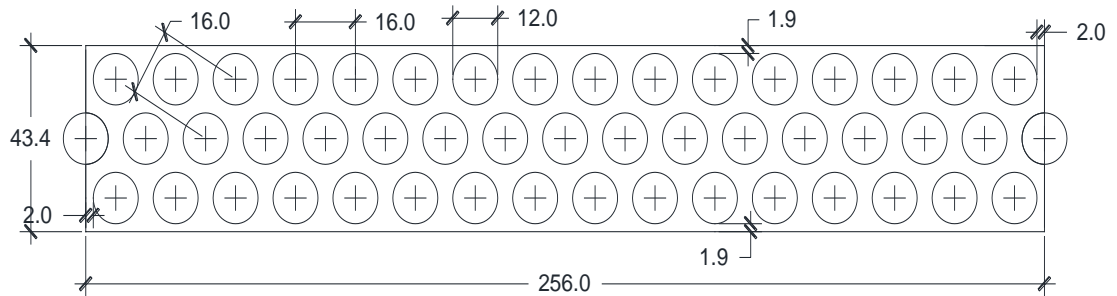


Figure 4.27 The detailed size of plate B₁ (mm).

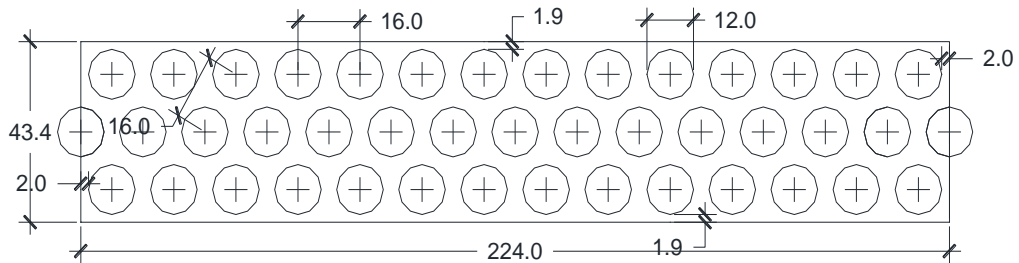


Figure 4.28 The Detailed Size of Plate B₂ (mm).

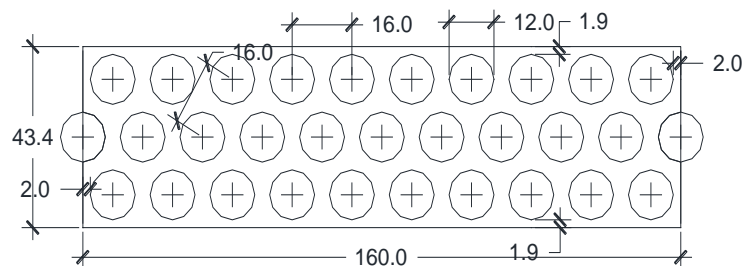


Figure 4.29 The Detailed Size of Plate B₃ (mm).

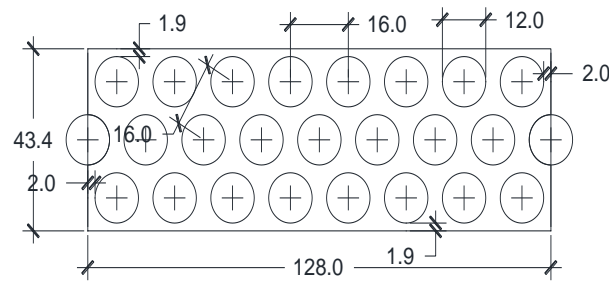


Figure 4.30 The Detailed Size of Plate B₄ (mm).

The third materials was specimens C. Specimens C were prepared from the perforated plate that was treated similar to specimens B in geometry but different in material. Actually, the objective of this experimental test was to define the characteristics of specimens C in both yield strength (F_y) and young's modulus (E) by comparing the results of the previous test. This materials would be utilized as reinforcement of base isolation, therefore the material properties must be discovered. The values of yield strength and young's modulus will be used to describe the material in finite element software.

4.2.3 Testing Procedure

In this section, experimental test setup for the specimens as well as loading procedure are illustrated. The experimental test was set up (see Fig 4.31) in order to obtain the desired data, such as yield strength (F_y) and young's modulus (E) of the perforated plate. The experimental test was conducted in the structural laboratory of Research Center for Human Settlement (Puslitbang Permukiman).

A testing method was realized in the machine tension test. In this stage, test type, material data (material thickness, test sample width, distance between the machine's clamping dies), traction speed, output file type are determined.

The experimentation program was based on the following elements:

- Thickness of the chosen test samples $t = 1.0$ mm
- Set of three test samples
- Speed with which the test sample is stressed at 0.5 mm/s.

d. Acquired output data: breaking load (kN), breaking elongation (mm), maximal stress achieved in the material (MPa), relative elongation corresponding of the maximal stress in the material (%). Beneath the above-mentioned data, the primary data of such test are saved; the characteristic curve in coordinates force (kN) - displacement (mm).



Figure 4.31 The specimens are mounted on the machine.

4.2.4 Summary

All specimens' details for tension test are summarized in Table 4-1. In the first phase, specimens A and B were only involved in the experimental test. The test results would be used to confirm the previous data conducted by O' Donel, then would be applied to the second phase. With the variation of ratio (length to width), a proper test method for perforated plate to determine yield stress is expected.

Table 4.1 Specimens Data of Experimental (Uniaxial Tension) Test

No	Specimen	Label	Unit	Dimension (mm)		Notes
				Length	Width	
1	A	A1	1	210	30	Specimens made of solid plate
		A2	1	210	30	
		A3	1	210	30	
2	B	B1	3	256	43.3	Perforated plate made of solid plate
		B2	3	224	43.3	
		B3	3	160	43.3	
		B4	3	128	43.3	
3	C	C1	3	256	43.3	Perforated Plate Material
		C2	3	224	43.3	
		C3	3	160	43.3	
		C4	3	128	43.3	

4.3 Fabrication of Base Isolation

4.3.1 Introduction

In this section, manufacture process of base isolation are described. A series of procedure was conducted to produce good quality specimen by cooperating with home industry that had a lot of experience in rubber manufacture although the equipment used in manufacturing process of base isolation are able to be classified as traditional apparatus with human labor. In this project, there was only one types of rubber utilized in the manufacturing process denoted rubber-A. The total number of base isolation was two specimens divided into: one specimens for vertical and the one for horizontal. The circular shape was selected

as the dimension for base isolation with 200 mm in diameter and 129 mm in total thickness. The base isolation consists of 2 end-steel plate, 19 perforated plate layers and 20 rubber layers with the thickness of 5 mm, 1 mm, and 5 mm, respectively. The details of base isolation are illustrated in Fig 4.32 and 4.33.

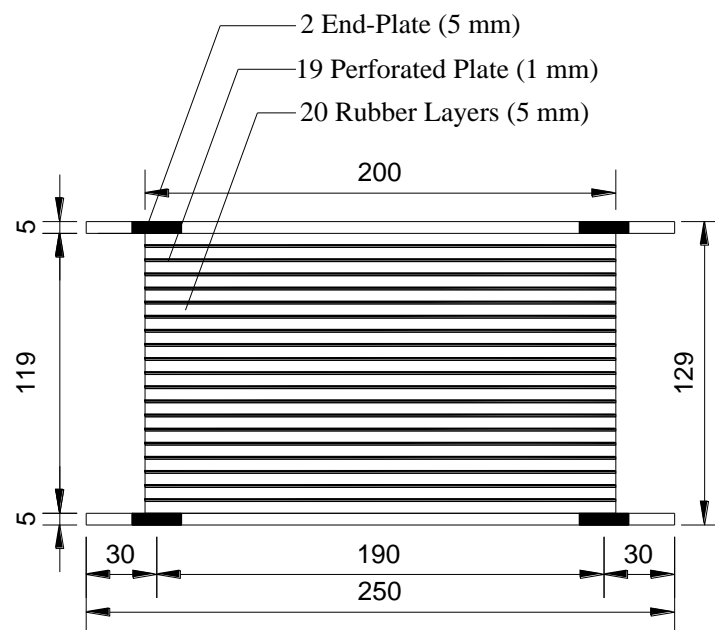


Figure 4.32 Cross section of the base isolation.

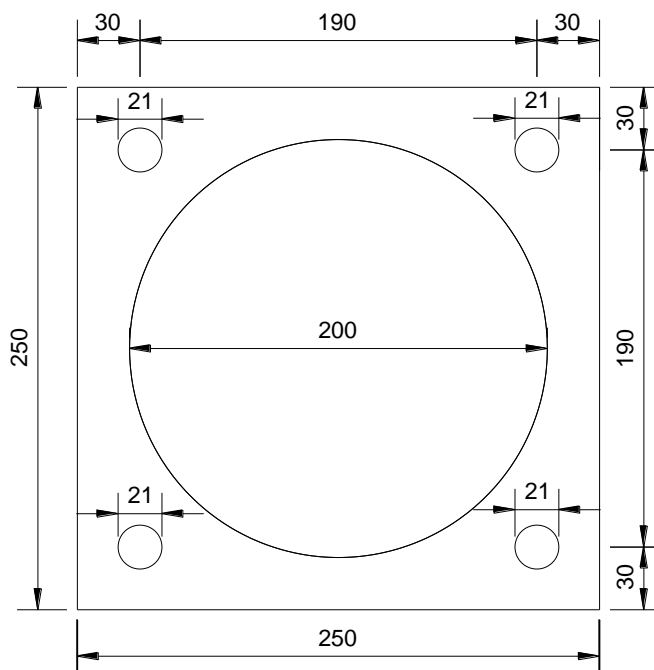


Figure 4.33 Top view of the base isolation.

4.3.2 Preparation of Material.

In this project, base isolation consisted of 3 parts of material; rubber, perforated plate and end-steel plate. The production process cooperated with home industry to produce base isolation system. Therefore the heating system was very simple and operated manually using hydraulic jack in vertical direction. Basically, the heating system was constructed using truss frame to support the vertical hydraulic jack. The truss system must be stiff to provide a good supporting to the hydraulic jack. The support was constructed using two WF frame in horizontal direction. The base plate was made of steel plate to support the molding system and located on the bottom of vertical hydraulic jack. The vertical hydraulic jack was employed to compress the specimen during the heating process as shown in Fig 4.34.



Figure 4.34 Heating system for producing base isolation.

After completing the heating system, the next step in preparing material was creating the mold. The mold was fabricated using steel material and designed similar to the shape of the base isolation that was in circular shape. In creating the mold, it must be ensured that the center of the base isolation was in a proper position and it was not shifted during the heating process. Therefore, four holes in the corner of top and bottom plate in the mold were created to guarantee the end plate did not move freely in lateral direction during the heating process. The details of mold dimension are described in Fig 4.35.

Unlike the mold preparation, the preparation process for perforated plate was easier. Earlier, the perforated plate must be established in circular shape in accordance with the dimension of the base isolation (200 mm). Then, the perforated plate must be cleaned and smeared with a layer of adhesive to make sure it will be attached firmly on the rubber during the heating process as shown in Fig 4.36.

It was somewhat different in the rubber preparation process, raw material for rubber is called *compound* that will be changed into rubber after experiencing the heating process. In this case, the compound was a layer with certain thickness corresponds to the preliminary design size. The compound layer would be cut in circular shape in accordance with the base isolation dimension. Defining the appropriate thickness of compound must be carried out carefully, since it would make the installation process on the mold more difficult. The details of rubber compound are shown in Fig 4.37.



Figure 4.35 Preparation of the mold of base isolation.



Figure 4.36 Preparation of the perforated plate before heating process.



Figure 4.37 Rubber compound layer for base isolation.

The last step in this process was preparing end-steel plate before the heating process as shown in Fig 4.38. The inner surface of end-plate must had rough layers to increase the bond between rubber and plate, therefore the plate was scrubbed with a grinder. Further step, similar with perforated plate, end-steel plate was cleaned and smeared with a layer of adhesive to make sure it will be attached firmly on the rubber during the heating process.



Figure 4.38 Preparation of end-steel plate.

4.3.3 Vulcanization Process

In this section, experimental setup for the specimens are described. The setup contains step by step procedures of vulcanization of base isolation under pressure in the mold. The components were arranged in accordance with the initial design concept of the base isolation that placed the end-steel plate on both the top and bottom level then rubber layers and perforated plates were in the middle. After the preparation processes of material component were completed, the next step was arranging all components into one as illustrated in Fig 4.39 and 4.40. The detailed procedure of the heating process of base isolation are as followed:



Figure 4.39 Arrangement process of rubber and perforated plate.



Figure 4.40 Arrangement result with 20 rubber layers and 19 perforated plates.

- After the arrangement processes of rubber and perforated plate were done, the next step was to set up the mold into heating frame as shown in Fig 4.41. In this case, the process begun with placing the bottom end plate on the heating plate and adjusting the position by locking according to holes in the corner plate. It was conducted to make sure that the components were located in the center. Then, it was followed by locating the molding on the end-plate.

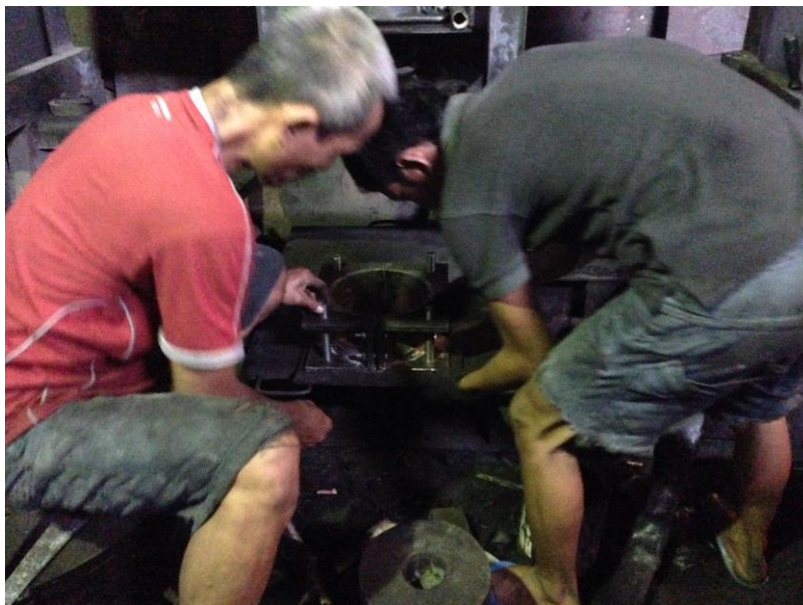


Figure 4.41 Set up the mold into heating frame.

- After the mold setup was complete. It would be continued by placing the rubber-perforated layer into the mold. As shown in Fig 4.42, the height of rubber-perforated layers was similar to the height of mold. The following step was to locate the end plate on the top of rubber and followed by heating plate on the top of end plate. Then, all of them would be locked using pins in four holes corner. By using hydraulic jack, the height of the supported plate was adjusted to the proper position. The heating process was able to start.

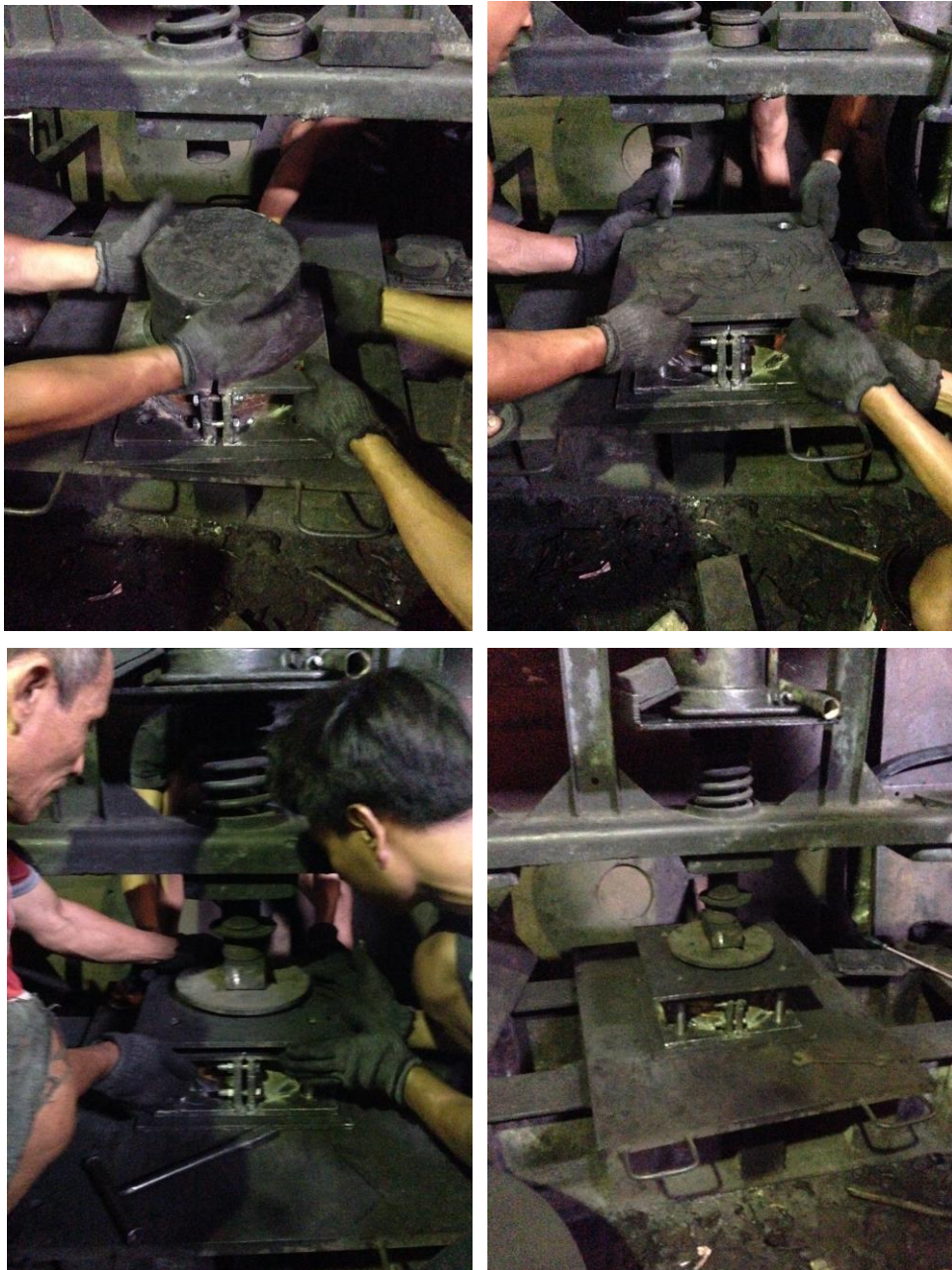


Figure 4.42 Set up the rubber-perforated layers into heating frame.

- A series of setup had been conducted to prepare the vulcanization of base isolation. The final step of this process was heating of rubber-perforated in a mold that spent approximately 2 hours per 1 unit as shown in Fig 4.43. In the heating process, the molding plate was burned through the heating plate and periphery of the mold. The heat was distributed from the surroundings of the mold into the center of the base isolation at the same time. Therefore, all parts of rubber in the mold were expected to be cooked at the same time. After two hours, the final results were illustrated in Fig 4.44.



Figure 4.43 Heating process of base isolation.



(a)



(b)

Figure 4.44 Final result of heating process of base isolation.

4.3.4 Summary

In this chapter, the design and preparation of specimens are described. The vulcanization process used in this research was under pressure in a mold. The rubber industry was considered as a partner in manufacturing process with traditional devices. The heating system spent approximately 2 hours for 1 base isolation. The number of base isolation produced in this step was two specimens with circular shape that consist of 1 specimen for vertical test and 1 specimen for horizontal test as shown in Fig 4.45. The constant thickness of rubber compound layers are considerably important for obtaining a good quality base isolation.



Figure 4.45 Two specimens of isolator with circular shape.

4.4 Base Isolation Test Procedure

4.4.1 Introduction

Base isolation is one of the best devices that had been proven satisfying in reducing earthquake force that is induced to the building. The ability in lengthening fundamental period of the upper structure is the special characteristic of base isolation and considerably important to ensure the acceleration of earthquake reduces significantly. It depends on how the horizontal stiffness are provided in the design process corresponds to the target period of the

superstructure. In addition, high vertical stiffness provided in base isolation that is a hundred times of the horizontal stiffness is one of the advantages of base isolation as dissipation device in the building structure. It means that base isolations are able to be applied for high axial load with their remaining performance in lateral load. In other word, two components that plays an important role in design process of base isolation are vertical stiffness and horizontal stiffness.

In this chapter, the details of procedure in deriving the horizontal and vertical stiffness are presented. The first phase, horizontal test was carried out by combining constant axial compressive load and reversed cyclic lateral displacement to derive the horizontal stiffness. The second phase, vertical test was conducted using reversed cyclic compressive load to investigate the vertical stiffness of base isolation. Moreover, the British standard (BS EN) code was used as the fundamental procedure in the experimental program. The details of test specimens, test set up and instrumentation are described in this chapter.

4.4.2 Experimental Test Setup

This section summarizes the experimental test setup of base isolation which was tested to investigate the vertical and horizontal characteristic of base isolation. The tests were conducted in the R & D Center of Settlement, Ministry of Public Works and Housing, Cileunyi, Bandung, Indonesia. Basically, the apparatus test was specially designed for testing of concrete column. Therefore, to satisfy the requirement for testing of base isolation, additional frame was added on the top and bottom to locate the isolator in the mid-high of test apparatus. The schematic of horizontal and vertical test are shown Fig 4.46 and Fig 4.47, respectively. In conducting both horizontal and vertical test, there were slight differences in the testing setup. The setup details of each test are illustrated below:

(a). Setup of Horizontal Test

The horizontal test must be carried out to derive the horizontal stiffness of base isolation. The test apparatus has a displacement capacity of ± 100 mm in horizontal direction and a load capacity of 500 kN in vertical direction. The vertical and horizontal actuators are able to perform with displacement and load

control. Many sensors were used to monitor the response of the specimen during the test in order to understand the specimen behavior under lateral test. Fig 4.48 present information of instrumentation and device loaction during lateral test.

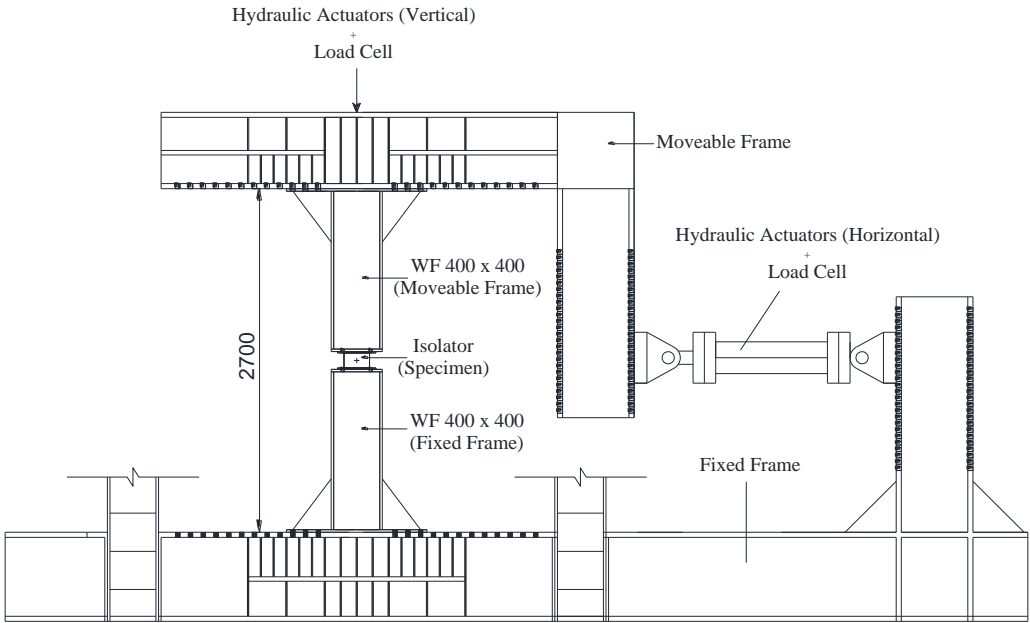


Figure 4.46. Schematic of test apparatus for lateral.

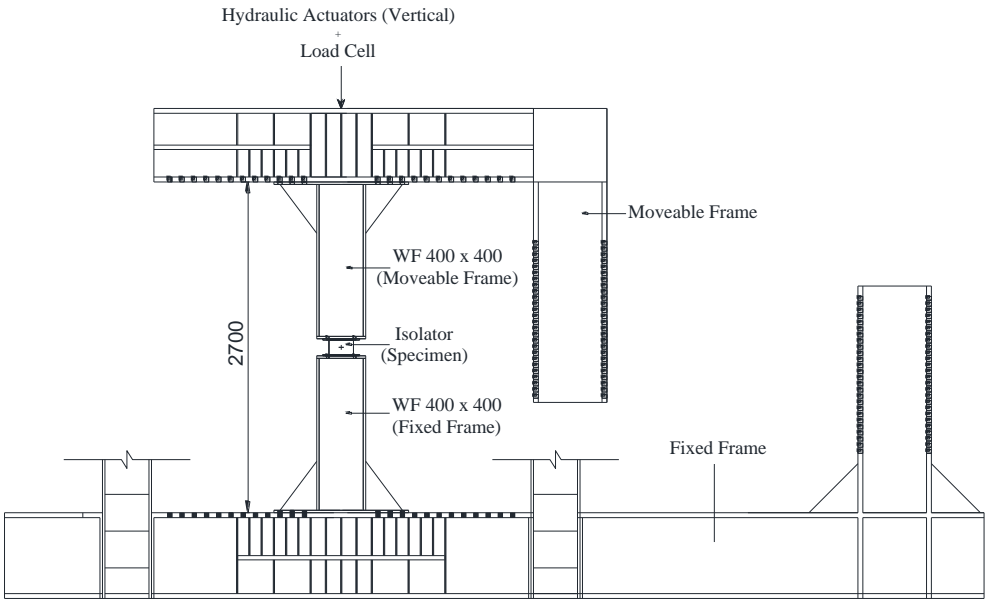
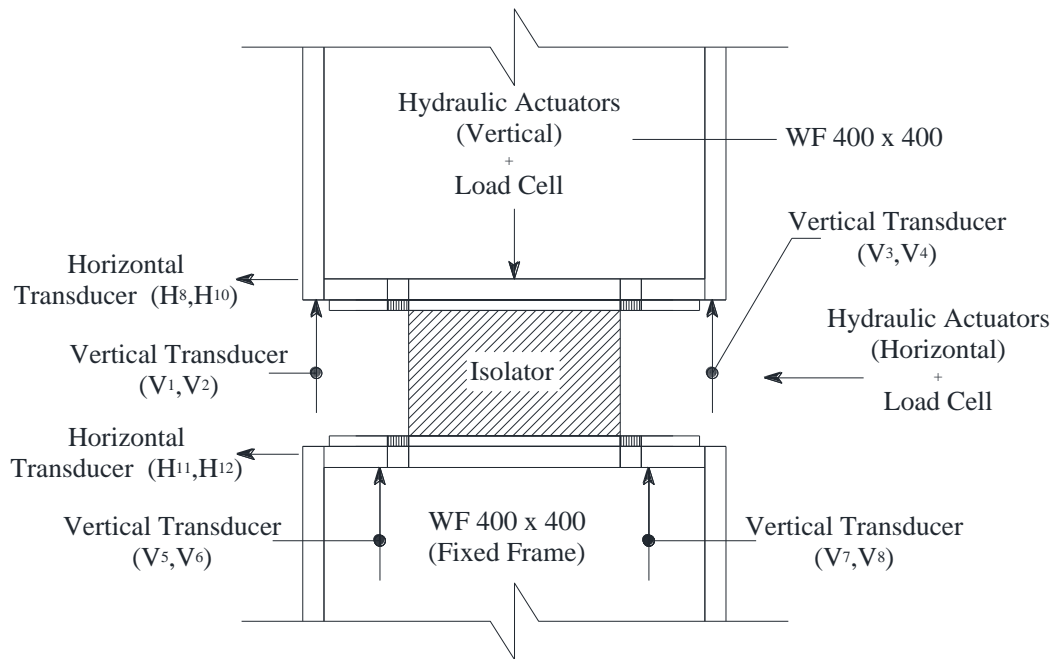


Figure 4.47 Schematic of test apparatus for compression.



(a)



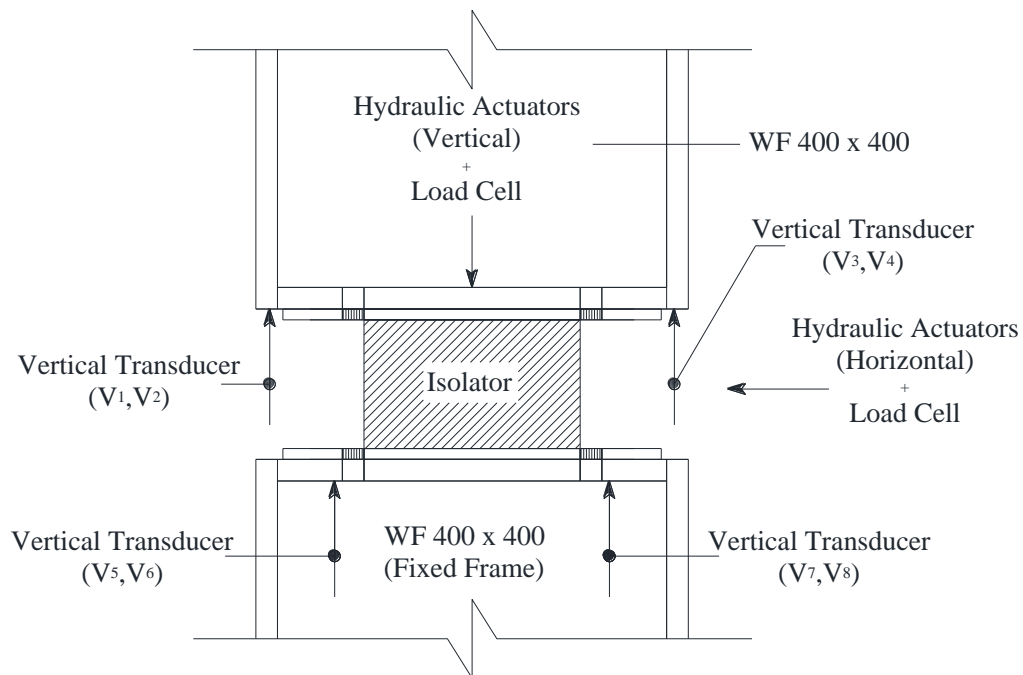
(b)

Figure 4.48 The Instrumentation setup for lateral test.

(a) Photograph; (b) Schematic of instrument setup.



(a)



(b)

Figure 4.49 The Instrumentation setup for compression test.

(a) Photograph; (b) Schematic of instrument setup.

(b). Setup of Vertical Test

The vertical test was slightly different from the horizontal test. In this step, the vertical actuator was only needed to carry out the test. Therefore, a number of sensors used to record lateral displacement and horizontal actuator were neglected and only one specimen was used to perform this test. The testing setup for the vertical test are illustrated in Fig 4.49. Similar with horizontal test, additional sensors were required to observe the vertical characteristics.

4.4.3 Testing Procedure

(a). Horizontal Test

Horizontal test of base isolation had been conducted according to BS EN 15129:2009. The specimens were subjected to constant vertical load then sheared freely in horizontal direction. Initially, the specimens were monotonically loaded to a compressive force of 80 kN at zero horizontal displacement by hydraulic actuator. Once the compressive load was achieved, the vertical reaction frame connected with horizontal actuator was fluctuated over three sinusoidal cycles for each shear strain (i.e. 5%, 10%, 20%, 50%, and 100%) at a frequency of 0.5 Hz . After shear displacement was complete, then the specimens were monotonically unloaded. In the horizontal test, lateral displacement was performed using horizontal displacement control and vertical load was conducted using vertical load control. The loading history of the horizontal test is presented in Fig 4.50 as sinusoidal displacement.

The specimen behavior was characterized by the following parameters during the horizontal test. During the horizontal test, the specimen was characterized by the applied horizontal load and the horizontal displacement of the top frame. The imposed horizontal load was computed as shear load measured by load cell located on the horizontal actuator. The relative horizontal displacement located on the left side of frame was averaged from two LVDT data (H_9 and H_{10}).

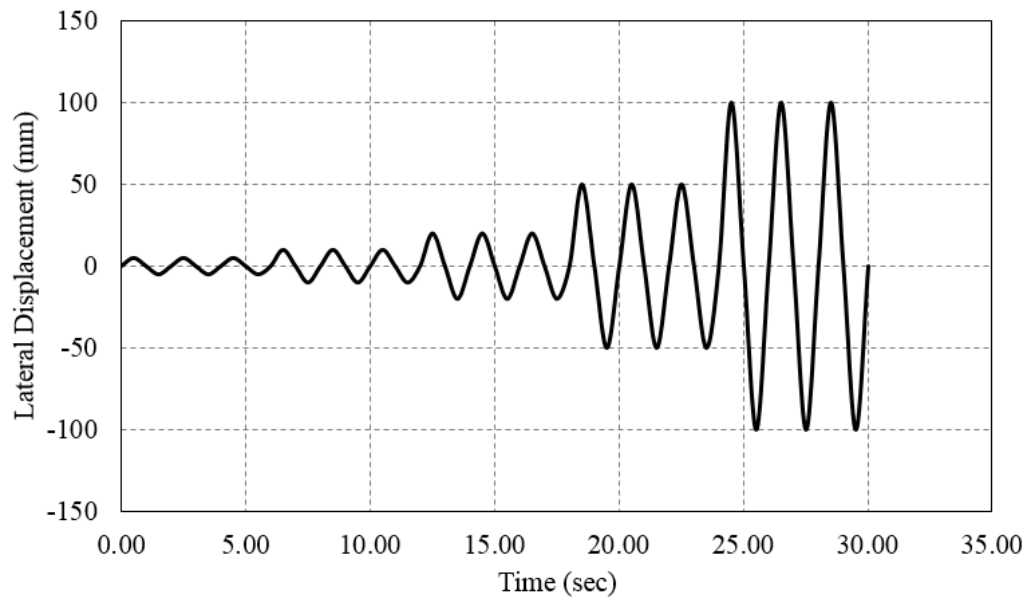


Figure 4.50 Loading history of horizontal test.

(b). Vertical Test

In this chapter, testing procedure of the vertical test is described. As mentioned earlier, the British standard code was used as the fundamental procedure in experimental program. The BS EN 1337-3: 2005 standard was used as the fundamental procedure for vertical test. In vertical test, the specimens were monotonically loaded to a compressive force at zero horizontal displacement. In order to observe the vertical characteristic of isolator, the specimen was loaded in multi vertical load started with 10 kN, 20 kN, 30kN, 40 kN, 80 kN, 100 kN, 150 kN, 200 kN and terminated by 250 kN.

The vertical load was performed using load control. Once the compressive load was achieved, it was fluctuated $\pm 1/3$ of force over three sinusoidal cycles at loading rate of 5.0 ± 0.5 Mpa/min (2.6 kN/sec) and then monotonically unloaded. The loading history for all of compression load are presented in Fig 4.51 to 4.59.

The specimen behavior was characterized by the following parameters during the horizontal test. The vertical load was obtained from the load cell located on the top of frame. The relative vertical displacement between the end plate of the specimen was averaged from four LVDT data (V_1, V_2, V_3 and V_4) that were located at the four corners of the end plates.

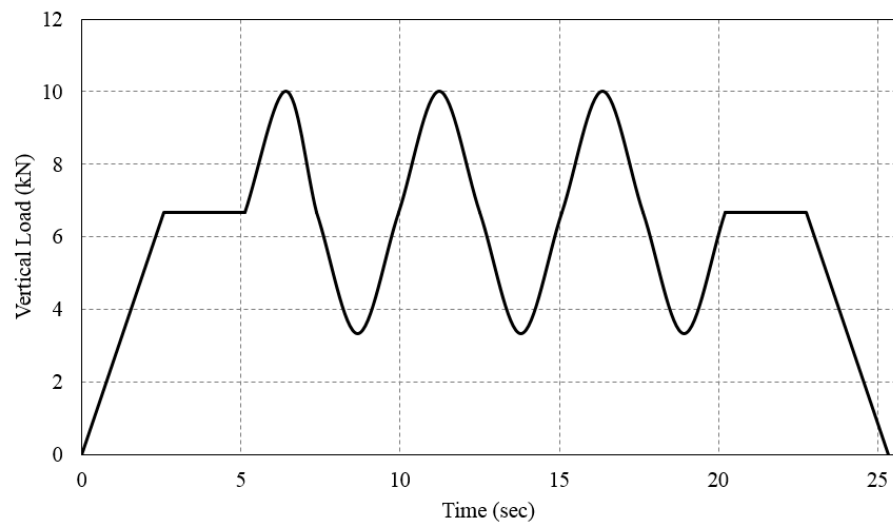


Figure 4.51 Loading history of vertical test of 10 kN.

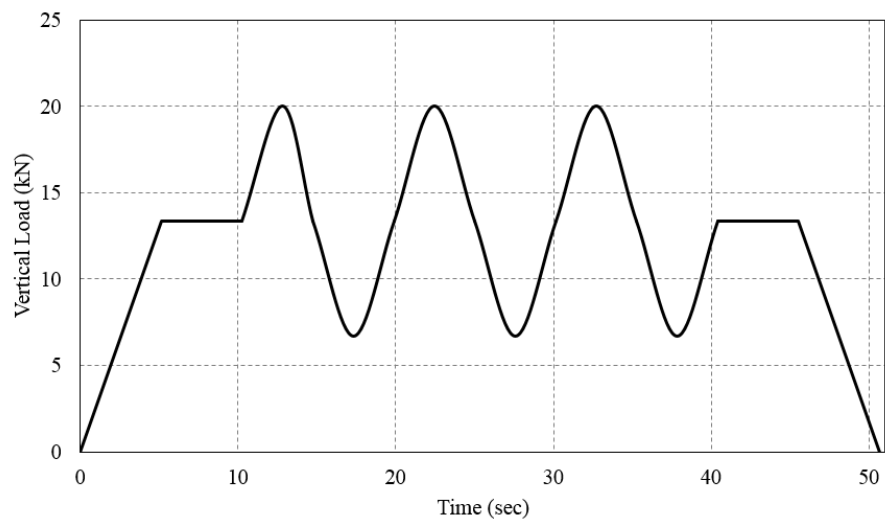


Figure 4.52 Loading history of vertical test of 20 kN.

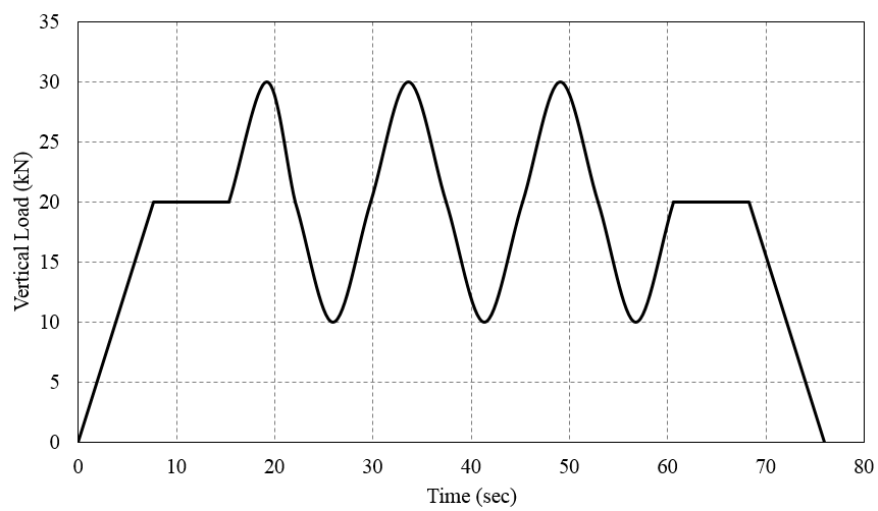


Figure 4.53 Loading history of vertical test of 30 kN.

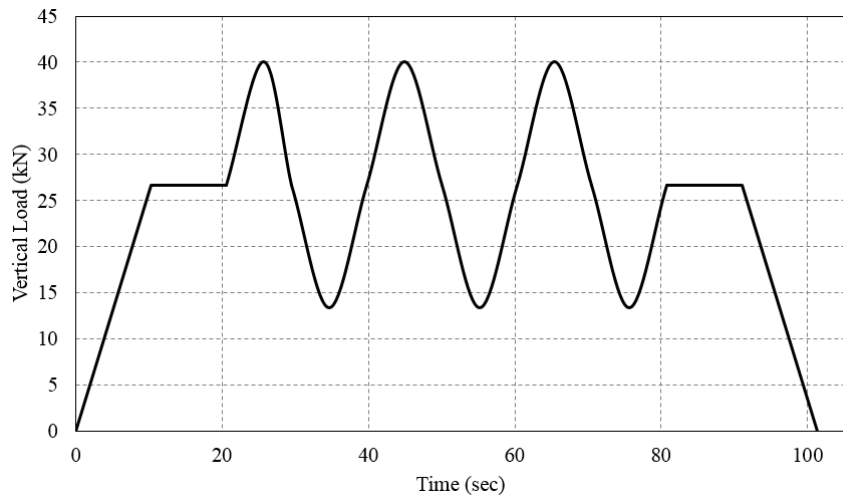


Figure 4.54 Loading history of vertical test of 40 kN.

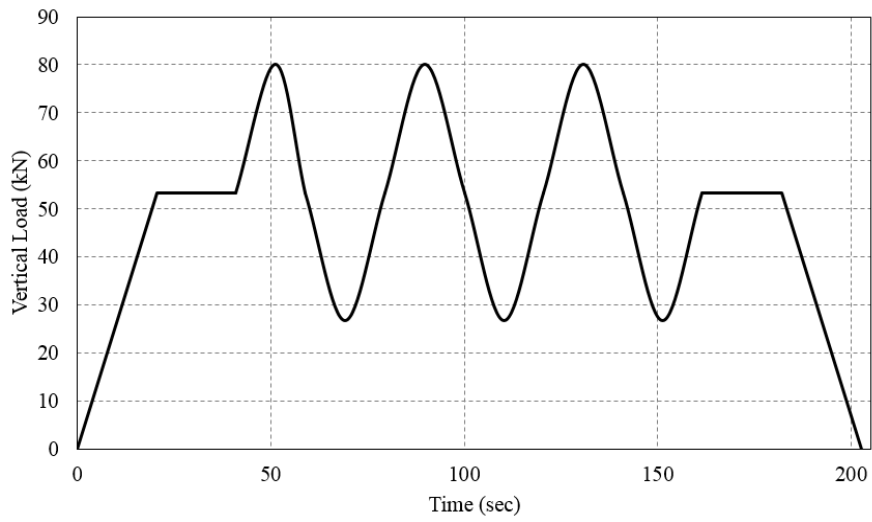


Figure 4.55 Loading history of vertical test of 80 kN.

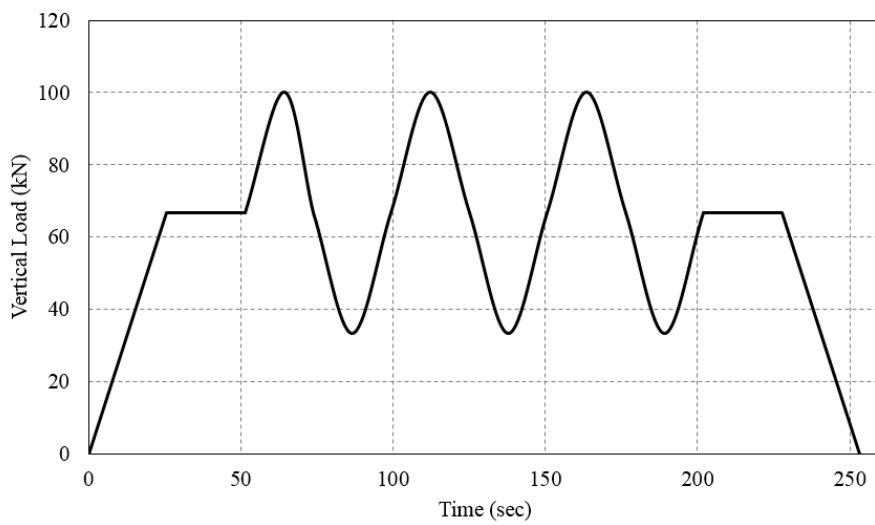


Figure 4.56 Loading history of vertical test of 100 kN.

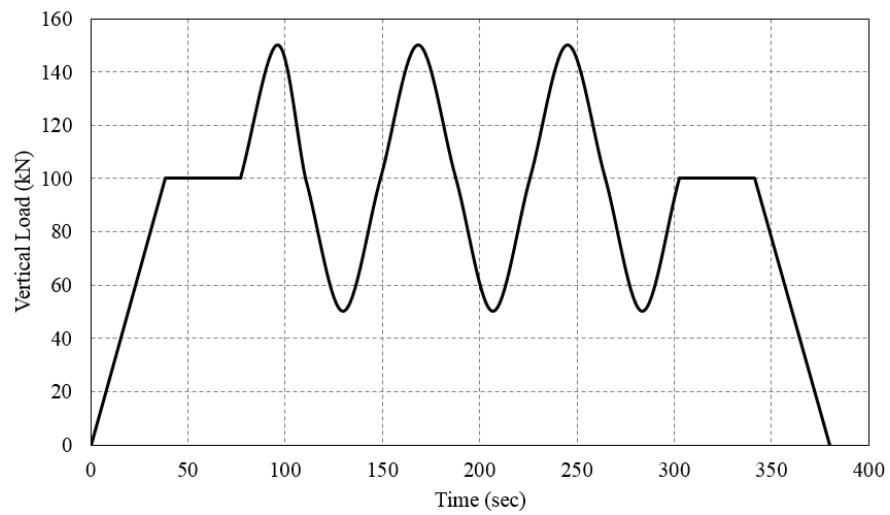


Figure 4.57 Loading history of vertical test of 150 kN.

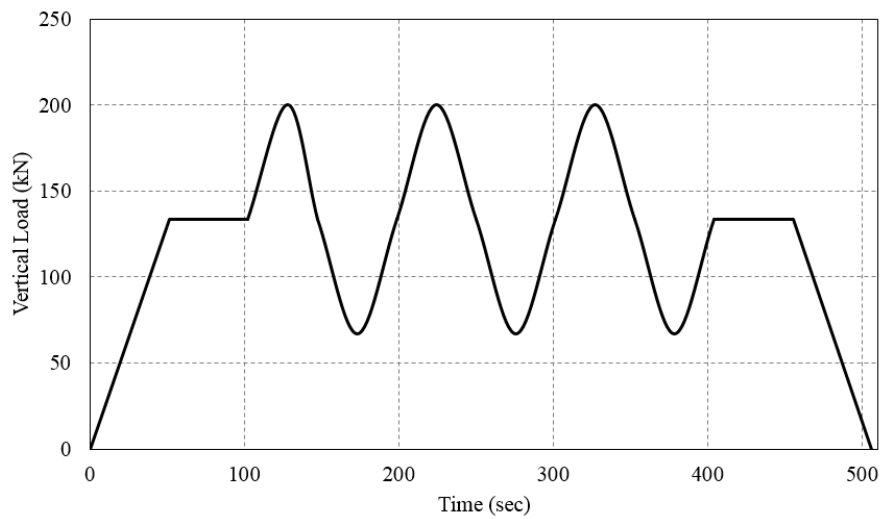


Figure 4.58 Loading history of vertical test of 200 kN.

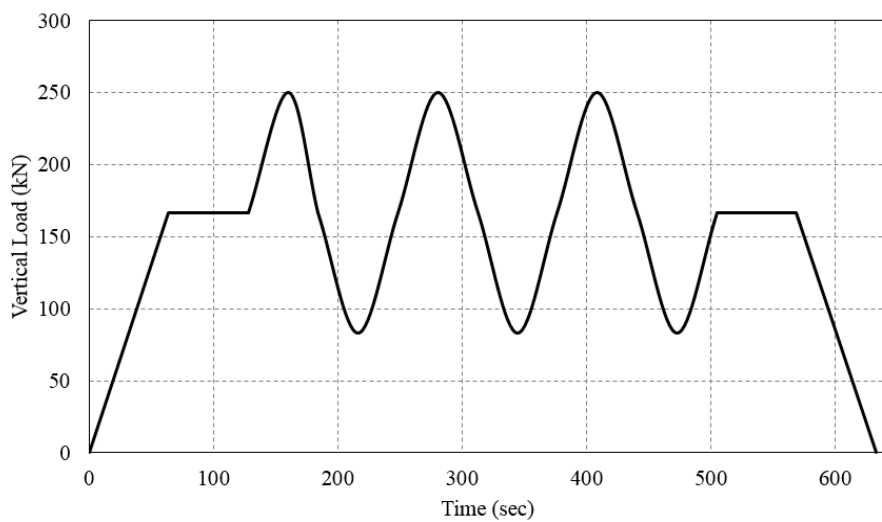


Figure 4.59 Loading history of vertical test of 250 kN.

4.4.4 Summary

In this section, testing procedures of the experimental test are illustrated. There were two types of experimental test, vertical test and horizontal test. Actually, vertical and horizontal test were conducted to derive the vertical stiffness and horizontal stiffness of base isolation, respectively. All of the tests adopted the British Standard (BS) as the fundamental procedure to obtain the base isolation characteristics. In performing vertical test, BS EN 1337-3:2005 was used as the basic procedure in obtaining vertical characteristics. At least one specimen was used in vertical test. The test performed with multi axial load (10 kN, 20 kN, 30 kN, 40 kN, 80 kN, 100 kN, 150 kN, 200 kN and 250 kN) to observe the characteristic of isolator under different axial load.

In other case, BS EN 15129:2009 was applied for the horizontal test to derive lateral characteristics of isolator. There was one specimen used in this test for deriving the lateral characteristics. In performing horizontal test, five different level of lateral displacement (i.e. 5%, 10%, 20%, 50%, and 100%) at a frequency of 0.5 Hz was used to investigate the characteristic of isolator under lateral load.



Figure 4.60 A number of experimental specimens.

A series of test has been completed. A number of specimens test has been obtained as shown in Fig 4.60. The characteristics of base isolation are observed,

typically for horizontal stiffness. Horizontal stiffness is a critical issue in this research. The values of horizontal stiffness are expected to be more flexible for obtaining the primary objective of this research, which is creating base isolation system for light structures with a fundamental period of 2 second.

"This page is intentionally left blank"

CHAPTER 5

DATA ANALYSIS

5.1 Rubber Material

5.1.1 Arrangement of Stress- Strain Data Test

In this chapter, detailing procedure to obtain stress-strain data from experimental test results are described specifically. It is required in modeling rubber material on finite element program, especially by ANSYS. This step must be conducted since the result derived from experimental are somewhat different than required by finite element software. Therefore, arrangement of experimental data test must be carried out to match with input files that required in finite element program.

As described earlier, the results from experimental test are loading-unloading curve with slow cyclic loading (SCL). The rubber specimens are stretched to certain strain level then released to zero strain while the stress- strain data are recorded during the test. It was repeated until the curve exhibits stable behavior, as shown in Fig. 2.2.

The structural properties of elastomers change significantly during the first several times that the material experiences straining. This behavior is commonly referred to as the Mullin's effect. If an elastomer is loaded to a set strain level followed by complete unloading to zero stress several times, the change in structural properties from cycle to cycle as measured by the stress strain function will diminish. When the stress strain function no longer changes significantly, the material may be considered to be stable for strain levels below that particular set strain maximum. If the rubber is taken to a new higher strain level, the structural properties will again change significantly.

Commonly, the stress- strain curve of hyperelastic experimental test are categorized to be three type, they are loading curve at first strain, unlading curve and loading curve, as shown in Fig. 5.1

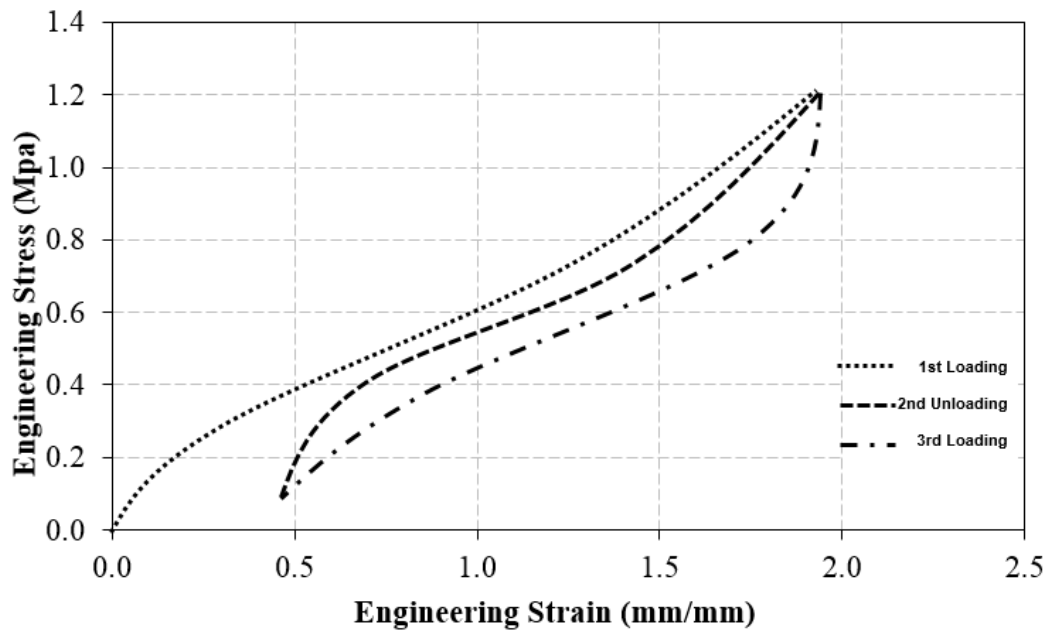


Figure 5.1 Type of curve on experimental test data.

Several observations can be made regarding the behavior in Fig 5.1, which are true to a varying degree for all elastomers.

1. The stress strain function for the 1st time an elastomer is strained is never again repeated. It is a unique event.

2. The stress strain function does stabilize after between 3 and 20 repetitions for most elastomers.

3. The stress strain function will again change significantly if the material experiences strains greater than the previous stabilized level. In general, the stress strain function is sensitive to the maximum strain experienced.

4. The stress strain function of the material while increasing strain is different than the stress strain function of the material while decreasing strain.

5. After the initial straining, the material does not return to zero strain at zero stress. There is some degree of permanent deformation.

Because the required data input into finite element program as a single stress-strain curve model, one must input a stress strain function that is relevant to the loading situation expected in the application. Naturally, this may be difficult

because the very purpose of the analysis is to learn about the stress strain condition in the part. However, there are a few guidelines that may be considered.

a. If the focus of the analysis is to examine the first time straining of an elastomeric part, then use the first time stress strain curves from material tests. This might be the case when examining the stresses experienced when installing a part for the first time.

b. If the focus of the analysis is to understand the typical structural condition of a part in service, use stress strain curves derived by cycling a material until it is stable and extracting the stabilized increasing strain curve.

c. If the focus of the analysis is to understand the unloading performance of a part in service by examining the minimum stress conditions, extract a stabilized decreasing strain curve.

d. Perform experiments at strain levels that are reasonable for the application. Large strains that greatly exceed those that the part will experience will alter the material properties such that they are unrealistic for the application of interest.

Generally, the determine of strain level of data test depends on its application that how the rubber will behave in real case. In this research, the increasing strain curve are utilized as input files into finite element program for all of the test. The strain level at 100%, are selected for uniaxial test, planar shear test and equal biaxial extension test. Meanwhile, the strain level for volumetric test is selected at strain 10%. The details procedure for all test are described as follows:

5.1.1.1 The Stress- Strain Data Test of Uniaxial Tension.

The uniaxial tension test has been carried out with 3 samples; sample A, sample B and sample C. In other word, there will be three stress- strain data for uniaxial test only. The average of three stress- strain data will be used as input file into finite element program. As discuss earlier, the stabilized loading is going to be used as input file into finite element software. The stress- strain data used for uniaxial tension analysis are stress and strain, as shown in Fig 5.4; 4.5 and 4.6, that are sample A, sample B and Sample C, respectively. The selecting curve data

for sample-A at 100% strain level, are given below (Fig 5.2). In addition to, a piece of the data needs to be cut from a large data set because the stress strain “slice” has non zero initial stress and strain point, as shown in Fig 5.3.

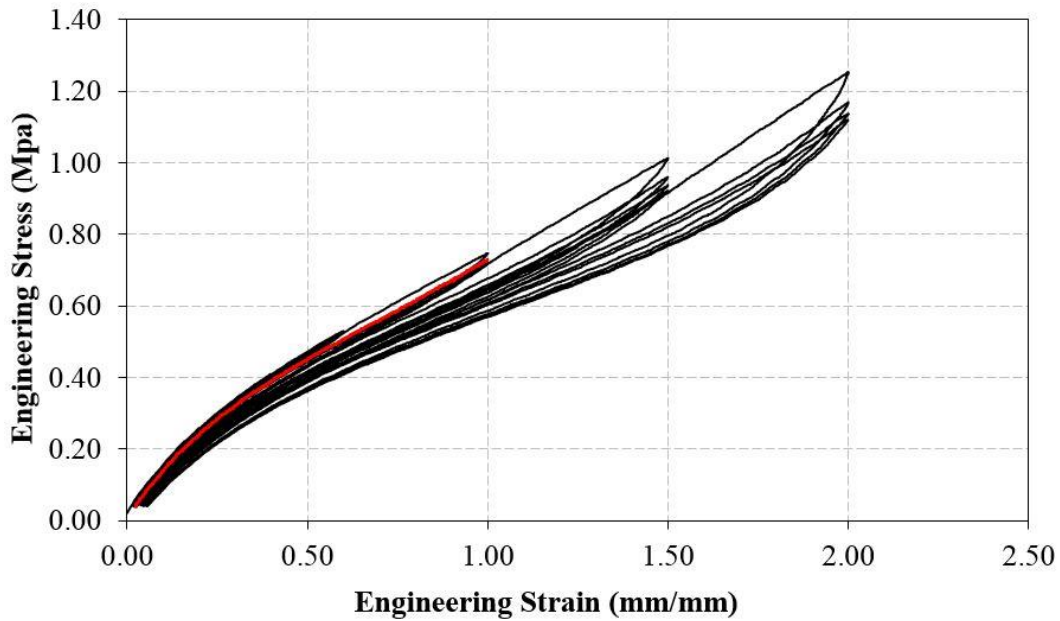


Figure 5.2 Selecting curve (red line) uniaxial tension data for sample A at 100% strain level.

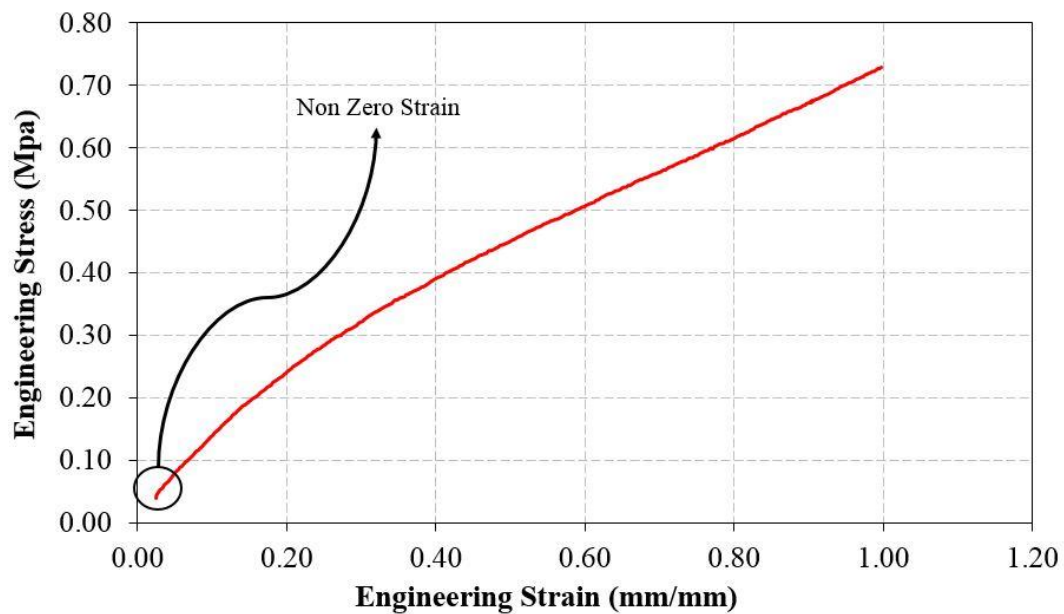


Figure 5.3 Single view for selecting curve (red line) uniaxial tension data for sample A at 100% Strain Level.

In order to reduce the number of data points in the data set, corrections need to be made due to the initial condition of selecting curve has non zero initial stress and strain. The following alterations need to occur:

1. Slice out the selected curve (as shown in Fig 5.3).
2. Subtract and note the offset strain.
3. Divide all strain values by (1+ offset strain) to account for the “new” larger stabilized gage length. The formula is as follow:

$$\varepsilon' = \frac{\varepsilon_i - \varepsilon_0}{1 + \varepsilon_0} \quad (5.1)$$

where ε' is new strain ; ε_i original strain in i -th and ε_0 initial point on original strain.

4. Multiply all stress values by (1+ offset stress) to account for “new” smaller stabilized cross section area. The formula is given by:

$$\sigma' = (\sigma_i - \sigma_0) \times (1 + \varepsilon_0) \quad (5.2)$$

where σ' is new stress ; σ_i original stress in i -th; σ_0 initial point on original stress; and ε_0 initial point on original strain. The data format is given in Fig 5.4.

5. The first stress value should be very near zero but shift the stress values this small amount so that zero strain has exactly zero stress. The result of modified curve for tension test are illustrated in Fig 5.5.

Column=	A	B	C	D
Row	ε'	s'	ε	s
			$=(A1-\$A\$1)/(\$1+\$A\$1)$	$=(B1-\$B\$1)*(\$1+\$A\$1)$
1	0.024865	0.044164	0.000000	0.000000
2	0.027446	0.047640	0.002518	0.003562
3	0.030118	0.050550	0.005126	0.006545
4	0.032790	0.053932	0.007733	0.010011
5	0.035508	0.058183	0.010385	0.014368
6	0.037627	0.061932	0.012452	0.018210
7	0.040195	0.065326	0.014958	0.021688
8	0.042770	0.068040	0.017471	0.024470
9	0.044459	0.071635	0.019119	0.028154
10	0.046675	0.074816	0.021281	0.031414
.	0.049128	0.077069	0.023674	0.033723
.	0.051793	0.079955	0.026275	0.036681
.	0.053915	0.083869	0.028345	0.040692
etc	0.056067	0.085873	0.030445	0.042746

$$\varepsilon' = \frac{\varepsilon_i - \varepsilon_0}{1 + \varepsilon_0}$$

$$\sigma' = (\sigma_i - \sigma_0) \times (1 + \varepsilon_0)$$

Figure 5.4 Reduced extracted data format for uniaxial tension.

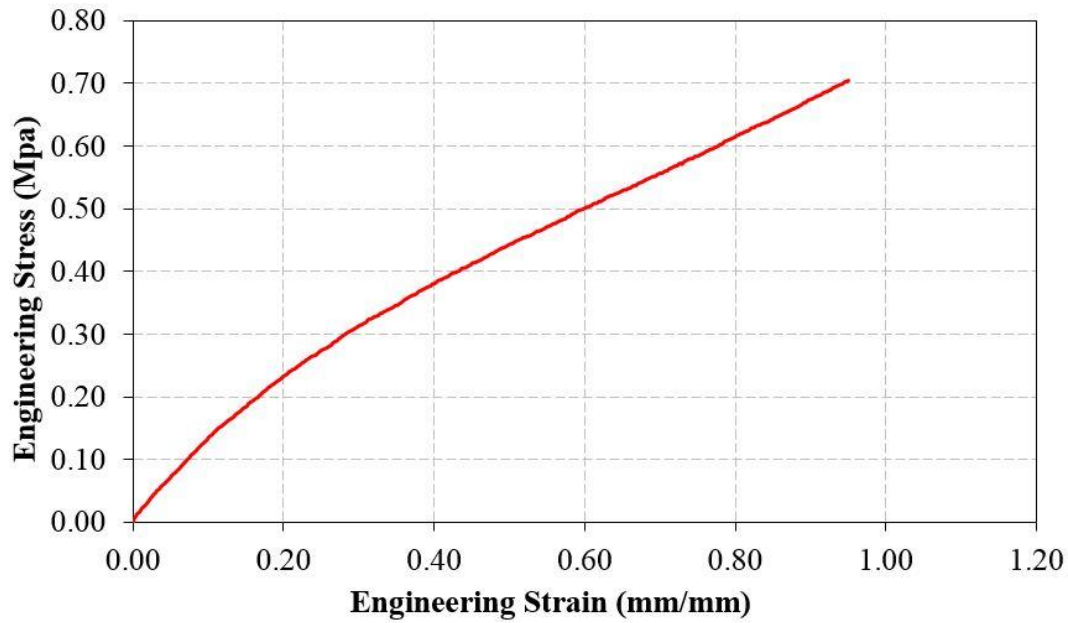


Figure 5.5 Modified of selecting curve data for sample-A at 100% strain level.

As described previous section, there are three sample test that conducted for uniaxial tension test. The remining stress-strain data, sample-B and sample-C, will be considered with similar method such as sample-A, in order to derive the selection curve stress-strain data. The results of all the test are presented in Fig 5.6.

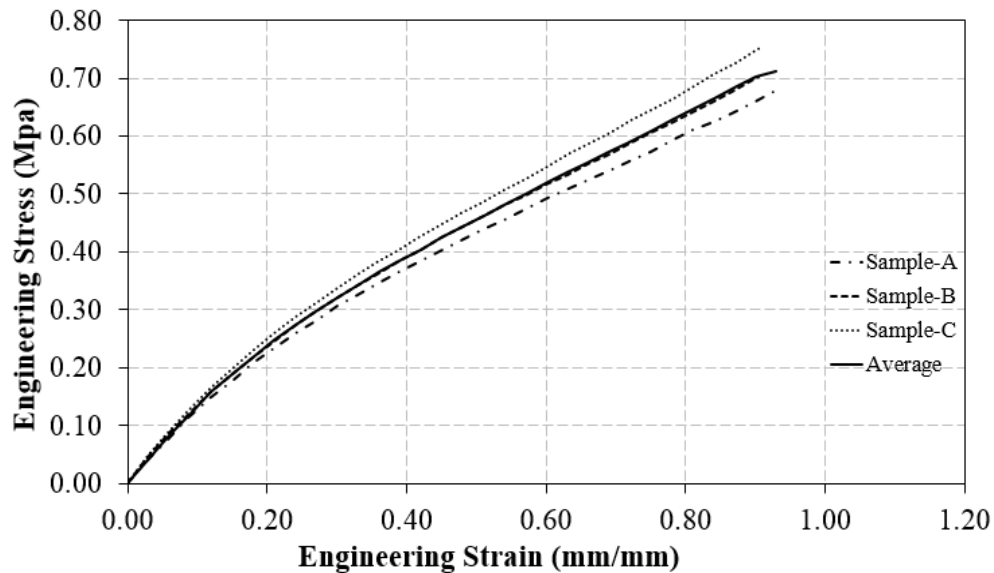


Figure 5.6 Selecting curve of tension test with three data test at 100% Strain Level.

5.1.1.2 The Stress- Strain Data Test of Planar Shear.

The planar shear test were carried out with 3 samples; sample A, sample B and sample C. In other word, there will be three stress- strain data for planar shear test only. The average of three stress- strain data will be used as input file into finite element program. As discuss earlier, the stabilized loading is going to be used as input file into finite element software. The stress- strain data used for planar shear analysis are stress and strain, as shown in Fig 5.10; 4.11 and 4.12, that are sample A, sample B and Sample C, respectively. The selecting curve data for sample-A at 100% strain level, are given below (Fig 5.7). In addition to, a piece of the data needs to be cut from a large data set because the stress strain “slice” has non zero initial stress and strain point, as shown in Fig 5.8.

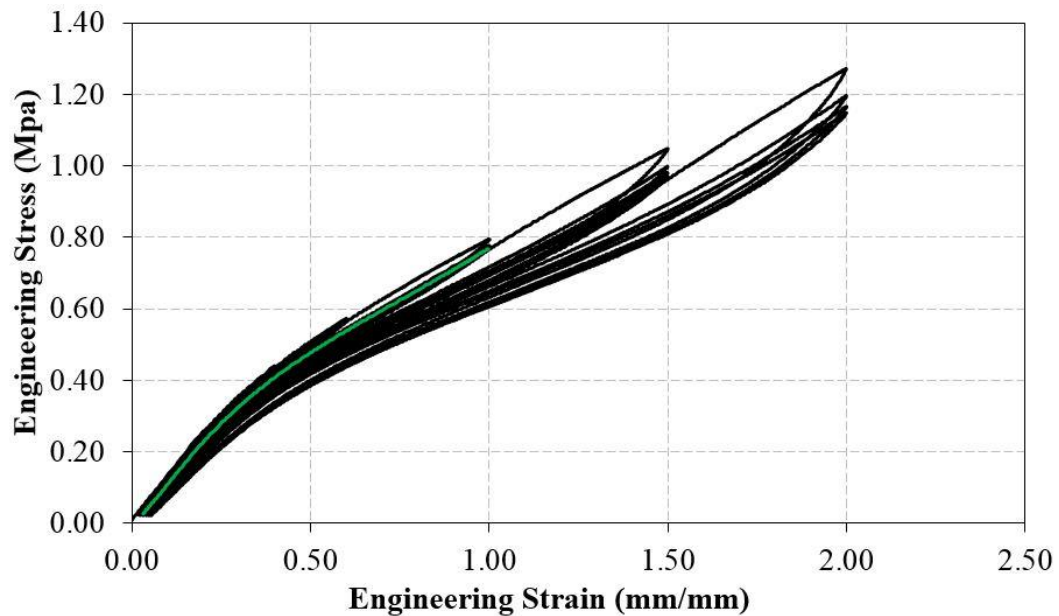


Figure 5.7 Selecting curve (green line) planar shear data for sample-A at 100% Strain Level.

The first stress value should be very near zero but shift the stress values this small amount so that zero strain has exactly zero stress. The modified method is equal to uniaxial tension test. The result of arranged curve for planar shear test are shown in Fig 5.9.

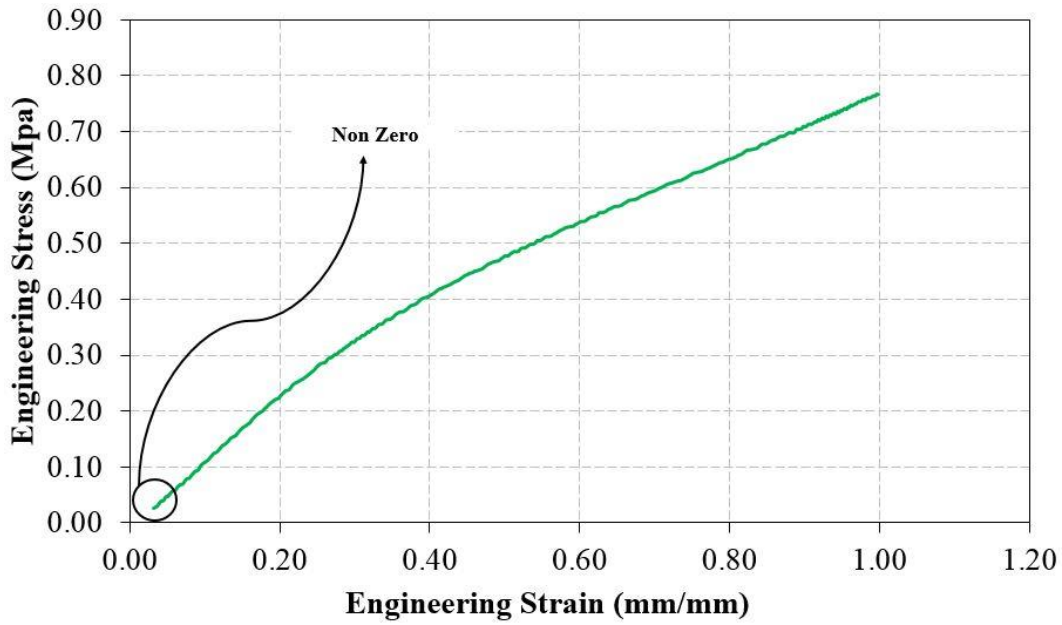


Figure 5.8 Single view for selecting curve (green line) planar shear data for sample-A at 100% Strain Level.

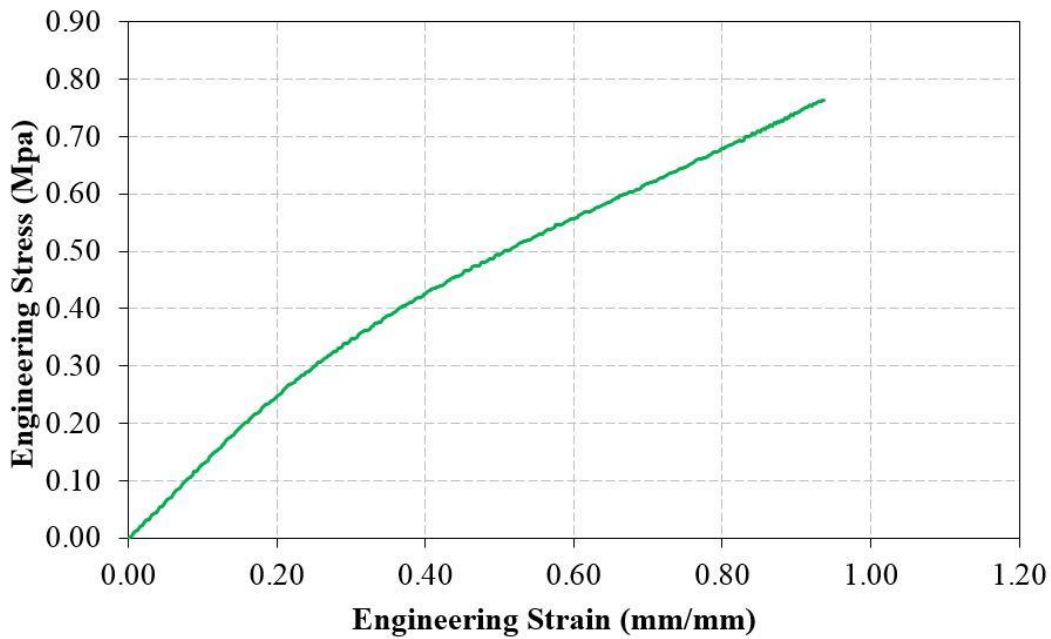


Figure 5.9 Modified of selecting curve planar shear data for sample-A at 100% strain level.

As described previous section, there are three sample test that conducted for planar shear test. The remining stress-strain data, sample-B and sample-C, will be considered with similar method such as sample-A, in order to derive the selection curve stress-strain data. The results of all the test are presented in Fig 5.10.

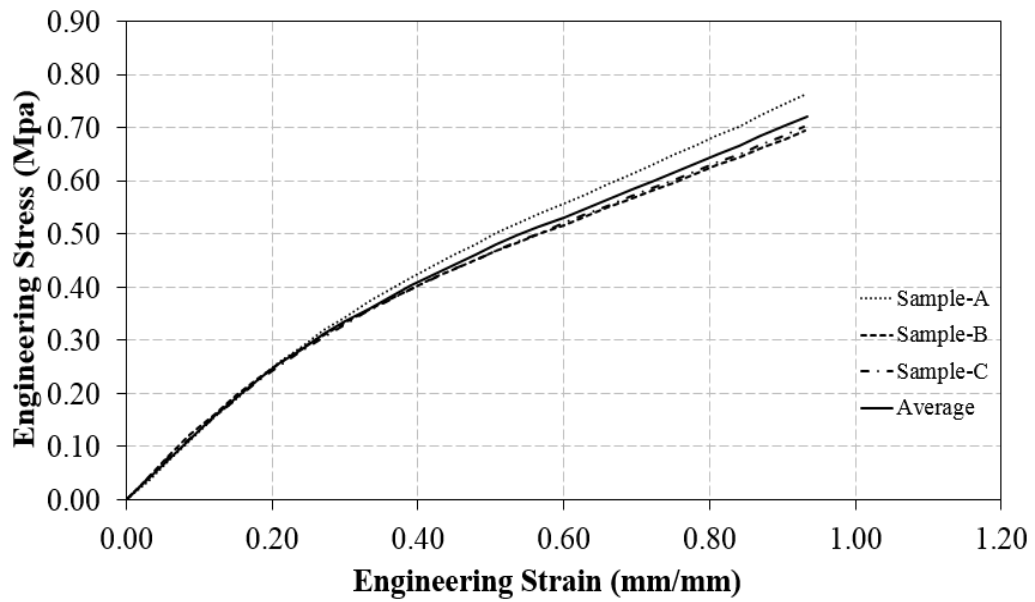


Figure 5.10 Selecting curve of planar shear test with three data test at 100% strain level.

5.1.1.3 The Stress- Strain Data Test of Equal Biaxial.

Similarly with pervious test, the equal biaxial test were conducted with 3 samples; sample A, sample B and sample C. In other word, there would be three stress- strain data for equal biaxial test only. The average of three stress- strain data will be used as input file into finite element program. The stabilized loading is going to be used as input file into finite element software. The stress- strain data used for equal biaxial analysis are stress and strain, as shown in Fig 5.16; 4.17 and 4.18, that are sample A, sample B and Sample C, respectively. The selecting curve data for sample-A at 100% strain level, are given below (Fig 5.11). In addition to, a piece of the data needs to be cut from a large data set because the stress strain “slice” has non zero initial stress and strain point, as shown in Fig 5.12.

The first stress value of selecting curve should be very near zero but shift the stress values this small amount so that zero strain has exactly zero stress. The modified method is equal to equal biaxial test. The result of arranged curve for planar shear test are shown in Fig 5.13.

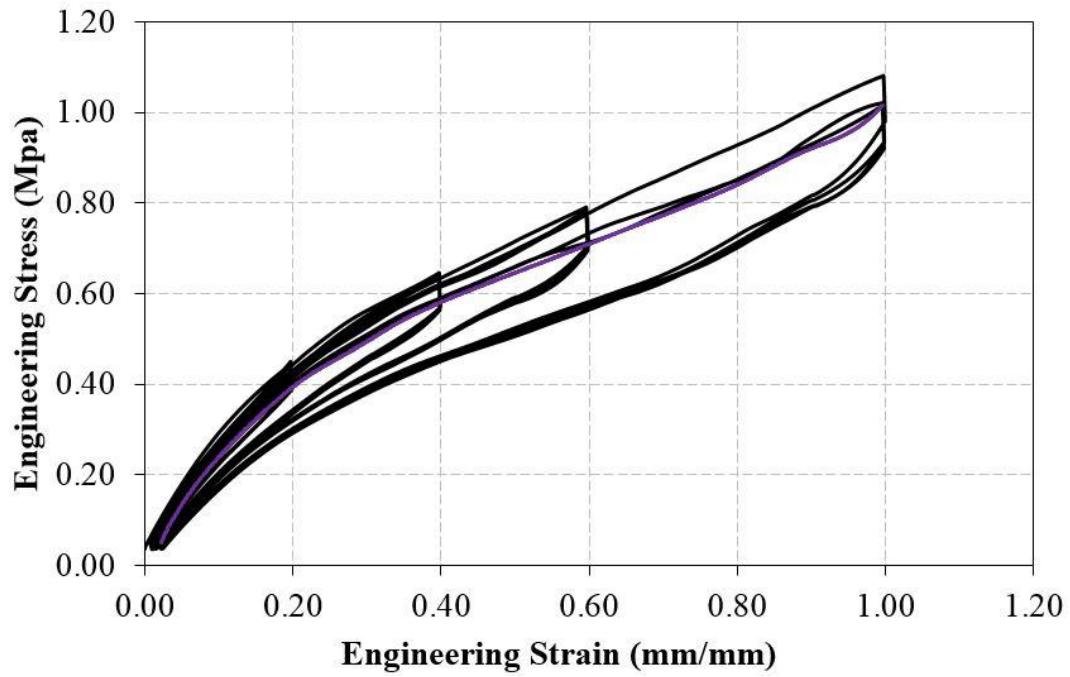


Figure 5.11 Selecting curve (purple line) equal biaxial data for sample-A at 100% strain level.

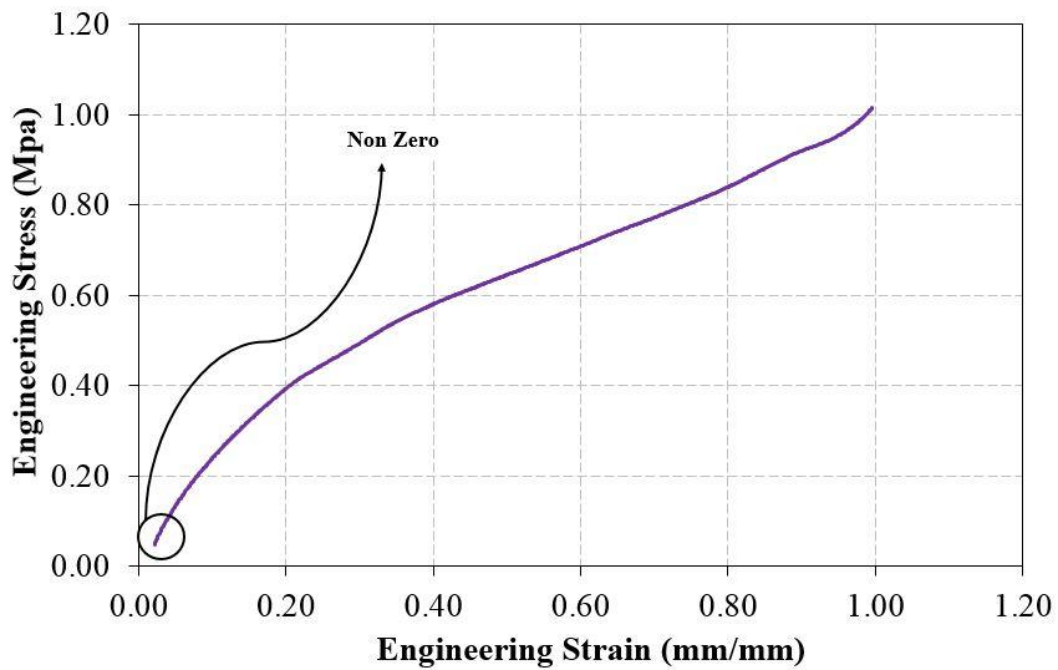


Figure 5.12 Single view for selecting curve (purple line) equal biaxial data for sample-A at 100% Strain Level.

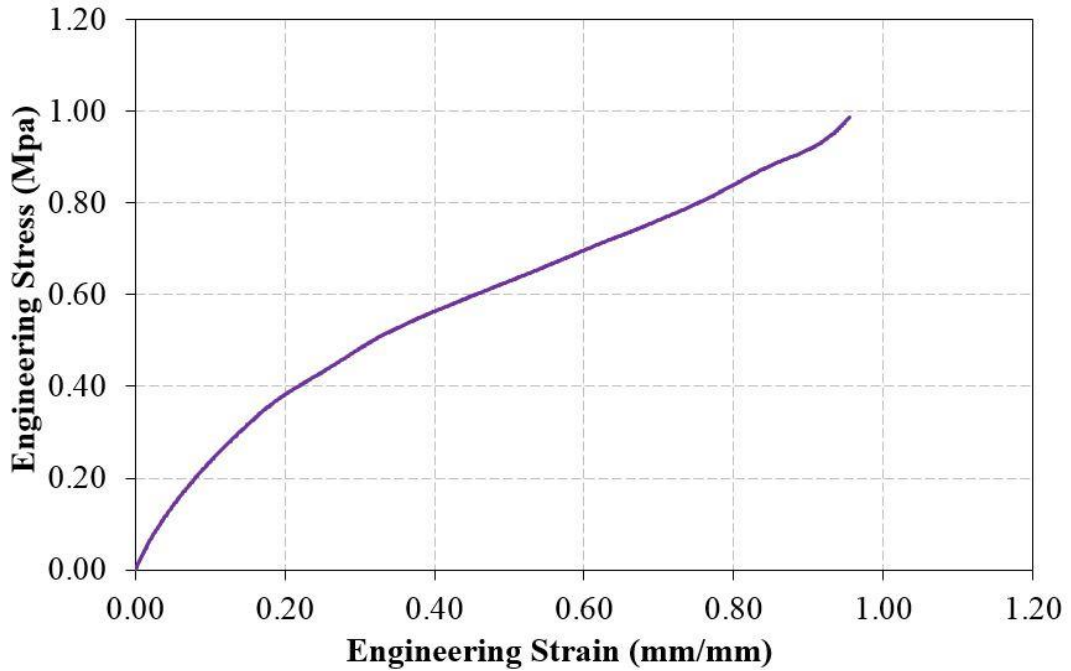


Figure 5.13 Modified of selecting curve equal biaxial data for sample-A at 100% strain level.

As mentioned earlier, three sample are conducted to derive vary data test in equal biaxial test. A remining stress- strain data test, such as sample-B and sample-C, are similarly considered as sample-A that described above for determining selection curve. The curves for all specimen are given in Fig 5.14.

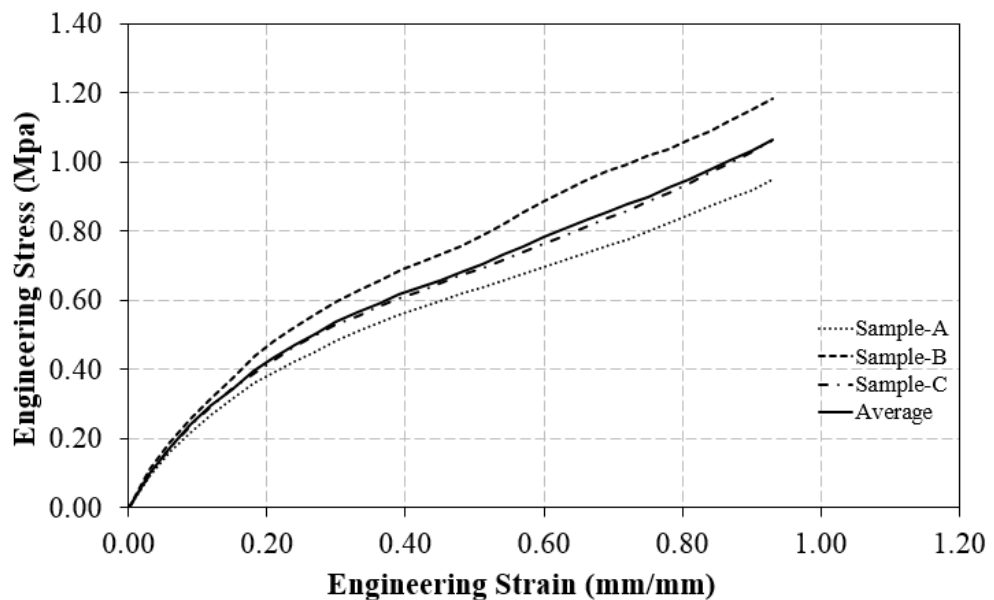


Figure 5.14 A Number of selecting curve of equal biaxial test (100% Strain).

5.1.1.4 The Stress- Strain Data Test of Volumetric.

In volumetric compression experiment, there is almost no “softening” of material. However, during the initial loading of the specimen in the fixture, some air is displaced. As such, the initial volume needs to be corrected. The slow cyclic loading approach is used primarily to find the new start volume by loading the specimen and unloading to a near zero stress point which is the new start position. This may be repeated a few times.

The stress- strain data used for equal biaxial analysis are stress and strain, as shown in Fig 5.22; 4.23 and 4.24, that are sample A, sample B and Sample C, respectively. The selecting curve data for sample-A at 10% strain level, are given below (Fig 5.15). In addition to, a piece of the data needs to be cut from a large data set because the stress strain “slice” has non zero initial stress and strain point, as shown in Fig 5.16.

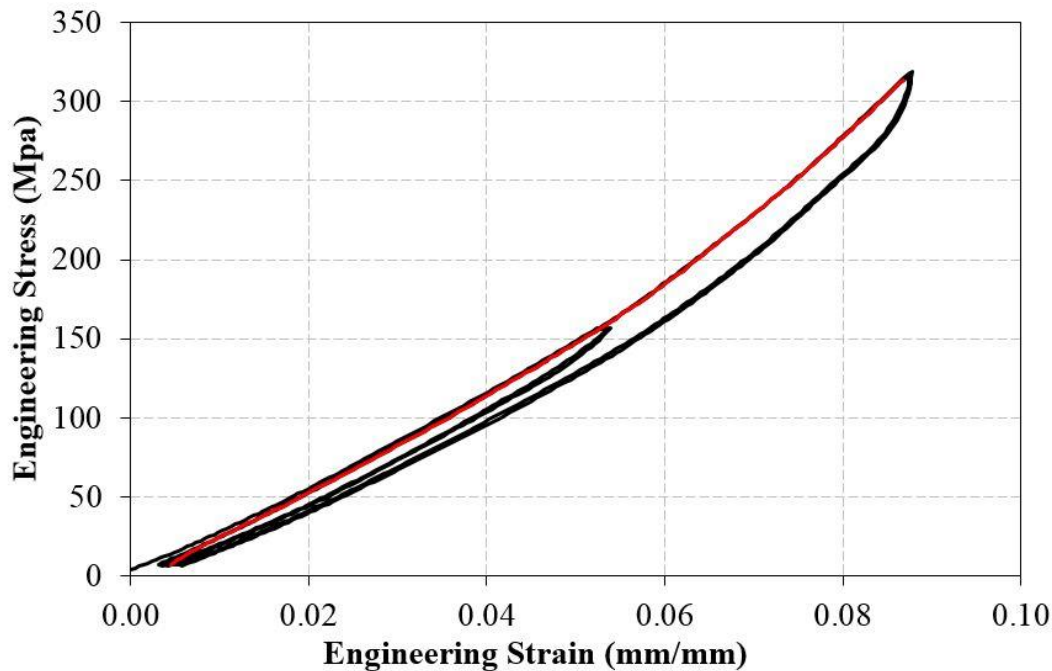


Figure 5.15 Selecting curve (red line) volumetric data for sample-A.

The volumetric compression experiment is performed to measure the relationship between hydrostatic and volume change in dense elastomer. The stress- strain experimental data experiments may need to be modified for input into curve fitters in finite element program. The volumetric compression experimental data may be used in curve fitters.

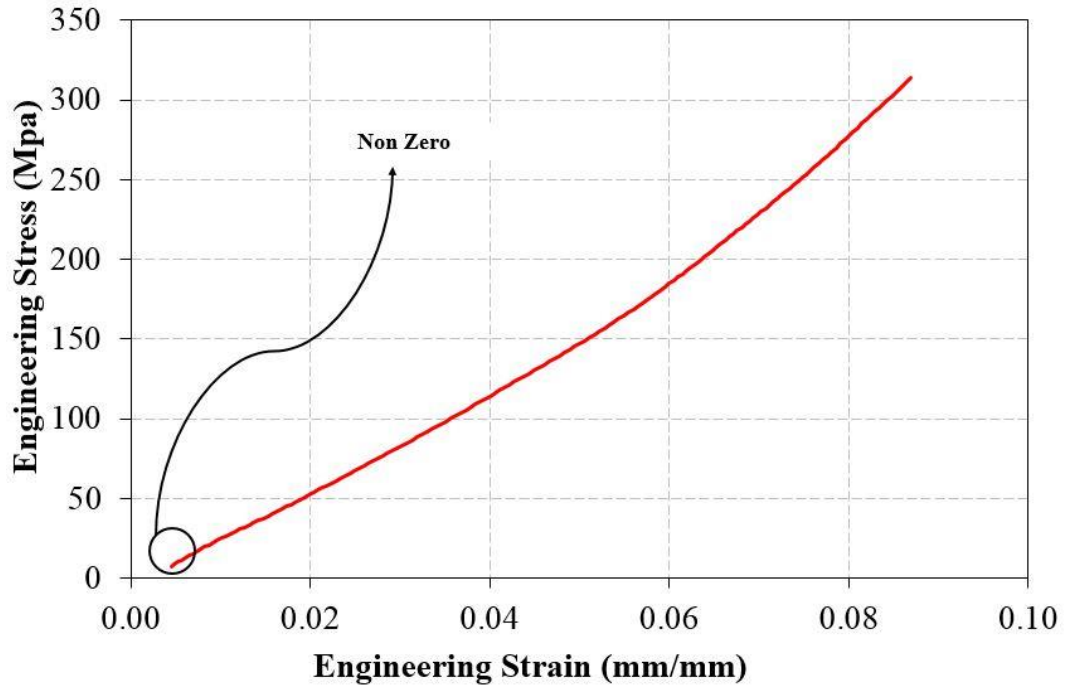


Figure 5.16 Single view for selecting curve (red line) volumetric data for sample-A.

In order to reduce the number of data points of volumetric, the procedure is somewhat different in calculating “new” stress. The following alterations need to occur:

1. Slice out the selected curve (as shown in Fig 5.16).
2. Subtract and note the offset strain.
3. Divide all strain values by (1+ offset strain) to account for the “new” larger stabilized gage length. The formula is as follow in Eq 5.1.
4. Multiply all stress values by (1+ offset stress) to account for “new” smaller stabilized cross section area. The formula is given by:

$$\sigma' = (\sigma_i - \sigma_0) \quad (5.3)$$

where σ' is new stress ; σ_i original stress in i -th; σ_0 initial point on original stress; The data format is given in Fig 5.17.

5. The first stress value should be very near zero but shift the stress values this small amount so that zero strain has exactly zero stress. The result of modified curve for tension test are illustrated in Fig 5.17.

Column=	A	B	C	D
Row	$\Delta V/V'$	σ'	$\Delta V/V$ =(A1-\$A\$1)/(1+\$A\$1)	σ =(B1-\$B\$1)
1	0.004551	7.359	0.000000	0.000
2	0.004906	8.705	0.000353	1.346
3	0.005277	10.053	0.000723	2.694
4	0.005661	11.403	0.001105	4.044
5	0.006060	12.755	0.001502	5.396
6	0.006471	14.110	0.001911	6.751
7	0.006894	15.467	0.002332	8.108
8	0.007329	16.828	0.002765	9.469
9	0.007775	18.191	0.003209	10.832
10	0.008231	19.557	0.003663	12.198
.	0.008697	20.927	0.004127	13.568
.	0.009172	22.300	0.004600	14.941
.	0.009655	23.677	0.005081	16.318
etc	0.010145	25.057	0.005569	17.698

$$\varepsilon' = \frac{\varepsilon_i - \varepsilon_0}{1 + \varepsilon_0}$$

$$\sigma' = (\sigma_i - \sigma_0)$$

Figure 5.17 Reduced extracted data format for volumetric test.

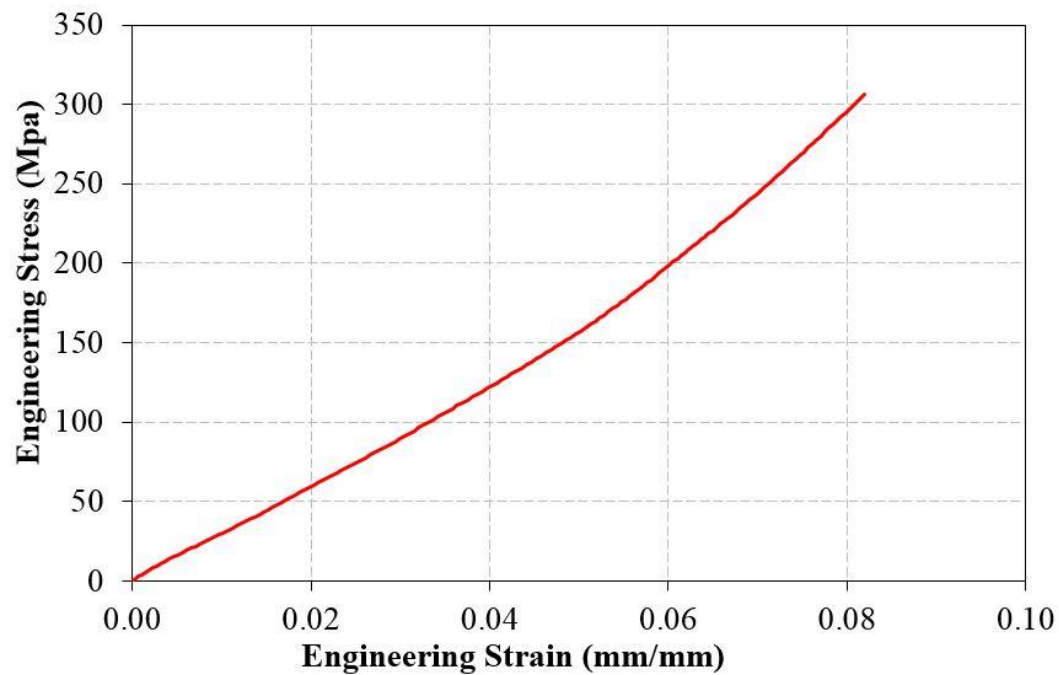


Figure 5.18 Modified of selecting curve of volumetric test data for sample-A.

Similarly, three sample are conducted to derive vary data test in volumetric test. A remining stress- strain data test, such as sample-B and sample-C, are equally considered as sample-A that described above for determining selection curve. The curves for all specimen are given in Fig 5.19.

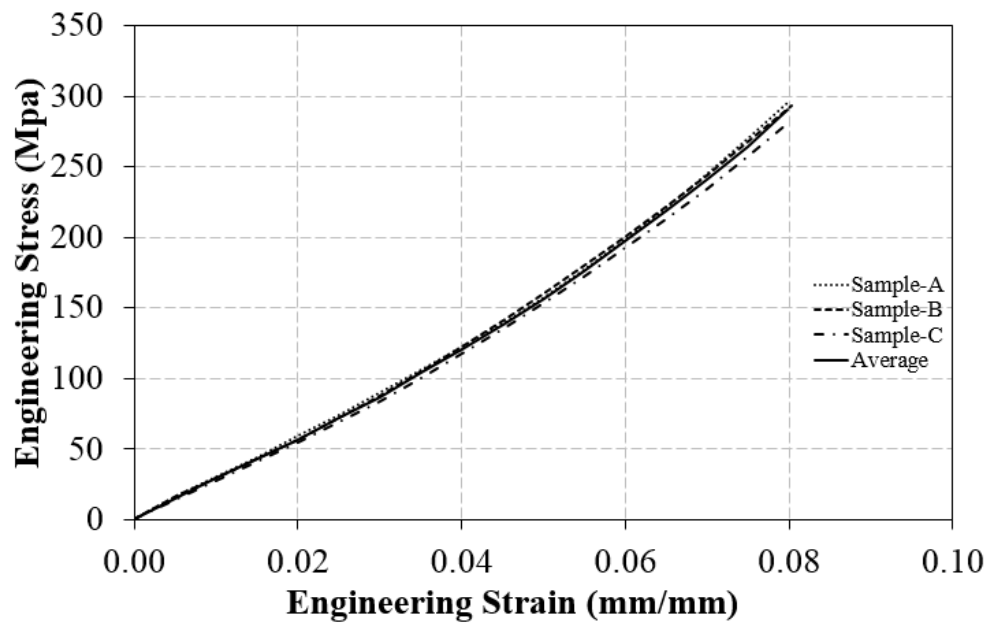


Figure 5.19 A Number of selecting curve of volumetric test.

In ANSYS program, to describe the incompressible behavior, the input file for volumetric data test are presented as volume ratio. Therefore, the selecting curve, particularly average value as shown in Fig 5.19, would be transformed into volume ratio by subtract the strain values from 1.0. The proper form of input file into ANSYS program are illustrated in Fig 5.20.

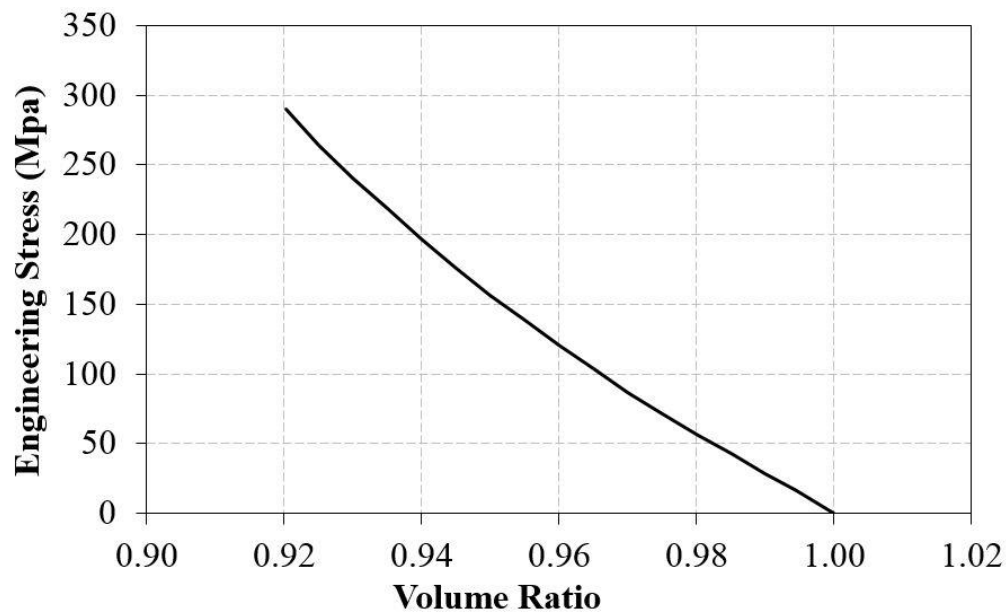


Figure 5.20 An Input file form for volumetric test on ANSYS.

5.1.1.5 Summary.

The primary objective of testing rubber material is to define and satisfy the input requirements of mathematical material models that exist in structural, non-linear finite element analysis software. A number of test are conducted including uniaxial tension test, planar shear test, equal biaxial test, volumetric test and stress relaxation test. Generally, a series data tests of uniaxial, planar and equal biaxial are performed in order to illustrated shear behavior of rubber by determining constant shear, denoted as C_{ij} . Then, volumetric test is to describe incompressible of rubber by defining the constant volume, denoted D_i . Finally, the requirement collecting data that would be input into the finite element software are obtained as describe in the previous section. The data are as shown in Fig 5.21 and 5.22.

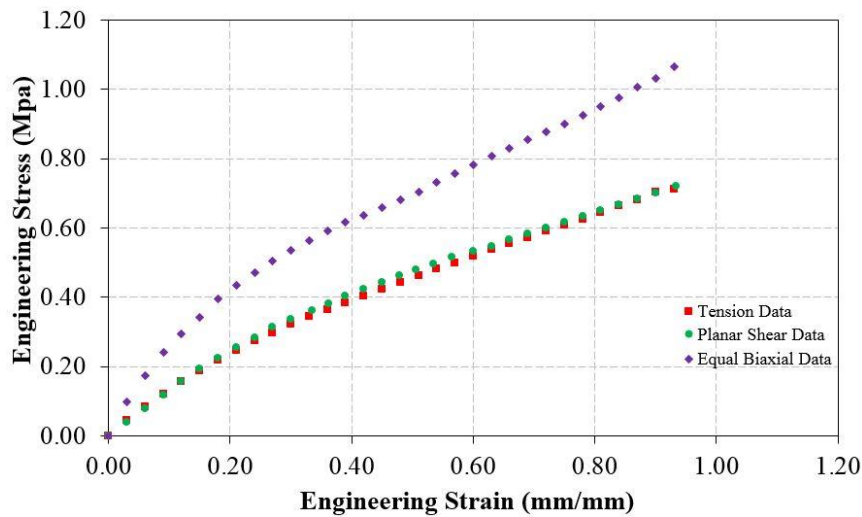


Figure 5.21 Input data files of Uniaxial, Planar and Equal Data Test.

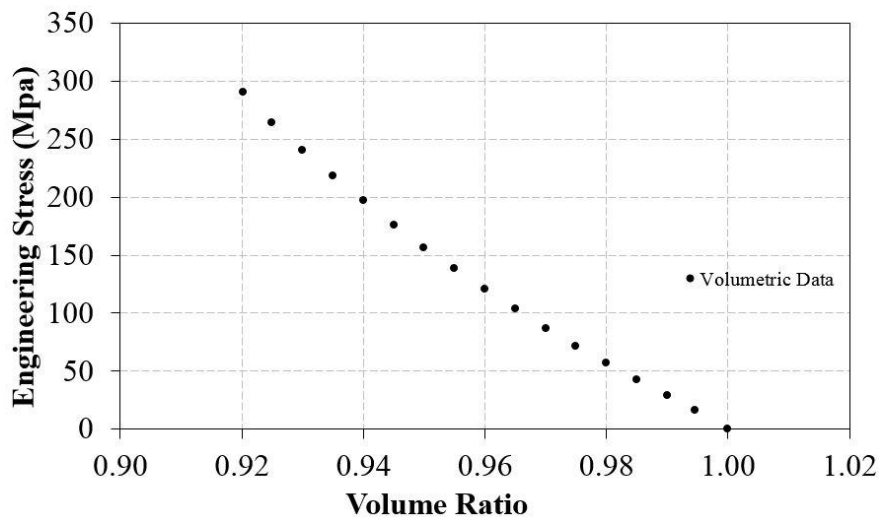


Figure 5.22 Input data file of volumetric test.

5.1.2 Selecting Constitutive Model.

In this chapter, an approach method are proposed to define the appropriate strain energy function (SEF) of hyperelastic material. A series finite element (FE) analysis for all material rubber testing including tension test, planar shear test, equal biaxial test and volumetric model, are performed to determine the selecting constitutive model. The FE result will be compared and validated with experimental test data that illustrated in Fig 5.21 and 5.22. The constitutive model that exhibits a good agreement with all experimental data, would be selected as mathematical model to represent the rubber behavior on finite element program. A commercial software program of ANSYS are utilized in this study, especially static structural ANSYS workbench. It means that the FE model would be assumed in static condition.

In this analysis, a number of hyperelastic material models which are considered in finite element analysis of rubber testing are Neo-Hookean, Mooney-Rivlin, Yeoh, Ogden and Arruda-Boyce. In other word, there would be four finite element modeling and each of them would be considered the six hyperelastic material model. The detail of finite element analysis are presented below:

5.1.2.1 Modeling Uniaxial Tension Test.

In this section, modeling finite element analysis of uniaxial tension test are presented. The loading conditions of FE analysis are somewhat different with experimental test which using cycle loading on the specimen. The typical loading used in FE of uniaxial tension is single loading that is performed in longitudinal direction of model intended to capture a pure tension behavior of rubber with various of hyperelastic constitutive models.

In order to obtain pure tensile strain on the FE model, the dimension in loading direction must be longer than the width and thickness. The FE dimension of uniaxial tension model are illustrated in Fig 5.23. The specimen is typically a dog bone-shape with effective gauge length is about 50mm. To simplify the FE analysis, the specimen is only modeled according to gauge length (50 mm). The determining appropriate clamp area on the model is to be the important issue to derived best result.

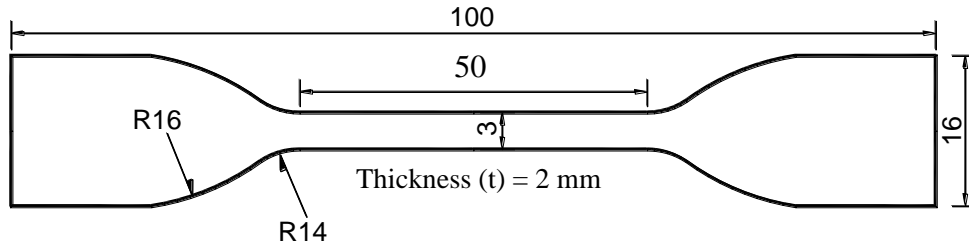


Figure 5.23 FE model dimension of uniaxial tension.

The uniaxial tension model is stretched to maximum displacement approximately 50 mm with loading rate is about 0.01 mm/mm/sec. The displacement control is used in this case while the forces are recorded during the stretching. The relationship between applied force and deformation are derived to calculate the stress-strain of uniaxial tension. To obtain the stress, the forces are divided with area cross section of model such as:

$$\sigma = \frac{F}{A} \quad (5.4)$$

where σ is stress (MPa); F is tension forces (N) and A is cross section area (mm^2) of model that is calculated as follow:

$$A = \text{thickness} \times \text{width} = 2 \times 3 = 6 \text{ mm}^2$$

In other hand, the strain of model is considered by dividing the actual displacement to initial length of gauge. The calculation is given by

$$\varepsilon = \frac{\Delta L}{L} \quad (5.5)$$

where ε is strain (mm/mm); ΔL actual displacement (mm) and L is gauge length (50 mm). The maximum strain level is achieved since the model undergo the maximum displacement, the calculation as follow:

$$\varepsilon = \frac{\Delta L}{L} = \frac{50 \text{ mm}}{50 \text{ mm}} = 1$$

The strain level of 1 is considered in finite element analysis according to the selecting strain on the uniaxial tension test data as illustrated in Fig 5.21. The results of FE with six constitutive models, would be compared with the actual test data in order to observe the appropriate SEF in representing uniaxial tension behavior. The deformation of FE model under pure tension are shown in Fig 5.24.

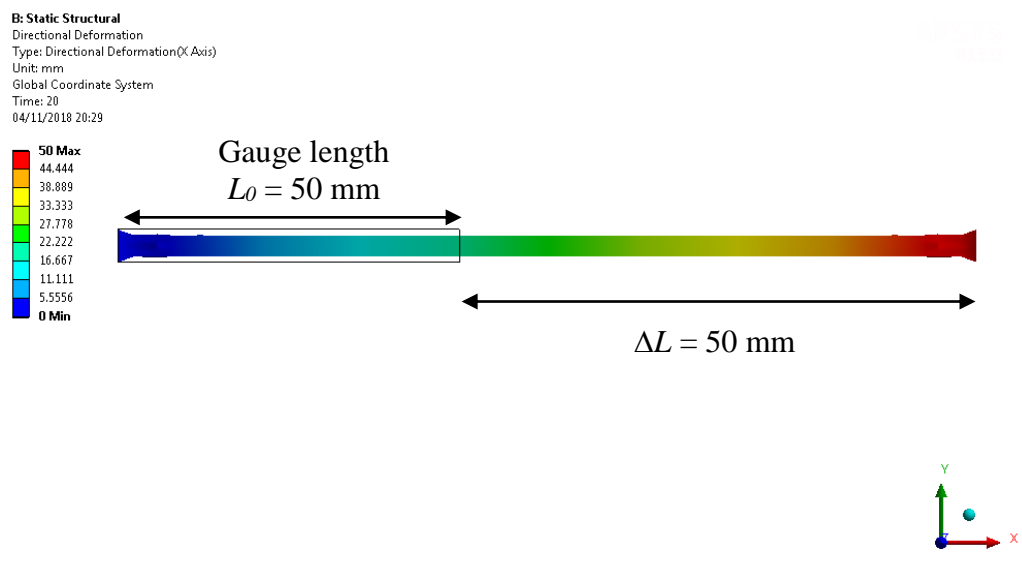


Figure 5.24 The deformation state of FE model under pure tension.

A number of hyperelastic model that available in ANSYS, are utilized to present the rubber material. The relationship between stress and strain that compare with experimental data of uniaxial tension test are presented on Fig 5.25. As mention earlier, there are six constitutive model involved in FE analysis. As shown in Fig 5.25, experimental data is denoted as red curve. Among the constitutive model, both Mooney-Rivlin and Ogden model exhibit a good agreement with experimental data test beginning at start point until maximum strain.

However, these results illustrated in figure above, are not sufficient to decide the proper material model for representing rubber behavior. The models must be able to perform consistently in other deformation state. Therefore, further FE analysis are carried out including planar shear, equal biaxial and volumetric.

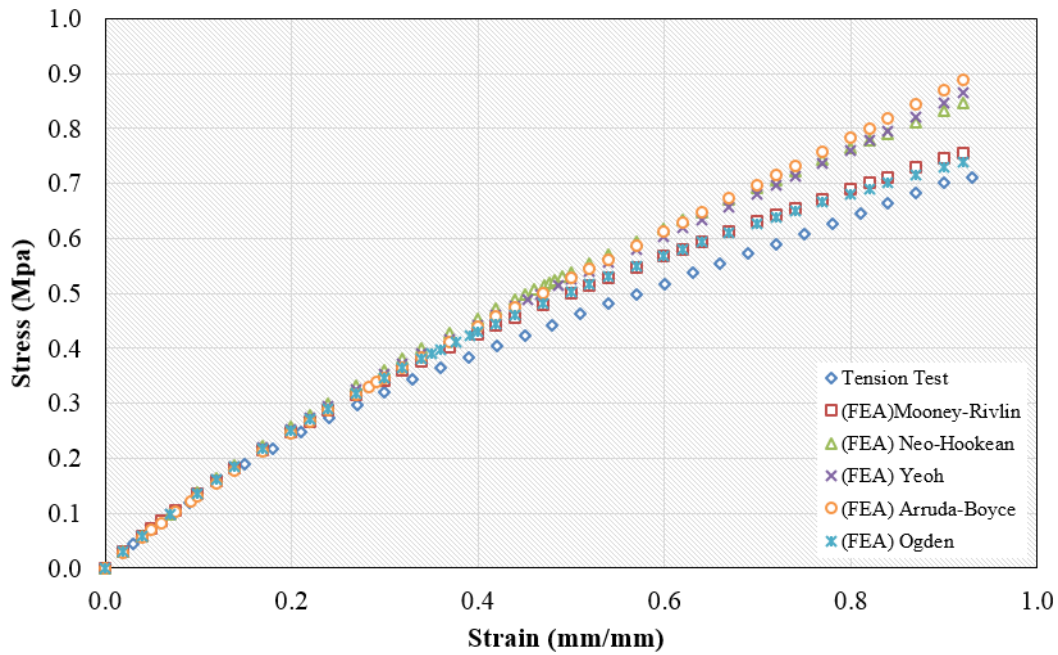


Figure 5.25 Fitting FE of uniaxial tension model with experimental data.

5.1.2.2 Modeling Planar Shear Test.

In this section, modeling finite element analysis of planar shear test are presented. The loading conditions of FE analysis are somewhat different with experimental test which using cycle loading on the specimen. The typical loading utilized in FE of planar shear is single loading and performed in perpendicular of width direction of model. The loading condition is intended to capture a pure shear behavior of rubber with various of hyperelastic constitutive models.

In order to obtain pure shear strain on the FE model, the dimension in width direction of FE model must be longer at least 10 times as much as the gauge length. The material is cut from sheet and is about 150 mm wide and 15 mm tall. The FE dimension of planar shear model are illustrated in Fig 5.26. The model was grip fixed on the one side and keep freely in other side in longitudinal loading direction. The determining appropriate clamp area on the model is to be the important issue to derived appropriate result.

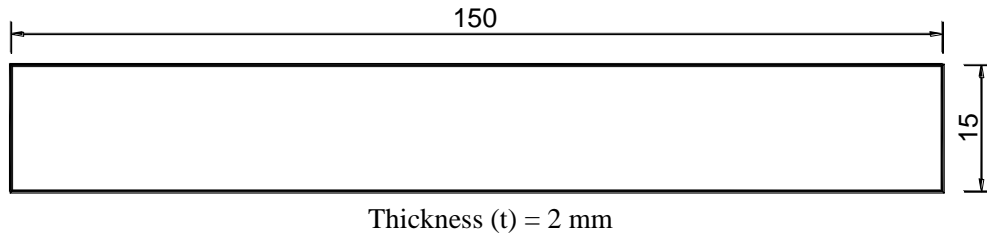


Figure 5.26 FE model dimension of planar shear.

The planar shear model is stretched to maximum displacement approximately 15 mm (100% of effective gauge length) with loading rate is about 0.01 mm/mm/sec. The displacement control is used in this case while the forces are recorded during the stretching. The relationship between applied force and deformation are derived to calculate the stress-strain of planar shear. To obtain the stress-strain values of FE planar shear model, the stress and strain are obtained similarly in Equation (5.3) and (5.4), respectively. The cross section of FE planar shear model is calculated as follow :

$$A = \text{thickness} \times \text{width} = 2 \times 150 = 300 \text{mm}^2$$

The maximum strain level is achieved since the model undergo the maximum displacement, that is given by :

$$\varepsilon = \frac{\Delta L}{L} = \frac{15 \text{mm}}{15 \text{mm}} = 1$$

The strain level of 1 is considered in finite element analysis according to the selecting strain on the planar shear test data as illustrated in Fig 5.21. The results of FE with six constitutive models, would be compared with the actual test data in order to observe the appropriate SEF in representing planar shear behavior. The deformation of FE model under pure shear are shown in Fig 5.27.

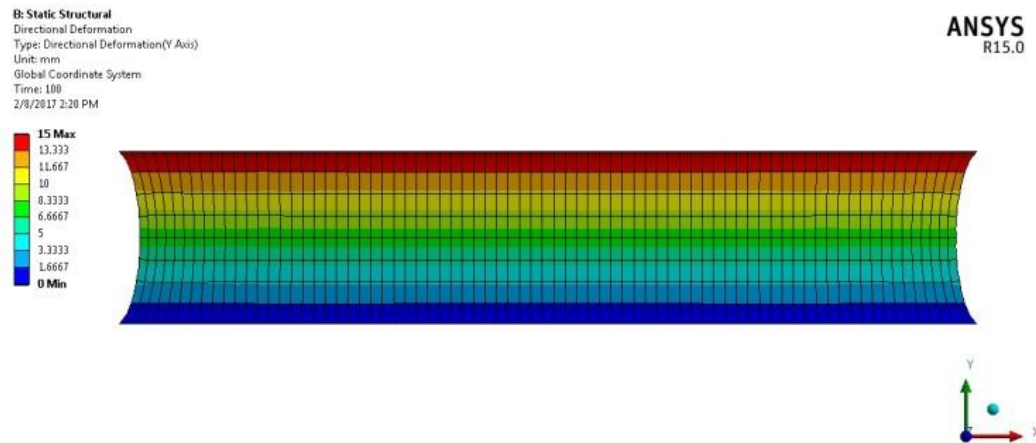


Figure 5.27 The deformation state of FE model under pure shear.

A number of hyperelastic model that available in ANSYS, are utilized to present the rubber material. The relationship between stress and strain that compare with experimental data of planar shear test are presented on Fig 5.28. As mention earlier, there are six constitutive model involved in FE analysis. As shown in Fig 5.28, experimental data is denoted as red curve. Although the fitting results are not as good as uniaxial tension, the pattern of deform shape remain describing that both Mooney-Rivlin and Ogden model illustrate a good agreement with experimental planar shear data than the others model. From two FE analysis (uniaxial tension and planar shear), the temporary conclusion could be taken that both Mooney- Rivlin and Ogden model are more dominant to be selected as proper SEF of rubber material than the others model. The remaining FE analysis (equal biaxial and volumetric) would make sure which one of both model are appropriate to represent rubber behavior on finite element program.

5.1.2.3 Modeling Equal Biaxial Test.

In this section, modeling finite element analysis of equal biaxial test are presented. The loading conditions of FE analysis are somewhat different with experimental test which using cycle loading on the specimen. The typical loading utilized in FE of equal biaxial is single loading and performed in radial direction of model. The loading condition is intended to capture a pure radial strain of rubber that are also equivalent to pure compression conditions.

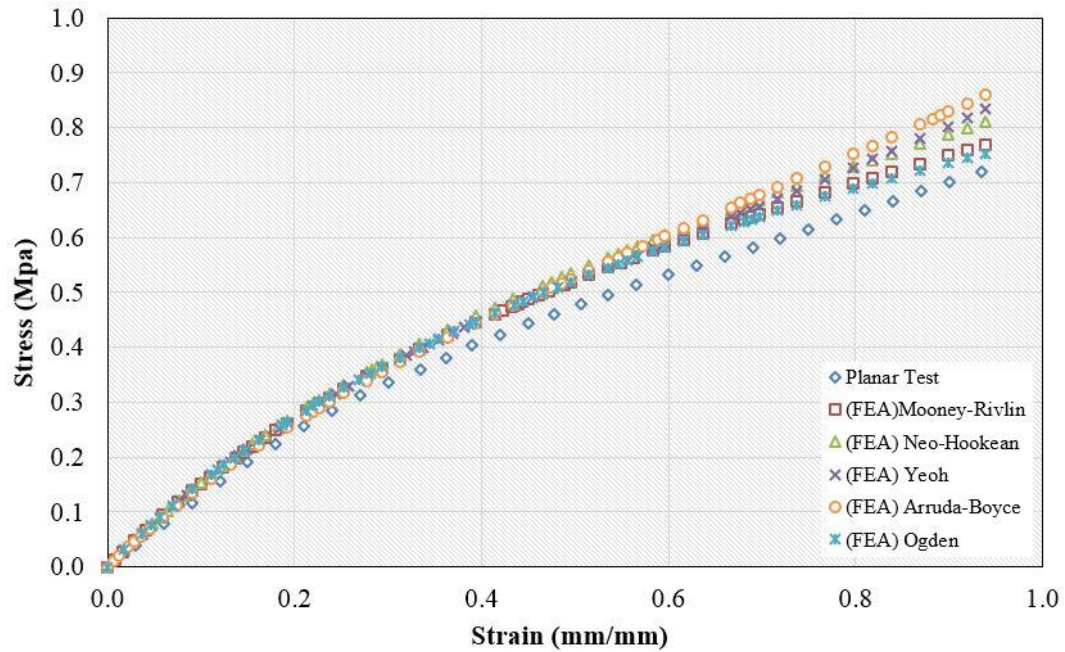


Figure 5.28 Fitting FE of planar shear model with experimental data.

In order to obtain pure strain in radial on the FE model, the dimension is performed in circular shape that is cut from sheets and is 75mm in diameter with an effective area 50 mm in diameter. The loading condition of equal biaxial FE model is somewhat different than the previous FE analysis (uniaxial and planar). The model would have 16 “clamps” that would be pulled at the same time to the desired strain level. The model was gripped fixed on the clamps and kept freely in radial direction. The determining appropriate clamp area on the model is to be the important issue to derive appropriate results. These conditions enable for the model experiencing pure radial stretching. The FE dimension of equal biaxial model are illustrated in Fig 5.29.

The deformation state of equal biaxial model is considerably different than either uniaxial tension or planar shear. The gauge length is approximately 25 mm as shown in Fig 5.29. Since the clamp edges of the model are subjected to tension in radial direction, the measured displacement on clamps are different than measured in the effective area (50 mm in diameter), particularly in gauge length. It is caused the effective area is stiffer than clamp edges. It means that in order to achieve 100% strain level, the clamp edges must be pulled more than 12.5 mm.

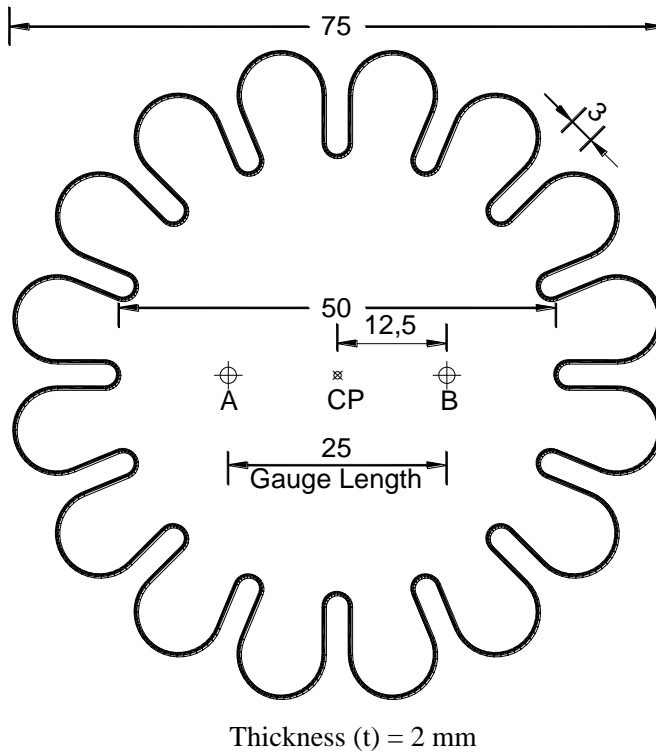


Figure 5.29 FE model dimension of equal biaxial.

It is considerably difficult to make sure how much the displacement must be subjected to the clamp edges to derive a particular strain level on the effective area (point A or point B). Therefore, a trial and error is conducted to derived the desired strain level by finite element analysis.

In this analysis, the strain level of equal biaxial are selected in 20% of effective gauge length. It means that the total length of gauge is to be 30mm increasing 5mm of initial length. By trial and error, in order to achieve 20% strain level, the clamps must be pulled until approximately 8,3 mm from initial position in radial direction. The relationship between applied force and deformation at point A or B (see Fig 5.33) are derived to calculate the stress-strain of equal biaxial. The critical point in calculating stress for equal biaxial is total forces that applied on the model are exist 16 forces. Therefore, the stress consideration are as follow :

$$\sigma = \frac{\sum_{i=1}^{16} F_i}{t_r \times \pi \times d_{eff}} \quad (5.6)$$

where σ is stress (MPa); $\sum_{i=1}^{16} F_i$ is total force (N) of clamps in radial direction; d_{eff} is 50mm diameter of effective area and t_r is thickness of rubber sheet (mm).

As mentioned earlier, the additional displacement of gauge length is approximately 5mm (20% strain level). The calculation of the strain is considered by dividing the change in length of gauge to original gauge distance. The strain level at 20% is achieved since the model undergo the particular displacement, the calculation as follow:

$$\varepsilon = \frac{\Delta L}{L} = \frac{5mm}{25mm} = 0,2$$

Actually, the determining strain level (20%) is because of the prediction of rubber strain in radial direction application on base isolation is not exceed more than 20%, therefore only 20% is considered here. The deformation of FE equal biaxial model under pure strain in radial direction are shown in Fig 5.30. A number of hyperelastic model that available in ANSYS, are utilized to present the rubber material. The relationship between stress and strain that compare with experimental data of equal biaxial test are illustrated on Fig 5.31. As mention earlier, there are six constitutive model involved in FE analysis. See in Fig 5.31 above, the similar phenomena are exhibited of both Mooney-Rivlin and Ogden model from the previous FE model (uniaxial and planar shear). These model consistently show a good fit, starting at zero strain until maximum strain, with experimental data in tension model, planar shear model and equal biaxial model.

Basically, the strain energy function (SEF) of rubber material consists of two strain function, they are strain function to change the shape (W_d) and strain function to change the volume (W_v). The general form of strain energy function as shown in Eq (2). The one of characterize of W_d is the constant value (C_{ij}) that are derived from fitting the uniaxial, planar shear and equal biaxial test data. In other word, the phenomena that illustrated by Mooney-Rivlin and Ogden (in tension, planar and biaxial model), are insufficient to determine one of them as the appropriate SEF for rubber due to the behavior on the strain function of volume

(W_v) is not clearly yet. Therefore, the volumetric FE model is needed to validate the trending of Mooney-Rivlin and Ogden model in describing rubber behavior.

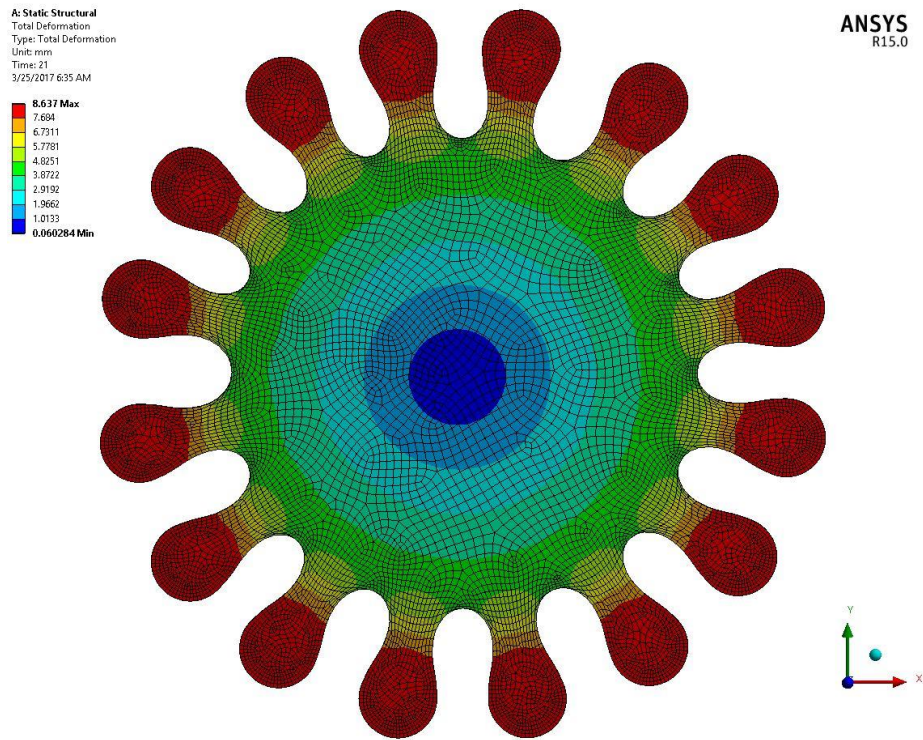


Figure 5.30 The deformation state of FE model under pure radial strain.

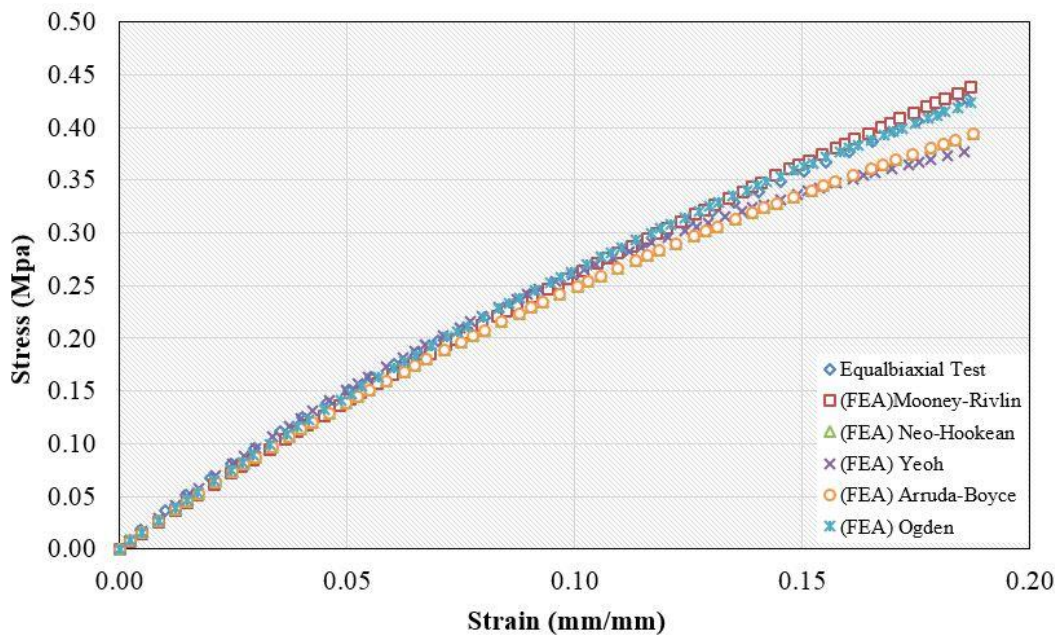


Figure 5.31 Fitting FE of equal biaxial model with experimental data.

5.1.2.4 Modeling Volumetric Test.

In this section, modeling finite element analysis of volumetric test are presented. The loading conditions of FE analysis are somewhat different with experimental test which using cycle loading on the specimen. The typical loading utilized in FE of volumetric is single loading as hydrostatic pressure. The boundary conditions are arranged to make sure the model undergoing pure compression to observe the incompressible behavior. The actual dimension of volumetric specimens consist of five circular disk with diameter of 6.35 mm illustrated in Fig 5.32. However in FEA, five circular disk was modeled as cylinder with 10 mm in tall and 6.35 mm in diameter. Fixed constrain was performed in the bottom and constrain in lateral direction was applied on the body to ensure the movement only in longitudinal direction under pure compression.

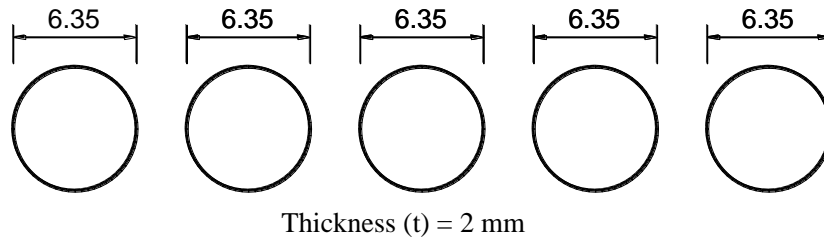


Figure 5.32 Actual dimension of volumetric specimens.

The axial load in longitudinal direction is applied with displacement control to particular displacement approximately 1 mm with loading rate is about 0.01 mm/mm/sec. The relationship between applied force and deformation are captured during the simulation for calculating the stress-strain of volumetric. The different among the previous FEA, the stress of volumetric is hydrostatic pressure (MPa). Commonly, the formula used for stress and strain analysis are similar with Equation (5.3) and (5.4), respectively.

The cross section of FE volumetric model is calculated as follow :

$$A = \frac{1}{4} \pi D^2 = \frac{1}{4} \times 3.14 \times 6.35^2 = 31.65 \text{ mm}^2$$

Due to the model is constrained in all direction except in longitudinal, the displacement are taken only in 1 mm (10% strain level). The term of strain in volumetric always change with volume ratio. In the principal, the concept is similar with general strain, but this term is used to illustrate the compressible behavior. Thus the equation of volume ratio could be as follow:

$$\frac{\Delta V}{V_0} \approx 1 - \varepsilon = 1 - \frac{\Delta L}{L} \quad (5.7)$$

where ΔV is change in volume under hydrostatic pressure and V_0 is initial state of model. The deformation of FE volumetric model under pure compression in longitudinal direction are shown in Fig 5.33.

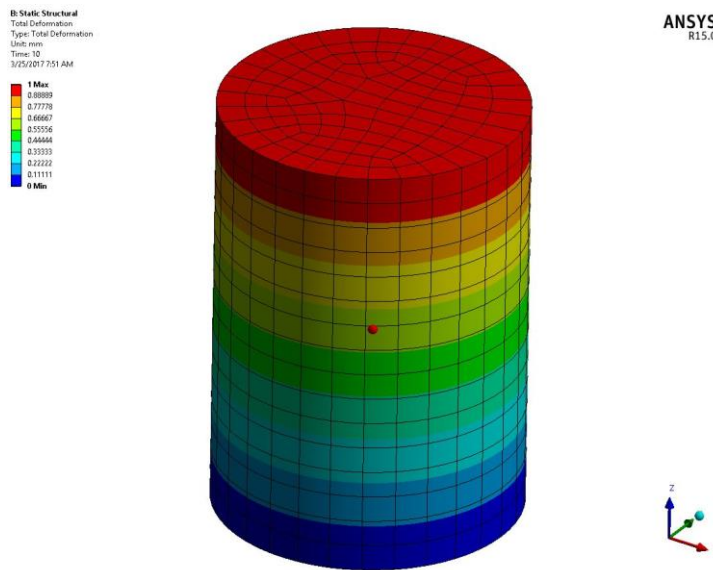


Figure 5.33 The deformation state of FE volumetric model under pure compression.

A number of hyperelastic model that available in ANSYS, are used to present the rubber material. The relationship between hydrostatic pressure and volume ratio that compare with experimental data of volumetric test are presented on Fig 5.34. In this step, the different behavior are exhibited by both Mooney-Rivlin and Ogden model that in prior to analysis they always give similar

characteristic. In the Fig 5.34, it is clear that Mooney- Rivlin are not able to maintain its good fitting under pure compression. Otherwise with the Ogden model that always remains indicating the consistently of its behavior in representing the material behavior in all of deform state.

5.1.2.5 Summary

A series finite element analysis (FEA) are carried out to predict the proper SEF of rubber material. The FEA are conducted due to the curve fitting process by experimental data are insufficient describing the hyperelastic behavior. In the first three simulation (uniaxial, planar and equalbiaxial), both Mooney-Rivlin and Ogden model exhibit a similar characteristic in describing rubber characteristic. In other word, if the FEA are only used without compressible effect, both of them are probably able to used as SEF to illustrate mechanical characteristic of rubber. However, in volumetric simulation Mooney-Rivlin are not able to capture the compressible effect, while the Ogden consistently show a good agreement to experimental data test for all deform state. It is clear that Ogden model are considerably appropriate for selecting as SEF of rubber material. The further FE analysis of base isolation are to be evidence for Ogden as correct selecting constitutive model in representing mechanical characteristic of rubber material in FE program.

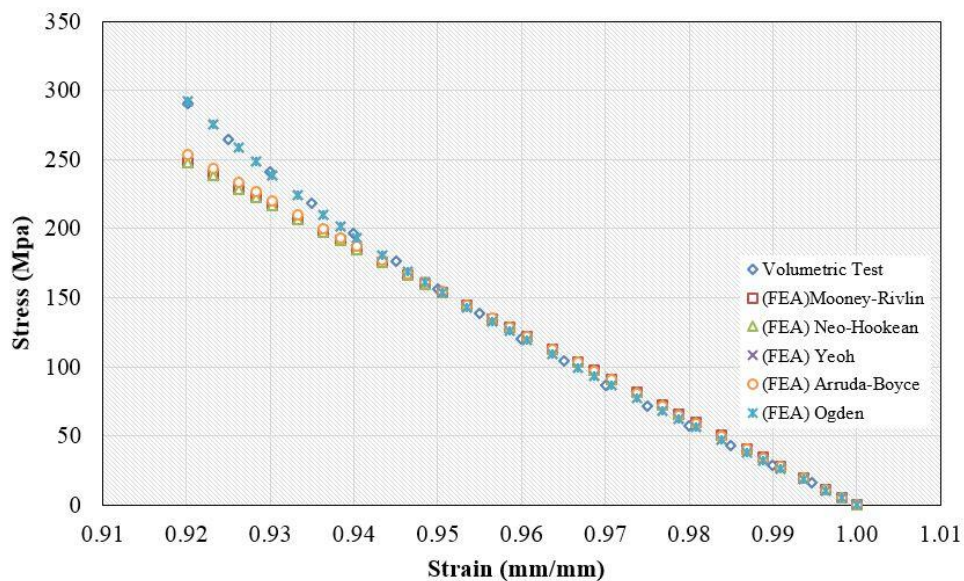


Figure 5.34 Fitting FE of volumetric model with experimental data.

5.2 Perforated Plate

5.2.1 Strength Analysis of Perforated Plate.

In chapter 3.2, the procedure of testing have been explained briefly. Now, the detail analysis for defining material properties are presented. In this section, the test results both specimens -A and specimens -B, as shown in Fig 5.31, are considered to define the relationship between perforated plate and full plate. As illustrated earlier that the main aim of analysis is in order to determine the appropriate test method in defining strength of perforated plate. Therefore, a series experimental test was conducted. In this section, analysis of tension test of specimen A, B and C are presented. The detail of results test are given below:

a. Anaysis of Specimens A.

Specimens-A (see Fig 5.32) are utilized for tension test in order to obtain the yield strength of solid plate. Three specimens were conducted in tension test and the results are as follow in Fig 5.35 – 5.37 and Table 5.1.

As illustrated above, the value of yield strength of specimens A are approximately 317 MPa. This value would be compared with experimental test result of specimens B. The ratio of yield strength between specimens B to specimens A would be considered as coefficient to obtain the strength of specimens C. The resume of experiemental test resulted are presented in Table 5.1.

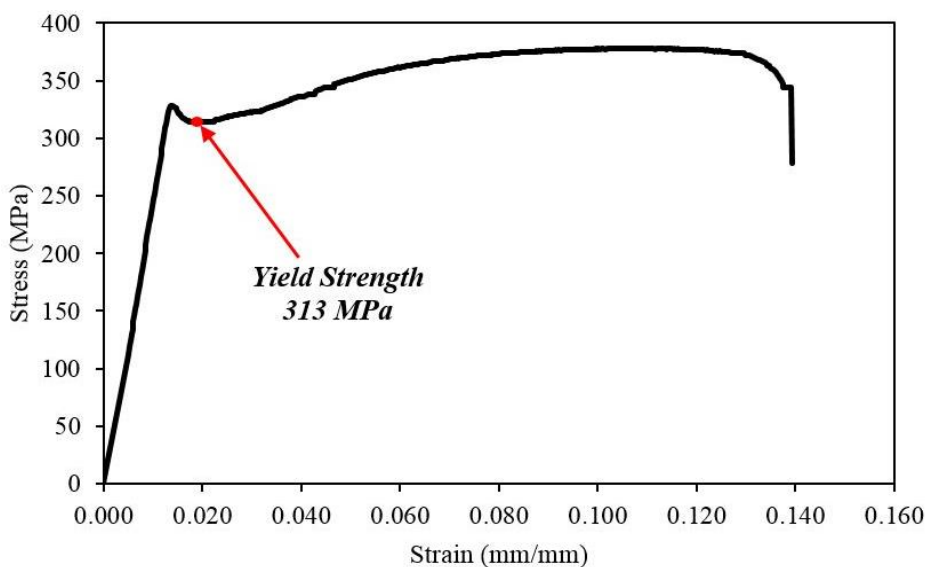


Figure 5.35 Stress – strain relationship of specimen A-1.

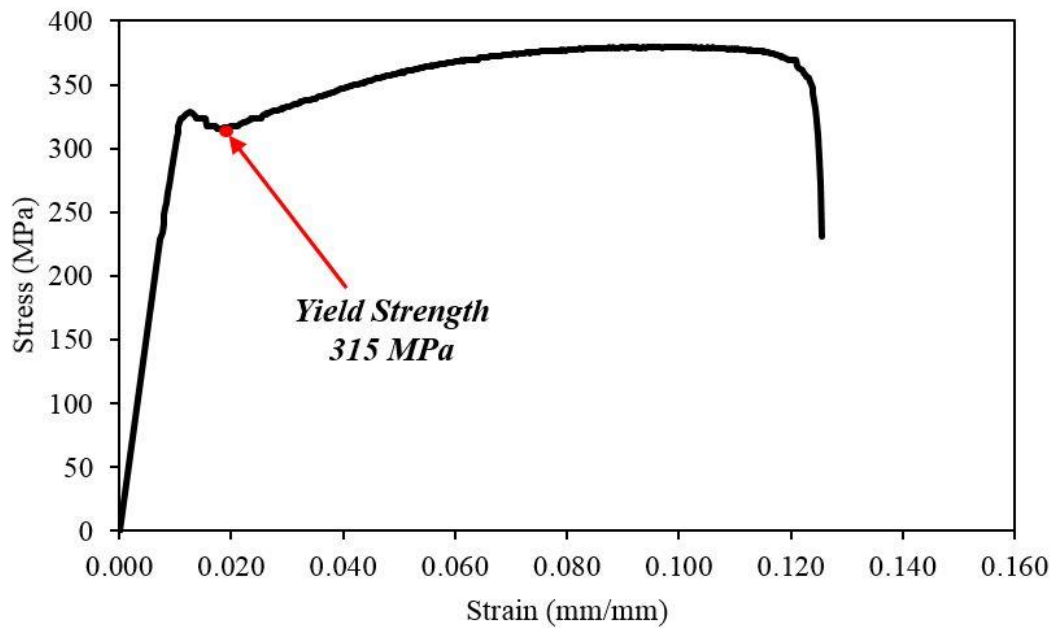


Figure 5.36 Stress – strain relationship of specimen A-2.

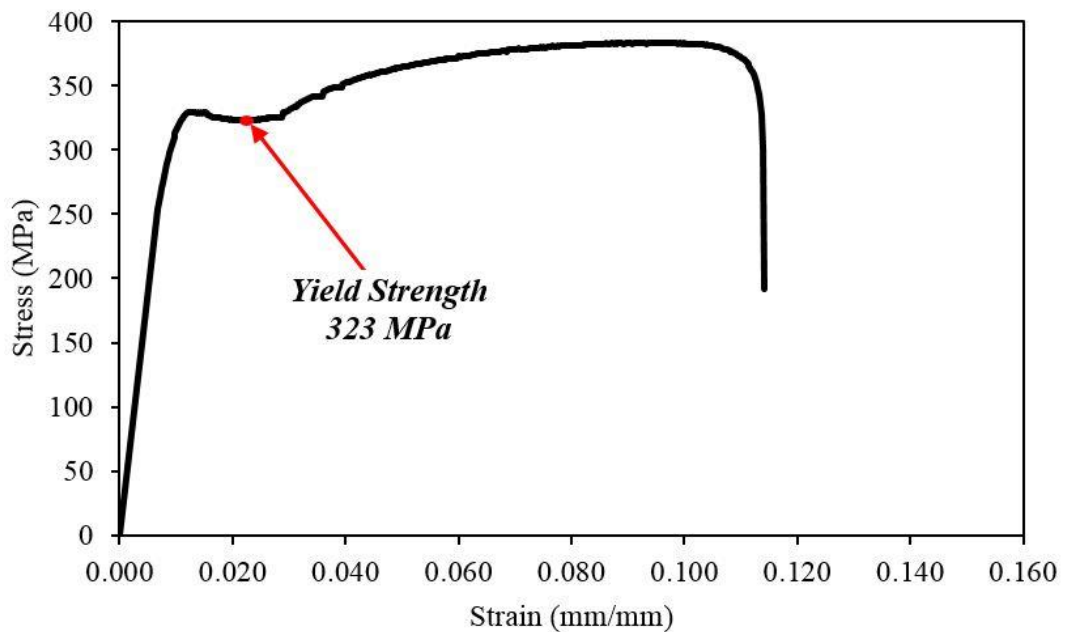


Figure 5.37 Stress – strain relationship of specimen A-3.

a. Analysis of Specimens B.

In this section, analysis data of experimental test of specimens B are presented. The specimens B are similar with specimen A. The difference is in the shape. Using identical material with specimens A, the plate was pierced as follows perforated plate pattern. As shown in Fig 5.25, the specimens B were divided into 4 types of specimens and each type consists of 3 samples. The total number

of specimens B are 12 samples. The stress-strain resulted from experimental are presented in Fig 5.38 to 5.40.

Tabel 5.1 Experimental test results of plate-A.

Material	Area (mm ²)	Yield Strength (MPa)	Tensile Strength (MPa)	Young's Modulus (MPa)	Elongation at Break (%)
A-1	13	314	378	24,802	14.691
A-2	13	315	380	26,177	14.644
A-3	13	323	383	26,120	14.260
Avarage		317	380	25,700	14.532

- Specimens B1.

The results test of specimens B1-1; B1-2; B1-3 are presented in Fig 5.38 to 5.40 and Table 5.2.

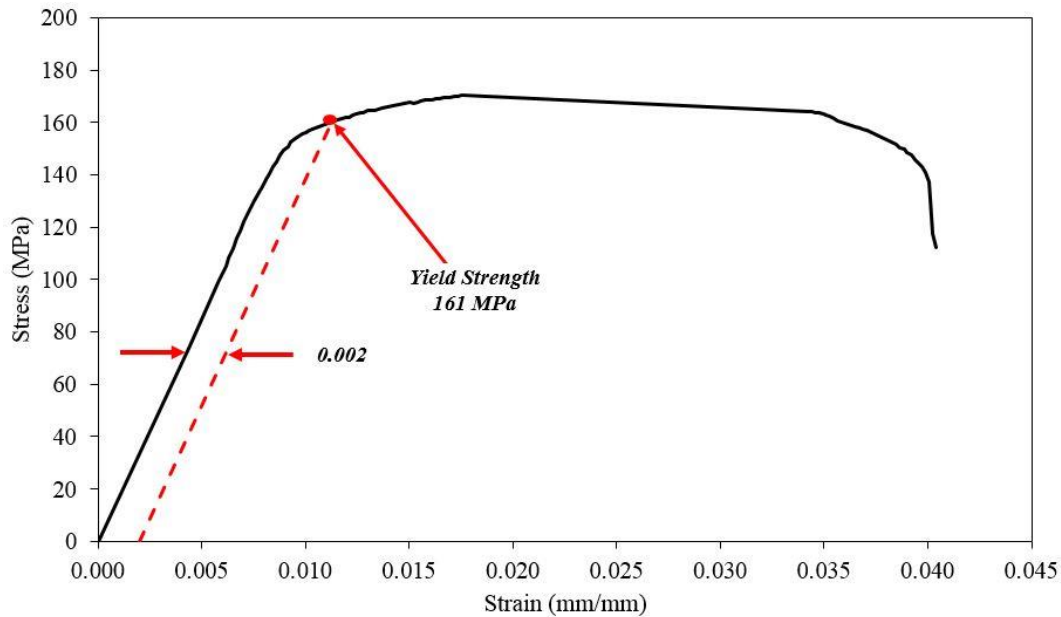


Figure 5.38 Stress – strain relationship of specimen B1-1.

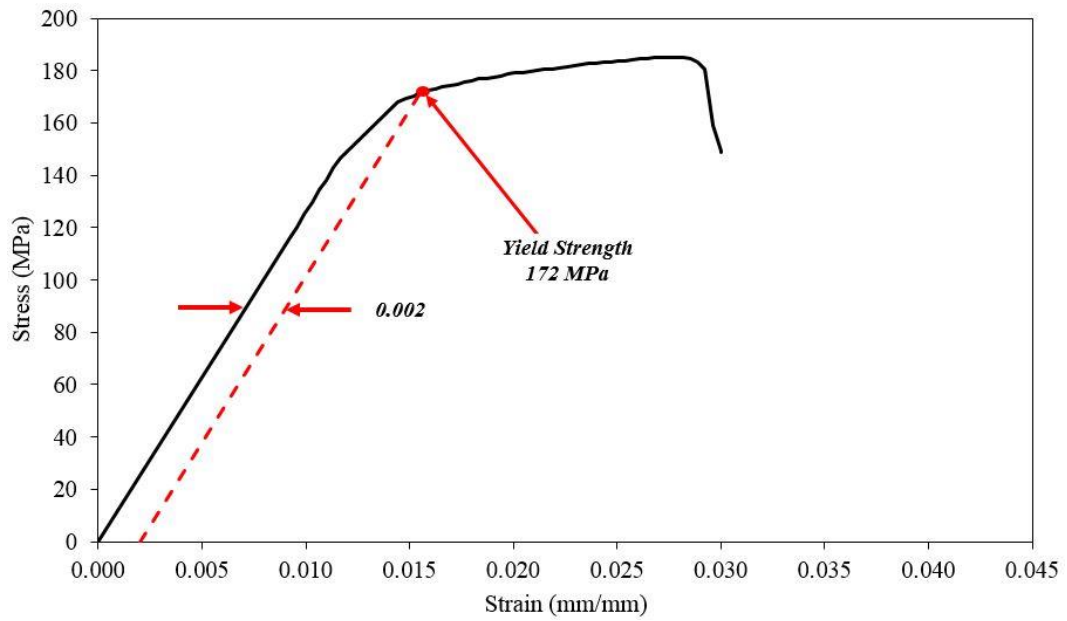


Figure 5.39 Stress – strain relationship of specimen B1-2.

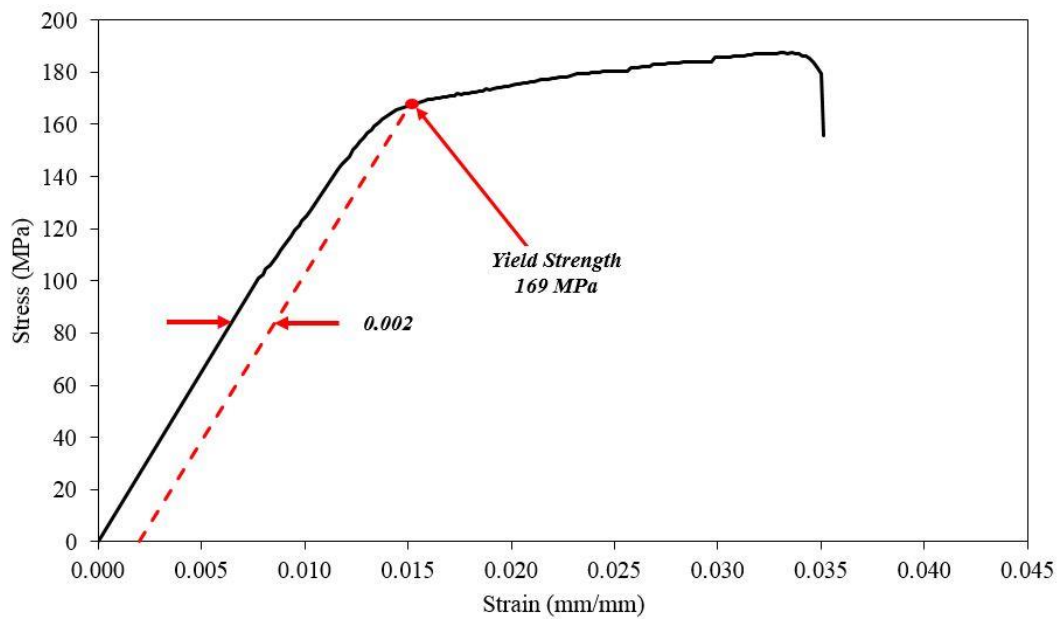


Figure 5.40 Stress – strain relationship of specimen B1-3.

Tabel 5.2 Experimental test results of specimens B1.

Material	Area (mm ²)	Yield Strength (MPa)	Tensile Strength (MPa)	Young's Modulus (MPa)	Elongation at Break (%)
B1-1	19.71	161	170	16,839	5.162
B1-2	19.71	172	185	12,700	4.169
B1-3	19.71	169	187	12,235	4.574
Avarage		167	181	13,925	4.635

- Specimens B2.

The results test of specimens B2 : B2-1; B2-2; B2-3 are presented in Fig 5.41 to 5.43 and Table 5.3.

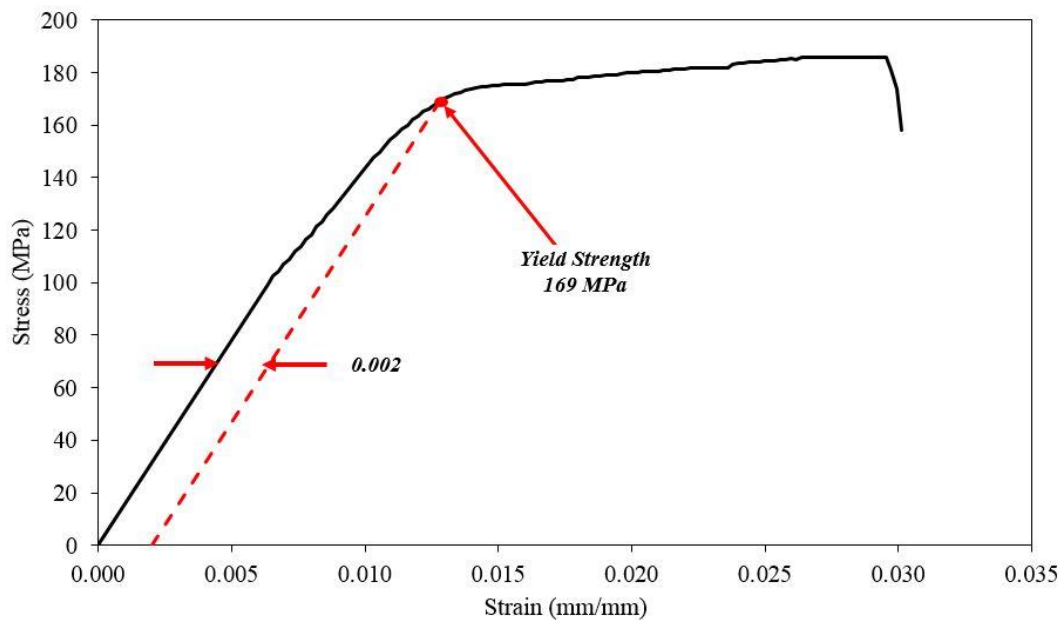


Figure 5.41 Stress – strain relationship of specimen B2-1.

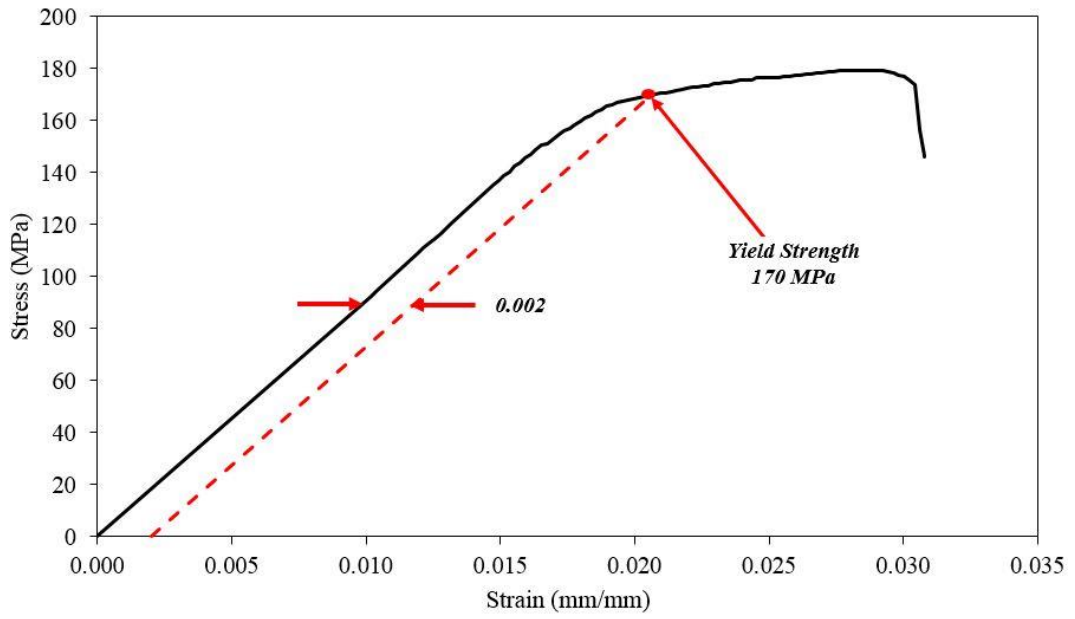


Figure 5.42 Stress – strain relationship of specimen B2-2.

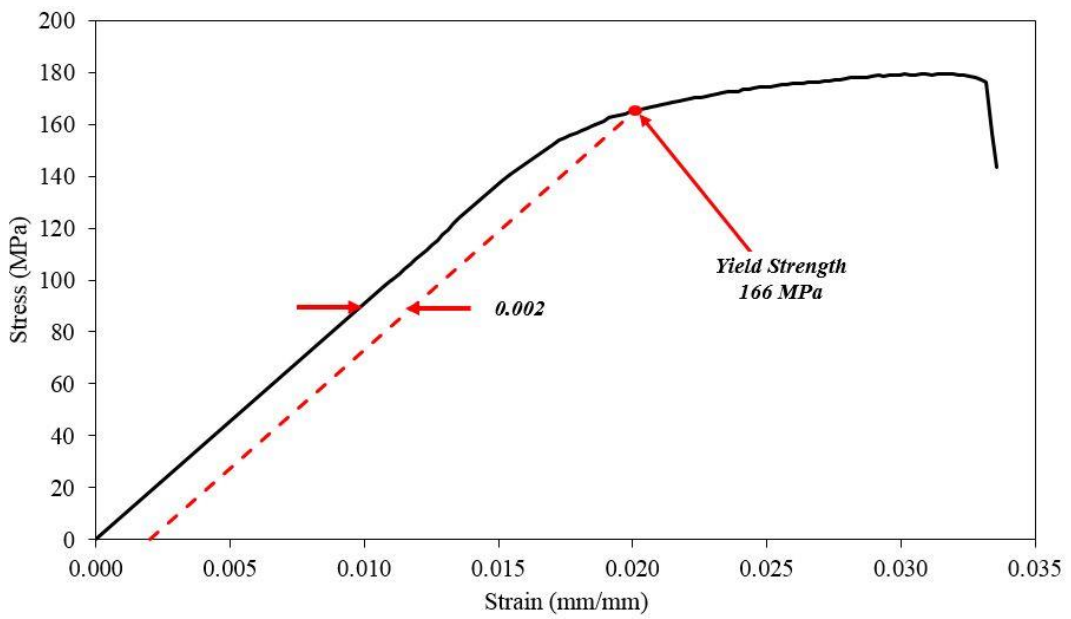


Figure 5.43 Stress – strain relationship of specimen B2-3.

Tabel 5.3 Experimental test results of specimens B2.

Material	Area (mm ²)	Yield Strength (MPa)	Tensile Strength (MPa)	Young's Modulus (MPa)	Elongation at Break (%)
B2-1	19.71	169	186	15,136	5.979
B2-2	19.71	170	179	8,994	4.596
B2-3	19.71	166	180	9,066	4.778
Avarage		168	182	11,065	5.118

- Specimens B3.

The results test of specimens B3 : B3-1; B3-2; B3-3 are presented in Fig 5.44 to 5.46 and Table 5.4.

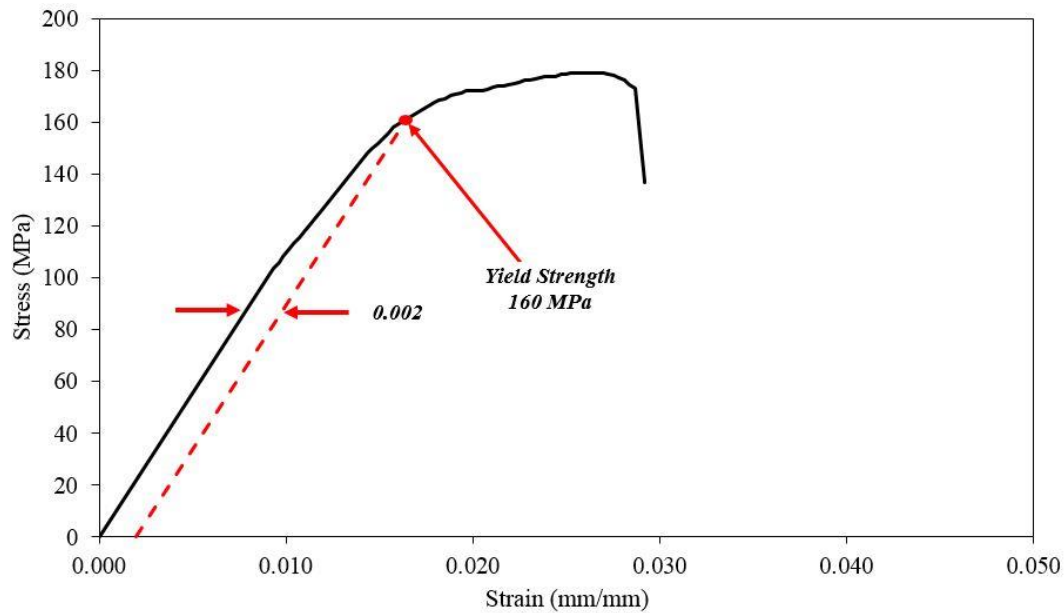


Figure 5.44 Stress – strain relationship of specimen B3-1.

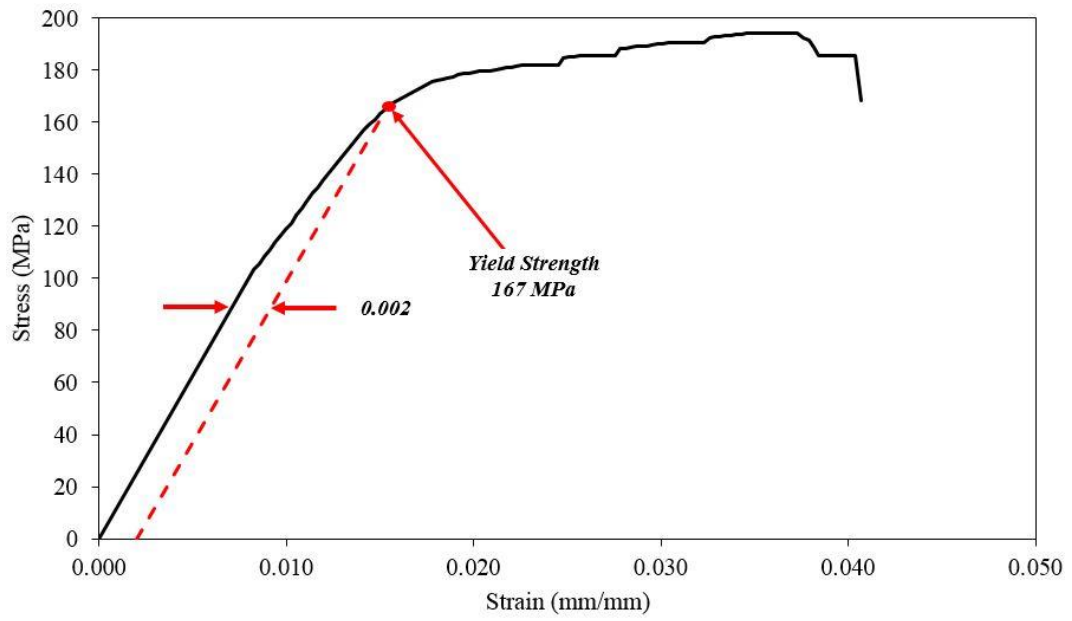


Figure 5.45 Stress – strain relationship of specimen B3-2.

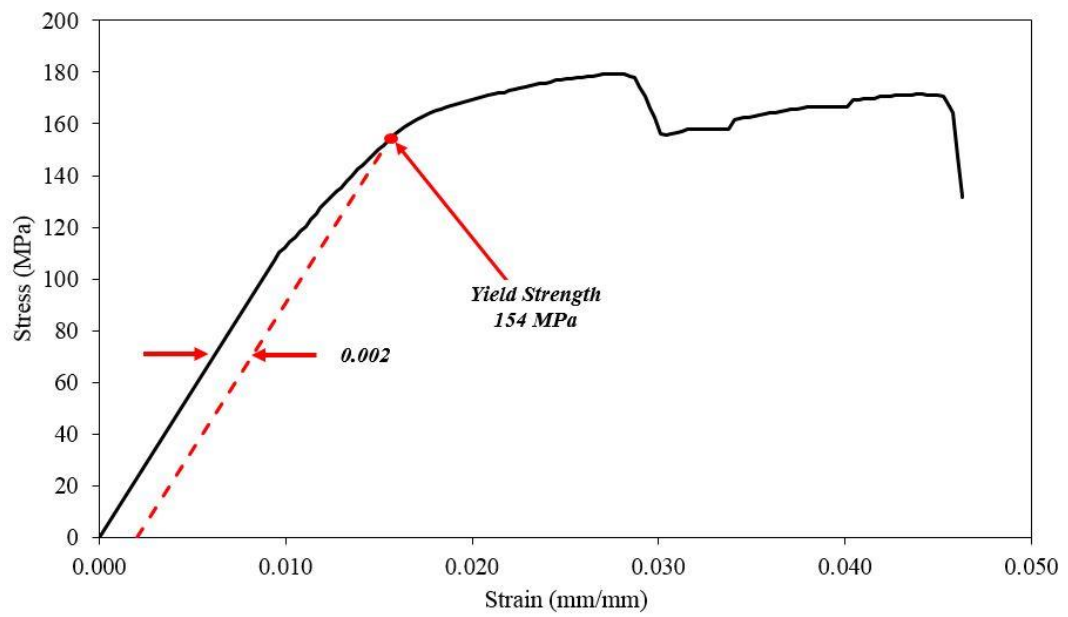


Figure 5.46 Stress – strain relationship of specimen B3-3.

Tabel 5.4 Experimental test results of specimens B3.

Material	Area (mm ²)	Yield Strength (MPa)	Tensile Strength (MPa)	Young's Modulus (MPa)	Elongation at Break (%)
B3-1	19.71	160	179	11,523	5.344
B3-2	19.71	167	194	12,313	7.274
B3-3	19.71	154	179	12,313	7.866
Avarage		160	184	12,050	6.828

- Specimens B4.

The results test of specimens B3 : : B4-1; B4-2; B4-3 are presented in Fig 5.47 to 5.49 and Table 5.5.

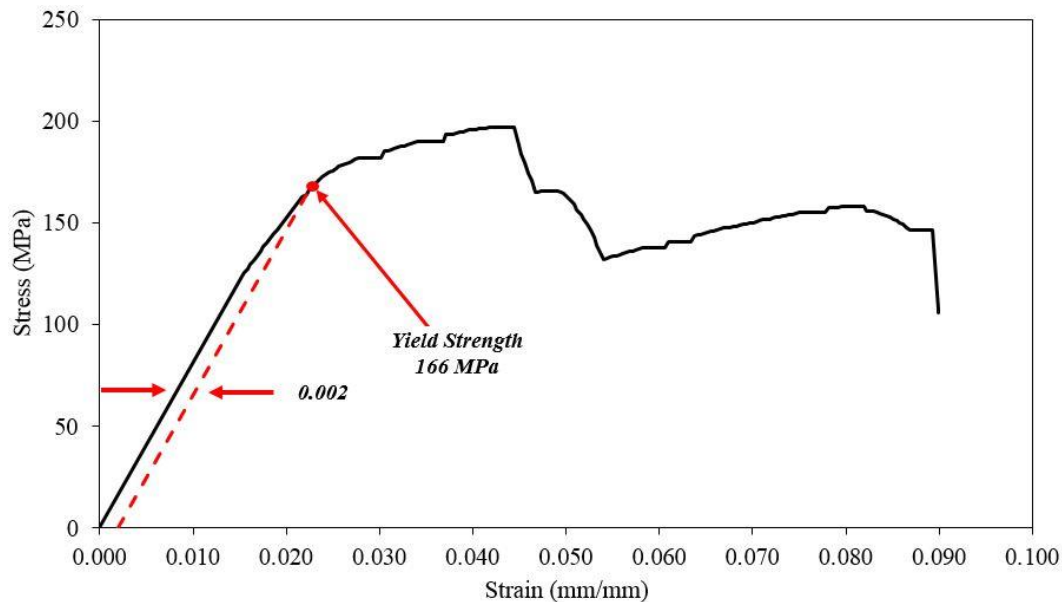


Figure 5.47 Stress – strain relationship of specimen B4-1.

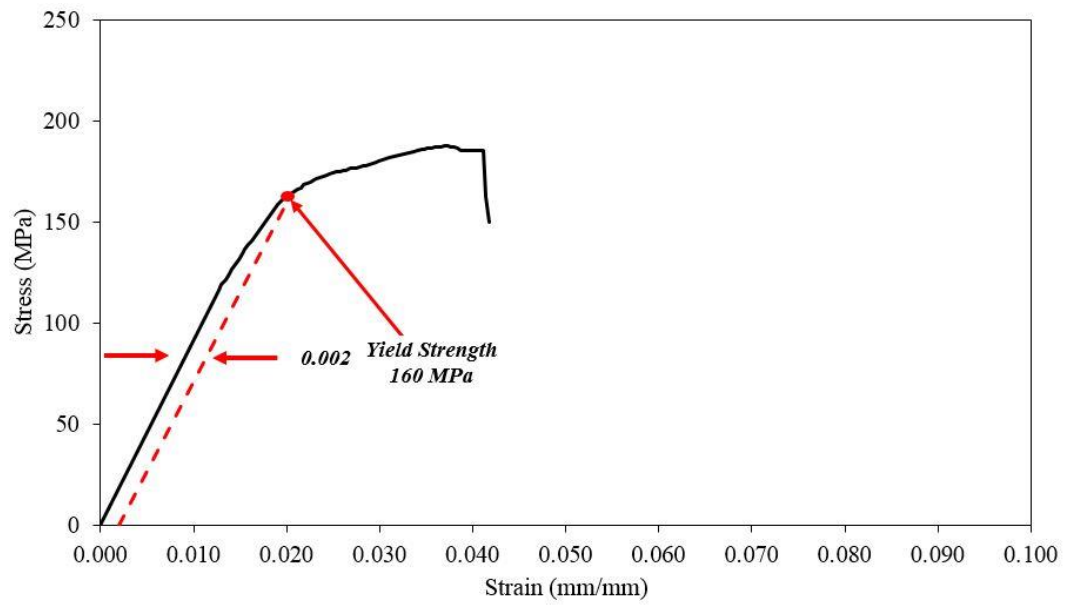


Figure 5.48 Stress – strain relationship of specimen B4-2.

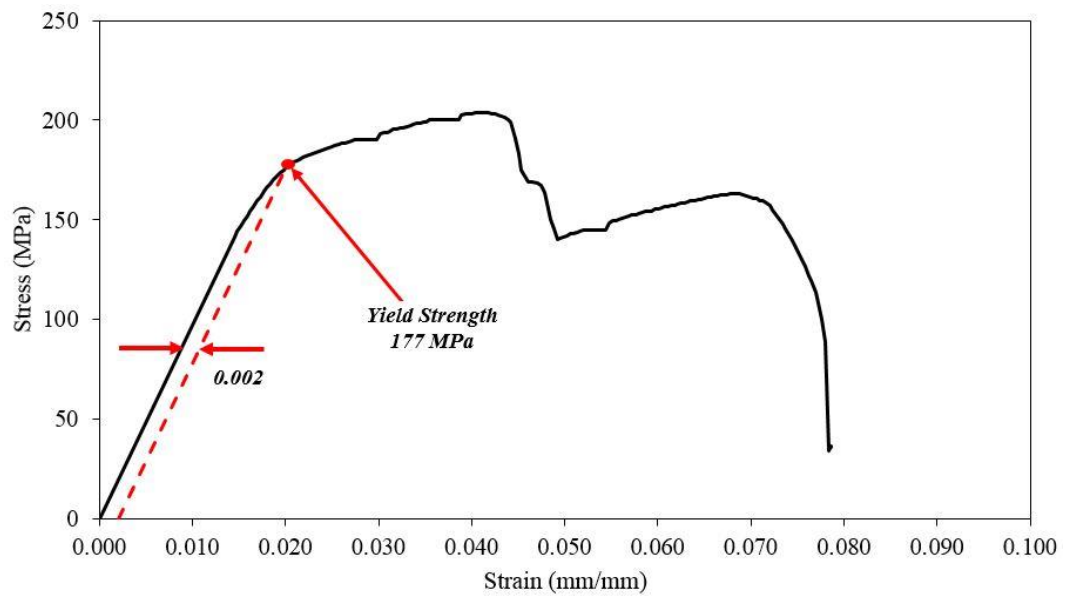


Figure 5.49 Stress – strain relationship of specimen B4-3.

Tabel 5.5 Experimental test results of specimens B4.

Material	Area (mm ²)	Yield Strength (MPa)	Tensile Strength (MPa)	Young's Modulus (MPa)	Elongation at Break (%)
B4-1	19.71	166	197	8,126	12.340
B4-2	19.71	160	187	9,221	6.602
B4-3	19.71	177	204	9,760	9.980
Avarage		168	196	9,036	9.641

The experimental test results of specimens B has been illustrated above. The avarage value of each type specimens has been obtained typically for yields strength. As described earlier, the length dimension of specimens were different while wide dimension are similar. These condition were conducted in order to derive the effect of ratio of length to wide on the material properties, esspecially yield strength. However, the values of experimental test of specimens B indicate that the ratio of length to wide has no effect on the material parameters. In other word, the test results illustrate that the value for all type specimen are similar. Since the results of test are identical, the avarage values of specimens B are presented clearly. These result would be compared to specimens A to obtain the coefficient of modification. The resume of experimental test of specimens B are given below in Table 5.6.

The analysis results both specimens A and specimens B are obtained as decribed above. Furthermore, Calculating the coefficient of modification used to predict the strength of perforated plate are conducted. There are two parameters considered in this analysis that are yield strength (f_y) and Young's modulus (E). These values are calculated since requaired for modeling in finite element software. Refer to IPA, the coefficients of modification are able to obtained by comparing the properties of specimen B to specimen A as illustrated below:

Tabel 5.6 Resume of experimental test results of specimens B.

Material	Area (mm ²)	Yield Strength (MPa)	Tensile Strength (MPa)	Young's Modulus (MPa)	Elongation at Break (%)
B1	19.71	167	181	13,925	4.635
B2	19.71	168	182	11,065	5.118
B3	19.71	160	184	12,050	6.828
B4	19.71	168	196	9,036	9.641
Avarage		166	186	11,519	6.555

- The coefficient of yield strength, denoted as C_y :

In obtaining the coefficient of yield strength, yield strength of specimen B is divided to yield strength of specimen A. The coefficient are used to predict the actual strength of perforated plate. The detail calculation is presented below:

$$C_y = \frac{f_y^*}{f_y} = \frac{166}{317} = 0.52$$

Where :

f_y^* = yield strength of perforated plate (specimens B).

f_y = yield strength of solid plate (specimens A).

- The coefficient of Young's modulus, denoted as C_e :

Similar with yield strength, the coefficient of Young modulus is also derived by comparing the specimen B to specimen A. The result are illustrated below:

$$C_e = \frac{E^*}{E} = \frac{11,519}{25,700} = 0.45$$

Where :

E^* = Young's modulus of perforated plate (specimens B).

E = Young's modulus of solid plate (specimens A).

5.2.2 Yield Strength of Perforated Plate

A series analysis has been conducted in previous section, to obtain the coefficient modification of perforated plate for yield strength and Young's modulus. It means that the actual strength of perforated plate (specimens C) are able to define. However, analysis data of experimental tension test of specimens C must be carried out. The pattern of result should be identical with specimens B since the geometric was similar. The coefficient of modification has been derived through previous analysis involving specimens A and specimens B. The values are used to find out the real strength of perforated plate, denoted specimen C. Prior to calculate the properties of specimens C, a series analysis must be conducted similarly with analysis in specimens B. It is carried out to make sure that the characteristic of specimen B and specimens C, that was different material, are identical. The detail analysis of specimens C are as follow:

- Specimens C1.

The results test of specimens C1-1; C1-2; C1-3 are presented in Fig 5.50 to 5.52 and Table 5.7.

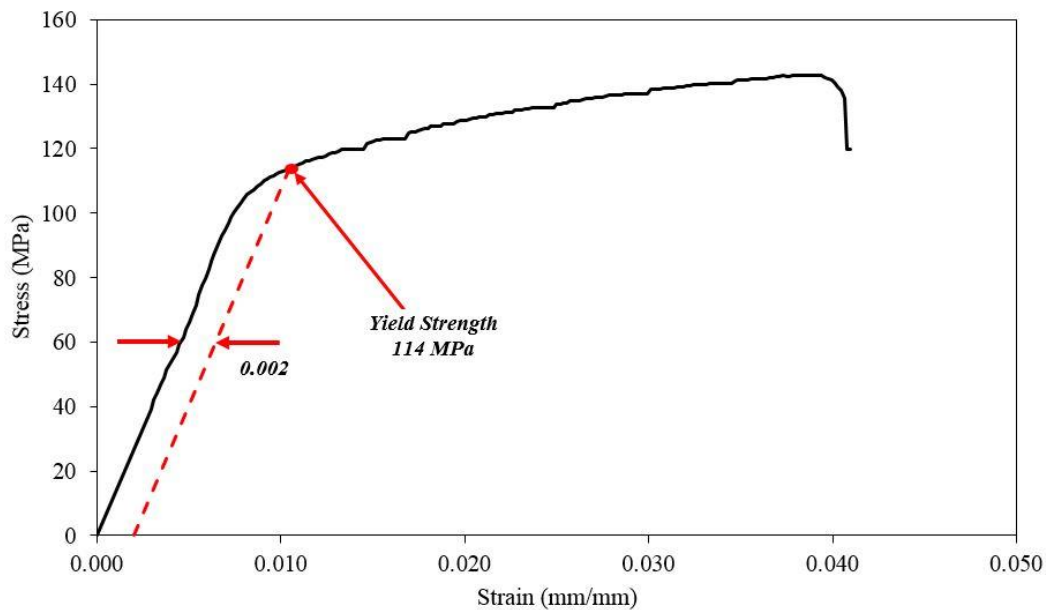


Figure 5.50 Stress – strain relationship of specimen C1-1.

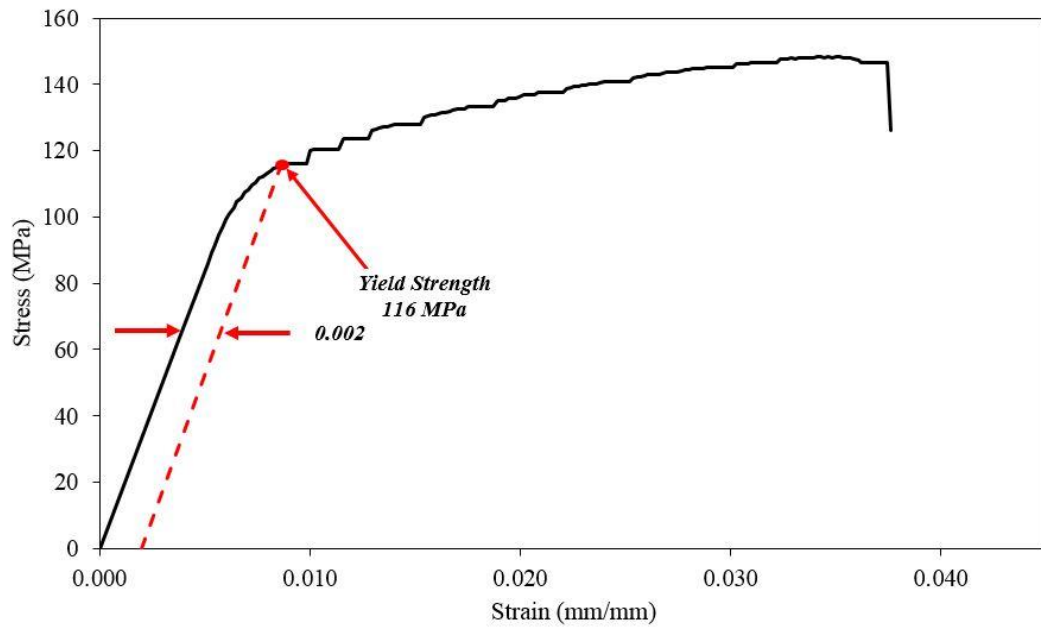


Figure 5.51 Stress – strain relationship of specimen C1-2.

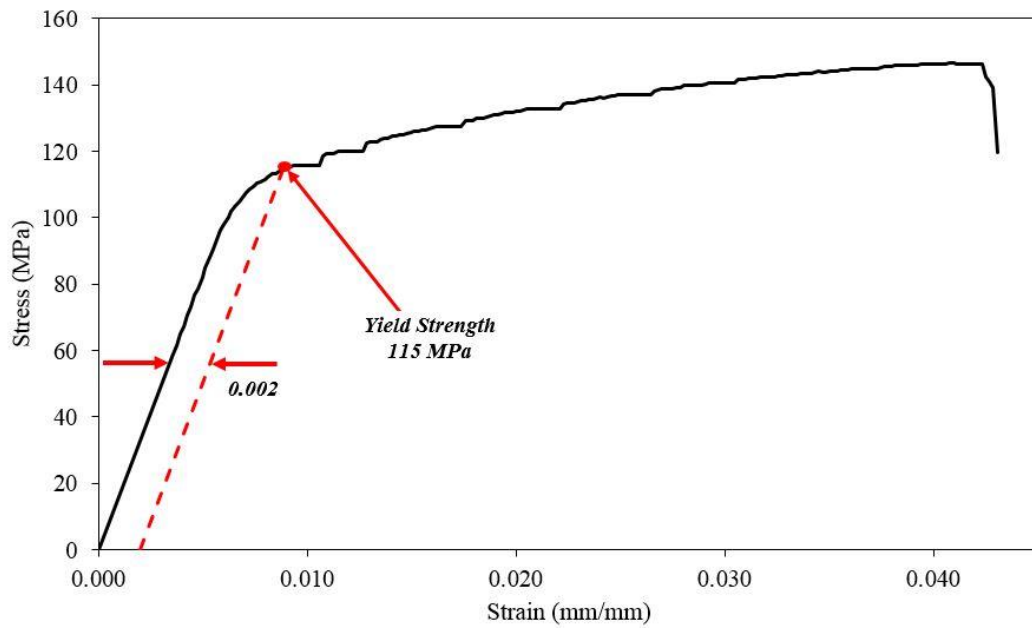


Figure 5.52 Stress – strain relationship of specimen C1-3.

Tabel 5.7 Experimental test results of specimens C1.

Material	Area (mm ²)	Yield Strength (Mpa)	Tensile Strength (Mpa)	Young's Modulus (Mpa)	Elongation at Break (%)
C1-1	19.71	114	143	13,430	4.897
C1-2	19.71	116	148	17,415	4.461
C1-3	19.71	115	147	16,040	5.127
Avarage		115	146	15,628	4.828

- Specimens C2.

The results test of specimens C2-1; C2-2; C2-3 are presented in Fig 5.53 to 5.55 and Table 5.8.

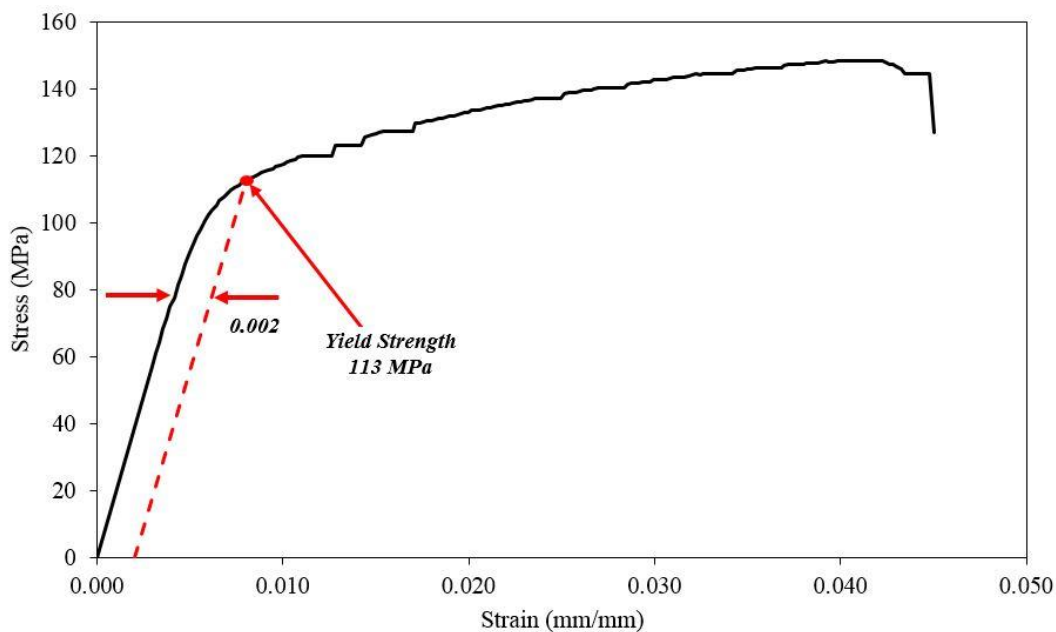


Figure 5.53 Stress – strain relationship of specimen C2-1.

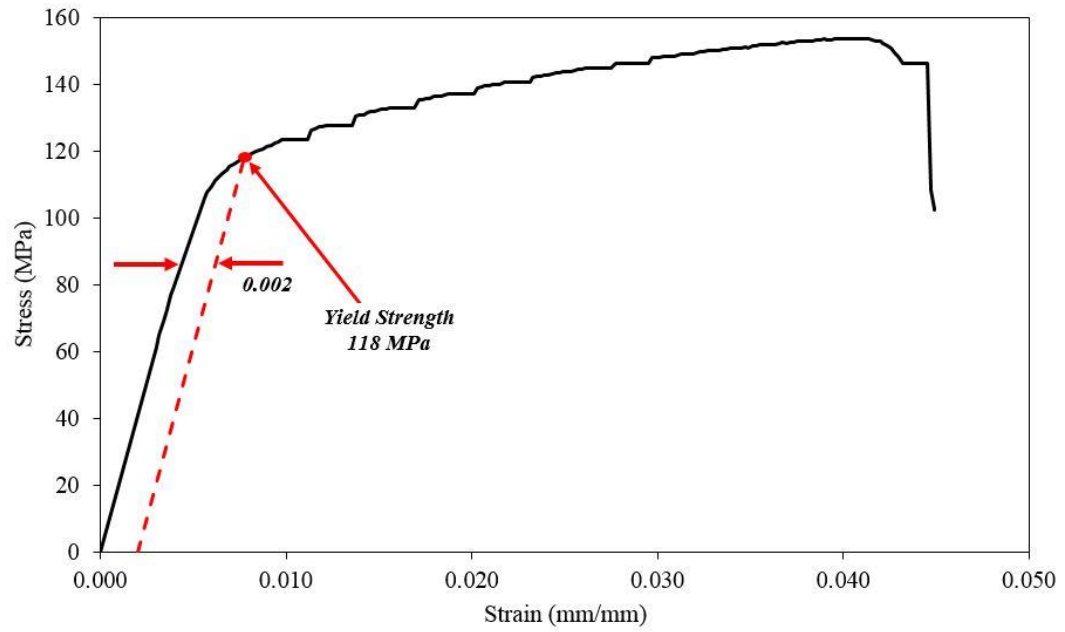


Figure 5.54 Stress – strain relationship of specimen C2-2.

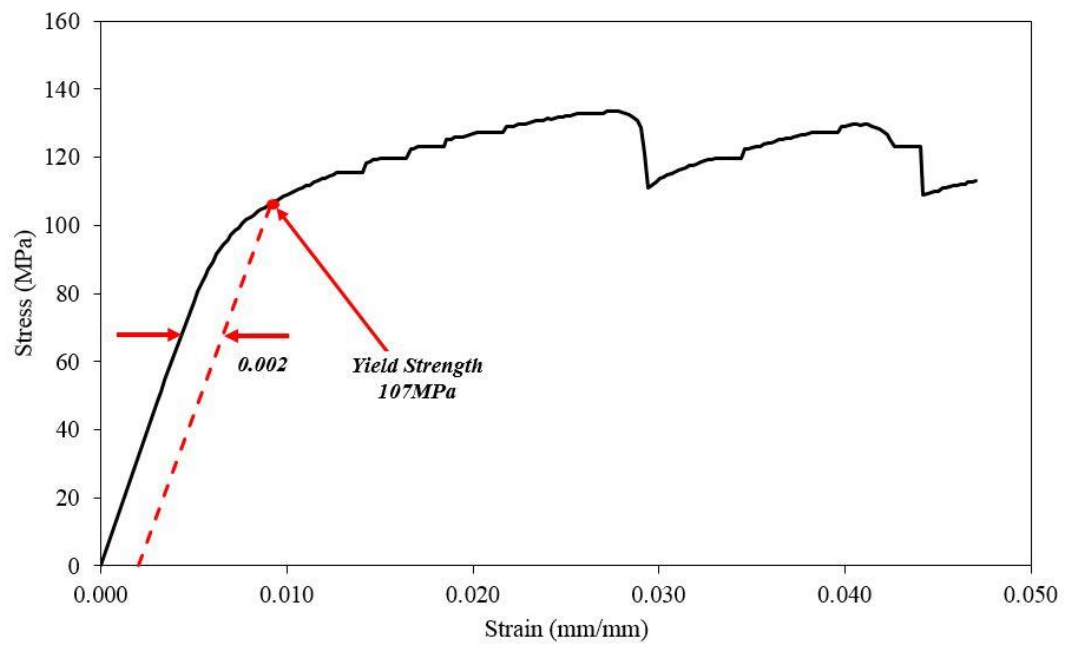


Figure 5.55 Stress – strain relationship of specimen C2-3.

Tabel 5.8 Experimental test results of specimens C2.

Material	Area (mm ²)	Yield Strength (MPa)	Tensile Strength (MPa)	Young's Modulus (MPa)	Elongation at Break (%)
C2-1	19.71	113	148	18,728	5.619
C2-2	19.71	118	154	20,525	5.294
C2-3	19.71	107	133	14,802	7.683
Avarage		113	145	18,019	6.199

- Specimens C3.

The results test of specimens C3-1; C3-2; C3-3 are presented in Fig 5.56 to 5.58 and Table 5.9.

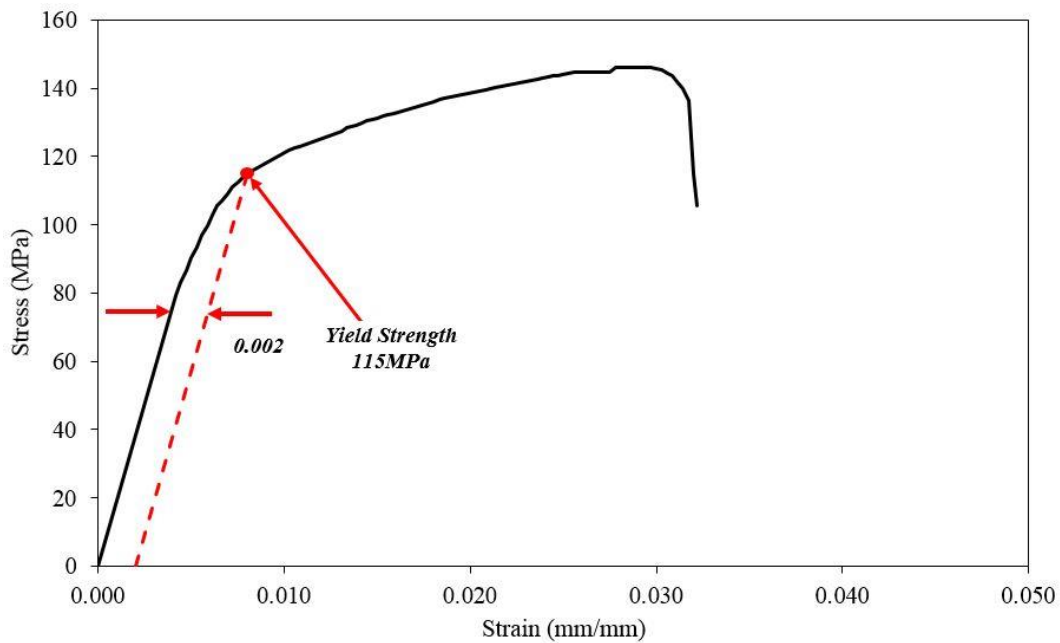


Figure 5.56 Stress – strain relationship of specimen C3-1.

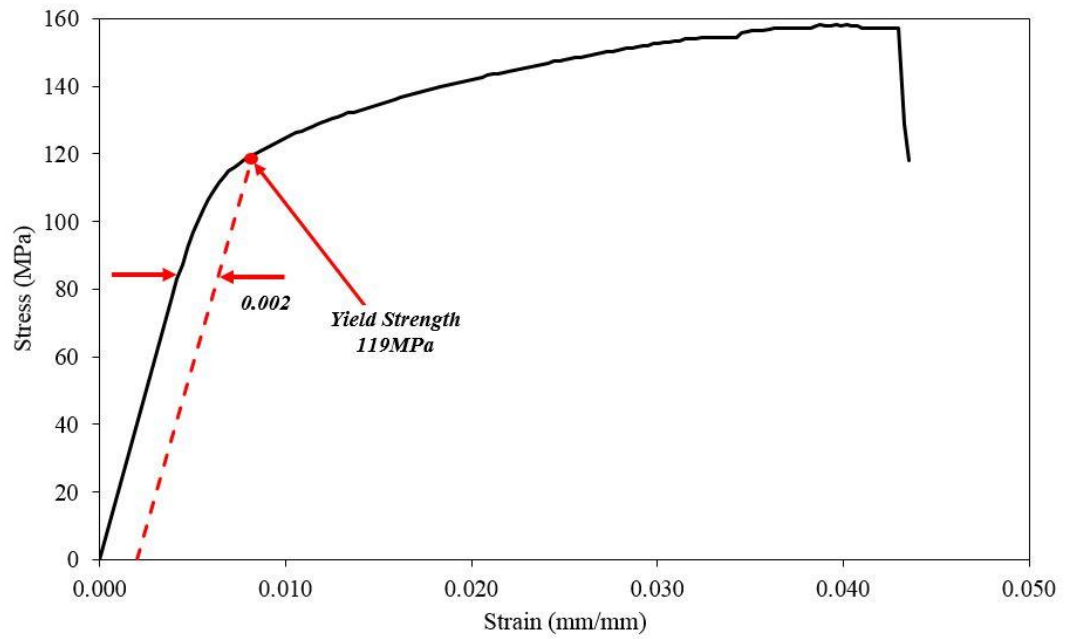


Figure 5.57 Stress – strain relationship of specimen C3-2.

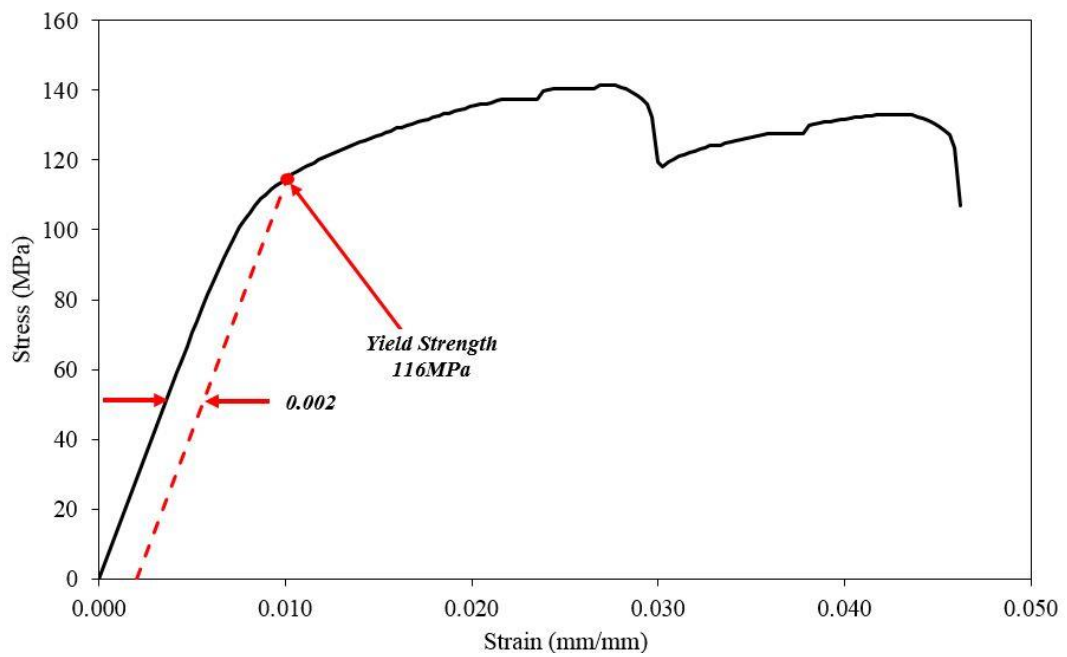


Figure 5.58 Stress – strain relationship of specimen C3-3.

Tabel 5.9 Experimental test results of specimens C3.

Material	Area (mm ²)	Yield Strength (MPa)	Tensile Strength (MPa)	Young's Modulus (MPa)	Elongation at Break (%)
C3-1	19.71	115	146	18,901	4.659
C3-2	19.71	119	158	20,358	5.226
C3-3	19.71	116	142	13,841	5.363
Avarage		117	149	17,700	5.082

- Specimens C4.

The results test of specimens C4-1; C4-2; C4-3 are presented in Fig 5.59 to 5.61 and Table 5.10.

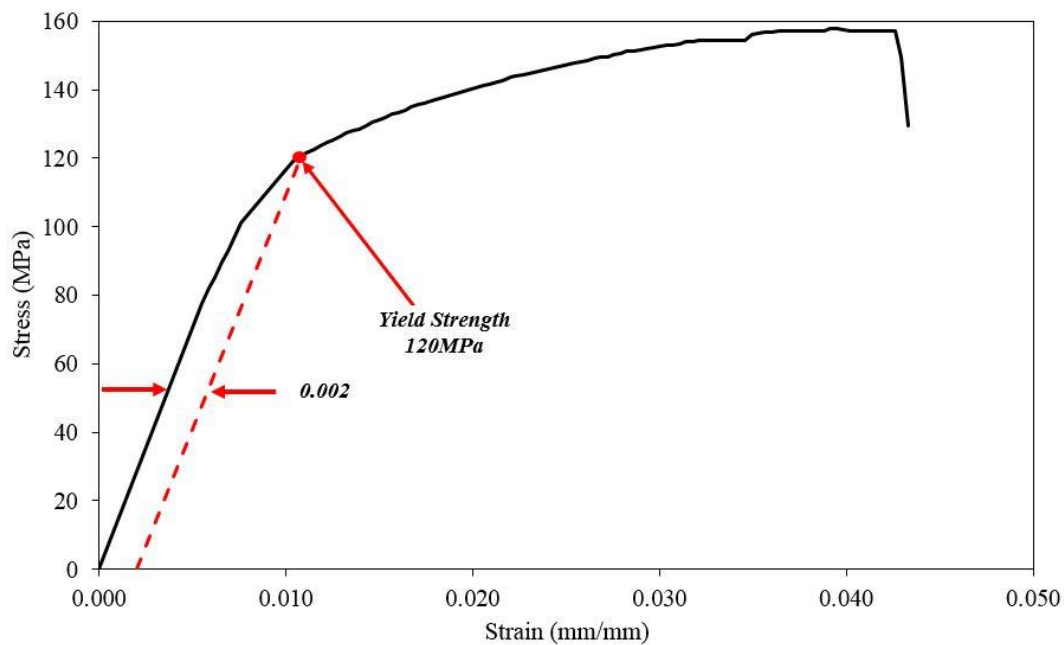


Figure 5.59 Stress – strain relationship of specimen C4-1.

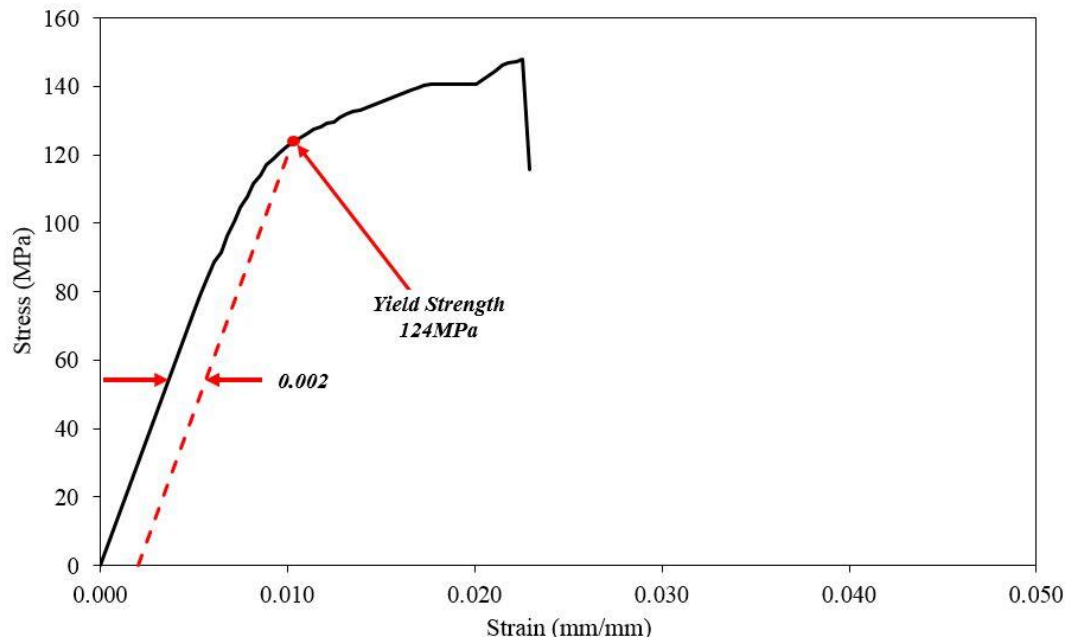


Figure 5.60 Stress – strain relationship of specimen C4-2.

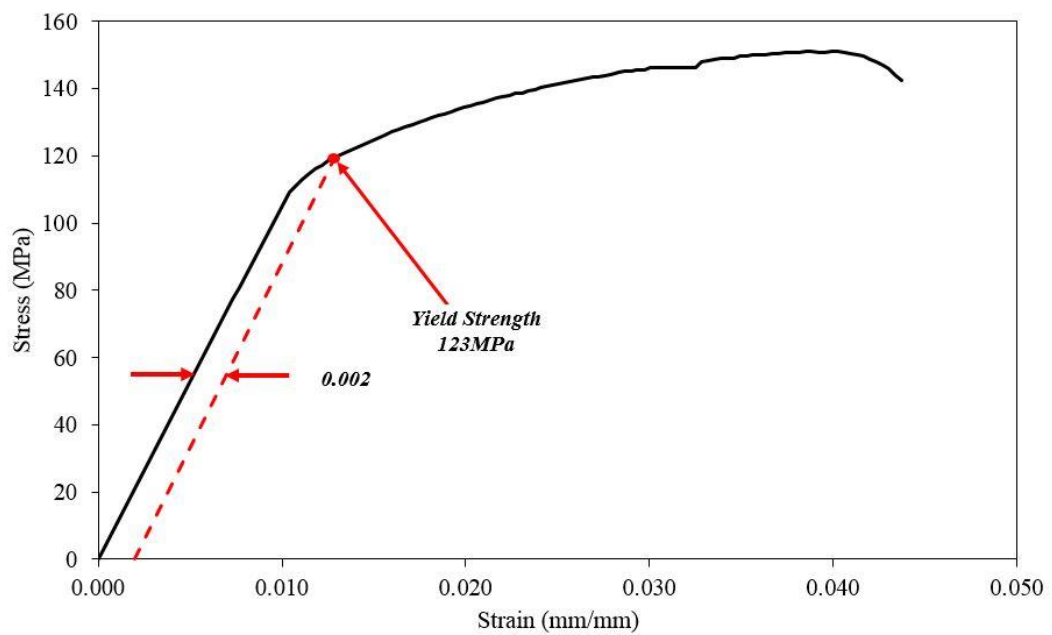


Figure 5.61 Stress – strain relationship of specimen C4-3.

Tabel 5.10 Experimental test results of specimens C4.

Material	Area (mm ²)	Yield Strength (MPa)	Tensile Strength (MPa)	Young's Modulus (MPa)	Elongation at Break (%)
C4-1	19.71	120	158	13,733	5.660
C4-2	19.71	124	148	14,933	4.165
C4-3	19.71	123	135	10,993	8.813
Avarage		122	147	13,220	6.213

Tabel 5.11 Resume of experimental test results of specimens C.

Material	Area (mm ²)	Yield Strength (MPa)	Tensile Strength (MPa)	Young's Modulus (MPa)	Elongation at Break (%)
C1	19.71	115	146	15,628	4.828
C2	19.71	113	145	18,019	6.199
C3	19.71	117	149	17,700	5.082
C4	19.71	122	147	13,220	6.213
Avarage		117	147	16,142	5.580

A series experimental tension test on specimens C were conducted to observe the material characteristic. Similar testing method, such as specimens B, was also applied on specimens C. The results test indicate identical characteristic between specimen B and specimen C for four type specimens. The resume of experimental test was given in Table 5.11. As shown in Table 5.11, the

mechanical characteristic among specimens C (C1 to C2) seem identical. This phenomena was also find out in experimental results of specimens B. In other word, the actual strength of specimens C are able to obtain by using coefficient modification. The detail are as follow :

- Analysis the actual yield strength of specimen C:

The coefficient of yield strength presented here is only for perforated plate with 51% percentage open area (POA). The coefficient for yield strength C_y was obtained about 0.52. Therefore, the actual yield strength of specimen C are given below :

$$C_y = \frac{f_y^*}{f_y}$$

$$0.52 = \frac{117}{f_y}$$

$$f_y = \frac{117}{0.52} = 225MPa$$

Where :

f_y^* = yield strength of perforated plate (specimens C).

f_y = the actual yield strength of solid plate (specimens C).

- Analysis the actual Young's modulus of specimen C:

Similar with yield strength, the coefficient of Young modulus is also derived by multiplying the cofficient Young's modulus C_e . Therefore, the actual Young's modulus of specimen C are given below :

$$C_e = \frac{E^*}{E}$$

$$0.45 = \frac{16,142}{E}$$

$$E = \frac{16,142}{0.45} = 35,871MPa$$

Where :

E^* = Young's modulus of perforated plate (specimens C).

E = the actual Young's modulus of solid plate (specimens C).

5.2.3 Summary

A series experimental test and analysis has been carried out to observe the characteristic of perforated plate presented in section 4.2. Normally, perforated plate was applied as non-structural member that is not required the detail information related to material properties. Therefore, the information related to material quality was not available on the market. However, in this research project, perforated was employed as reinforcement to prevent bulging effect on isolator under compression replacing conventional steel plate. In other word, the information related to material properties, typically yield strength, are needed to analyze the stress of perforated plate under compression. The stress on reinforcement must be determined to make sure that the stress occurred on the perforated plate during service load do not exceed the yield strength of material. Therefore, experimental test must be carried out on the perforated plate to observe the material properties.

The appropriate experiments for perforated plate are not clearly yet defined by national or organizational standards organizations. This difficulty derives from the complex geometric of perforated plate. In section 5.2.1, an approach method has been conducted in order to know the appropriate test method of perforated plate. The experimental resulted two parameters that were coef of yield strength (C_y) and coef of Young's modulus (C_c) as shown in Table 5.12. The coefficients were used to identify the actual strength of perforated plate that was presented in section 5.2.2 and Table 5.13.

Table 5.12 The coefficient of perforated plate

Coef of yield strength (C_y)	Coef of Young's modulus (C_c)
0.52	0.45

Table 5.13 Material properties of perforated plate

Yield strength (f_y)	Young's modulus (E_c)
225 MPa	35,871 MPa

5.3 Isolated Structure

5.3.1 Introduction

The main objective of this research work is to develop low cost base isolation for housing in high seismic zone. Prior to analyze the isolator, it is preferable to consider the characteristic of super structure that using base isolation, well-known as isolated structure (*IS*). It was regarded important to understand well to determine the target period of super structure and to define the appropriate horizontal stiffness of isolator related to the weight of structure. Therefore, in this section a series analytical solution was conducted to observe the behavior of isolated structure to determine both optimum fundamental period and horizontal stiffness of isolators. There were two type of housing considered in this section, one- and two- storey.

In this study, one-and two-storey houses were investigated to define the effective range of the fundamental period due to seismic loads. The effective period of an isolated structure should be defined first to provide an optimal design of the isolated structure. This period is related to the ductility demand of the isolated structure, which significantly decreases with the insertion of a very flexible base isolation system.

The main reason of introducing a base isolation system in a building is to enhance the structural safety and integrity of the building that is subjected to severe earthquakes. Application of a base isolation system in residential houses, which have less self-weight than a multi-storey building, is not feasible due to the unavailability of base isolation systems for houses with low horizontal stiffness. Therefore, a residential house does not require a heavily reinforced isolation system. In addition, a relatively small horizontal stiffness is required to acquire the target natural period of a house. The ductility demand is limited to less than 1.5 to ensure that a structure behaves elastically, and the displacement of an isolator has to be carefully checked prior to a strong earthquake. A study should be conducted to ensure the performance of residential houses with low horizontal stiffness, particularly the ductility demand of the structures.

These considerations suggest that the performance of a lowrise buildings (houses) that utilizes base isolation should be explored to pursue an optimal

design and certain safety level. Structures should be analysed for different isolator's horizontal stiffness values with an assumed isolation ratio value. In this study, a nonlinear time history analysis (NLTHA) method is performed to observe the response of a base-isolated reinforced concrete (RC) structure that is subjected to several selected earthquake motions.

5.3.2 Structural Modeling.

In the study, a typical residential building is considered; the plan view of a symmetric RC framed structure is shown in Figure 5.62 (a). The 3D frames are the assumed analytical models for the numerical investigations. Two cases are investigated: a one-storey building and a two-storey building. Only isolated analytical models of the buildings are shown in Figs. 5.62 (b) and (c); a rigid tie beam is assumed to be placed on the isolators at the base of the framed structures. Initially, RC frames with fixed bases have been designed according to the Indonesian National Standard (BSN, 2013), with the following assumptions: high-ductility/special moment frames (reduction factor: $R = 8$), high-risk seismic region (Aceh), PGA of 0.9 g, and soil profile SA (hard rock). A cylindrical compressive strength of 25 MPa (N/mm²) for concrete and a yield strength of 320 MPa (N/mm²) for steel have been assumed. The main properties of the structure are listed in Table 5.14

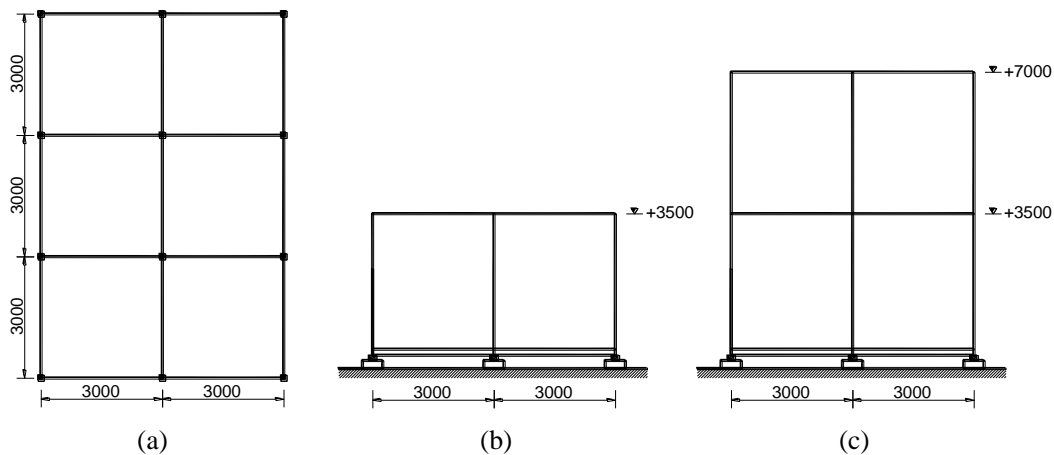


Figure 5.62 Analytical models of isolated frames: (a) Plan view; (b) Elevation of one-storey building; and (c) Elevation of two-storey building.

Tabel 5.14 Member cross-sectional dimensions (width depth, in Centimeter).

No	Storey	Columns	Girder	Beam
One-storey frames				
1	Base	-	15 x 25	-
	1	15 x 15	-	15 x 25
Two-storey frames				
2	Base	-	15 x 25	
	1	20 x 20	-	15 x 25
	2	20 x 20	-	15 x 25

The base-isolated frames are designed by assuming the same strength level for the corresponding fixed-base frames and considering the different strength distributions throughout each isolated framed structure according to its vibration modes (predominantly the first mode). Different values of the isolation ratio in an extensive range ($1 \leq \alpha_I \leq 10$) are considered; assuming $\alpha_I = 1$, the case of the fixed-base structure is analyzed. The variation in α_I value is obtained by selecting suitable values for the isolator stiffness properties. The behavior of the isolated structure is primarily dependent on the horizontal stiffness of the base isolator. The required horizontal stiffness of the isolation structure K_H is calculated as

$$K_H = m \times \left(\frac{2\pi}{T} \right)^2 \quad (5.8)$$

$$T_I = \alpha_I T_F \quad (5.9)$$

where m is the mass of the structure. The target fundamental period of the analytical models T_I , and the horizontal elastic stiffness of the isolator K_1 , K_2 , K_3 and K_4 as shown in Fig 5.76 which are generated from different values of the isolation ratio, are listed in Table 5.15.

5.3.3 Modeling Approach.

Regular form of 1- and 2 story buildings are designed according to Indonesia Building Code for the loading and dimensions described in the previous section. Then using the outcome member size and reinforcement, structure are modeled for nonlinear analysis. A three-dimensional model of each structure is created in SAP2000 v14.2.2 to carry out nonlinear time history analysis.

Beam and column elements are modeled as nonlinear frame elements with lumped plasticity by defining plastic hinges at both ends of beams and columns. SAP2000 provides default or the user-defined hinge properties options to model nonlinear behavior of components. The value assigned to each of these points vary depending on type of element, material properties, longitudinal and transverse steel content and axial load level on the element. It is possible to satisfy the performance criteria of elastic behavior by using base isolation on the structure. In order to guaranty the performance structure behave elastically, the ductility demand is restricted below 1.5 for isolated structure.

5.3.4 Ground Motion Selected.

Seven ground motion records selected are presented in Table 5.16 and Fig. 5.63 to 5.69. The parameters that need to be consider in identifying the scenario are those that have the most influence on ground motion spectral shape , in the following:

- a. Magnitude Dependence; In order to derive the magnitude influence on response spectral shape, the magnitude ranging about 4.9 to 7.9 in the NGA database.
- b. Distance; predominant period shifts to higher values with increase in distance from the fault for the given earthquake. For particular event, predominant period shifts from about 0.35 sec at the closes distance (0-20km) to 1.2 sec at farthest fault distance (120-140 km).
- c. Soil Condition; The spectral shape also depends on the site conditions. Predominant period of the spectra from rock soil type is generally lower than the soft soil type. The average spectral shape in Vs30 of 180-360 m.sec with that of 540-720 m/sec.

Tabel 5.15 Horizontal stiffness of isolators

Model	$\alpha_I = T_I/T_F$	T_I	K_H (MN/m)			
		(s)	Isolator 1	Isolator 2	Isolator 3	Isolator 4
(a). <i>One-storey frames</i>						
Model-1	1.0	$T_F = 0.4$	~	~	~	~
Model-2	1.5	0.60	0.504	0.822	0.844	1.315
Model-3	2.0	0.80	0.370	0.604	0.620	0.966
Model-4	2.5	1.00	0.251	0.409	0.420	0.655
Model-5	3.0	1.20	0.181	0.296	0.304	0.473
Model-6	3.5	1.40	0.126	0.205	0.211	0.329
Model-7	4.0	1.60	0.100	0.162	0.167	0.260
Model-8	4.5	1.80	0.076	0.123	0.126	0.197
Model-9	5.0	2.00	0.059	0.097	0.099	0.155
Model-10	5.5	2.20	0.050	0.082	0.084	0.131
Model-11	6.0	2.40	0.041	0.067	0.069	0.107
Model-12	6.5	2.60	0.036	0.058	0.060	0.093
Model-13	7.0	2.80	0.030	0.049	0.051	0.079
Model-14	7.5	3.00	0.027	0.044	0.045	0.070
Model-15	8.0	3.20	0.023	0.038	0.039	0.060
Model-16	8.5	3.40	0.021	0.034	0.035	0.054
Model-17	9.0	3.60	0.018	0.030	0.031	0.048
Model-18	9.5	3.80	0.017	0.027	0.028	0.043
Model-19	10	4.00	0.015	0.024	0.025	0.039
(b). <i>Two-storey frames</i>						
Model-1	1.0	$T_F = 0.7$	~	~	~	~
Model-2	1.5	1.1	0.475	0.824	0.797	1.337
Model-3	2.0	1.4	0.259	0.450	0.435	0.731
Model-4	2.5	1.8	0.152	0.265	0.560	0.429
Model-5	3.0	2.1	0.106	0.184	0.178	0.298
Model-6	3.5	2.5	0.074	0.129	0.125	0.209
Model-7	4.0	2.8	0.060	0.103	0.100	0.168
Model-8	4.5	3.2	0.045	0.079	0.076	0.128
Model-9	5.0	3.5	0.037	0.064	0.062	0.104
Model-10	5.5	3.9	0.030	0.052	0.050	0.084
Model-11	6.0	4.2	0.025	0.040	0.042	0.071
Model-12	6.5	4.6	0.021	0.037	0.036	0.060
Model-13	7.0	4.9	0.019	0.032	0.031	0.052
Model-14	7.5	5.3	0.016	0.028	0.027	0.046
Model-15	8.0	5.6	0.014	0.025	0.024	0.040
Model-16	8.5	6.0	0.013	0.022	0.021	0.036
Model-17	9.0	6.3	0.011	0.020	0.019	0.032
Model-18	9.5	6.7	0.010	0.018	0.017	0.029
Model-19	10.0	7.0	0.009	0.016	0.015	0.026

Tabel 5.16 Selected earthquake the ground motions.

No	Earthquake	Year	Station	Magnitude	PGA (g)
1	Tabas, Iran	1978	Tabas	7.4	0.85
2	San Fernando	1971	Pacoima	6.1	1.12
3	Northridge	1994	Alhambra - Fremont School	6.7	0.10
4	Landers	1992	Lucerne	7.3	0.72
5	Morgan Hill	1984	Anderson Dam (Downstream)	6.2	0.40
6	Loma Prieta	1989	APEEL 10 - Skyline	6.9	0.45
7	Italy	1980	Bagnoli Irpinio	6.9	0.15

The best way to avoid a biased sample is to select a random sample. This process statically allows us to treat the spectrum of this random sample as the "true" target spectrum. Therefore in selecting candidate records for nonlinear time history analysis , one needs to carefully identify records whose spectral shapes are close to each other.

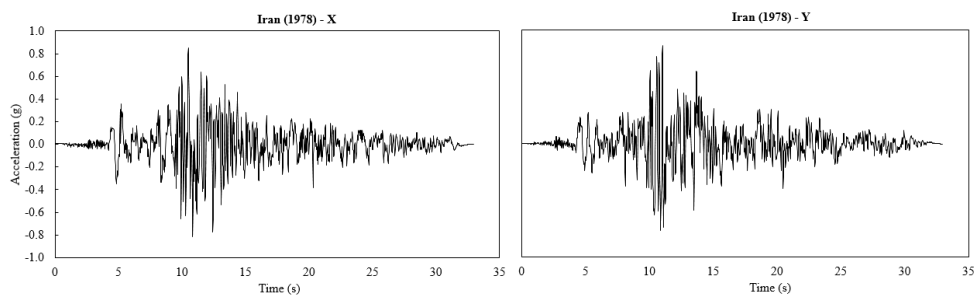


Figure 5.63 Ground motion of Tabas - Iran (1978) in X- and Y- direction.

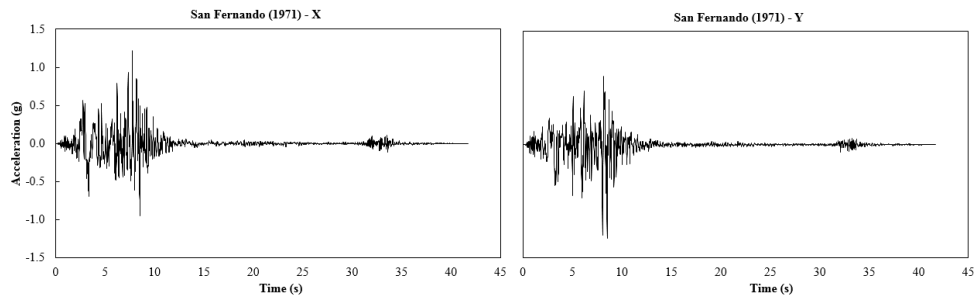


Figure 5.64 Ground motion of San Fernando (1971) in X- and Y- direction.

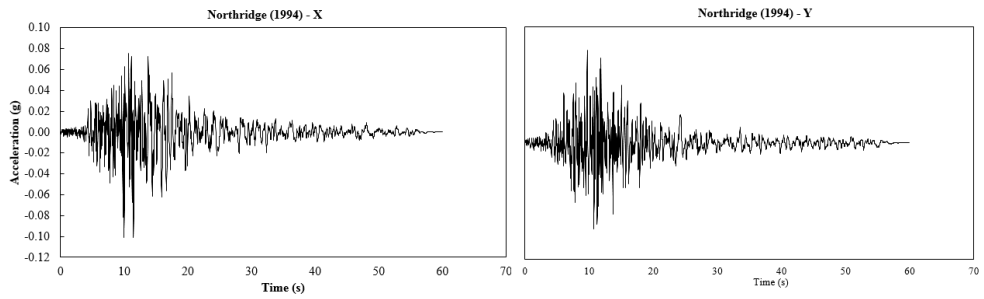


Figure 5.65 Ground motion of Northridge (1994) in X- and Y- direction.

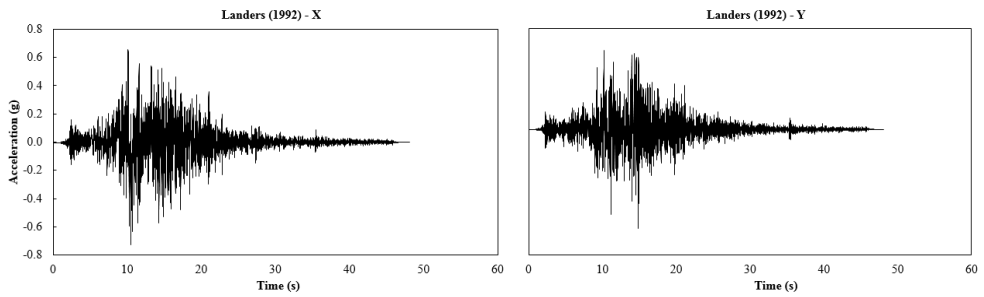


Figure 5.66 Ground motion of Landers (1992) in X- and Y- direction.

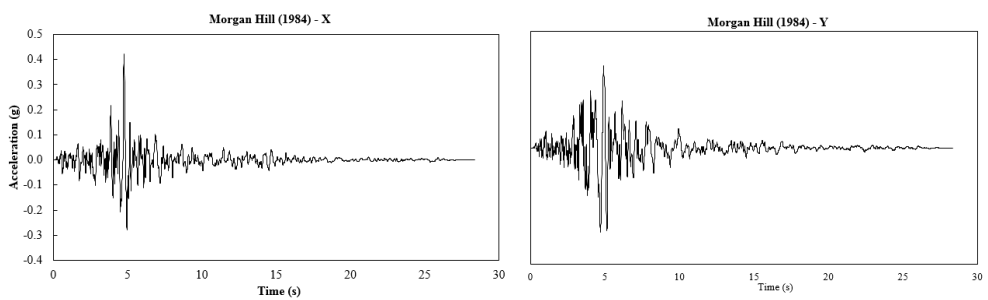


Figure 5.67 Ground motion of Morgan Hill (1984) in X- and Y- direction.

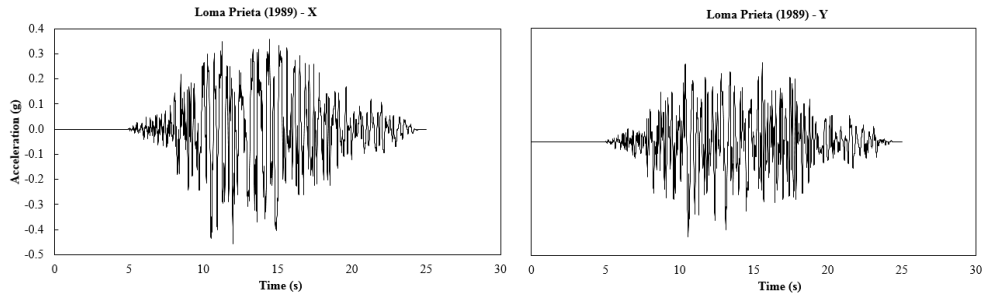


Figure 5.68 Ground motion of Loma Prieta (1989) in X- and Y- direction.

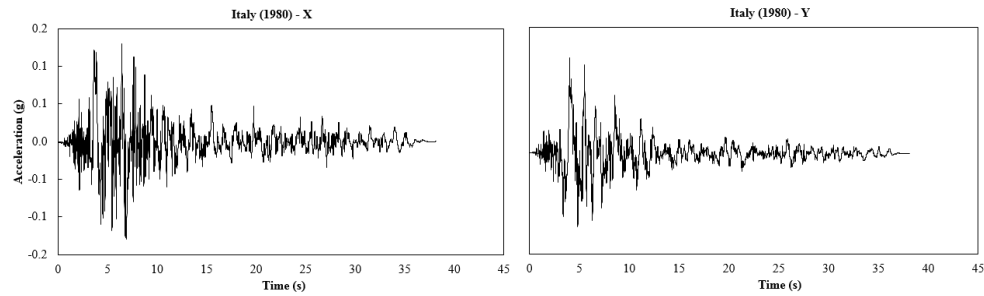


Figure 5.69 Ground motion of Italy (1980) in X- and Y- direction.

5.3.5 Ground Motion Scaling Prosedure.

According to ASCE 7-10 standard, ordinate of the target spectrum over the period range were $0.2T_I$ to $1.5T_I$. The target pseudo-acceleration spectrum for the buildings site was taken as the median of the 5% damped pseudo-acceleration response spectra corresponding to the average of the horizontal components of the unscaled records, related to Indonesia earthquake code. The pseudo-acceleration spectrums of the seven-ground motion were derived by using commercial program, as shown in Fig 5.70 and Fig 5.71.

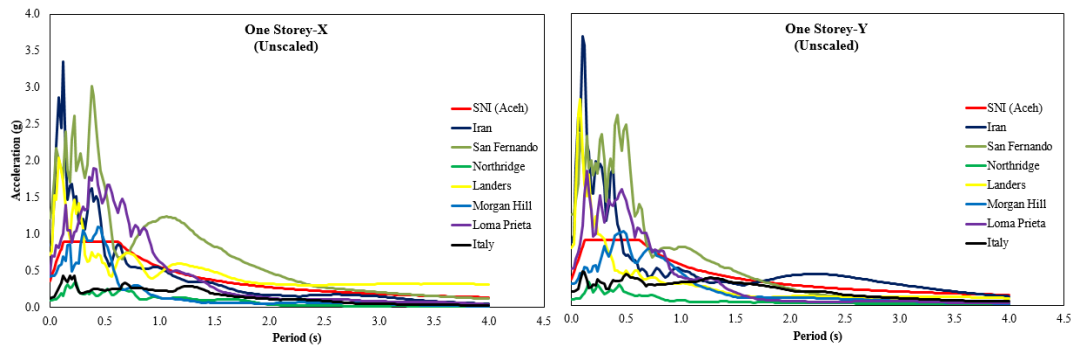


Figure 5.70 Unscaled response spectra of ground motion records (one storey).

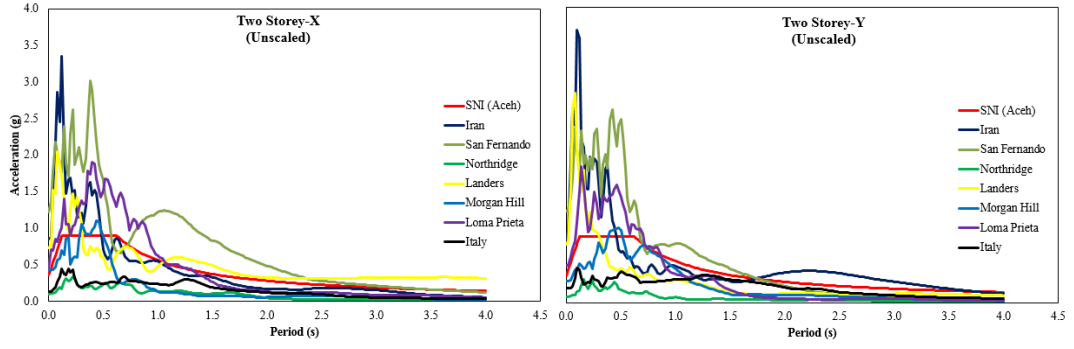


Figure 5.71 Unscaled response spectra of ground motion records (two storey).

Least Square Method, scaling technique used to match the spectrum, was proposed by (Kalkan and Chopra, 2010). Under this method, the input acceleration were multiplied by a scalar that minimizes the weighted sum of the errors between the ground motion spectra and the target spectrum. In order to obtain a minimum scale factor for each of seven records, residuals between the record's scaled spectrum and target spectrum is minimized between $0.2T_l$ and $1.5T_l$ trough a method of least square whereby square of sum of residuals is expressed as

$$\lambda = \sum_{i=1}^n [\bar{A}_i - (SF \times A_i)]^2 \quad (5.10)$$

where \bar{A}_i and A_i are the target spectral acceleration and record's (unscaled) spectral acceleration, respectively. The symbol i^{th} is spectral period, and n is the number of periods (log spaced) covered between $0.2T_l$ and $1.5T_l$. The aim is to find a values of SF that minimize the error. In multivariable calculus, we learn that this requires us to find the SF such that

$$\frac{d\lambda}{dSF} \cong 0$$

$$\lambda = \sum_{i=1}^n [\bar{A}_i^2 - 2\bar{A}_i.A_i.SF + A_i^2.SF^2]$$

$$\frac{d\lambda}{dSF} = \sum_{i=1}^n [2SF.A_i^2 - 2\bar{A}_i.A_i] = 0$$

$$SF = \frac{\sum_{i=1}^n \bar{A}_i A_i}{\sum_{i=1}^n A_i A_i} \quad (5.11)$$

Note that Eq 5.11, yields an optimal scaling factor to ensure the record's scaled spectrum match closely the target spectrum between $0.2T_l$ and $1.5T_l$. The scaled factor of record ground according to Eq 5.11, are shown in Table 5.17. Then, the scaled spectra acceleration were shown in Fig 5.72 and Fig 5.73.

Table 5.17 Scaling factor of ground motion.

No	Earthquake	Year	Station	Magnitude	Scaling Factor			
					One Storey		Two Stories	
					X	Y	X	Y
1	Tabas, Iran	1978	Tabas	7.4	0.514	0.449	0.745	0.660
2	San Fernando	1971	Pacoima	6.1	0.430	0.429	0.470	0.487
3	Northridge	1994	Alhambra - Fremont School	6.7	3.868	4.287	3.837	4.668
4	Landers	1992	Lucerne	7.3	0.749	0.669	0.985	1.086
5	Morgan Hill	1984	Anderson Dam (Downstream)	6.2	1.064	1.190	1.176	1.142
6	Loma Prieta	1989	APEEL 10 - Skyline	6.9	0.623	0.661	0.627	0.723
7	Italy	1980	Bagnoli Irpinio	6.9	2.958	2.576	2.862	2.512

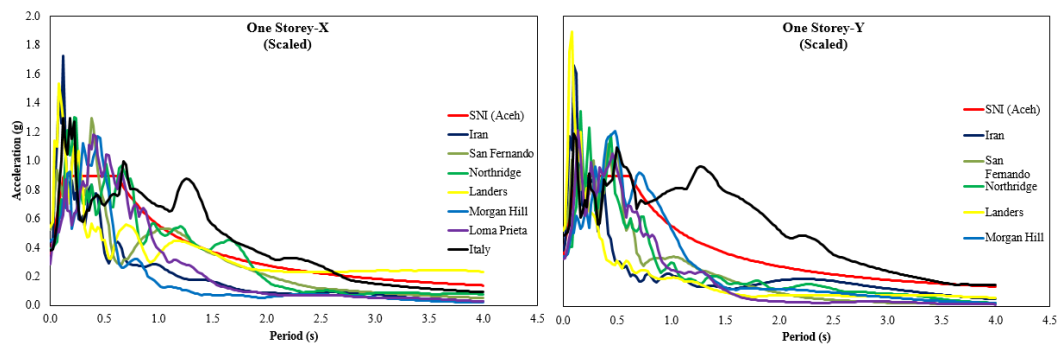


Fig 5.72 Scaled response spectra of ground motion records (one storey).

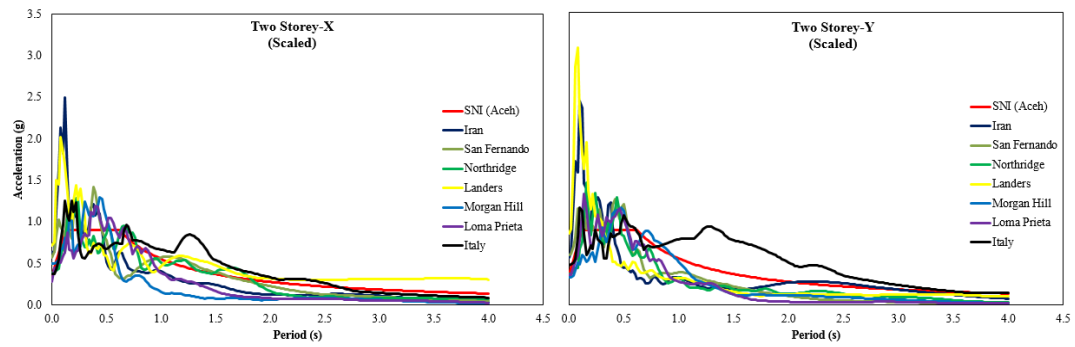


Fig 5.73 Scaled response spectra of ground motion records (two storey).

5.3.6 Results.

In order to study the dynamic response of the isolated structure due to earthquake loads, a numerical investigation was carried out assuming the isolation-ratio value in Table 5.15. The ground motion generated to match the design spectrum as shown in Fig 5.72 and Fig 5.73, are considered for studying the dynamic behavior of the structure subjected to strong earthquake. The results which follow are derived as an average value of these seven ground motions.

The structural system were subjected to sets of seven records modified according to ASCE 7 ground motion-scaling method. Regular form of 1- and 2 story buildings show a similar pattern in term of ductility demand. Considering the isolation ratio 1 is a fixed base structure, the pattern of ductility demand of the structure decrease significantly by following the increasing of the isolation ratio. It matches with basic concept of base isolation in order to lengthen the period of the structure, that means the increasing period of the structure lead to the ductility will be decrease. The top limit of ductility demand in this case is 1.5. The reason for this is to avoid high ductility in the structure above the isolation system as the period of the yielded structure may degrade and interact with that of the isolation system.

In contrast with displacement of isolator, the increase of isolation ratio causes the value of displacement of isolator increase significantly. The capability of the isolator under going horizontal displacement was restricted with the max shear strain (100%) of the isolator, which has max displacement, related to the height of isolator, about 150mm. The Fig 5.74 and Fig 5.75, show the results analysis,

according to ductility demand and displacement, of one- and two-storey low-rise buildings.

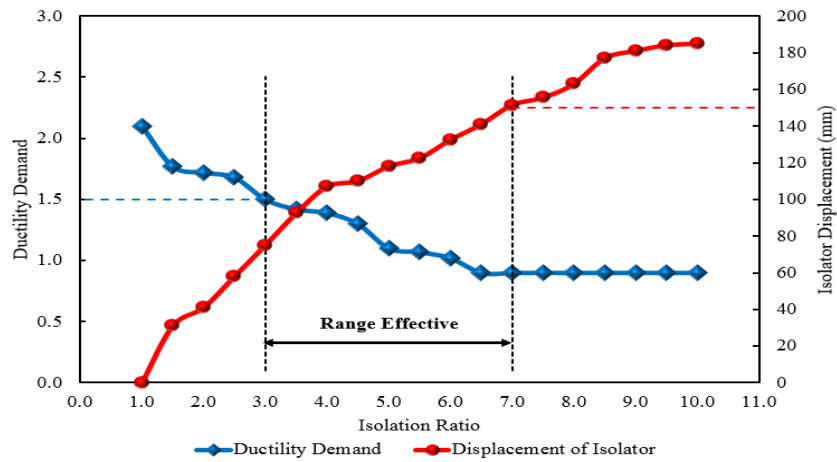


Figure 5.74 The range effective of the isolation ratio for one storey.

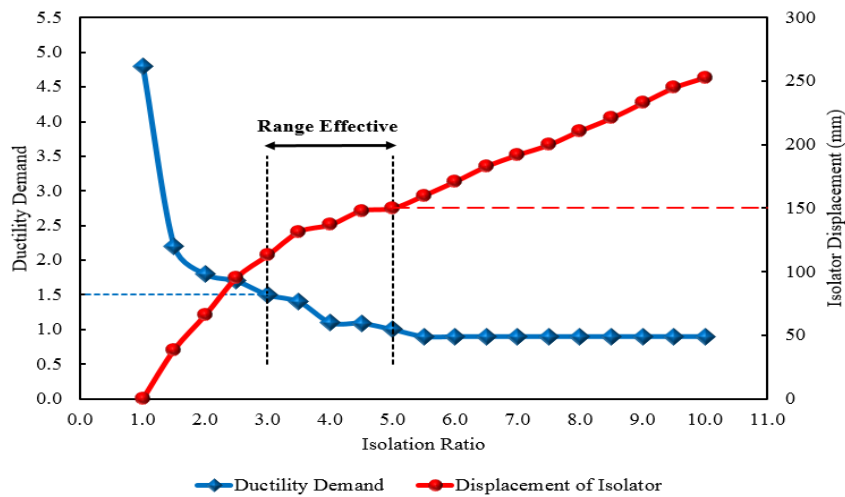


Figure 5.75 The range effective of the isolation ratio for two storey.

5.3.7 Summary.

The primary objective of using base isolation on the structure is to expect that the structure behaves elastically. In section 4.3, analysis of isolated structure is presented. There were two type of building structure studied in this research, one- and two- storey. The analysis resulted that the ranges effective of isolated structure for one- and two- storey were 3 to 7 and 3 to 5, respectively. It means that the effective fundamental period were 1.2 sec to 2.8 sec and 2.1 sec to 3.5 sec for one- and two storey, respectively.

The determination of fundamental period in design proses is a critical point to determine the lateral stiffness of isolator. It must be conducted to achieve the desired fundametal period. In this research, there were two parameters used in defining target of fundamental period, they were ductility demand of structure and lateral displacement of isolator. A single value must be selected to represent the period of isolated structure for low-rise building. Refer to some references (Kelly, 2001; Kelly, 1999), the fundamental period for isolated structure was suggested of about 1.5 sec to 2 sec. Therefore, in this research, the target of fundamental period for two isolated structures were selected of 2 sec. The selecting period of 2 sec for isolated structure is considered appropriate since it is still in range of effective isolation periode that is shown in Fig 5.74 and Fig 5.75. It means that to obtain the fundamental period of 2 sec, the isolation ratio used for one- and two- storey were 5 and 2.8, respectively. Subsequently, the fundamental period was employed in planning process of isolator as shwon in section 4.4. The dimension and the horizontal stiffness were designed to achieve fundamental period of approximately 2 second. In this period, the structures are expected to behave elastically under earthquake.

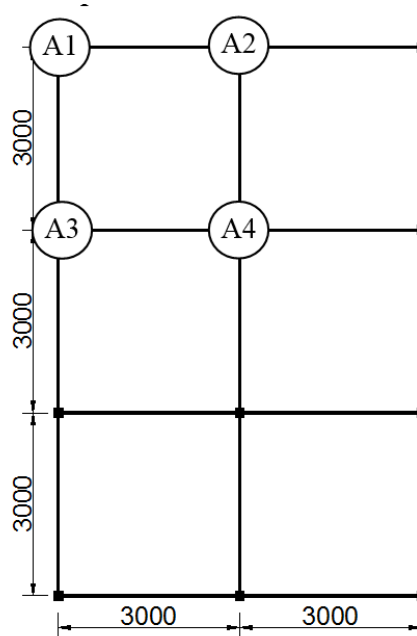


Figure 5.76 Plan view of isolated model for one- and two- storey.

In order to derive the target fundamental period of structure, the isolator must be provide and designed for each columns related to the axial force subjected to dead load and live load. The plane view of isolated model is illustrated in Fig 5.76. There are four join reaction denoted A1, A2, A3 and A4 that represent the isolated structure for one- and two- storey. The specifications of isolator which is required to create isolated having fundamental period of 2 sec are illustrated in Table 5.18 and 5.19.

Table 5.18 Characteristic of isolator for one storey.

Join	Axial force (ton)	t_r (mm)	Dia (mm)	K_H (Kg/m)	Shear Modulus (MPa)
A1	4.6	100	200	4,627.976	0.147
A2	7.5	100	200	7,545.612	0.240
A3	7.7	100	200	7,746.829	0.247
A4	12.0	100	200	12,072.980	0.384

Table 5.19 Characteristic of isolator for two storey.

Join	Axial force (ton)	t_r (mm)	Dia (mm)	K_H (Kg/m)	Shear Modulus (MPa)
A1	8.7	100	200	8,752.910	0.279
A2	15.1	100	200	15,191.833	0.484
A3	14.6	100	200	14,688.792	0.468
A4	24.5	100	200	24,649.000	0.785

The horizontal stiffness, described in Table 5.18 and 5.19, produce a fundamental period of approximately 2 second on the the isolated structure. The isolators are designed with similar dimension and different shear modulus of rubber material. In other word, the shear modulus (G) is the critical point for design process of isolator. Refer to some references, the smallest value of shear modulus is about 0.2 MPa. Therefore, the isolator for join A1 of one storey must be modified to achieve desired fundamental period due to the shear modulus is below of 0.2 MPa.

5.4 Preliminary Design of Base Isolation System.

In this chapter, design of base isolation using analytical method are presented. The aim is to determine the appropriate geometric of base isolation used in experimental test. This analysis is initial approach to define geometric of base isolation. Several assumption was employed in design process to derive preliminary of isolator. According to analysis of isolated structure, the target fundamental period of this research work is approximately 2 second. It means that horizontal stiffness of base isolation must be designed to move freely in horizontal direction in 2 second. The appropriate axial load was determined to achieve target period refer to horizontal stiffness. The detail calculation are presented below :

- **Axial load**

$$P = 8 \text{ ton} = 8,000 \text{ Kg} = 80,000 \text{ N}$$

- **Target Period of Isolated Structure**

- DBE (Design Basic Earthquake)

$$T_D = 2 \text{ second (refer to isolated structure analysis)}$$

- MCE (maximum Capacity Earthquake)

$$T_M = 2.3 \text{ second (refer to assumption)}$$

- **Stiffness Calculation**

- DBE (Design Basic Earthquake)

$$T_D = 2\pi \sqrt{\frac{W}{K_D \times g}}$$

$$2 \text{ sec} = 2\pi \sqrt{\frac{8,000 \text{ Kg}}{K_D \times 9.8 \text{ m/s}^2}}$$

$$K_D = 8,048.653 \text{ kg/m} = 8.048 \text{ ton/m}$$

- MCE (Maximum Capacity Earthquake)

$$T_M = 2\pi \sqrt{\frac{W}{K_M \times g}}$$

$$2.3 \text{ sec} = 2\pi \sqrt{\frac{8,000 \text{ Kg}}{K_M \times 9.8 \text{ m/s}^2}}$$

$$K_M = 6,085.983 \text{ kg/m} = 6.085 \text{ ton/m}$$

In calculate $K_{D,\max}$ and $K_{M,\max}$, it was assumed additional 10% about the mean stiffness values.

$$K_{D,\max} = 1.1 \times 8,048.653 \text{ kg/m} = 8,853.518 \text{ kg/m}$$

$$K_{M,\max} = 1.1 \times 6,085.938 \text{ kg/m} = 6,694.532 \text{ kg/m}$$

▪ Design Displacement

In this calculation, the structure was considered in Aceh with type of soil is hard rock. Therefore the parameter such as S_{D1} and S_{M1} were derived from SNI 1726:2012 refer to parameter of Aceh earthquake design.

$$D_D = \frac{g \times S_{D1} \times T_D}{4\pi^2 \times B_D} = \frac{9.8 \times 0.428 \times 2}{4\pi^2 \times 1.35} = 0.157 \text{ m} = 157 \text{ mm}$$

$$D_M = \frac{g \times S_{M1} \times T_M}{4\pi^2 \times B_D} = \frac{9.8 \times 0.642 \times 2.3}{4\pi^2 \times 1.35} = 0.272 \text{ m} = 272 \text{ mm}$$

▪ Minimum Design Displacement Permitted for Dynamic Analysis

$$D'_D = \frac{D_D}{\sqrt{1 + (T/T_D)^2}} = \frac{0.157 \text{ m}}{\sqrt{1 + (0.4/2)^2}} = 0.153 \text{ m}$$

$$D'_M = \frac{D_M}{\sqrt{1 + (T/T_M)^2}} = \frac{0.272 \text{ m}}{\sqrt{1 + (0.4/2.3)^2}} = 0.267 \text{ m}$$

▪ Minimum Base Shear Strength on the Isolation Interface

$$V_b = K_{D,\max} \times D_D = 8,853.518 \text{ kg/m} \times 0.157 \text{ m} = 1,390 \text{ kg} = 1.4 \text{ ton}$$

In Table 5.20, the base shear of Aceh related to type of soils are presented.

Tabel 5.20 Parameter design of Aceh.

Soils	S_{D1} (g)	S_{M1} (g)	D_D (m)	D_M (m)	V_b (Kg)
Hard Rock (SA)	0.428	0.642	0.157	0.267	1,390
Rock (SB)	0.557	0.835	0.205	0.353	1,815
Soft Rock (SC)	0.642	0.963	0.236	0.408	2,089
Stiff Soil (SD)	1.028	1.541	0.378	0.652	3,347

▪ **Estimation of rubber thickness**

In determine the total rubber thickness, the approach analysis was employed by assuming the max shear strain about 1.5. The detail is given below :

$$\gamma = \frac{D_D}{t_r}$$

$$t_r = \frac{D_D}{\gamma} = \frac{157}{1.5} = 102mm \approx 100mm$$

▪ **Estimation of loaded area of base isolation**

Prior to define the loaded area, the magnitude of shear modulus (G) of rubber material must be determined as primary parameter in design procedure. The initial shear modulus (G) is employed in preliminary process derived from experimental data presented in section 3.1. The initial shear modulus (G) of rubber is take into account from material constant of Ogden model derived from curve fitting process as shown in Table 6.1. By using Ogden model, the initial shear modulus is obtained as follow :

$$G = \frac{1}{2}(\mu_1\alpha_1 + \mu_2\alpha_2 + \mu_3\alpha_3)$$

$$G = \frac{1}{2}((-2,596.2 \times 0.12926) + (910.09 \times 0.21027) + (4,729.7 \times 0.03068))$$

$$G = 0.439 \text{ MPa}$$

The surface area of base isolation is able to estimate after the total rubber thickness was obtained. The detail is as follow :

$$K_H = \frac{G \times A}{t_r}$$

$$A = \frac{K_H \times t_r}{G} = \frac{80.48N/mm \times 100}{0.439} = 18,332.5mm^2$$

Therefore, the diameter of base isolation is as follow:

$$A = \frac{1}{4} \times \pi \times D^2$$

$$18,332.5 = \frac{1}{4} \times \pi \times D^2$$

$$D = \sqrt{\frac{18,332.5 \times 4}{\pi}} = 152.8mm \approx 200mm$$

▪ Initial Design of Base Isolation

The parameter design of base isolation is derived from previous analysis, diameter (D) and total thickness (t_r). Therefore, the design process of base isolation are able to initiate. The parameters design are given below :

- Diameter (D) and Total thickness of rubber (t_r)

$$D = 200 \text{ mm (diameter of base isolation)}$$

$$t_r = 100 \text{ mm (total thickness of rubber)}$$

- Perforated Plate

$$D_{hole} = 12 \text{ mm (diameter of hole)}$$

$$C = 16 \text{ mm (pitch)}$$

Reduction area of perforated plate is able to calculate using equation;

$$(\%) = \frac{D^2 \times 90.69}{C^2} = \frac{12^2 \times 90.69}{16^2} = 51\%$$

- Shape factor (S)

The shape factor used in design process are 10. Then, the rubber thickness for single rubber layer with circular shape is obtained as follow

$$t_{rubber} = \frac{D}{4 \times S} = \frac{200}{4 \times 10} = 5 \text{ mm (thickness of single rubber layer)}$$

- A Number of rubber layer and perforated plate.

$$\text{Rubber} : n = \frac{t_r}{t_{sr}} = \frac{100}{5} = 20 \text{ layers}$$

Perforated : $n = 20 - 1 = 19$ layers (Thickness of perforated plate is approximately 1 mm)

End-Steel : $n = 2$ plates (Thickness is 5 mm)

The total height of base isolation :

$$H = \text{Rubber} + \text{Perforated plate} + \text{End Steel plate}$$

$$H = 100 \text{ mm} + 19 \text{ mm} + 10 \text{ mm} = 129 \text{ mm.}$$

Finally, the initial dimension of base isolation is obtained as shown in Fig 5.77.

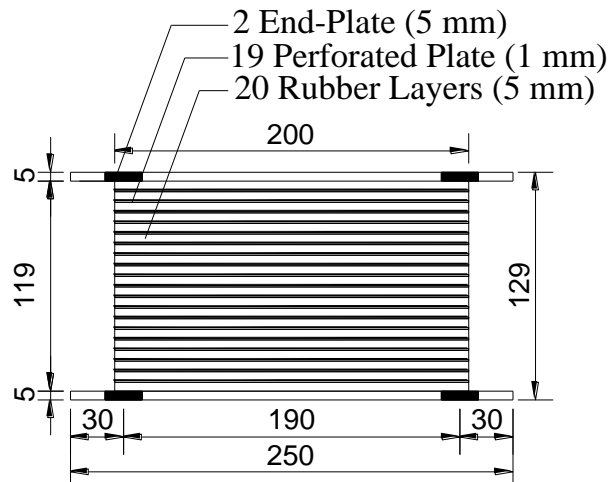


Figure 5.77. Dimension of base isolation.

▪ The Characteristic of base isolation

In this section, the characteristics of base isolation were predicted that are compression modulus (E_c), vertical stiffness (K_v), horizontal stiffness (K_H), Critical Load (P_{crit}) and Max Stress under compression (σ_{max}).

- Compression modulus (E_c)

$$E_c = \frac{6GS^2K}{6GS^2 + K}$$

In calculating compression modulus, E_c , some parameters were assumed to derive E_c . The values were Bulk modulus (K) and Shear modulus (G).

$$K = \text{Bulk Modulus} = 2,800 \text{ MPa}$$

$$G = \text{Shear Modulus} = 0.439 \text{ MPa}$$

$$E_c = \frac{6GS^2K}{6GS^2 + K} = \frac{6 \times 0.4 \times 10^2 \times 2,800}{6 \times 0.4 \times 10^2 + 2,800}$$

$$E_c = 241 \text{ MPa}$$

- Vertical Stiffness (K_v)

Since the perforated plates were employed as reinforcement, the loaded area of base isolation must consider the existing of holes. Therefore, the actual loaded area used in vertical calculation is as follow:

Full Plate area :

$$A = \frac{1}{4} \times \pi \times D^2 = \frac{1}{4} \times \pi \times 200mm^2 = 31,400 \text{ mm}^2 \text{ (Full plate)}$$

Reduction area, (A_c) :

$$A_c = (1 - 0.51) \times 31,400 = 15,386 \text{ mm}^2$$

Vertical Stiffness :

$$K_V = \frac{E_c \times A_c}{t_r} = \frac{241MPa \times 15,386mm^2}{100mm} = 37,080.26 \text{ N/mm} = \underline{\underline{3,708.026 \text{ t/m}}}$$

○ Horizontal Stiffness (K_H)

$$K_H = \frac{G \times A}{t_r} = \frac{0.439 \times 31,400}{100} = 137.846 \text{ N/mm} = \underline{\underline{13.785 \text{ t/m}}}$$

○ Critical Load (P_{crit})

Area for critical load

$$A_s = A \times \frac{h_{tot}}{t_r} = 31,400mm^2 \times \frac{(100+19)}{100} = 37,366 \text{ mm}^2$$

Shear stiffness per unit length

$$P_s = G \times A_s = 0.439 \times 37,366mm^2 = 16,403.674 \text{ N}$$

Euler buckling load

$$P_E = \frac{\pi^2 \times (EI)_{eff}}{h_{tot}^2}$$

$$I_s = \frac{1}{4} \times \pi \times R^4 \times \frac{h_{tot}}{t_r} = \frac{1}{4} \times \pi \times 100^4 \times \frac{119}{100} = 93,415,000 \text{ mm}^4$$

$$(EI)_{eff} = E_c \times \frac{I_s}{3} = 241MPa \times \frac{93,415,000}{3} = 7,504,338,333 \text{ Nmm}^2$$

$$P_E = \frac{\pi^2 \times (EI)_{eff}}{h_{tot}^2} = \frac{\pi^2 \times 7,504,338,333}{119^2} = 5,224,897.552 \text{ N}$$

Critical load

$$P_{crit} = \sqrt{P_s \times P_E} = 292,758.460 \text{ N} = 29.276 \text{ ton}$$

- Maximum pressure in the center of plate (σ_{\max})

$$\frac{\sigma_{\max}}{P_{ave}} = \frac{(3 + \nu)}{2} \times \frac{t_{rubber}}{t_{plate}}$$

$$P_{ave} = \frac{P}{A_c} = \frac{80,000N}{15,386} = 5.199 \text{ MPa}$$

then;

$$\sigma_{\max} = \frac{(3 + \nu)}{2} \times \frac{t_{rubber}}{t_{plate}} \times P_{ave} = \frac{(3 + 0.3)}{2} \times \frac{5}{1} \times 5.199 = 42.896 \text{ MPa}$$

The stress occurred must be lower than yield strength of reinforcement.

"This page is intentionally left blank"

CHAPTER 6

EXPERIMENTAL RESULTS

6.1 Introduction

In this chapter, the experimental test results of vertical and horizontal tests are presented. The detailed procedure of the test has been illustrated in the previous chapter. The primary objective in this research is to develop low-cost base isolation for light structures such as residential housing; 1- and 2-storey. The critical issue is how to produce the lowest horizontal stiffness from isolator product. A number of techniques was used to achieve this target started by designing isolator dimension, arranging rubber thickness, replacing material of reinforcement and then using special low grade rubber for obtaining low shear modulus. The novelty of this research is the application of perforated plate as reinforcement replacing steel-plate and the use of low grade rubber as the main material. A series of modification are regarded valuable to produce low-cost product of base isolation for residential housing in Indonesia. A rough estimation related to the cost of this product is approximately US\$.100 per unit. Based on the results, this product is expected to be produced widely in Indonesia to be applied in residential housing in high seismic zones.

6.2 Vertical Test Results

In this section, vertical test results of rubber A will be presented. As described earlier, the specimens were monotonically loaded to a compressive force at zero horizontal displacement. In order to observe the vertical characteristic of isolator, the specimen was loaded in multi vertical load started with 10 kN, 20 kN, 30 kN, 40 kN, 80 kN, 100 kN, 150 kN, 200 kN and terminated by 250 kN. The vertical load was performed using load control. Once the compressive load was achieved, it was fluctuated $\pm 1/3$ of force over three sinusoidal cycles at loading rate of 5.0 ± 0.5 Mpa/min (2.6 kN/sec) and then monotonically unloaded. The loading history for all of compression load are presented in Fig 4.59 to 4.68. The vertical test results are given below:

- Vertical characteristic of specimen subjected to axial load of 10 kN.

The results of vertical test subjected to axial load of 10 kN is presented in Figure 6.1. The vertical axis represents the vertical imposed load and the horizontal axis represents the relative displacement between base plate. The dashed straight line corresponds to the average stiffness of the specimen during the cyclic part of testing. The loading history are presented in Fig 6.53.

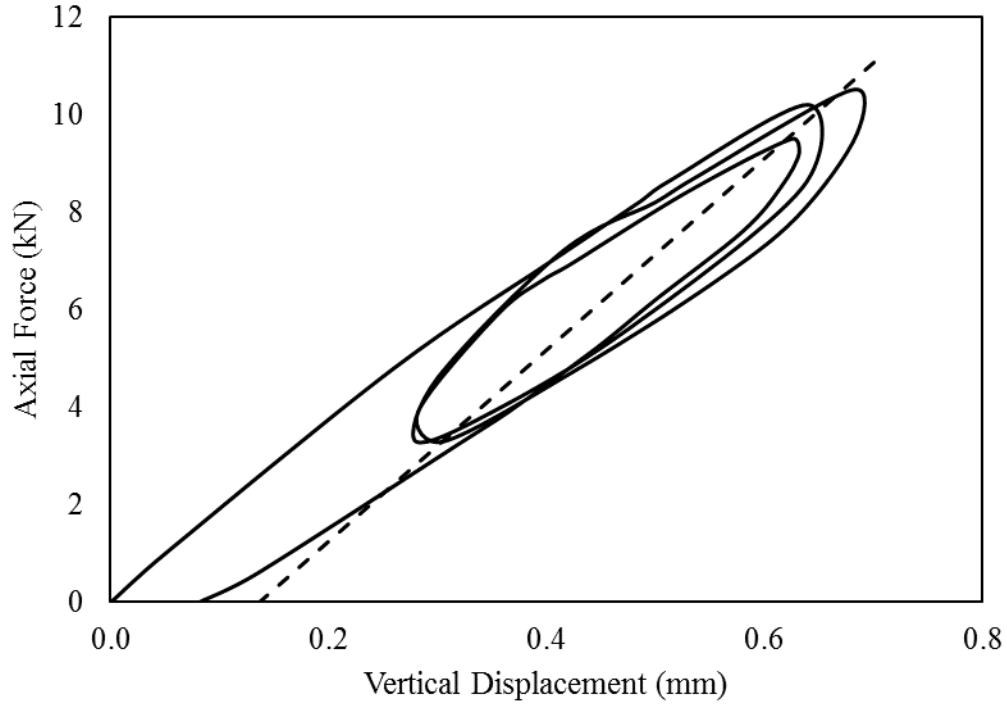


Figure 6.1 Vertical characteristic of specimen subjected to axial load of 10 kN.

The vertical stiffness was determined by using maximum and minimum forces, F , and maximum and minimum displacements, δ , observed in each cycle. In one test, there were three cycles of loaded-unloaded subjected to the specimens. The vertical stiffness would be calculated in each cycle then the average value would be considered as the final result.

1st Cycle:

$$K_{v-1st} = \frac{(F_{\max} - F_{\min})}{(\delta_{\max} - \delta_{\min})} = \frac{(10.200 - 3.300)}{(0.640 - 0.280)} = 19.167 \text{ kN/mm}$$

With the same procedure, the calculation of the 2nd cycles was carried out and illustrated in Table 6.1 below.

Table 6.1 Vertical stiffness of specimen subjected to axial load of 10 kN.

Cycle	Max		Min		Stiffness	Average
	$\delta_{max} (mm)$	$F_{max}(kN)$	$\delta_{min} (mm)$	$F_{min} (kN)$	kN/mm	(kN/mm)
1st	0.640	10.200	0.280	3.300	19.167	
2nd	0.680	10.500	0.306	3.300	19.251	19.653
3rd	0.625	9.500	0.323	3.300	20.542	

From Table 6.1, the vertical stiffness of isolator was obtained. It can be seen that the values in each cycle are identical, therefore the average value of the vertical stiffness, K_v , was **19.653 kN/mm**. Another parameter for the vertical characteristics of isolator system is compression modulus, denoted E_c . The value of E_c can be derived after the vertical stiffness of isolator is defined. Commonly, the equation of E_c is derived as follows:

$$K_v = \frac{E_c \times A}{t_r}$$

In general case, A is usually taken as the area of steel-plate. However in this research, A is taken as the area of perforated plate. Therefore, to determine the compression modulus, the perforated area should be determined. The detailed calculations are given below:

Area of full plate

$$A = \frac{1}{4} \times \pi \times D^2 = \frac{1}{4} \times \pi \times 200^2 = 31,400 \text{ mm}^2.$$

The full plate area would be reduced with the percentage of open area (POA) of the perforated plate. In this case, the POA of perforated plate used in isolator is approximately 51%. Then, the area of perforated (A_c) can be written as follows:

$$A_c = (1 - 0.51) \times A = (1 - 0.51) \times 31,400 = 15,386 \text{ mm}^2$$

Then, the compression modulus of sample A is determined by

$$E_c = \frac{K_v \times t_r}{A_c} = \frac{19,653 \text{ N/mm} \times 100 \text{ mm}}{15,386 \text{ mm}^2} = 127.736 \text{ MPa.}$$

- Vertical characteristic of specimen subjected to axial load of 20 kN.

The results of vertical test subjected to axial load of 20 kN is presented in Figure 6.2. The vertical axis represents the vertical imposed load and the horizontal axis represents the relative displacement between base plate. The dashed straight line corresponds to the average stiffness of the specimen during the cyclic part of testing. The loading history are presented in Fig 4.54.

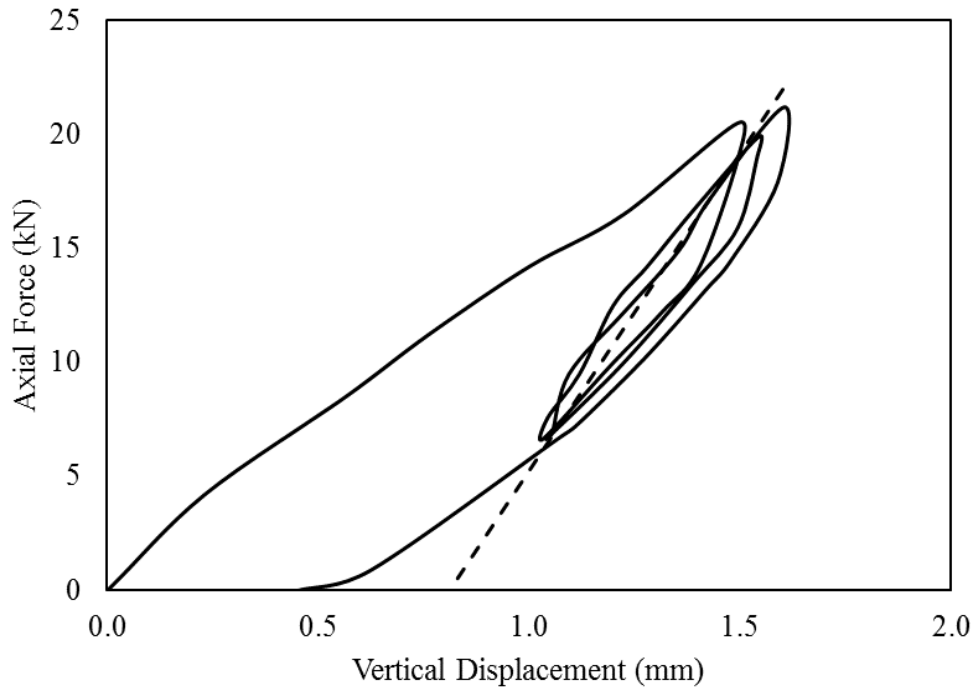


Figure 6.2 Vertical characteristic of specimen subjected to axial load of 20 kN.

Therefore, the vertical stiffness would be calculated in each cycle then the average value would be considered as the final result.

1st Cycle:

$$K_{v-1st} = \frac{(F_{\max} - F_{\min})}{(\delta_{\max} - \delta_{\min})} = \frac{(20.5 - 6.667)}{(1.495 - 1.034)} = 30.007 \text{ kN/mm}$$

With the same procedure, the calculation of the 2nd cycles was carried out and illustrated in Table 6.2 below.

Table 6.2 Vertical stiffness of specimen subjected to axial load of 20 kN.

Cycle	Max		Min		Stiffness (kN/mm)	Average (kN/mm)
	$\delta_{max} (mm)$	$F_{max}(kN)$	$\delta_{min} (mm)$	$F_{min} (kN)$		
1st	1.495	20.500	1.034	6.667	30.007	
2nd	1.545	19.00	1.042	6.667	26.318	27.812
3rd	1.605	21.200	1.069	6.667	27.112	

From Table 6.2, the vertical stiffness of isolator was obtained. It can be seen that the values in each cycle are identical, therefore the average value of the vertical stiffness, K_v , was **27.812 kN/mm**. Another parameter for the vertical characteristics of isolator system is compression modulus, denoted E_c . The value of E_c can be derived after the vertical stiffness of isolator is defined. Commonly, the equation of E_c is derived as follows:

$$K_v = \frac{E_c \times A}{t_r}$$

In general case, A is usually taken as the area of steel-plate. However in this research, A is taken as the area of perforated plate. Therefore, to determine the compression modulus, the perforated area should be determined. The detailed calculations are given below:

Area of full plate

$$A = \frac{1}{4} \times \pi \times D^2 = \frac{1}{4} \times \pi \times 200^2 = 31,400 \text{ mm}^2.$$

The full plate area would be reduced with the percentage of open area (POA) of the perforated plate. In this case, the POA of perforated plate used in isolator is approximately 51%. Then, the area of perforated (A_c) can be written as follows:

$$A_c = (1 - 0.51) \times A = (1 - 0.51) \times 31,400 = 15,386 \text{ mm}^2$$

Then, the compression modulus of sample A is determined by

$$E_c = \frac{K_v \times t_r}{A_c} = \frac{27,812 \text{ N/mm} \times 100 \text{ mm}}{15,386 \text{ mm}^2} = 180.763 \text{ MPa.}$$

- Vertical characteristic of specimen subjected to axial load of 30 kN.

The results of vertical test subjected to axial load of 30 kN is presented in Figure 6.3. The vertical axis represents the vertical imposed load and the horizontal axis represents the relative displacement between base plate. The dashed straight line corresponds to the average stiffness of the specimen during the cyclic part of testing. The loading history are presented in Fig 4.55.

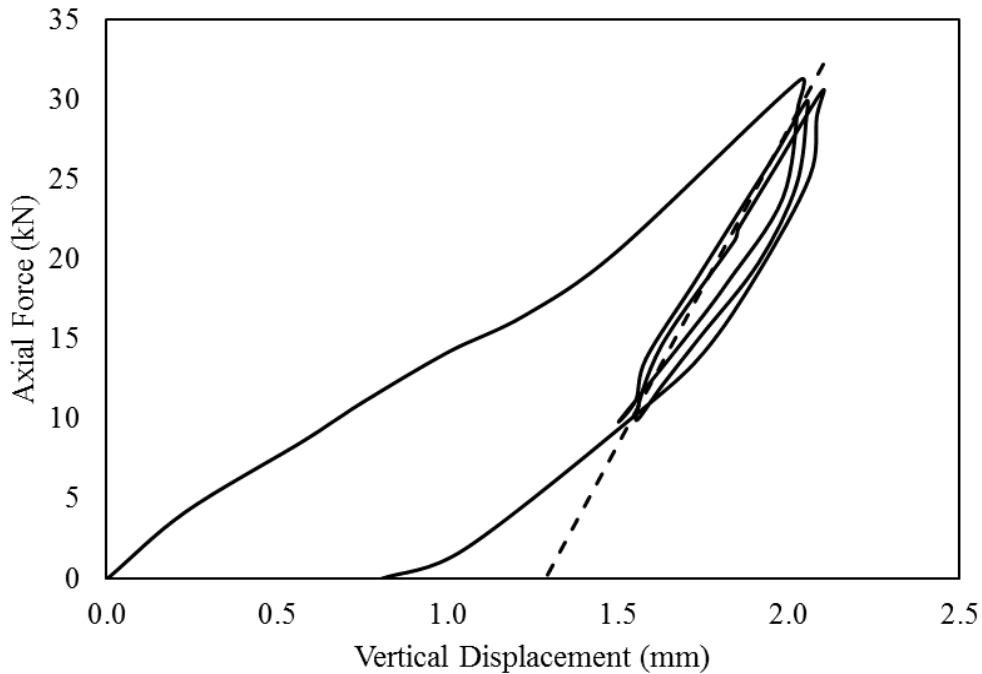


Figure 6.3 Vertical characteristic of specimen subjected to axial load of 30 kN.

Therefore, the vertical stiffness would be calculated in each cycle then the average value would be considered as the final result.

1st Cycle:

$$K_{v-1st} = \frac{(F_{\max} - F_{\min})}{(\delta_{\max} - \delta_{\min})} = \frac{(31.2 - 10.000)}{(2.030 - 1.505)} = 40.381 \text{ kN/mm}$$

With the same procedure, the calculation of the 2nd cycles was carried out and illustrated in Table 6.3 below.

Table 6.3 Vertical stiffness of specimen subjected to axial load of 30 kN.

Cycle	Max		Min		Stiffness (kN/mm)	Average (kN/mm)
	$\delta_{max} (mm)$	$F_{max}(kN)$	$\delta_{min} (mm)$	$F_{min} (kN)$		
1st	2.030	31.200	1.505	10.000	40.381	
2nd	2.050	29.900	1.550	10.000	39.800	39.537
3rd	2.095	30.500	1.585	10.900	38.431	

From Table 6.3, the vertical stiffness of isolator was obtained. It can be seen that the values in each cycle are identical, therefore the average value of the vertical stiffness, K_v , was **39.537 kN/mm**.

Another parameter for the vertical characteristics of isolator system is compression modulus, denoted E_c . The value of E_c can be derived after the vertical stiffness of isolator is defined. Commonly, the equation of E_c is derived as follows:

$$K_v = \frac{E_c \times A}{t_r}$$

In general case, A is usually taken as the area of steel-plate. However in this research, A is taken as the area of perforated plate. Therefore, to determine the compression modulus, the perforated area should be determined. The detailed calculations are given below:

Area of full plate

$$A = \frac{1}{4} \times \pi \times D^2 = \frac{1}{4} \times \pi \times 200^2 = 31,400 \text{ mm}^2.$$

The full plate area would be reduced with the percentage of open area (POA) of the perforated plate. In this case, the POA of perforated plate used in isolator is approximately 51%. Then, the area of perforated (A_c) can be written as follows:

$$A_c = (1 - 0.51) \times A = (1 - 0.51) \times 31,400 = 15,386 \text{ mm}^2$$

Then, the compression modulus of sample A is determined by

$$E_c = \frac{K_v \times t_r}{A_c} = \frac{39,537 \text{ N/mm} \times 100 \text{ mm}}{15,386 \text{ mm}^2} = 256.97 \text{ MPa.}$$

- Vertical characteristic of specimen subjected to axial load of 40 kN.

The results of vertical test subjected to axial load of 40 kN is presented in Figure 6.4. The vertical axis represents the vertical imposed load and the horizontal axis represents the relative displacement between base plate. The dashed straight line corresponds to the average stiffness of the specimen during the cyclic part of testing. The loading history are presented in Fig 3.56.

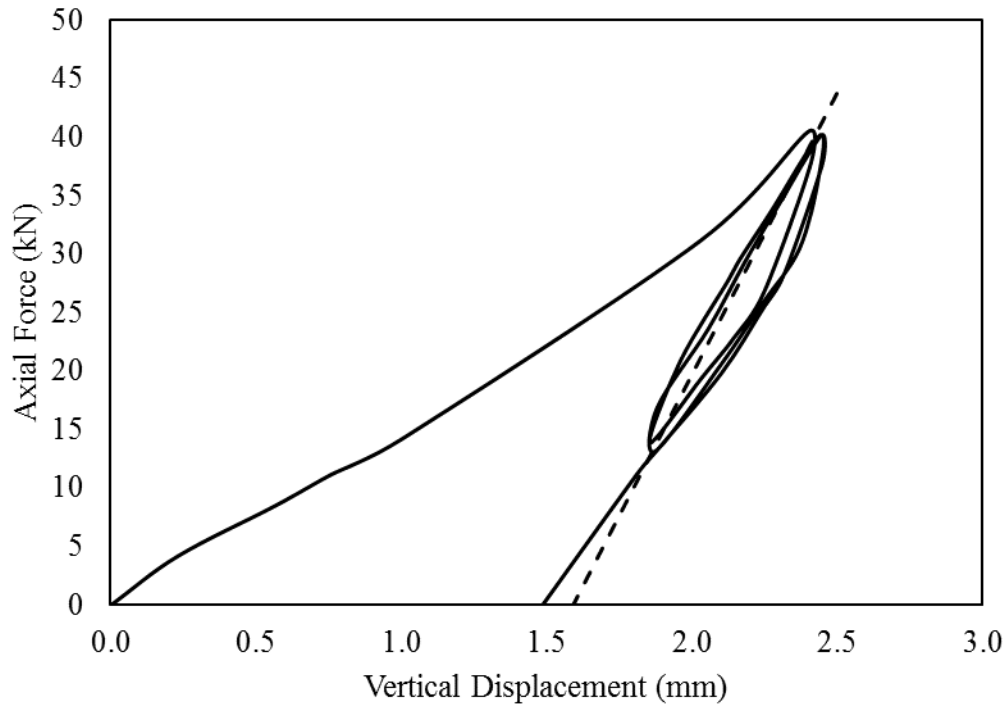


Figure 6.4 Vertical characteristic of specimen subjected to axial load of 40 kN.

Therefore, the vertical stiffness would be calculated in each cycle then the average value would be considered as the final result.

1st Cycle:

$$K_{v-1st} = \frac{(F_{\max} - F_{\min})}{(\delta_{\max} - \delta_{\min})} = \frac{(40.500 - 13.900)}{(2.400 - 1.855)} = 48.807 \text{ kN/mm}$$

With the same procedure, the calculation of the 2nd cycles was carried out and illustrated in Table 6.4 below.

Table 6.4 Vertical stiffness of specimen subjected to axial load of 40 kN.

Cycle	Max		Min		Stiffness (kN/mm)	Average (kN/mm)
	$\delta_{\max} (mm)$	$F_{\max}(kN)$	$\delta_{\min} (mm)$	$F_{\min} (kN)$		
1st	2.400	40.500	1.855	13.900	48.807	
2nd	2.440	40.200	1.875	13.200	47.788	48.091
3rd	2.445	40.200	1.881	13.300	47.679	

From Table 6.4, the vertical stiffness of isolator was obtained. It can be seen that the values in each cycle are identical, therefore the average value of the vertical stiffness, K_v , was **48.091 kN/mm**.

Another parameter for the vertical characteristics of isolator system is compression modulus, denoted E_c . The value of E_c can be derived after the vertical stiffness of isolator is defined. Commonly, the equation of E_c is derived as follows:

$$K_v = \frac{E_c \times A}{t_r}$$

In general case, A is usually taken as the area of steel-plate. However in this research, A is taken as the area of perforated plate. Therefore, to determine the compression modulus, the perforated area should be determined. The detailed calculations are given below:

Area of full plate

$$A = \frac{1}{4} \times \pi \times D^2 = \frac{1}{4} \times \pi \times 200^2 = 31,400 \text{ mm}^2.$$

The full plate area would be reduced with the percentage of open area (POA) of the perforated plate. In this case, the POA of perforated plate used in isolator is approximately 51%. Then, the area of perforated (A_c) can be written as follows:

$$A_c = (1 - 0.51) \times A = (1 - 0.51) \times 31,400 = 15,386 \text{ mm}^2$$

Then, the compression modulus of sample A is determined by

$$E_c = \frac{K_v \times t_r}{A_c} = \frac{48,091 \text{ N/mm} \times 100 \text{ mm}}{15,386 \text{ mm}^2} = 312.566 \text{ MPa}.$$

- Vertical characteristic of specimen subjected to axial load of 80 kN.

The results of vertical test subjected to axial load of 80 kN is presented in Figure 6.5. The vertical axis represents the vertical imposed load and the horizontal axis represents the relative displacement between base plate.

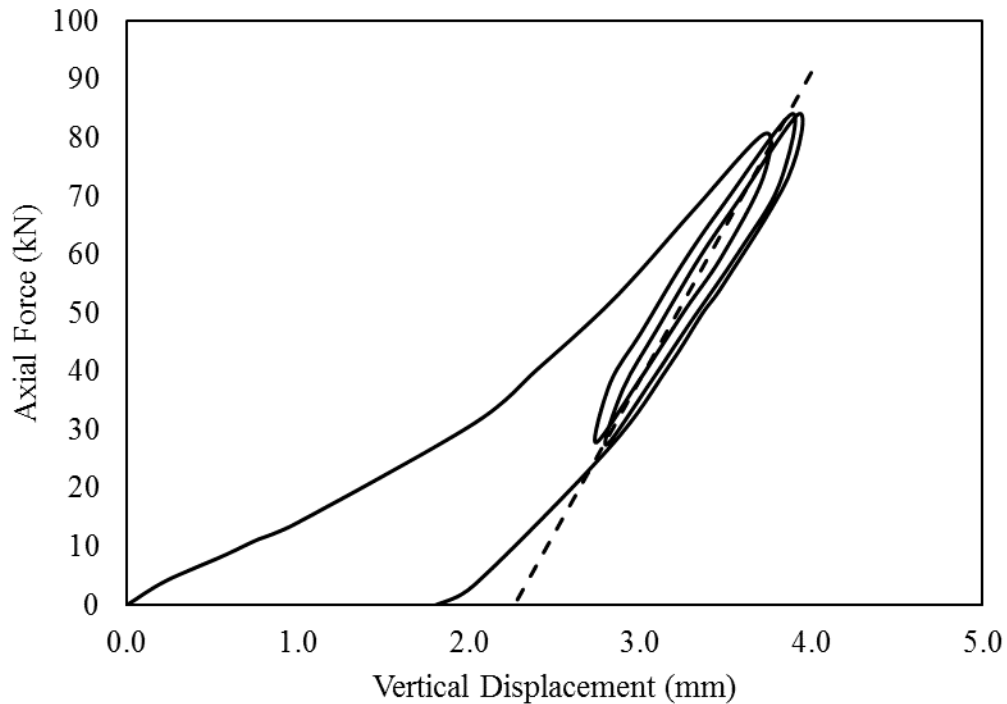


Figure 6.5 Vertical characteristic of specimen subjected to axial load of 80 kN.

The dashed straight line corresponds to the average stiffness of the specimen during the cyclic part of testing. The loading history are presented in Fig 4.57. Therefore, the vertical stiffness would be calculated in each cycle then the average value would be considered as the final result.

1st Cycle:

$$K_{v-1st} = \frac{(F_{\max} - F_{\min})}{(\delta_{\max} - \delta_{\min})} = \frac{(80.800 - 27.900)}{(3.725 - 2.740)} = 53.706 \text{ kN/mm}$$

With the same procedure, the calculation of the 2nd cycles was carried out and illustrated in Table 6.5 below.

Table 6.5 Vertical stiffness of specimen subjected to axial load of 80 kN.

Cycle	Max		Min		Stiffness	Average
	$\delta_{\max} (mm)$	$F_{\max}(kN)$	$\delta_{\min} (mm)$	$F_{\min} (kN)$	(kN/mm)	(kN/mm)
1st	3.725	80.800	2.740	27.900	53.706	
2nd	3.885	84.200	2.800	27.500	52.258	52.528
3rd	3.925	84.200	2.815	26.900	51.622	

From Table 6.4, the vertical stiffness of isolator was obtained. It can be seen that the values in each cycle are identical, therefore the average value of the vertical stiffness, K_v , was **52.528 kN/mm**. Another parameter for the vertical characteristics of isolator system is compression modulus, denoted E_c . The value of E_c can be derived after the vertical stiffness of isolator is defined. Commonly, the equation of E_c is derived as follows:

$$K_v = \frac{E_c \times A}{t_r}$$

In general case, A is usually taken as the area of steel-plate. However in this research, A is taken as the area of perforated plate. Therefore, to determine the compression modulus, the perforated area should be determined. The detailed calculations are given below:

Area of full plate

$$A = \frac{1}{4} \times \pi \times D^2 = \frac{1}{4} \times \pi \times 200^2 = 31,400 \text{ mm}^2.$$

The full plate area would be reduced with the percentage of open area (POA) of the perforated plate. In this case, the POA of perforated plate used in isolator is approximately 51%. Then, the area of perforated (A_c) can be written as follows:

$$A_c = (1 - 0.51) \times A = (1 - 0.51) \times 31,400 = 15,386 \text{ mm}^2$$

Then, the compression modulus of sample A is determined by

$$E_c = \frac{K_v \times t_r}{A_c} = \frac{52,528 \text{ N/mm} \times 100 \text{ mm}}{15,386 \text{ mm}^2} = 341.404 \text{ MPa}.$$

- Vertical characteristic of specimen subjected to axial load of 100 kN.

The results of vertical test subjected to axial load of 100 kN is presented in Figure 6.6. The vertical axis represents the vertical imposed load and the horizontal axis represents the relative displacement between base plate.

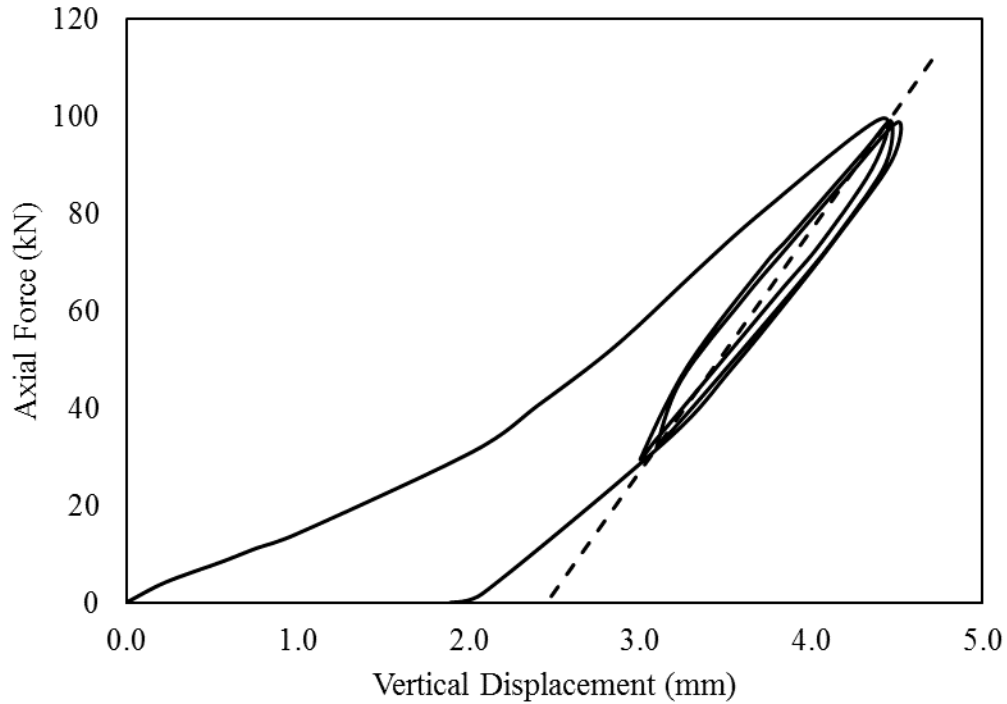


Figure 6.6 Vertical characteristic of specimen subjected to axial load of 100 kN.

The dashed straight line corresponds to the average stiffness of the specimen during the cyclic part of testing. The loading history are presented in Fig 4.58. Therefore, the vertical stiffness would be calculated in each cycle then the average value would be considered as the final result.

1st Cycle:

$$K_{v-1st} = \frac{(F_{\max} - F_{\min})}{(\delta_{\max} - \delta_{\min})} = \frac{(99.4 - 33.0)}{(4.395 - 3.079)} = 50.446 \text{ kN/mm}$$

With the same procedure, the calculation of the 2nd cycles was carried out and illustrated in Table 6.6 below.

Table 6.6 Vertical stiffness of specimen subjected to axial load of 100 kN.

Cycle	Max		Min		Stiffness	Average
	δ_{\max} (mm)	F_{\max} (kN)	δ_{\min} (mm)	F_{\min} (kN)	(kN/mm)	(kN/mm)
1st	4.395	99.400	3.079	33.000	50.446	
2nd	4.460	99.100	3,123	33.000	49.430	49.557
3rd	4.500	98.800	3,170	33.900	48.797	

From Table 6.6, the vertical stiffness of isolator was obtained. It can be seen that the values in each cycle are identical, therefore the average value of the vertical stiffness, K_v , was **49.557 kN/mm**.

Another parameter for the vertical characteristics of isolator system is compression modulus, denoted E_c . The value of E_c can be derived after the vertical stiffness of isolator is defined. Commonly, the equation of E_c is derived as follows:

$$K_v = \frac{E_c \times A}{t_r}$$

In general case, A is usually taken as the area of steel-plate. However in this research, A is taken as the area of perforated plate. Therefore, to determine the

compression modulus, the perforated area should be determined. The detailed calculations are given below:

Area of full plate

$$A = \frac{1}{4} \times \pi \times D^2 = \frac{1}{4} \times \pi \times 200^2 = 31,400 \text{ mm}^2.$$

The full plate area would be reduced with the percentage of open area (POA) of the perforated plate. In this case, the POA of perforated plate used in isolator is approximately 51%. Then, the area of perforated (A_c) can be written as follows:

$$A_c = (1 - 0.51) \times A = (1 - 0.51) \times 31,400 = 15,386 \text{ mm}^2$$

Then, the compression modulus of sample A is determined by

$$E_c = \frac{K_v \times t_r}{A_c} = \frac{49.557 \text{ N/mm} \times 100 \text{ mm}}{15,386 \text{ mm}^2} = 322.095 \text{ MPa}.$$

- Vertical characteristic of specimen subjected to axial load of 150 kN.

The results of vertical test subjected to axial load of 150 kN is presented in Figure 6.7. The vertical axis represents the vertical imposed load and the horizontal axis represents the relative displacement between base plate.

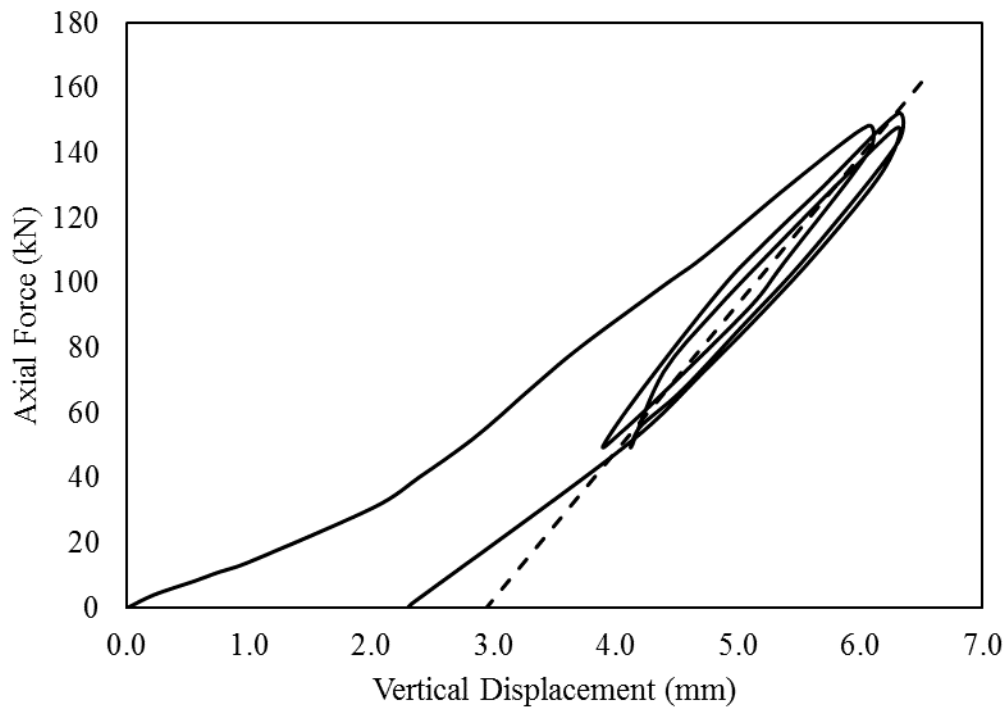


Figure 6.7 Vertical characteristic of specimen subjected to axial load of 150 kN.

The dashed straight line corresponds to the average stiffness of the specimen during the cyclic part of testing. The loading history are presented in Fig 4.59. Therefore, the vertical stiffness would be calculated in each cycle then the average value would be considered as the final result.

1st Cycle:

$$K_{v-1st} = \frac{(F_{\max} - F_{\min})}{(\delta_{\max} - \delta_{\min})} = \frac{(148.7 - 50.000)}{(6.070 - 3.900)} = 45.484 \text{ kN/mm}$$

With the same procedure, the calculation of the 2nd cycles was carried out and illustrated in Table 6.7 below.

Table 6.7 Vertical stiffness of specimen subjected to axial load of 150 kN.

Cycle	Max		Min		Stiffness	Average
	$\delta_{\max} (mm)$	$F_{\max} (kN)$	$\delta_{\min} (mm)$	$F_{\min} (kN)$	(kN/mm)	(kN/mm)
1st	6.070	148.700	3.900	50.000	45.484	
2nd	6.310	152.400	4.133	50.000	47.047	45.451
3rd	6.315	148.100	4.065	49.500	43.822	

From Table 6.7, the vertical stiffness of isolator was obtained. It can be seen that the values in each cycle are identical, therefore the average value of the vertical stiffness, K_v , was **45.451 kN/mm**.

Another parameter for the vertical characteristics of isolator system is compression modulus, denoted E_c . The value of E_c can be derived after the vertical stiffness of isolator is defined. Commonly, the equation of E_c is derived as follows:

$$K_v = \frac{E_c \times A}{t_r}$$

In general case, A is usually taken as the area of steel-plate. However in this research, A is taken as the area of perforated plate. Therefore, to determine the compression modulus, the perforated area should be determined. The detailed calculations are given below:

Area of full plate

$$A = \frac{1}{4} \times \pi \times D^2 = \frac{1}{4} \times \pi \times 200^2 = 31,400 \text{ mm}^2.$$

The full plate area would be reduced with the percentage of open area (POA) of the perforated plate. In this case, the POA of perforated plate used in isolator is approximately 51%. Then, the area of perforated (A_c) can be written as follows:

$$A_c = (1 - 0.51) \times A = (1 - 0.51) \times 31,400 = 15,386 \text{ mm}^2$$

Then, the compression modulus of sample A is determined by

$$E_c = \frac{K_v \times t_r}{A_c} = \frac{45,451 \text{ N/mm} \times 100 \text{ mm}}{15,386 \text{ mm}^2} = 295.406 \text{ MPa}.$$

- Vertical characteristic of specimen subjected to axial load of 200 kN.

The results of vertical test subjected to axial load of 200 kN is presented in Figure 6.8. The vertical axis represents the vertical imposed load and the horizontal axis represents the relative displacement between base plate.

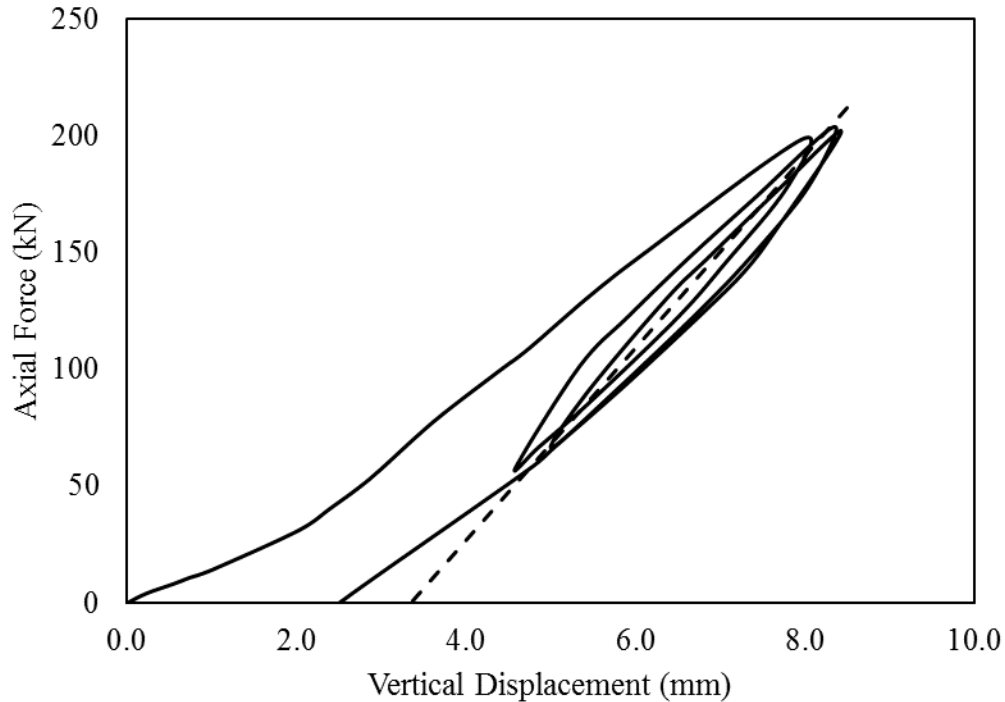


Figure 6.8 Vertical characteristic of specimen subjected to axial load of 200 kN.

The dashed straight line corresponds to the average stiffness of the specimen during the cyclic part of testing. The loading history are presented in Fig 4.60. Therefore, the vertical stiffness would be calculated in each cycle then the average value would be considered as the final result.

1st Cycle:

$$K_{v-1st} = \frac{(F_{\max} - F_{\min})}{(\delta_{\max} - \delta_{\min})} = \frac{(198.400 - 66.670)}{(7.965 - 4.855)} = 42.358 \text{ kN/mm}$$

With the same procedure, the calculation of the 2nd cycles was carried out and illustrated in Table 6.8 below.

Table 6.8 Vertical stiffness of specimen subjected to axial load of 200 kN.

Cycle	Max		Min		Stiffness	Average
	$\delta_{\max} (mm)$	$F_{\max} (kN)$	$\delta_{\min} (mm)$	$F_{\min} (kN)$	(kN/mm)	(kN/mm)
1st	7.965	198.400	4.855	66.670	42.358	
2nd	8.340	203.700	5.005	66.500	41.139	41.137
3rd	8.425	201.700	5.042	66.670	39.914	

From Table 6.8, the vertical stiffness of isolator was obtained. It can be seen that the values in each cycle are identical, therefore the average value of the vertical stiffness, K_v , was **41.137 kN/mm**. Another parameter for the vertical characteristics of isolator system is compression modulus, denoted E_c . The value of E_c can be derived after the vertical stiffness of isolator is defined. Commonly, the equation of E_c is derived as follows:

$$K_v = \frac{E_c \times A}{t_r}$$

In general case, A is usually taken as the area of steel-plate. However in this research, A is taken as the area of perforated plate. Therefore, to determine the compression modulus, the perforated area should be determined. The detailed calculations are given below:

Area of full plate

$$A = \frac{1}{4} \times \pi \times D^2 = \frac{1}{4} \times \pi \times 200^2 = 31,400 \text{ mm}^2.$$

The full plate area would be reduced with the percentage of open area (POA) of the perforated plate. In this case, the POA of perforated plate used in isolator is approximately 51%. Then, the area of perforated (A_c) can be written as follows:

$$A_c = (1 - 0.51) \times A = (1 - 0.51) \times 31,400 = 15,386 \text{ mm}^2$$

Then, the compression modulus of sample A is determined by

$$E_c = \frac{K_v \times t_r}{A_c} = \frac{41,137 \text{ N/mm} \times 100 \text{ mm}}{15,386 \text{ mm}^2} = 267.366 \text{ MPa}.$$

- Vertical characteristic of specimen subjected to axial load of 250 kN.

The results of vertical test subjected to axial load of 250 kN is presented in Figure 6.9. The vertical axis represents the vertical imposed load and the horizontal axis represents the relative displacement between base plate. The dashed straight line corresponds to the average stiffness of the specimen during the cyclic part of testing. The loading history are presented in Fig 4.61.

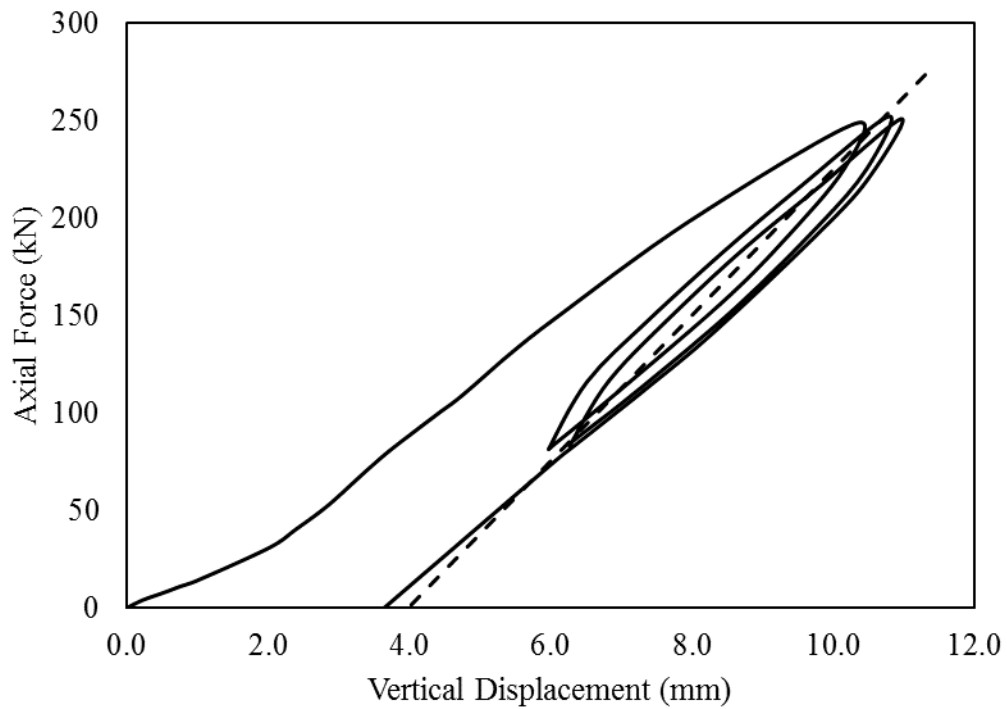


Figure 6.9 Vertical characteristic of specimen subjected to axial load of 250 kN.

Therefore, the vertical stiffness would be calculated in each cycle then the average value would be considered as the final result.

1st Cycle:

$$K_{v-1st} = \frac{(F_{\max} - F_{\min})}{(\delta_{\max} - \delta_{\min})} = \frac{(248.400 - 83.330)}{(10.310 - 6.027)} = 38.537 \text{ kN/mm}$$

With the same procedure, the calculation of the 2nd cycles was carried out and illustrated in Table 6.9 below.

Table 6.9 Vertical stiffness of specimen subjected to axial load of 250 kN.

Cycle	Max		Min		Stiffness (kN/mm)	Average (kN/mm)
	$\delta_{\max} (mm)$	$F_{\max}(kN)$	$\delta_{\min} (mm)$	$F_{\min} (kN)$		
1st	10.310	248.400	6.027	83.333	38.537	
2nd	10.775	252.000	6.270	83.333	37.444	37.404
3rd	10.955	250.700	6.336	83.333	36.233	

From Table 6.9, the vertical stiffness of isolator was obtained. It can be seen that the values in each cycle are identical, therefore the average value of the vertical stiffness, K_v , was **37.404 kN/mm**. Another parameter for the vertical characteristics of isolator system is compression modulus, denoted E_c . The value of E_c can be derived after the vertical stiffness of isolator is defined. Commonly, the equation of E_c is derived as follows:

$$K_v = \frac{E_c \times A}{t_r}$$

In general case, A is usually taken as the area of steel-plate. However in this research, A is taken as the area of perforated plate. Therefore, to determine the compression modulus, the perforated area should be determined. The detailed calculations are given below:

Area of full plate

$$A = \frac{1}{4} \times \pi \times D^2 = \frac{1}{4} \times \pi \times 200^2 = 31,400 \text{ mm}^2.$$

The full plate area would be reduced with the percentage of open area (POA) of the perforated plate. In this case, the POA of perforated plate used in isolator is approximately 51%. Then, the area of perforated (A_c) can be written as follows:

$$A_c = (1 - 0.51) \times A = (1 - 0.51) \times 31,400 = 15,386 \text{ mm}^2$$

Then, the compression modulus of sample A is determined by

$$E_c = \frac{K_v \times t_r}{A_c} = \frac{37,404 \text{ N/mm} \times 100 \text{ mm}}{15,386 \text{ mm}^2} = 234.107 \text{ MPa}.$$

6.3 Horizontal Test Results

The samples of perforated-reinforced elastomer isolators was tested in shear to obtain the horizontal characteristics of isolator. The specimen was subjected to constant compression load and shear freely in lateral direction. The primary objective of the experimental test is to determine the horizontal characteristics of isolator involving horizontal stiffness and damping ratio. The hysteresis loops obtained during the tests were analyzed to derive a number of different performance parameters for perforated-reinforced bearings.

The test apparatus has a displacement capacity of ± 100 mm in horizontal direction and a load capacity of 500 kN in vertical direction. The shear strain considered on the test involved 4 levels (for instance 5 mm, 10 mm, 20 mm, 50 mm, and 100 mm) based on the total thickness of rubber. That test was carried out to investigate the characteristics of isolator under lateral load in every single shear strain. The detailed analysis of experimental test results in every single shear strain are described below:

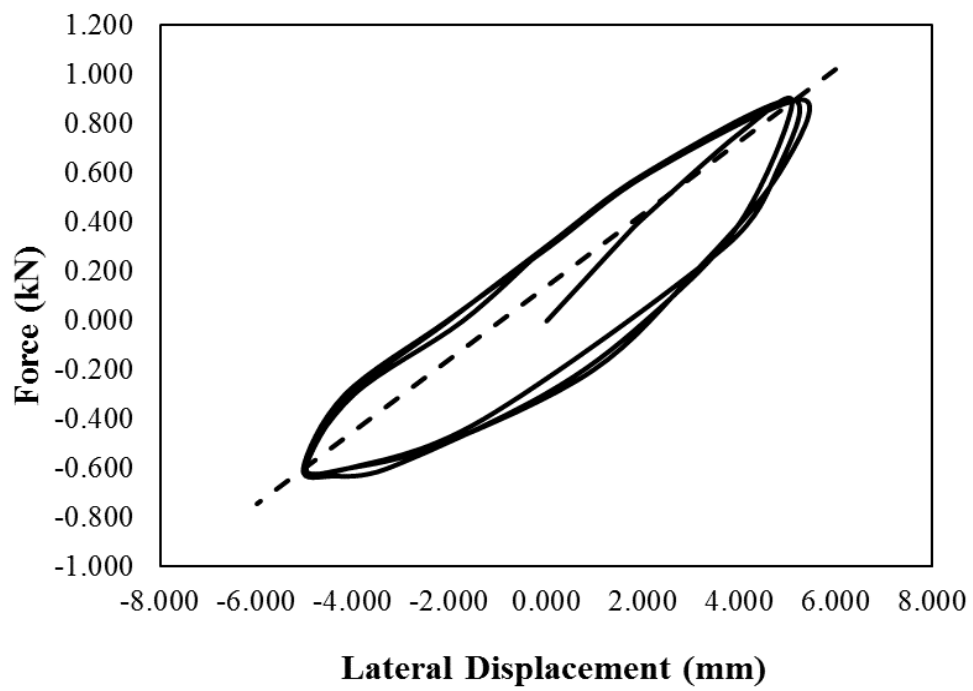
a. Shear Strain 5% (5 mm):

The results of horizontal test of specimen in shear at strain 5% are presented in Fig 6.10. The vertical axis represents the horizontal imposed load and the horizontal axis represents the horizontal displacement. The dashed straight

line corresponds to the horizontal average stiffness of the specimen during the cyclic part of the testing.



(a)



(b)

Figure 6.10 Horizontal test result at 5% shear deformation; (a). Photograph of specimen (b). Force-displacement relationship.

The stiffness (5%): The horizontal stiffness would be considered in each cycle denoted effective stiffness, then the average value would be considered to represent the isolator. The details of analysis are presented below:

1st Cycle:

$$K_{H-1st} = \frac{(F_{\max} - F_{\min})}{(\delta_{\max} - \delta_{\min})}$$

$$K_{H-1st} = \frac{(0.890 - (-0.6))}{(5.100 - (-5.025))} = 0.147 \text{ kN/mm}$$

With the same procedure, the calculations of the 2nd and 3rd cycles were conducted and presented in Table 6.10 below.

Table 6.10 Horizontal test results in 5% shear strain.

Cycle	Max		Min		K_{H-Eff} (kN/mm)	K_{H-Ave} (kN/mm)
	$\delta_{\max} (mm)$	$F_{\max} (kN)$	$\delta_{\min} (mm)$	$F_{\min} (kN)$		
1st	5.100	0.890	-5.025	-0.600	0.147	
2nd	5.295	0.900	-4.965	-0.600	0.146	0.147
3rd	5.085	0.900	-5.010	-0.600	0.149	

The damping ratio (5%): The hysteresis loops were analyzed to obtain the equivalent viscous damping ratio of the bearing for each test. A hysteresis loop represents the plot of force against displacement, therefore the area contained within such a loop represents the energy dissipated by the bearing. In calculating damping ratio, hysteresis loop in the middle cycle (2nd) was used. The calculations of dissipation energy of bearing in shear strain 5% are given below:

Stored or elastic energy (W_s):

$$\Delta_{\max} = \frac{(\delta_{\max} + |\delta_{\min}|)}{2} = \frac{(5.295 + |-4.965|)}{2} = 5.13 \text{ mm}$$

$$W_s = \frac{K_H \times (\Delta_{\max})^2}{2} = \frac{0.147 \times (5.13)^2}{2} = 1.938 \text{ kN-mm}$$

Dissipated energy (W_d):

The dissipated energy is equal to the hysteresis loop area. A hysteresis loop represents the plot of force (in kN) against displacement (in mm). By using Autocad software, the area in the 2nd cycle obtained is as follows:

$$W_d = 4.756 \text{ kN-mm.}$$

Therefore, the equivalent viscous damping ratio of isolator in shear strain 5% is illustrated below:

$$\xi_{5mm} = \frac{W_d}{(4\pi \times W_s)} \times 100\% = \frac{4.756}{(4\pi \times 1.938)} \times 100\% = 19.533 \%$$

b. Shear Strain 10% (10 mm) :

The results of horizontal test of specimen in shear at strain 10% are presented in Fig 6.11. The vertical axis represents the horizontal imposed load and the horizontal axis represents the horizontal displacement. The dashed straight line corresponds to the horizontal average stiffness of the specimen during the cyclic part of the testing.

The stiffness (10%): The horizontal stiffness would be considered in each cycle denoted effective stiffness, then the average value would be considered to represent the isolator. The details of analysis are presented below:

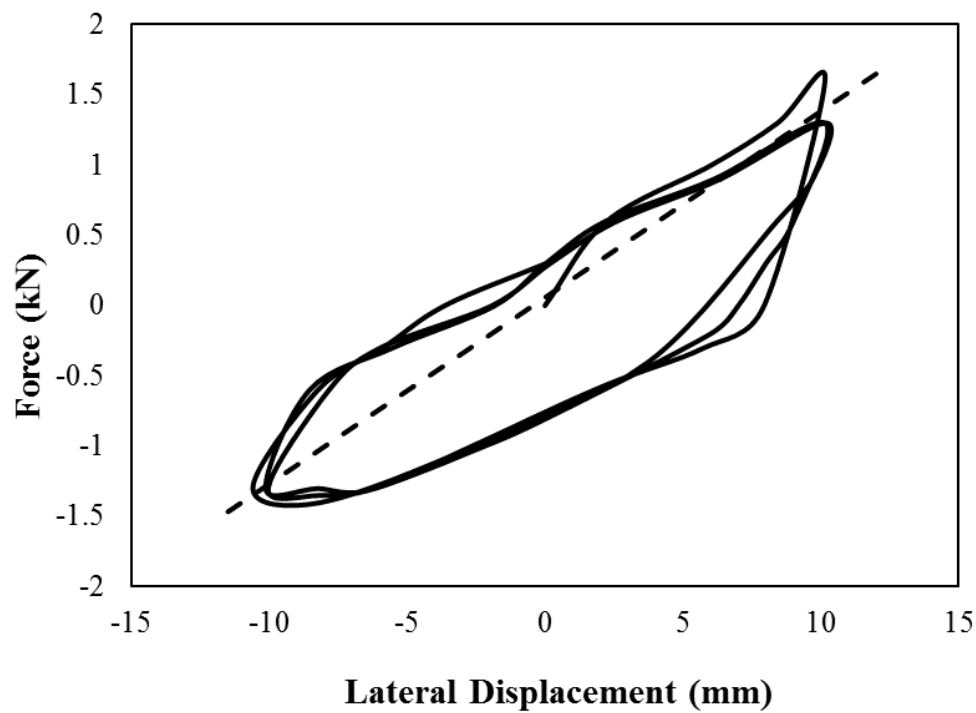
1st Cycle:

$$K_{H-1st} = \frac{(F_{\max} - F_{\min})}{(\delta_{\max} - \delta_{\min})}$$

$$K_{H-1st} = \frac{(1.3 - (-1.3))}{(10.140 - (-10.020))} = 0.129 \text{ kN/mm}$$



(a)



(b)

Figure 6.11 Horizontal test result at 10% shear deformation; (a). Photograph of specimen (b). Force-displacement relationship.

With the same procedure, the calculations of the 2nd and 3rd cycles were conducted and presented in Table 6.11 below.

Table 6.11 Horizontal test results in 10% shear strain (10 mm).

Cycle	Max		Min		K_{H-Eff} (kN/mm)	K_{H-Ave} (kN/mm)
	δ_{max} (mm)	F_{max} (kN)	δ_{min} (mm)	F_{min} (kN)		
1st	10.140	1.600	-10.110	-1.300	0.143	
2nd	10.140	1.300	-10.020	-1.300	0.129	0.133
3rd	10.170	1.300	-10.575	-1.300	0.125	

The damping ratio (10%): In calculating damping ratio, hysteresis loop in the middle cycle (2nd) was used. The calculations of dissipation energy of bearing in shear strain 10% are given below:

Stored or elastic energy (W_s):

$$\Delta_{max} = \frac{(\delta_{max} + |\delta_{min}|)}{2} = \frac{(10.140 + |-10.020|)}{2} = 10.080 \text{ mm}$$

$$W_s = \frac{K_H \times (\Delta_{max})^2}{2} = \frac{0.133 \times (10.080)^2}{2} = 6.732 \text{ kN-mm}$$

Dissipated energy (W_d):

The dissipated energy is equal to the hysteresis loop area. A hysteresis loop represents the plot of force (in *kN*) against displacement (in *mm*). By using Autocad software, the area in the 2nd cycle obtained is as follows:

$$W_d = 20.229 \text{ kN-mm.}$$

Therefore, the equivalent viscous damping ratio of isolator in shear strain 10% is illustrated below:

$$\xi_{10mm} = \frac{W_d}{(4\pi \times W_s)} \times 100\% = \frac{20.229}{(4\pi \times 6.732)} \times 100\% = 23.926 \%$$

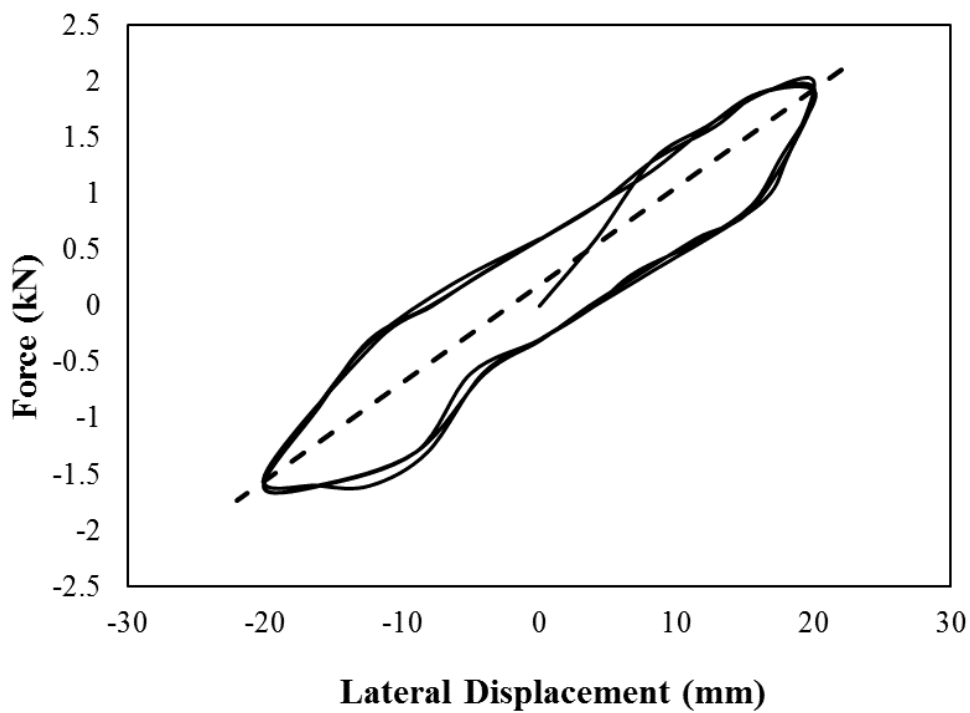
c. *Shear Strain 20% (20 mm):*

The results of horizontal test of specimen in shear at strain 20% are presented in Fig 6.12. The vertical axis represents the horizontal imposed load and the horizontal axis represents the horizontal displacement. The dashed straight

line corresponds to the horizontal average stiffness of the specimen during the cyclic part of the testing.



(a)



(b)

Figure 6.12 Horizontal test result at 20% shear deformation; (a). Photograph of specimen (b). Force-displacement relationship.

The stiffness (20%): The horizontal stiffness would be considered in each cycle denoted effective stiffness, then the average value would be considered to represent the isolator. The details of analysis are presented below:

1st Cycle:

$$K_{H-1st} = \frac{(F_{\max} - F_{\min})}{(\delta_{\max} - \delta_{\min})}$$

$$K_{H-1st} = \frac{(1.900 - (-1.600))}{(20.1 - (-20.130))} = 0.087 \text{ kN/mm}$$

With the same procedure, the calculations of the 2nd and 3rd cycles were conducted and presented in Table 6.12 below.

Table 6.12 Horizontal test results in 20% shear strain (20 mm).

Cycle	Max		Min		K_{H-Eff} (kN/mm)	K_{H-Ave} (kN/mm)
	$\delta_{\max} (mm)$	$F_{\max} (kN)$	$\delta_{\min} (mm)$	$F_{\min} (kN)$		
1st	20.025	2.000	-20.025	-1.500	0.087	
2nd	20.100	1.900	-20.130	-1.600	0.087	0.087
3rd	20.145	1.900	-20.100	-1.600	0.087	

The damping ratio (20%): In calculating damping ratio, hysteresis loop in the middle cycle (2nd) was used. The calculations of dissipation energy of bearing in shear strain 20% are given below:

Stored or elastic energy (W_s):

$$\Delta_{\max} = \frac{(\delta_{\max} + |\delta_{\min}|)}{2} = \frac{(20.100 + |-20.130|)}{2} = 20.115 \text{ mm}$$

$$W_s = \frac{K_H \times (\Delta_{\max})^2}{2} = \frac{0.087 \times (20.115)^2}{2} = 17.625 \text{ kN-mm}$$

Dissipated energy (W_d):

The dissipated energy is equal to the hysteresis loop area. A hysteresis loop represents the plot of force (in kN) against displacement (in mm). By using Autocad software, the area in the 2nd cycle obtained is as follows:

$$W_d = 36.861 \text{ kN-mm.}$$

Therefore, the equivalent viscous damping ratio of isolator in shear strain 20% is illustrated below:

$$\xi_{20mm} = \frac{W_d}{(4\pi \times W_s)} \times 100\% = \frac{36.861}{(4\pi \times 17.625)} \times 100\% = 16.651 \%$$

d. Shear Strain 50% (50 mm):

The results of horizontal test of specimen in shear at strain 50% are presented in Fig 6.13. The vertical axis represents the horizontal imposed load and the horizontal axis represents the horizontal displacement. The dashed straight line corresponds to the horizontal average stiffness of the specimen during the cyclic part of the testing.

The stiffness (50%): The horizontal stiffness would be considered in each cycle denoted effective stiffness, then the average value would be considered to represent the isolator. The details of analysis are presented below:

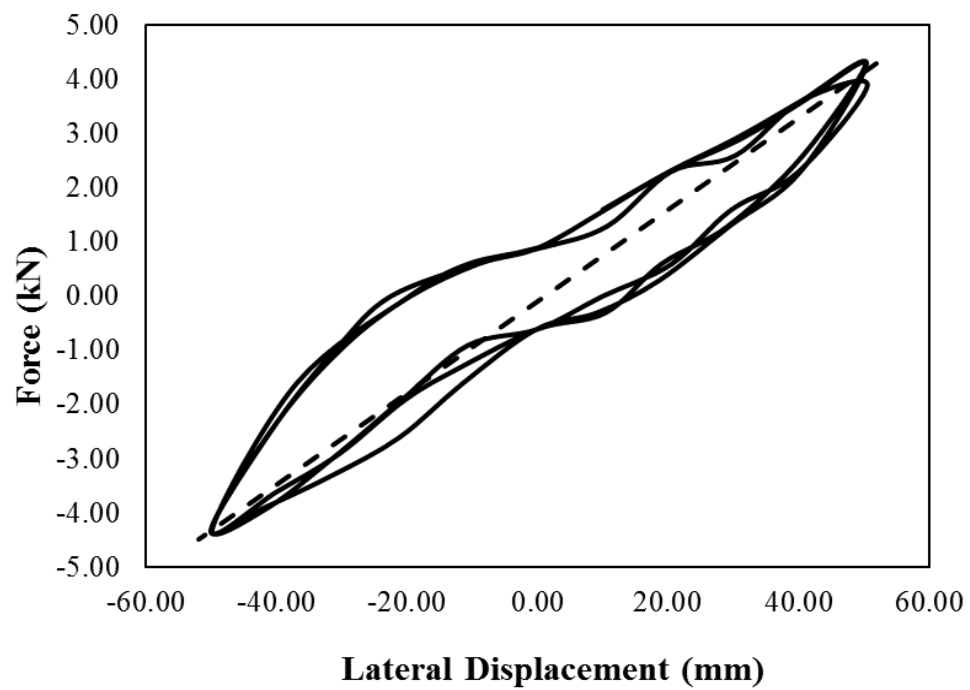
1st Cycle:

$$K_{H-1st} = \frac{(F_{\max} - F_{\min})}{(\delta_{\max} - \delta_{\min})}$$
$$K_{H-1st} = \frac{(4.30 - (-4.30))}{(50.310 - (-49.860))} = 0.086 \text{ kN/mm}$$

With the same procedure, the calculations of the 2nd and 3rd cycles were conducted and presented in Table 6.13 below.



(a)



(b)

Figure 6.13 Horizontal test result at 50% shear deformation; (a). Photograph of specimen (b). Force-displacement relationship.

Table 6.13 Horizontal test results in 50% shear strain (50 mm).

Cycle	Max		Min		K_{H-Eff} (kN/mm)	K_{H-Ave} (kN/mm)
	$\delta_{max} (mm)$	$F_{max}(kN)$	$\delta_{min} (mm)$	$F_{min} (kN)$		
1st	50.415	4.300	-50.040	-4.300	0.086	
2nd	50.310	4.300	-49.860	-4.300	0.086	0.084
3rd	50.565	3.900	-49.950	-4.300	0.082	

The damping ratio (50%): In calculating damping ratio, hysteresis loop in the middle cycle (2nd) was used. The calculations of dissipation energy of bearing in shear strain 50% are given below:

Stored or elastic energy (W_s):

$$\Delta_{max} = \frac{(\delta_{max} + |\delta_{min}|)}{2} = \frac{(50.310 + |-49.860|)}{2} = 50.085 \text{ mm}$$

$$W_s = \frac{K_H \times (\Delta_{max})^2}{2} = \frac{0.084 \times (50.085)^2}{2} = 105.794 \text{ kN-mm}$$

Dissipated energy (W_d):

The dissipated energy is equal to the hysteresis loop area. A hysteresis loop represents the plot of force (in kN) against displacement (in mm). By using Autocad software, the area in the 2nd cycle obtained is as follows:

$$W_d = 170.292 \text{ kN-mm.}$$

Therefore, the equivalent viscous damping ratio of isolator in shear strain 50% is illustrated below:

$$\xi_{50mm} = \frac{W_d}{(4\pi \times W_s)} \times 100\% = \frac{170.292}{(4\pi \times 105.794)} \times 100\% = 12.816 \%$$

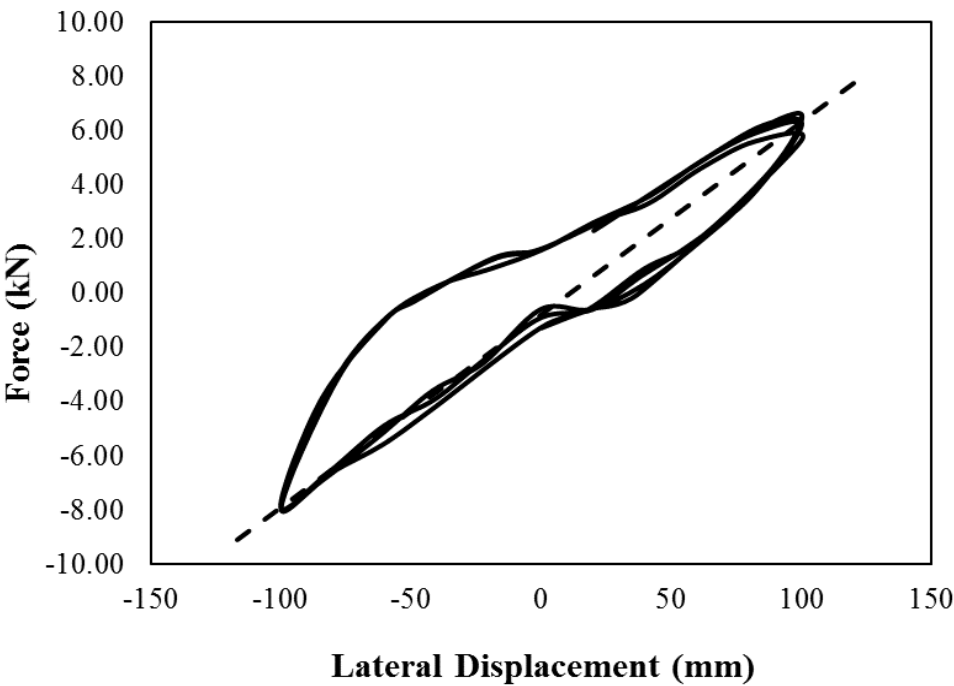
e. Shear Strain 100% (100 mm):

The results of horizontal test of specimen in shear at strain 100% are presented in Fig 6.14. The vertical axis represents the horizontal imposed load and the horizontal axis represents the horizontal displacement. The dashed straight

line corresponds to the horizontal average stiffness of the specimen during the cyclic part of the testing. The results of horizontal test of specimen in shear at strain 100% are given below:



(a)



(b)

Figure 6.14 Horizontal test result at 100% shear deformation; (a). Photograph of specimen (b). Force-displacement relationship.

The stiffness (100%): The horizontal stiffness would be considered in each cycle denoted effective stiffness, then the average value would be considered to represent the isolator. The details of analysis are presented below:

1st Cycle:

$$K_{H-1st} = \frac{(F_{\max} - F_{\min})}{(\delta_{\max} - \delta_{\min})}$$

$$K_{H-1st} = \frac{(6.20 - (-7.90))}{(100.230 - (-99.990))} = 0.071 \text{ kN/mm}$$

With the same procedure, the calculations of the 2nd and 3rd cycles were conducted and presented in Table 6.14 below.

Table 6.14 Horizontal test results in 100% shear strain (100 mm).

Cycle	Max		Min		K_{H-Eff} (kN/mm)	K_{H-Ave} (kN/mm)
	$\delta_{\max} (mm)$	$F_{\max} (kN)$	$\delta_{\min} (mm)$	$F_{\min} (kN)$		
1st	100.155	6.600	-100.005	-7.900	0.072	
2nd	100.230	6.200	-99.990	-7.900	0.070	0.071
3rd	100.035	6.200	-100.170	-7.900	0.070	

The damping ratio (100%): In calculating damping ratio, hysteresis loop in the middle cycle (2nd) was used. The calculations of dissipation energy of bearing in shear strain 100% are given below:

Stored or elastic energy (W_s):

$$\Delta_{\max} = \frac{(\delta_{\max} + |\delta_{\min}|)}{2} = \frac{(100.23 + |-99.990|)}{2} = 100.110 \text{ mm}$$

$$W_s = \frac{K_H \times (\Delta_{\max})^2}{2} = \frac{0.071 \times (100.110)^2}{2} = 356.270 \text{ kN-mm}$$

Dissipated energy (W_d):

The dissipated energy is equal to the hysteresis loop area. A hysteresis loop represents the plot of force (in kN) against displacement (in mm). By using Autocad software, the area in the 2nd cycle obtained is as follows:

$$W_d = 629.17 \text{ kN-mm.}$$

Therefore, the equivalent viscous damping ratio of isolator in shear strain 100% is illustrated below:

$$\xi_{100mm} = \frac{W_d}{(4\pi \times W_s)} \times 100\% = \frac{629.17}{(4\pi \times 356.270)} \times 100\% = 14.060 \%$$

6.4 Summary of Experimental Test.

In this section, resume of the experimental test are presented. A series of experimental test has been conducted to observe the characteristics of Perforated-Reinforced Elastomeric Isolators (PREIs) under compression and lateral load that are presented below:

6.4.1 Vertical Test

The primary objective in conducting vertical test is to observe the characteristic of PREIs under pure compression. The resume of vertical test results are illustrated in Table 6.15 and Figure 6.15. The most important parameters on the vertical test are vertical stiffness and compression modulus. The use of perforated plates on isolator are studied to observe its influence on both vertical stiffness and compression modulus.

In this case, the perforated plate is considered as rigid reinforcement that is similar with initial assumption on the reinforcement of SREIs. The difference is only on the reinforcement area due to existence the holes on perforated plate. Therefore, the basic concept of SREIs is still used in PREIs analysis.

The limitation of apparatus test become the primary obstacles in research. In addition, the number of isolator was also insufficient to represent the experimental test result. Therefore, to verify the experimental test, FE analysis is conducted. Further discussion are presented in the subsequent section.

Table 6.15 Resume of the vertical characteristics of isolator.

Specimen	Axial Force (kN)	Vertical Stiffness K_v (kN/mm)	Compression Modulus E_c (MPa)
A	10	19.65	128
	20	27.81	181
	30	39.54	257
	40	48.09	313
	80	52.53	341
	100	49.56	322
	150	45.45	295
	200	41.14	267
	250	37.40	243
Average		40.130	260.82

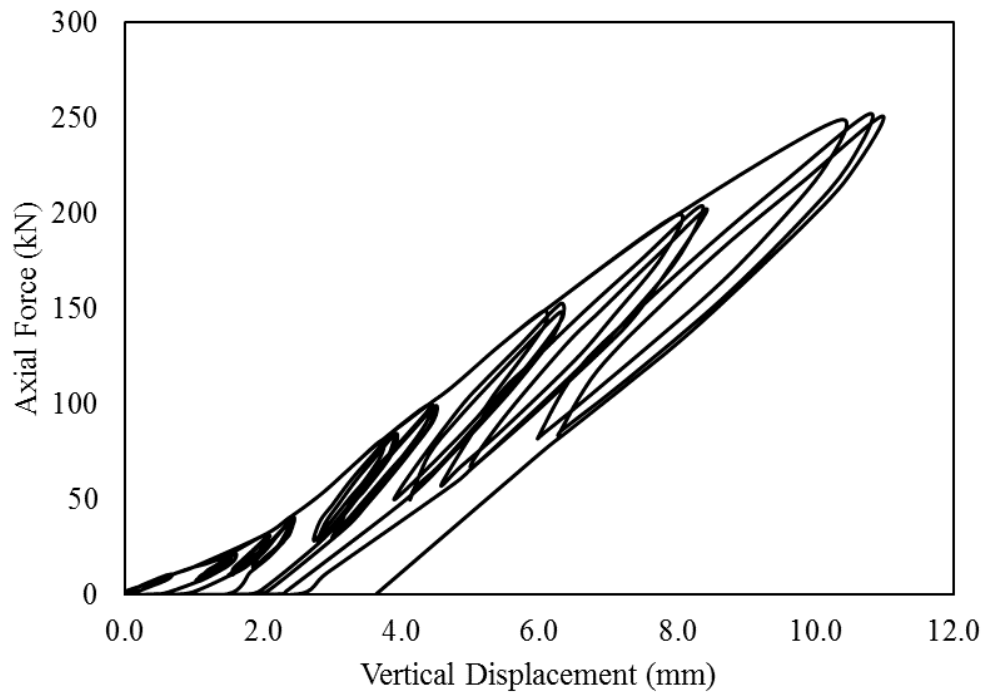


Figure 6.15 Vertical test result of isolator in multi axial load.

6.4.2 HorizontalTest

The resume of horizontal test results are illustrated in Table 6.16 and Figure 6.15. The primary objective in conducting horizontal test is to observe the characteristic of PREIs under lateral load.

Table 6.16 Resume of the lateral characteristics of isolator.

No	Shear strain (mm)	Horizontal stiffness (kN/mm)	Damping (%)	Shear Modulus (MPa)
1	5	0.147	19.53	0.469
2	10	0.133	23.93	0.422
3	20	0.087	16.65	0.277
4	50	0.084	12.82	0.269
5	100	0.071	14.06	0.226
Average		0.104	17.40	0.333

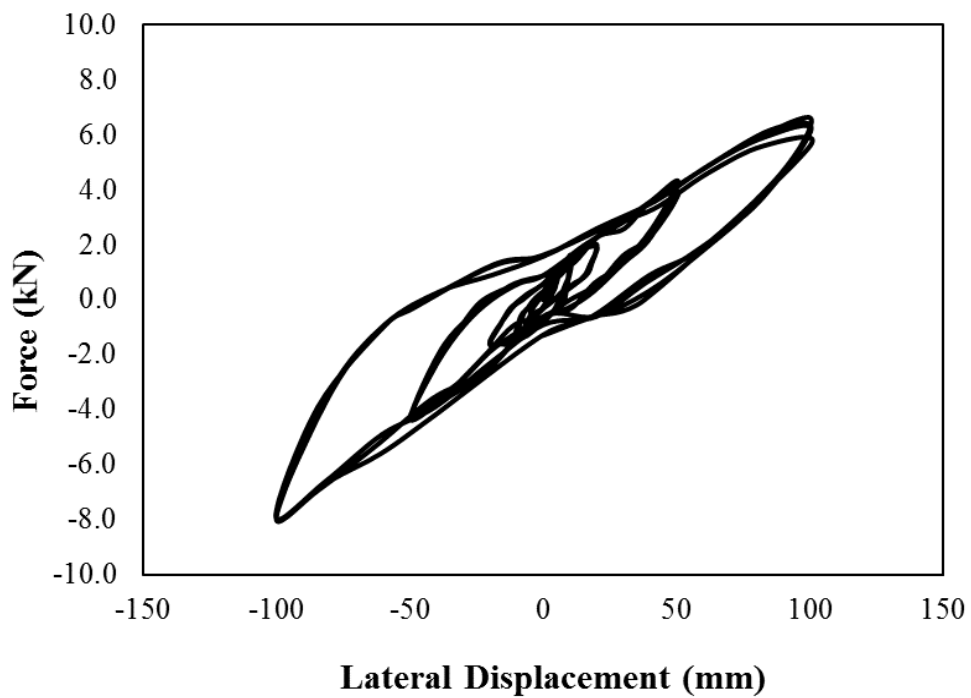


Figure 6.16 Horizontal test result of isolator in multi shear strain.

The most important parameters on the horizontal test are horizontal stiffness and shear modulus. The use of perforated plates on isolator are studied to observe its influence on both horizontal stiffness and shear modulus. As discussed earlier, the reinforcement has no effect on the horizontal stiffness of isolator. It means that the holes on the perforated plate are able to neglected in calculation of horizontal stiffness of PREIs. The limitation of apparatus test become the primary obstacles in this test. Therefore, to verify the experimental test, FE analysis is conducted presented in the subsequent section.

CHAPTER 7

FINITE ELEMENT ANALYSIS

7.1 Introduction

Finite element (FE) analysis is an alternative method in solving nonlinear problems in engineering fields. Many studies of the global characteristics of elastomer isolators by means of FE analysis have been conducted to investigate the principal stress and strain distribution in an elastomeric bearing. Modeling the ultimate behavior of elastomeric isolator is challenging for finite element since the problem involves a lot of settings such as the change of contact conditions, sliding, large strain (elastomer behavior) and near-incompressibility of the rubber.

In this chapter, a series of finite element (FE) analysis of isolators was carried out using the general-purpose commercially available FE software program of ANSYS. The main objective of FE analysis was to investigate the relationship between force-displacement of isolator under vertical and horizontal load. In addition, since the number of specimens used in the experimental test was limited, the FE analysis was employed to verify the experimental data test and conduct further analysis of isolator in different conditions. In modeling FE, there were three materials used to illustrate the isolators, such as rubber materials, perforated plates and end-steel plates. Due to the running process of finite element involved highly nonlinear material, for example rubber, high spec computers were required to solve nonlinear problems of isolator model in ANSYS. The details of finite element analysis are elaborated below.

7.2 Material Properties

In modeling isolator by ANSYS, there were three kinds of material involved in this analysis. These materials consist of rubber, end-steel plate, and perforated plate. The details of material properties for each element are presented below.

a. Rubber material

The four experimental data test are required to represent hyperelastic material in FE program, ANSYS. In section 4.1.2, selecting process of appropriate

constitutive model of hyperelastic material has been carried out. Ogden model is found to be the most appropriate model in representing rubber material in ANSYS. The curve fitting process is conducted using ANSYS program to derive the coefficient of Ogden. The coefficients of Ogden model are presented in Table 7.1.

Table 7.1 Coefficients for material constitutive models

Constitutive Model	Value	Unit
Ogden		
μ_1	-2,596.2	MPa
μ_2	910.09	MPa
μ_3	4,729.7	MPa
α_1	0.12926	-
α_2	0.21027	-
α_3	0.03068	-
D_1	0.00068928	MPa ⁻¹
D_2	6.5679E-05	MPa ⁻¹
D_3	6.503E-07	MPa ⁻¹

b. End-plate

In modeling end-steel plate of isolator, steel material was used to illustrate this element on ANSYS software. The material properties of steel were assumed from the default material from ANSYS program considered in linear condition. The detailed material properties for steel material illustrating end-plate are described in Table 7.2

c. Perforated Plate

Material properties of perforated plate were based on the experimental tension test results of perforated plate. The perforated plate was considered as rigid reinforcement. The detailed material properties illustrating perforated plate are given in Table 7.3.

Table 7.2 Material properties of end-plate (Steel material).

Property		Value	Unit
Density		7,850	Kg/m ³
Isotropic Elasticity	Young's Modulus	200,000	MPa
	Poisson's Ratio (ν)	0.3	
	Bulk Modulus	1,6667E+5	MPa
	Shear Modulus	7,6923E+4	MPa
Tensile Yield Strength		250	MPa
Tensile Ultimate Strength		460	MPa

Table 7.3 Material properties of perforated plate.

Property		Value	Unit
Density		7,850	Kg/m ³
Isotropic Elasticity	Young's Modulus	35,871	MPa
	Poisson's Ratio (ν)	0.3	
	Bulk Modulus	4,2667E+5	MPa
	Shear Modulus	1,9692E+4	MPa
Yield Strength		225	MPa
Tensile Strength		283	MPa

7.3 Contact Mechanism between Perforated and Rubber

The contact mechanics is part of mechanical engineering that provides necessary information for the safe and energy efficient design of technical system. It also represents the deformation of solids that touch each other at one or more points. The complex contact analysis under large deformation makes the ANSYS well suited for the analysis of PREIs. A bonded contact was defined between the rubber and perforated plate to prevent any slip along the interface (Engelen et al., 2014). The use of bonded as contact at the interface between rubber and perforated plate was assumed that it was no gaps and no sliding during the

deformation. The Augmented Lagrange was used as formulation during nonlinear analysis since it is better conditioning and is less sensitive to the magnitude of the contact stiffness coefficient.

7.4 Finite Element of Vertical Analysis

In this section, FE analysis of vertical test is presented. Since the limited of specimen, the FE analysis was conducted to verify the experimental data test result, especially for vertical test. The FE analysis was regarded significant to carry out verification in order to ensure the appropriate results of experimental data test of rubber-A by using FE analysis. The detailed settings on FE program, for instance: modeling, mesh condition, loading condition and boundary condition, are presented below:

7.4.1 Modeling Geometric of Isolator

As described earlier, finite element (FE) analysis was used for verifying the experimental data test and conducting further analysis with different conditions. Therefore, the geometry was modeled according to the actual dimension of isolator design illustrated in Fig 7.1.

The shape of isolator employed in this research was circular shape with a diameter of 200 mm and total thickness of 129 mm. The isolator contains alternating horizontal layers of rubber and reinforcement. There were 2 layers of end-steel plate, 20 layers of rubber and 19 layers of perforated plate with a thickness of 5 mm, 5 mm and 1 mm, respectively. In ANSYS program, the rubber, perforated plate and end-steel plate layers were modeled using SOLID186 that represented as hexahedron element with 20-nodes. According to ANSYS element library, this element has three translation degrees of freedom (DOF) at each node along x-, y-, and z- directions.

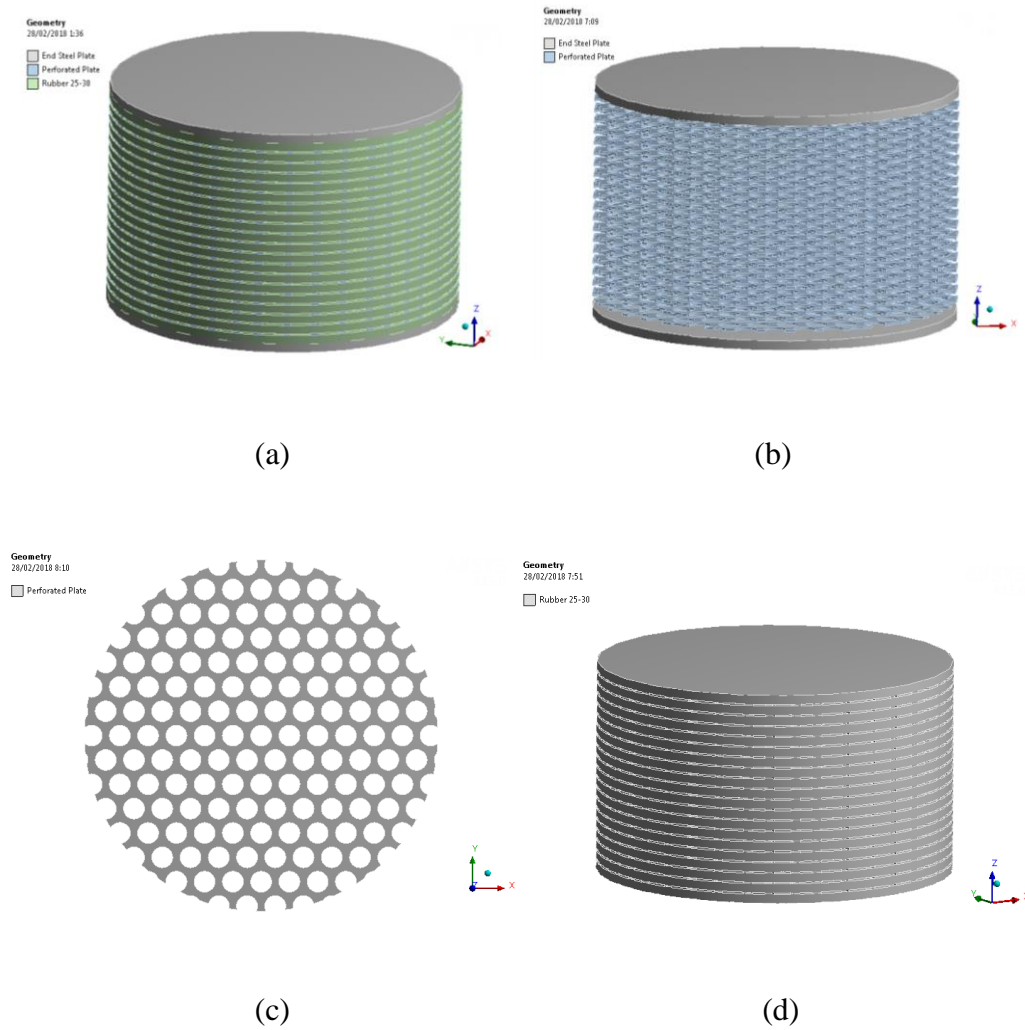


Figure 7.1 The geometric of isolator in finite element software, (a.) full model; (b.) perforated and end-steel plate, (c.) perforated plate and (d.) rubber.

In modeling the elements, a unique case occurred in modeling rubber material. Since the existence of holes on the plate, the rubber material was provided to fulfill the holes of perforated plate named *pin*, as shown in Fig 7.2. It generated between the layers of rubber that were interconnected from the top until the bottom layers of rubber. Due to the complexity of meshing process in FE program, the *pin* element was not possible to merge with rubber layer. Therefore, it was created separately with rubber layer however it has similar material properties.

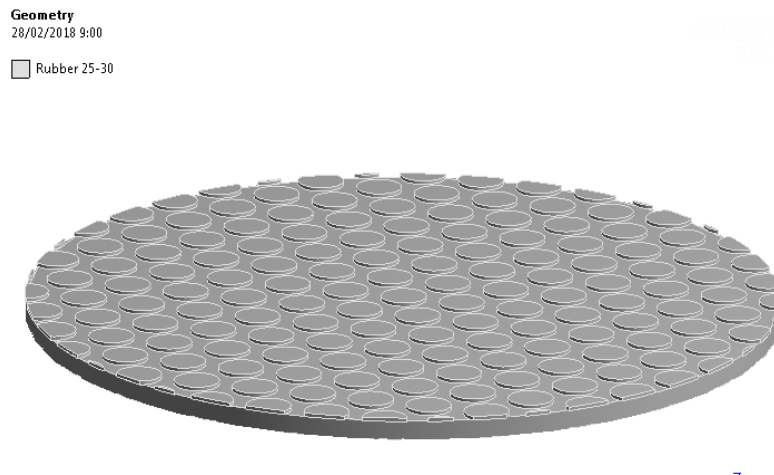


Figure 7.2 Preview of modeling the rubber in the holes (*pin*) of perforated plate.

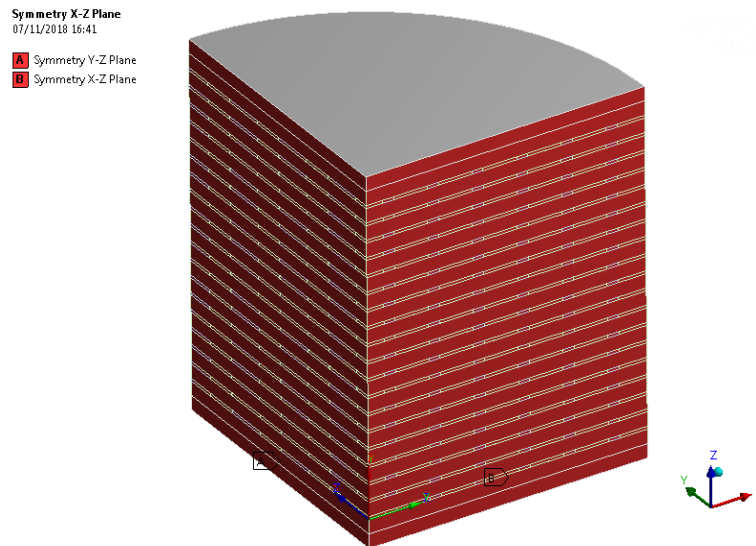


Figure 7.3 Finite element models for vertical analysis.

In addition, since the running process was time consuming, the FE model was modeled in a quarter from the overall isolator model for vertical analysis. The models are illustrated in Fig 7.3. In Fig 7.3, the model was only subjected to compression load in z -direction, therefore a quarter model was employed in FE analysis. In this condition, the model was arranged symmetrically in both y - z and x - z planes. The symmetries in both x - z and y - z planes produced free translations of the model in x - and z -directions as well as in y - and z -directions, respectively. Basically, simplified model was used due to the restricted capability of computers to process highly nonlinear calculation from hyperelastic

material. In further research, higher specification of computer is required to conduct nonlinear analysis of hyperelastic material.

7.4.2 Mesh Condition

The further analysis is carried out using finite element method by modeling 3D model of isolator in ANSYS program. The mesh condition of FE models is a critical issue in FE. Therefore, the quality of mesh must be considered carefully. In this research, hexahedron element was employed for the mesh shape in modeling isolator in ANSYS. Hexahedron, known as brick element, is able to fill a given volume more efficiently than other mesh shapes. It takes approximately 5 to 6 tetrahedrons to fill 1 brick. Fewer elements lead to faster solutions times. Hexahedron meshes are generally more uniform and it is easier to control the element distribution. In other word, hexahedron (well known as brick element) is more efficient and controllable.

In ANSYS program, the quality of mesh is measured by mesh metric, known as *skewness*. The skewness is one of the primary quality measures for a mesh. The skewness is a measure of the relative distortion of an element compared to its ideal shape and is scaled from 0 (Excellent) to 1 (Unacceptable). Highly skewed faces and cells are unacceptable because the equations being solved assume that the cells are relatively equilateral/equiangular. The skewness method is equiangular for every element type. The degrees of mesh quality related to *skewness* are shown in Table 7.4

Table 7.4 Measure the quality of mesh in ANSYS.

Value of skewness	Quality
1	Degenerate
0.9 - < 1	Bad
0.75 - 0.9	Poor
0.5 - 0.75	Fair
0.25 - 0.5	Good
>0 - 0.25	Excellent
0	Equilateral

In modeling FE model of isolator, mesh quality and time consumption are the main considerations to define mesh size of the elements. Therefore, the mesh sizes were set 2, 5, and 10 mm for the perforated plates, rubber layers, and end-plates, respectively. The skewness value of the FE model with specified size was found approximately 0.227. It means that the mesh quality for FE models are categorized as excellent. The mesh models are illustrated in Fig 7.4 below.

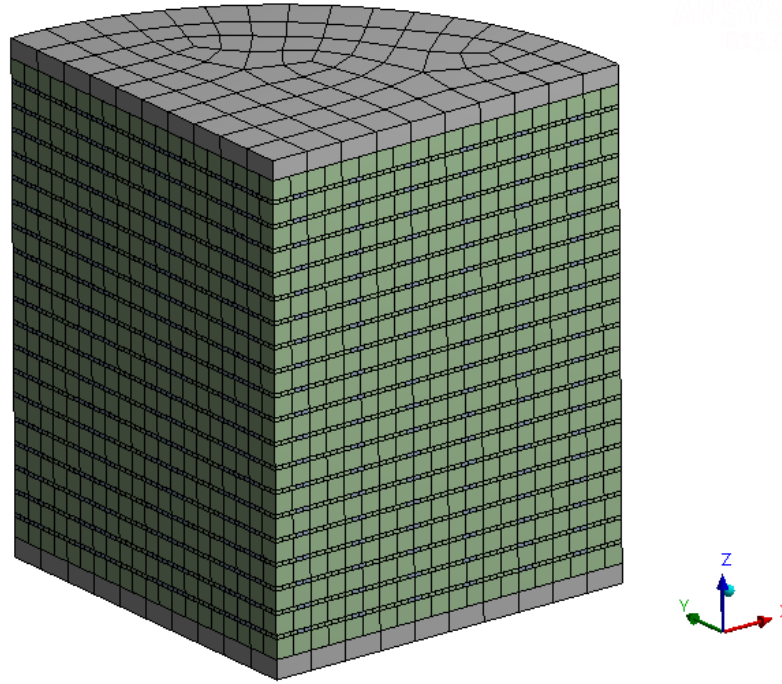


Figure 7.4 Mesh condition on FE models for vertical analysis.

7.4.3 Loading Condition

In this section, the loading conditions of FE model are presented. The loading conditions for vertical analysis are slightly different with experimental data test. In FE analysis, it was decided to use single load which was applied on the top side of isolator model in z direction. The model was subjected to axial load of approximately 80 kN (2.548 MPa) with zero lateral displacement.

The loading rate used on the FE model was similar with experimental test of 2.6 kN/sec. The loading of vertical analysis employed in FE program is presented in Fig 7.5. In other word, the FE result of vertical analysis only capture the backbone the experimental test. In addition, it was very effective in reducing time consuming in running process. The finite element program used employs the

Newton-Raphson method to solve the nonlinear problem. The load is subdivided into a series of load increments that can be applied over several load steps.

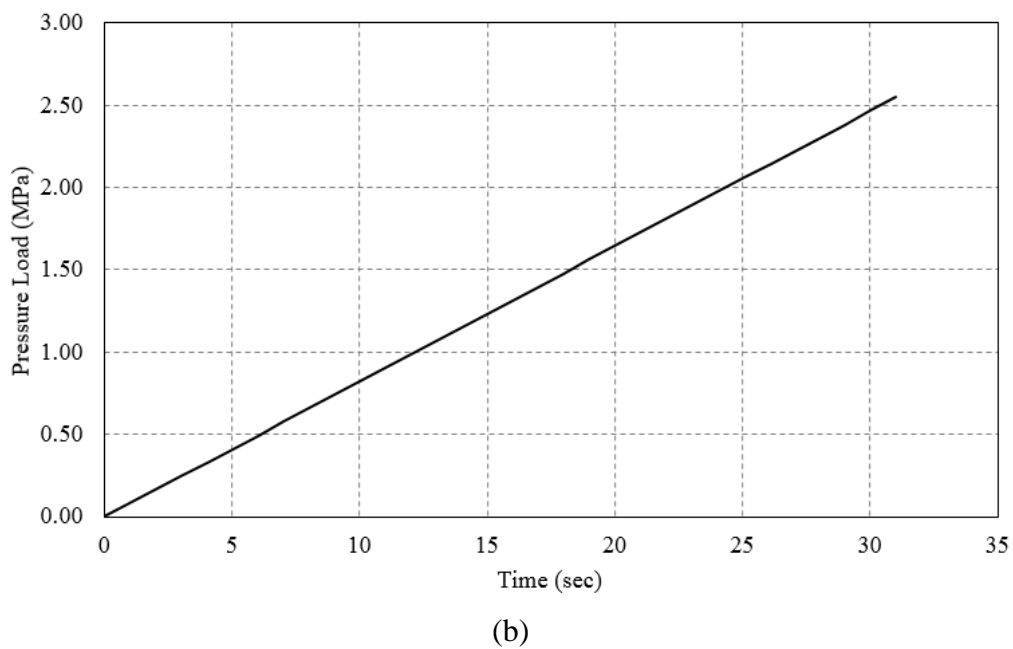
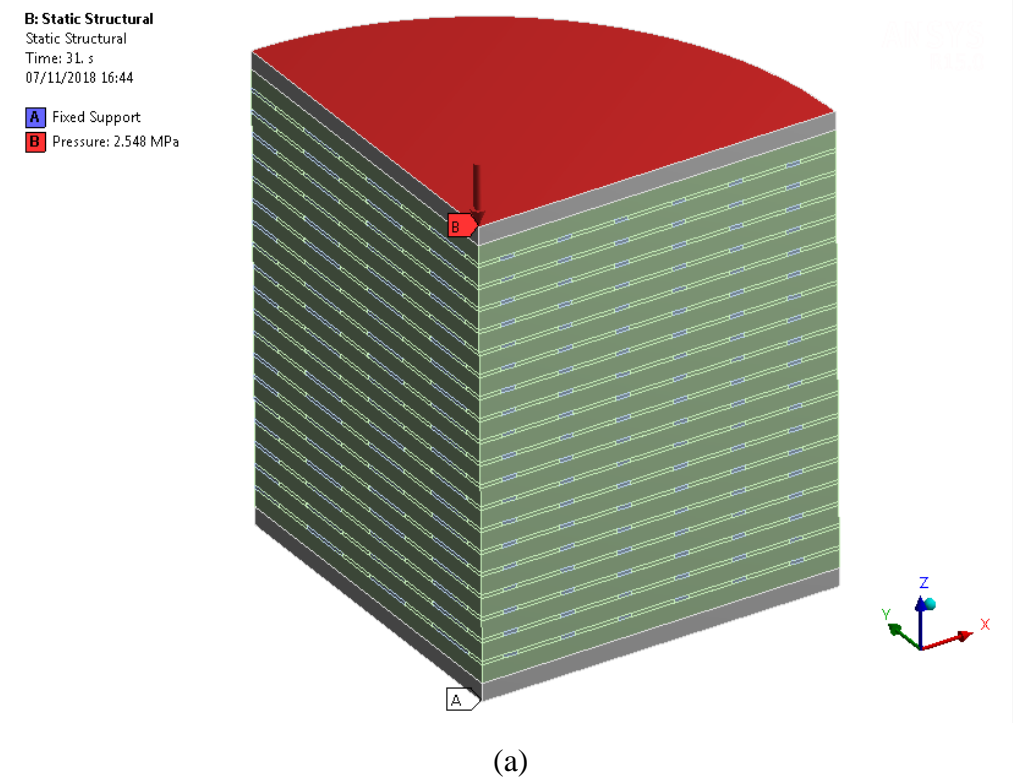


Figure 7.5 The loading condition of vertical analysis on FE program;
(a). Modeling in ANSYS; (b). Graph of vertical load.

7.4.4 Boundary Condition

In this section, the boundary conditions of FE model are presented. The boundary conditions between lateral and compression models are slightly different since the FE loading conditions are also different.

The boundary condition of compression model is somewhat simpler since the loading condition is only in z -direction (compression load). The bottom side of isolator is arranged as the fixed base in all directions to simulate the real condition of isolator on the application that is bolted on the foundation. In addition, the top side of the end steel plate was only free in z -direction and fixed in both x - and y -direction. In this condition, the model was arranged symmetrically in both y - z and x - z planes. The symmetries in both x - z and y - z planes produced free translations of the model in x - and z -directions as well as in y - and z -directions, respectively.

7.4.5 Finite Element Result of Vertical Analysis

In this section, FE result of vertical test is presented. A series of FE setting has been conducted to obtain appropriate result in modeling hyperelastic material, especially in vertical analysis of isolator. The FE result is employed to ensure that experimental test qualify to be considered as representative of actual behavior of isolator under compression load. It is caused the number of specimen in experimental test was only one specimen. In order to proof it, the experimental data test and FE result is compared in compression condition. The deformed shape of FE under compression load is illustrated in Fig. 7.6.

The backbone of experimental test data is used to compare with FE result illustrated in Fig 7.7. The FE result indicates that experimental data test is clearly different with experimental test data. It will be validated with analytical method to make sure the appropriate result between FE and experimental. The percentage of relative error between the experimental results and FE analysis is obtained by averaging the RMS error illustrated in Eq (71).



Figure 7.6 Deformed shape of isolator under pure compression load.

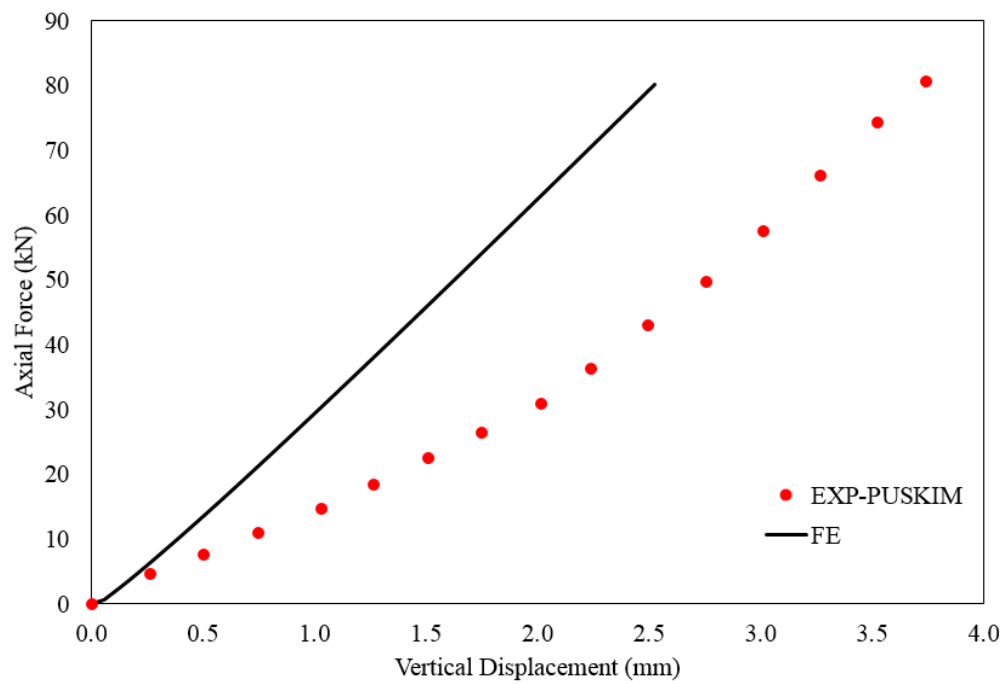


Figure 7.7 Comparison of vertical analysis between FE and experimental data of isolators.

$$RMS_{avg}Error = \frac{1}{N} \sqrt{\sum_{i=1}^N \left(\frac{|F_{exp} - F_{FE}|}{F_{exp}} \right)} \quad (7.1)$$

where N is the number of data point derived by FE analysis. The symbol F_{FE} and F_{exp} are finite element forces and experimental forces, respectively. The error was found to be 27.288% for PREIs model using FE analysis.

7.5 Finite Element of Horizontal Analysis

In this chapter, the FE analysis of horizontal test is presented as a subsequent study of lateral characteristic of isolator. Moreover, FE was also conducted to confirm that Ogden is an appropriate constitutive model to represent hyperelastic material in FE program. The lateral FE analysis was considerably different from the vertical test, due to the difference in both geometry and loading condition. The detailed settings on FE program, for instance: modeling, mesh condition, loading condition and boundary condition, are presented below:

7.5.1 Modeling Geometric of Isolator

As described earlier, finite element (FE) analysis was used for verifying the experimental data test and conducting further analysis with different conditions. Therefore, the geometry was modeled according to the actual dimension of isolator design. For horizontal analysis, FE setting is somewhat different than vertical typically for modeling perforated plate as reinforcement of isolator. Simplification in modeling perforated plate is conducted in order to reduce time consuming while running FE program. Basically, the geometric of FE model is similar as shown in Fig 7.9, however there are different setting in modeling horizontal analysis compare to vertical model, as follow :

- a. The isolator was modeled as half of model.

In this case, the isolator was only presented as half of model as shown in Fig 7.8. The primary reason is to reduce time consuming in running process. In addition, the loading condition of horizontal analysis allows to employ a half

model in running process due to the geometric is symmetric in XZ Plane. In lateral analysis, the model was subjected to compression load in z-direction then continued to shear laterally in x-direction. In this condition, the model was arranged symmetrically in y-z planes. The symmetries in y-z planes produced free translations of the model in x- and z-direction. With this condition, the half model of isolator is considered sufficient in representing the full model of isolator. The detail of loading condition will be presented in further section.

b. The perforated plate was modeled as full plate

Basically, simplified model was used due to the restricted capability of computers to process highly nonlinear calculation of hyperelastic material. Somewhat different with vertical analysis, the model of lateral analysis employs a half of model as shown in Fig 7.8. It means that the number of elements and nodes are increase significantly. In addition, the existance of holes on perforated plate require small size in meshing process. Therefore, to simplified the model and reduce the number of elements and nodes, the idealization of using full plate in modeling reinforcement in lateral analysis is decided. The holes of perforated plate are neglected and replaced by full plate. The considerations to determine this concept are based on :

1. The area of reinforcement has no effect on the lateral stiffness calculation (Kelly, 1999; Kelly and Shakhzod, 2001).
2. The reinforcement has no effect on the lateral stiffness of isolator (Kelly and Konstantinidis 2007, 2009, 2011; Engelen et al., 2014).

Since FE model of perforated plate is modified, the number of elements and nodes of isolator are highly different compared to initial model, as shown in Fig 7.9.

As shown in Fig 7.9 (a), the mesh size of initial model were set 2, 2, 5, and 5 mm for the pin, perforated plates, rubber layers, and end-plates, respectively. The total nodes and elements are 1,060,020 and 129,183, respectively. The number of elements and nodes are extremely excessive and it lead to running process considerably consuming time. Therefore, the model as shown in Fig 7.9 (b) is defined to reduce the number of node and element.

Symmetry Z-X Plane
07/11/2018 16:48
Symmetry Z-X Plane

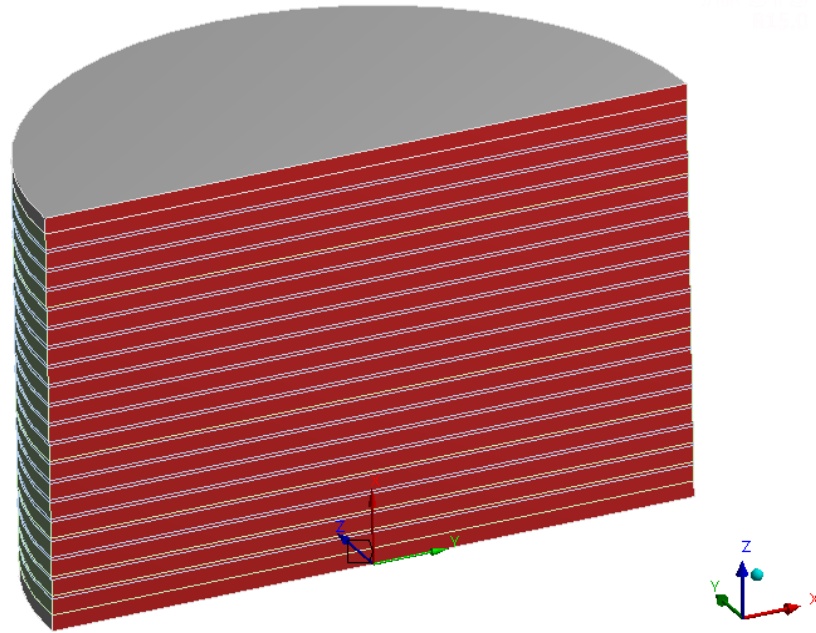


Figure 7.8 FE model for horizontal analysis.

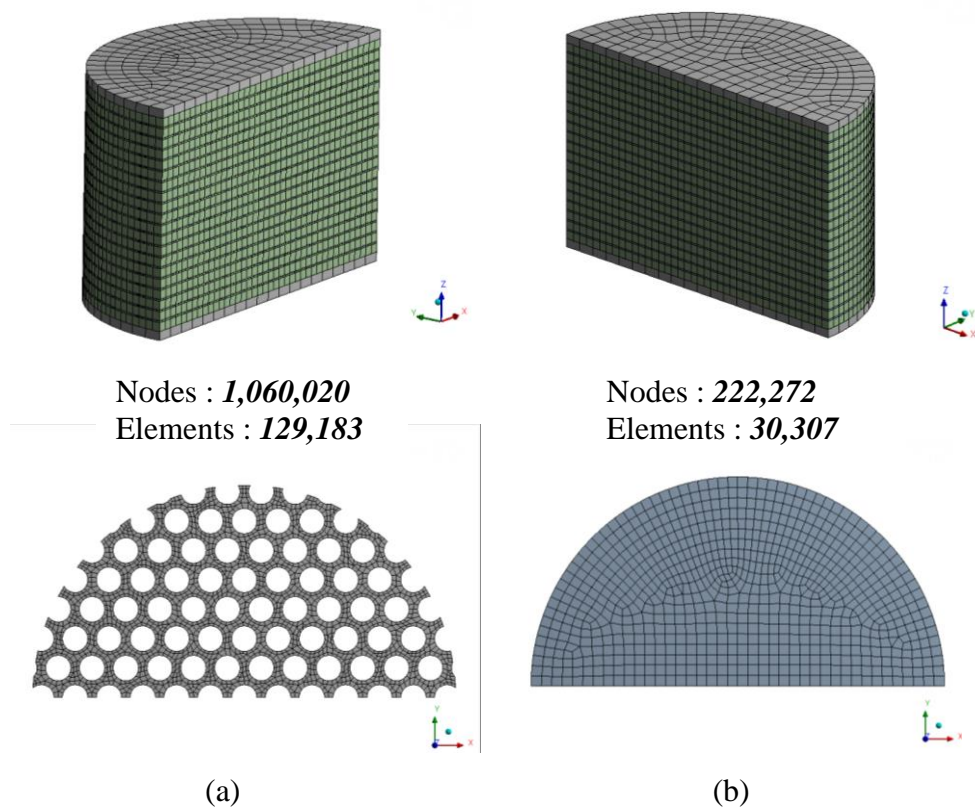


Figure 7.9 Modification model of lateral analysis;
(a). Initial model and (b). Modified model.

Fig 7.9 (b) is only consist of rubber, end plate and steel plate. The mesh size were set 5 mm for the all components. The total number of nodes and element are 222,272 and 30,307, respectively. This condition significantly reduces time consuming of FE of lateral analysis. The skewness value of the FE model with specified size is found approximately 0.06. It means that the mesh quality for FE models are categorized as excellent.

7.5.2 Loading Condition

In this section, the loading conditions of FE model of lateral analysis are presented. The loading conditions for lateral analysis are slightly different with experimental data test. Similar to the vertical test, the FE results of lateral analysis was only fitted to the backbone of the experimental test results (Spizzuoco et al., 2014). Therefore, the loading condition was simpler than the actual test.

In modeling loading condition on FE program, single loading was employed to describe compression load and lateral displacement. The model was subjected to axial load of approximately 80 kN and continued to move freely in lateral direction until 100 mm with a frequency of 0.5 Hz. The loading of lateral analysis employed in FE program is presented in Fig 7.10.

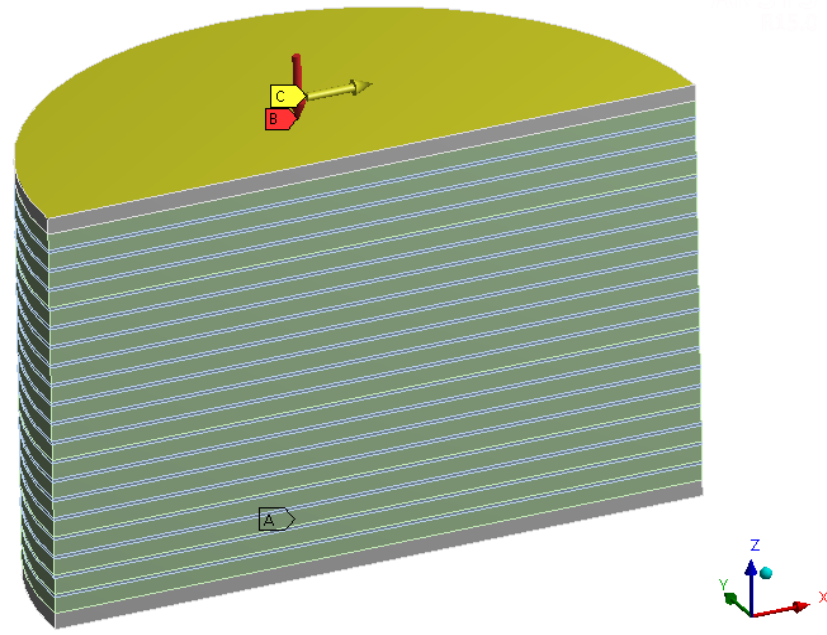
7.5.3 Boundary Condition

In this section, the boundary conditions of FE model of lateral analysis are presented. The boundary conditions between lateral and compression models are slightly different since the FE loading conditions and geometric are also different. In lateral analysis, the model was subjected to two kind of loading that were axial force with single load and continued with lateral displacement in x-direction. Therefore, typical boundary condition was adjusted to obtain the appropriate behavior. The setting of boundary conditions of lateral analysis are as follow:

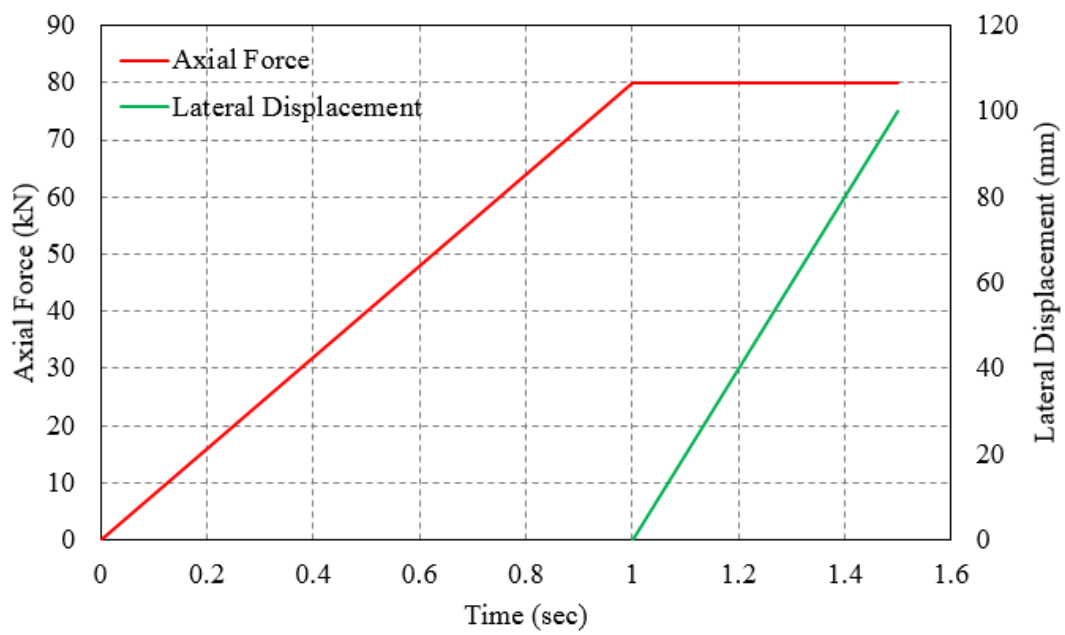
1. The bottom side of isolator is arranged as the fixed base in all directions to simulate the real condition of isolator on the application that is bolted on the foundation.

B: Static Structural
 Static Structural
 Time: 1.5 s
 07/11/2018 16:49

A Fixed Support
B Pressure: 2.548 MPa
C Remote Displacement



(a)



(b)

Figure 7.10 The loading condition of lateral analysis on FE program;

(a). Modeling in ANSYS; (b). Graph of horizontal load.

2. The top side of the end steel plate was only free in z- and x- direction and fixed in y- direction.
3. In addition, the model was arranged symmetrically in x-z planes. The symmetries in x-z planes produced free translations of the model in x- and z-directions.

7.5.4 Finite Element Result of Lateral Analysis

In this section, FE result of lateral test is presented. A series of FE setting has been conducted to obtain appropriate result in modeling hyperelastic material especially in lateral analysis of isolator. In solving nonlinear lateral analysis, Newton-Raphson was also used on FE program.

In finite element analysis, the model arranged moving down in z-direction due to axial load and undergoing displacement in lateral due to lateral force. The data pairs of force-displacement were recorded during the running process to fit with the experimental data. The deformed shape of FE model in lateral analysis is presented in Fig 7.11.

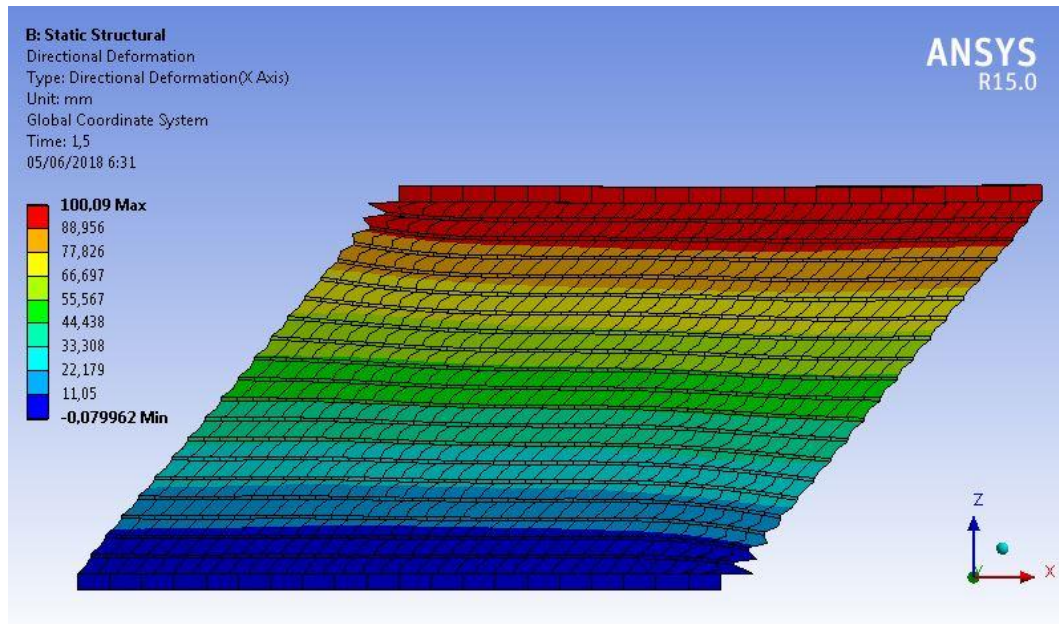


Figure 7.11 Deformed shape of isolator under lateral load.

Similar to vertical analysis, the agreement between experimental and FE results was considered related to the backbone of the experimental data test. The comparison between experimental and FE analysis are presented in Fig 7.12. The

FE results exhibit a good agreement with the experimental data in lateral condition. The error was found of about 19.02% for the PREI model using FE analysis. Furthermore, the FE model must be verified using analytical method to ensure the appropriate characteristic of isolator under lateral displacement.

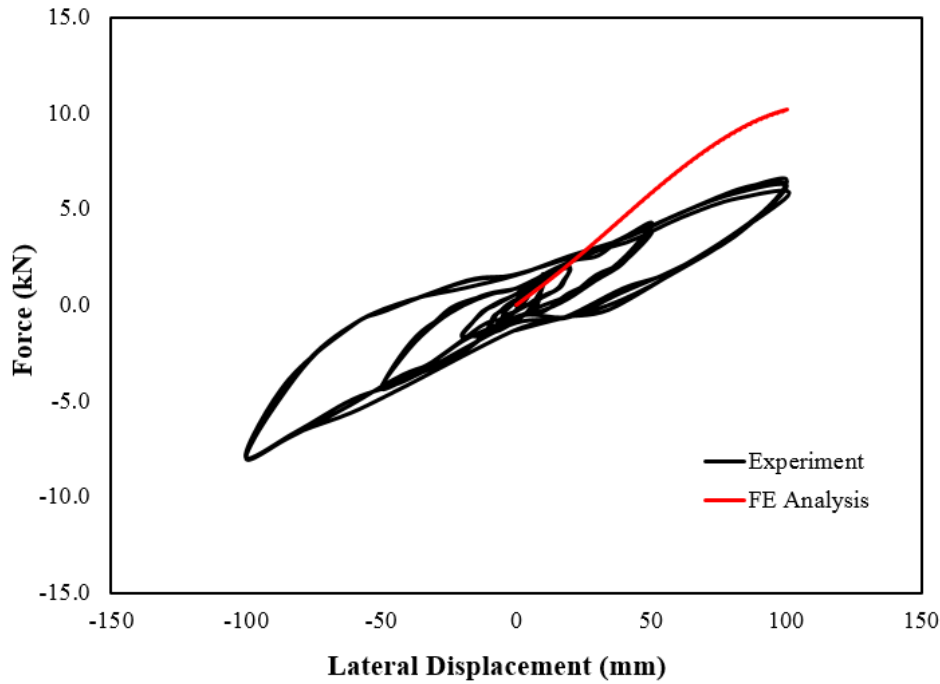


Figure 7.12 Comparison of lateral analysis between FE and experimental data of isolators.

7.6 Analytical Method

7.6.1 Characteristic of PREIs using analytical

This section presents analytical result of base isolation related to the characteristic of vertical and horizontal test. As described earlier, the limitation of apparatus test and specimens number caused that the results test cannot be verified properly. Therefore, FE and analytical method are required to make sure the appropriate experimental test results.

The FE analysis has been presented in previous section that illustrated the different characteristic of FE compare to the experimental test. The analytical method is needed to verify the FE result. Since the initial assumption of perforated as rigid reinforcement, the basic concept of SREIs is used to observe the

characteristic of isolator under lateral and axial load. The detail analysis is presented below:

- Estimation of critical axial load (P_{crit})

The critical axial load is required to observe the buckling load of isolator with no lateral-force. The estimation of critical load used in this analysis is 300 kN according to maximum axial load of experimental test.

$$P_{crit} = 300kN \text{ (Experimental data test).}$$

- Shear modulus (G) of isolator

In lateral characteristic of isolator, the horizontal stiffness is influenced by the vertical load (Kelly, 1999). When the load carried by the isolator is comparable to the buckling load to the buckling load, the horizontal stiffness is reduced. The reduction is derived by using the linear elastic analysis and is presented by

$$K_H = \frac{GA_s}{h} \times \left[1 - \left(\frac{P}{P_{crit}} \right)^2 \right] \quad (7.2)$$

where G is shear modulus of rubber, A_s is effective shear area, h is the total height of isolator (rubber plus perforated plate) and P is loaded carried by isolator (80 kN). The horizontal stiffness, K_H , used in this analysis is obtained from FE of approximately 102 N/mm, illustrated in Fig 7.12. The detail calculations are presented below

$$A_s = \frac{A \times h}{t_r} = \frac{31,400 \times (100 + 19)}{100} = 37,366 mm^2$$

$$K_H = \frac{GA_s}{h} \times \left[1 - \left(\frac{P}{P_{crit}} \right)^2 \right]$$

$$102 = \frac{G \times 37,366}{119} \times \left[1 - \left(\frac{80,000N}{300,000N} \right)^2 \right]$$

$$G = 0.35 MPa$$

The shear modulus of isolator under axial load of 80 kN is about 0.35 *MPa*.

- Vertical stiffness (KV)

Prior to calculate the vertical stiffness, the compression modulus of rubber-steel composite (E_c) must be defined as a follow:

$$E_c = \frac{6GS^2K}{(6GS^2 + K)} \quad (7.3)$$

where :

G = shear modulus ($G = 0.35$ *MPa*)

S = Shape factor ($S = 10$)

K = Bulk modulus derived from volumetric test ($K = 2,800$ *MPa*)

$$E_c = \frac{6GS^2K}{(6GS^2 + K)} = \frac{6 \times 0.35 \times 10^2 \times 2,800}{(6 \times 0.35 \times 10^2 + 2,800)}$$

$$E_c = 195 \text{ MPa}$$

The compression modulus of isolator is about 195 *MPa*. After the compression modulus defined, the vertical stiffness of isolator is able to calculate as follow

$$K_v = \frac{E_c \times A_c}{t_r}$$

where A_c is the cross-sectional area of the isolator (in this chase it is taken as the area of perforated plate with POA of 51%).

$$A_c = (1 - 0.51) \times 31,400 \text{ mm}^2 = 15,386 \text{ mm}^2$$

$$t_r = \text{total thickness of rubber (100 mm).}$$

$$K_v = \frac{E_c \times A_c}{t_r} = \frac{195 \times 15,386}{100} = 30,003 \text{ N/mm} = 30 \text{ kN/mm}$$

- Fundamental period

The target of fundamental period of isolated structure described in previous section is about 2 second. Therefore, the stiffness of isolator under axial load of 80 kN is expected to achieve the target. With this analytical result, the estimation of fundamental period of isolator subjected to axial load of 80 kN is presented below:

$$T = 2\pi \sqrt{\frac{P}{K_H \times g}} = 2\pi \sqrt{\frac{8000}{10200 \times 9.8}} = 1.8 \text{ Second.}$$

with this result, the stiffness of isolator (under axial load of 80 kN) is able to apply for the low-rise building with fundamental period of 2 sec.

7.6.2 Bilinear model of PREIs

This section presents modeling isolator using bilinear model. In practice all isolation are modeled by a bilinear model based on the three parameters K_1 , K_2 , and Q as shown in Fig 7.13. A number assumption are made to complete the calculation corresponding to literatures and previos experiments. The detail of calculations are presented below

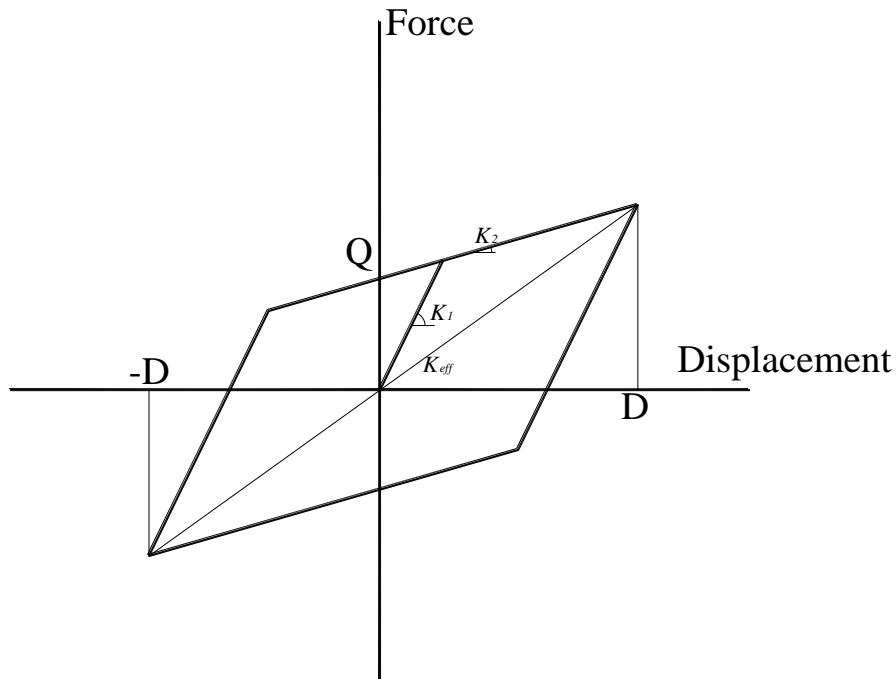


Figure 7.13 Parameters of basic hyteresis loop.

■ Parameters

In order to model bilinear, the horizontal stiffness is obtained from FE analysis that is about 0.102 kN/mm. The displacement, denoted D , is determined of 100mm. The elastic stiffness, K_1 , is assumed of $2.3K_2$ while the damping is estimated of 8% catagorized as low damping. This quantity is employed to calculate the parameters of K_1 , K_2 and Q .

$$K_H = 0.102 \text{ kN/mm}$$

$$D = 100 \text{ mm}$$

$$K_1 = 2.3K_2$$

$$\beta = 8\% \text{ (low damping isolation system)}$$

- Nondimensional characteristic strength

$$a = \frac{K_1 - K_2}{K_2} = \frac{2.3K_2 - K_2}{K_2} = 1.3$$

Determine parameter y :

$$\beta = \frac{2a}{\pi} \times \frac{(y-1)}{(y+a)y}$$

$$0.08 = \frac{2 \times 1.3}{\pi} \times \frac{(y-1)}{(y+1.3)y}; \text{ it is found that}$$

$$y = 7.706$$

- Yield displacement (D_y)

$$D_y = \frac{D}{y} = \frac{100}{7.706} = 12.977 \text{ mm}$$

- Stiffness of K_1 and K_2

$$K_{eff} = K_2 + \frac{Q}{D}$$

$$\text{where } Q = a \times K_2 \times D_y = 1.3 \times K_2 \times 12.977 = 16.87K_2$$

$$0.102 = K_2 + \frac{16.87K_2}{100}$$

$$10.2 = \frac{100K_2 + 16.87K_2}{100}$$

$$K_2 = 0.087 \text{ kN/mm}$$

Therefore,

$$K_1 = 2.3 \times K_2 = 2.3 \times 0.087 \text{ kN/mm} = 0.20 \text{ kN/mm}$$

And

$$Q = 16.87 \times K_2 = 16.87 \times 0.087 = 1.468 \text{ kN}$$

- The damping ratio of bilinear model at 100% shear strain.

In calculating damping ratio, bilinear model as shown in Fig7.14 was used. The calculations of dissipation energy of bilinear in shear strain 100% are given below:

Stored or elastic energy (W_s):

$$\Delta_{\max} = \frac{(\delta_{\max} + |\delta_{\min}|)}{2} = \frac{(100 + |-100|)}{2} = 100 \text{ mm}$$

$$W_s = \frac{K_H \times (\Delta_{\max})^2}{2} = \frac{0.102 \times (100)^2}{2} = 510 \text{ kN-mm}$$

Dissipated energy (W_d):

The dissipated energy is equal to the hysteresis loop area. A hysteresis loop represents the plot of force (in kN) against displacement (in mm). By using Autocad software, the area in the 2nd cycle obtained is as follows:

$$W_d = 513.382 \text{ kN-mm.}$$

Therefore, the equivalent viscous damping ratio of bilinear model in shear strain 100% is illustrated below:

$$\xi_{100mm} = \frac{W_d}{(4\pi \times W_s)} \times 100\% = \frac{513.382}{(4\pi \times 510)} \times 100\% = 8.01 \text{ \%}.$$

All parameter required to illustrate the bilinear model are obtained. The bilinear model is employed to verify the FE model and experimental test result. The bilinear model of PREIs under 80 kN with displacement of 100 mm are presented in Fig 7.14. Furthermore, the bilinear model is compared to FE results and experimental test that is shown in Fig 7.15.

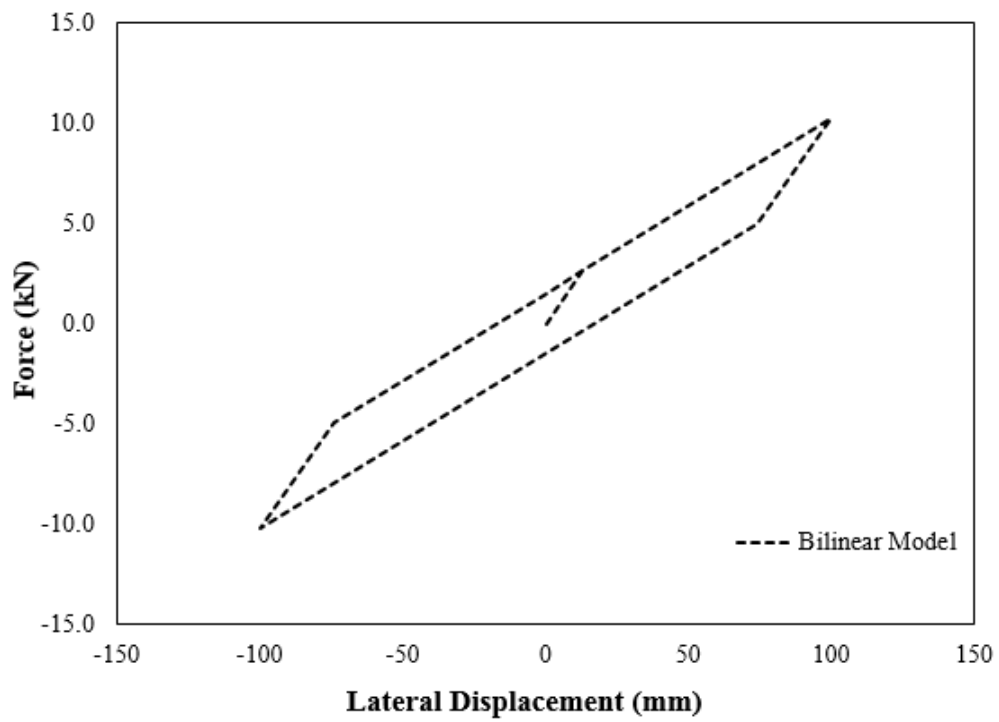


Figure 7.14 Bilinear model of PREIs under lateral displacement (100 mm).

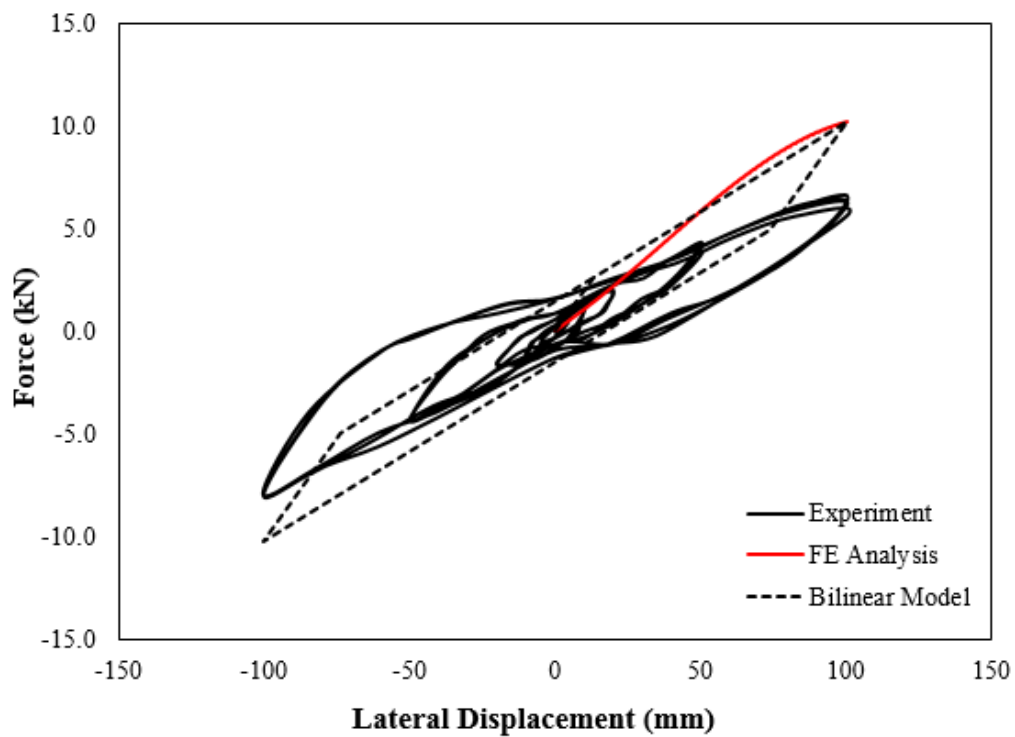


Figure 7.15 Bilinear model of PREIs compare to FE and experimental test result.

7.7 Lateral characteristic of PREIs under different vertical load

In this section, FE analysis of PREIs under different axial load are presented. It is conducted to observe the horizontal stiffness of isolator under compression. The FE analysis is employed to investigate the effect of axial load on the horizontal stiffness. The FE setting is identical with previous lateral analysis as described in section 7.5 except the axial load that varied of 40 kN, 80 kN and 120 kN. These axial load is selected to represent vertical load of low-rise building as illustrated in Table 4.18. The results are presented in Fig 7.16 and Table 7.5 as follow:

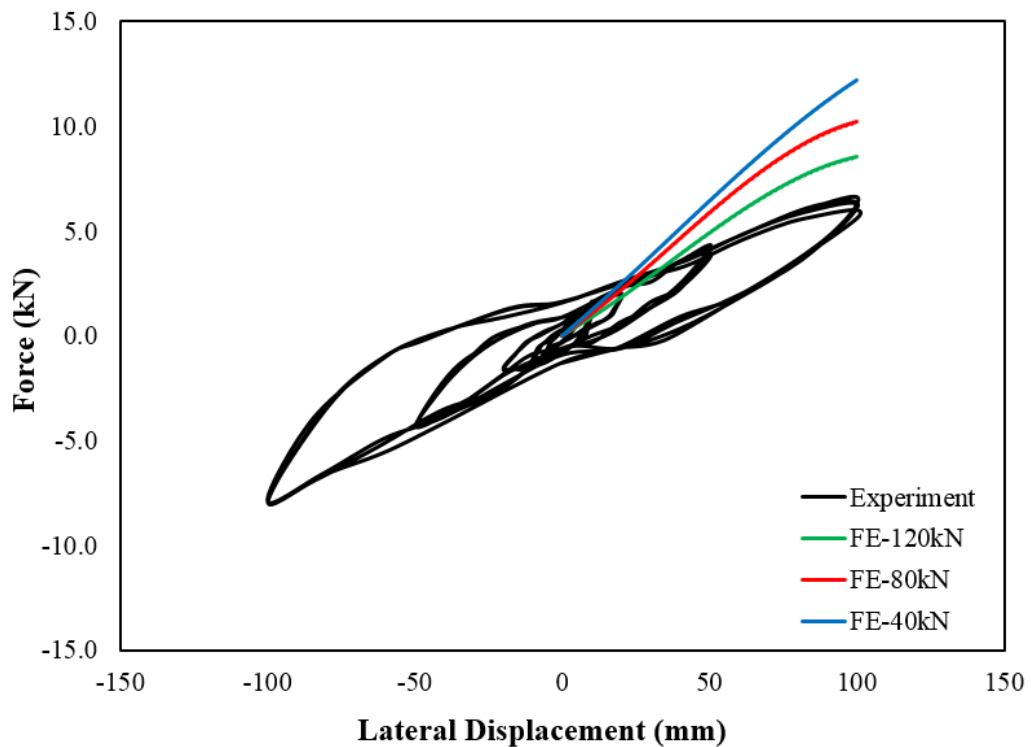


Figure 7.16 Lateral characteristic of PREIs under different vertical load.

Table 7.5 Lateral characteristic of PREIs.

Axial (kN)	Horizontal Stiffness (kN/mm)	Shear Modulus (MPa)	Fundamental Period (Sec)
0	0.147	0.47	-
40	0.122	0.40	1.15
80	0.102	0.35	1.8
120	0.086	0.33	2.40

7.8 Stability under large lateral displacement

In calculating max lateral displacement of isolator, it depends on the axial force subjected to the isolator. It is presented as follow :

$$\frac{P}{P_{crit}} < 0.6$$

$$\frac{80kN}{300kN} < 0.6$$

$$0.267 < 0.6$$

Therefore, the critical displacement of isolator is :

$$d = 1 - \left[\frac{1}{2} \left(\frac{3\pi}{4} \right)^{\frac{2}{3}} \times \left(\frac{P}{P_{crit}} \right)^{\frac{4}{3}} \right] \text{ where } d \text{ is constant.}$$

$$d = 1 - \left[\frac{1}{2} \left(\frac{3\pi}{4} \right)^{\frac{2}{3}} \times \left(\frac{80}{300} \right)^{\frac{4}{3}} \right]$$

$$d = 0.847$$

$$\text{where } d = \frac{D_{crit}}{2R}$$

$$D_{crit} = d \times 2R$$

$$D_{crit} = 0.847 \times 2 \times 100mm = 169.5mm \approx 170mm$$

The critical lateral displacement (D_{crit}) of PREIs under axial load (80 kN) is 170 mm.

7.9 Summary of FE analysis

Finite element is known as a powerful method in predicting material characteristics involving linear and nonlinear analysis. A series of FE analysis has been conducted on PREIs in order to verify the experimental data test and carry out further analysis of PREIs design. A limited number of specimen in this research project became the primary reason why FE was used to predict the characteristics of isolator. The FE analysis considered in this reasearch are vertical and horizontal analysis that represent vertical test and horizontal test of PREIs, respectively.

The analytical and FE are required to verify the appropriate results for presenting the behavior of isolator. According to Fig 7.7 and 7.12, it illustrates that the experimental test results and FE analysis cannot perform good agreement. The analytical method is required to prove the appropriate result of isolator design. Table 7.6 and 7.7 illustrates the values of characteristics among analytical, FE and experimental results.

Table 7.6 Comparison of vertical characteristics of PREIs.

Vertical Stiffness (kN/mm)			Compression Modulus (MPa)		
Analysis	FE	Experiment	Analysis	FE	Experiment
30	33.2	40.13	195	216	260

Table 7.7 Comparison of horizontal characteristics of PREIs.

Horizontal Stiffness (kN/mm)			Shear Modulus (MPa)		
Analysis	FE	Experiment	Analysis	FE	Experiment
0.102	0.102	0.71	0.35	0.35	0.23

According to Table 7.5 and 7.6, the results derived from FE are considered to be in good agreement with the analytical results, and the FE model is qualified to be employed for further analysis refer to parametric study using FE analysis.

"This page is intentionally left blank"

CHAPTER 8

FINITE ELEMENT STUDY OF MODIFIED ISOLATOR

8.1 Introduction

The primary aim of research project is to develop low-cost base isolation sistem for low-rise building in high seismic zone. In this research project, perforated plate is employed as alternatif material to replace steel plate as reinforcement on conventional steel-reinforced elastomeric isolator (SREIs). The replacement of steel plate with perforated plate is expected to reduce significantly the cost and weight of isolator.

The critical point in developing isolator for low-rise building (light structure) is how to derive the lowest horizontal stiffness of isolator to obtain the target of fundamental period of the structure. In this research work, low-rise building is expected to be have fundamental period of approximately 2 second, as described in Chapter 5.3. The horizontal stiffness is influenced by axial force subjected to the isolator. The lower axial force subjected to the isolator, it means the lower horizontal stiffness is required to obtain the target of fundamental period of light structure. In this study, the number of attempts were conducted by using perforated plate as reinforcement and using low-grade of rubber material to derive lower horizontal stiffness.

According to experimental test result, perforated-reinforced elastomeric isolators (PREIs) used in this study is able to create the structure belong a fundamental period of about 2 second with an axial load of 80 kN. However, this results are insufficient to apply on the low-rise building typically for one storey due to the lowest axial force, as discuss on chapter 4, is approximately 40 kN. An alternative method is required to enhance the lateral characteristic of PREIs by reducing the horizontal stiffness significantly. The viable method was proposed by Engelen (Engelen et al 2014; Osgooei et al 2015) by modifying the geometric of isolator to enhance the lateral response characteristic of isolator. The modifying geometric of isolator is by cutting holes in the center portion of the isolator or removing sections from the sides. It was carried out to increase the lateral response of isolator.

Therefore, to enhance the lateral response of PREIs, the modifying geometric is also conducted by removing section in the center portion of the isolator. This modified is extremely expected to reduce significantly the horizontal stiffness of PREIs under lower axial load, typically for 40 kN.

In this chapter, the modified circular perforated-reinforced elastomeric isolators (MC-PREIs) are investigated. The primary objective of the study is to reduce horizontal stiffness of PREIs. In this case, FE analysis is employed to investigate the lateral and vertical response of MR-PREIs with an axial load of about 40 kN. The detail of analysis of MR-PREIs using FE analysis are presented below.

8.2 Geometry of FE model of MC-PREIs

In this section, geometry of finite element model of modified circular perforated-reinforced elastomeric isolators (MC-PREIs) are presented. The modifying geometrics become an alternatif method in order to enhance the lateral response of isolator. It is expected to reduce significantly the horizontal stiffness of isolator under combination load.

The geometry of the isolators are circular with ratio between total thickness and diameter of 0.5. During the design process, the circular shape was selected for base isolation with a diameter of 200 mm. It was bounded with two steel end plates at the top and bottom surfaces for connecting the isolator to the upper and the lower structure. The isolators contained alternating horizontal rubber layers and perforated plate as reinforcement. There were 20 rubber layers in the isolator, with a thickness of 5 mm for a single layer. There were 19 layers of perforated plate reinforcement with a thickness of 1 mm for a single plate. By adding the two steel end plates on to the isolator, the total height of the base isolation was 129 mm. The detail dimensions of the isolator considered in this research work are illustrated and similar with previous section as shown in Fig 5.81 and Fig 8.9.

The geometry of FE models were identical with initial model, except fot interior modification to the hole in the center of the siolator, with a certain diameter (d). The study considered two type of isolators; one unmodified and

three modified models. The unmodified model was denoted as M0, while the three modified models were denoted as M1, M2, and M3 with interior modification of 50 mm, 75 mm and 100 mm, respectively. The FE result describe the characteristic of modified model compare to the unmodified model in vertical and lateral response. The detail of the FE models are illustrated in Fig 8.1 and Table 8.1. The models will be employed in vertical and horizontal analysis.

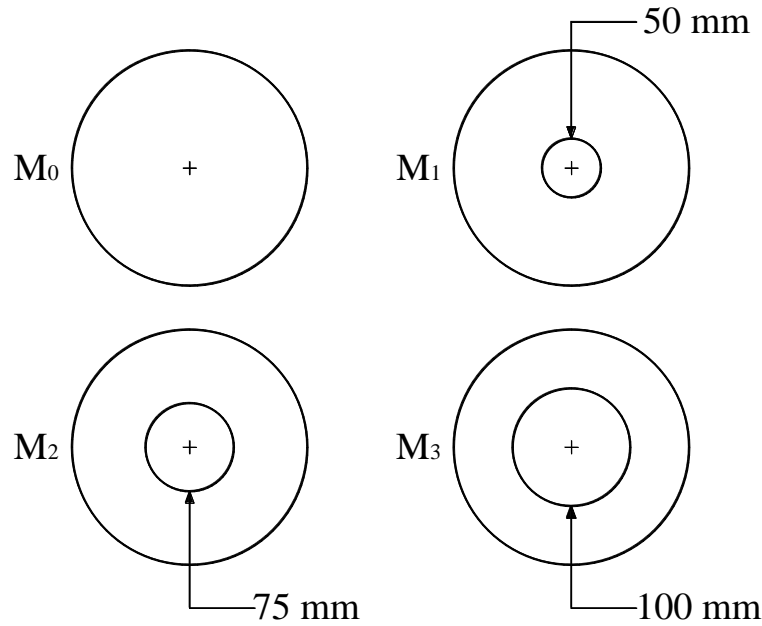


Figure 8.1. Plan view of FE model of modified isolators.

Tabel 8.1. Specimens geometric characteristics.

FE model	d (mm)	D (mm)	Area (mm ²)	d/D	Area removed (%)
M ₀	0	200	31,400	0.00	0.00
M ₁	50	200	29,438	0.25	6.25
M ₂	75	200	26,984	0.38	14.06
M ₃	100	200	23,550	0.50	25.00

8.3 Finite element study on vertical response of MC-PREIs.

This section presents the vertical characteristics of Modified Circular Perforated-Reinforced Elastomeric Isolators (MC-PREIs) under compression. Research on base isolation was undertaken to derive the lowest horizontal

stiffness to obtain the fundamental period of an isolated structure, typically for light structures, such as residential housing. In order to achieve this purpose, geometric modifications were introduced by reducing the loaded area of the isolators. Prior to observing the horizontal characteristic, the vertical stiffness of MC-PREIs was considered to ensure that the interior modification influences the vertical characteristic of the isolator. In this study, experimental vertical test results of Perforated-Reinforced Elastomeric Isolators (PREIs) were used to verify three-dimensional (3D) finite element (FE) model analyses of ANSYS. Furthermore, the 3D finite element models were used to undertake a parametric study on three MC-PREI configurations with different geometries. The FE method investigation considered the influence of the geometric modifications on the vertical stiffness and the compression modulus, in addition to strain and stress distribution in the perforated reinforcement and elastomer. The series analysis are presented below:

8.3.1 FE model of MC-PREIs for vertical analysis

As illustrated in Fig 8.1, the modified isolators consist of 3 type correspond to interior diameter of models. In modeling FE analysis, the MC-PREIs were modeled only a quarter from the overall isolator model. This condition is similar with initial analysis in section 7.4.1. It was carried out to reduce time consuming along running process. The model was arranged symmetrically in both y-z and x-z planes. The symmetries in both x-z and y-z planes produced free translations of the model in x- and z-directions as well as in y- and z-directions, respectively. The finite element models of MC-PREIs used in vertical analysis are illustrated in Fig 8.1 and Fig 8.2. The simplified model was utilized since the restricted capability of computers to process highly nonlinear calculation from hyperelastic material.

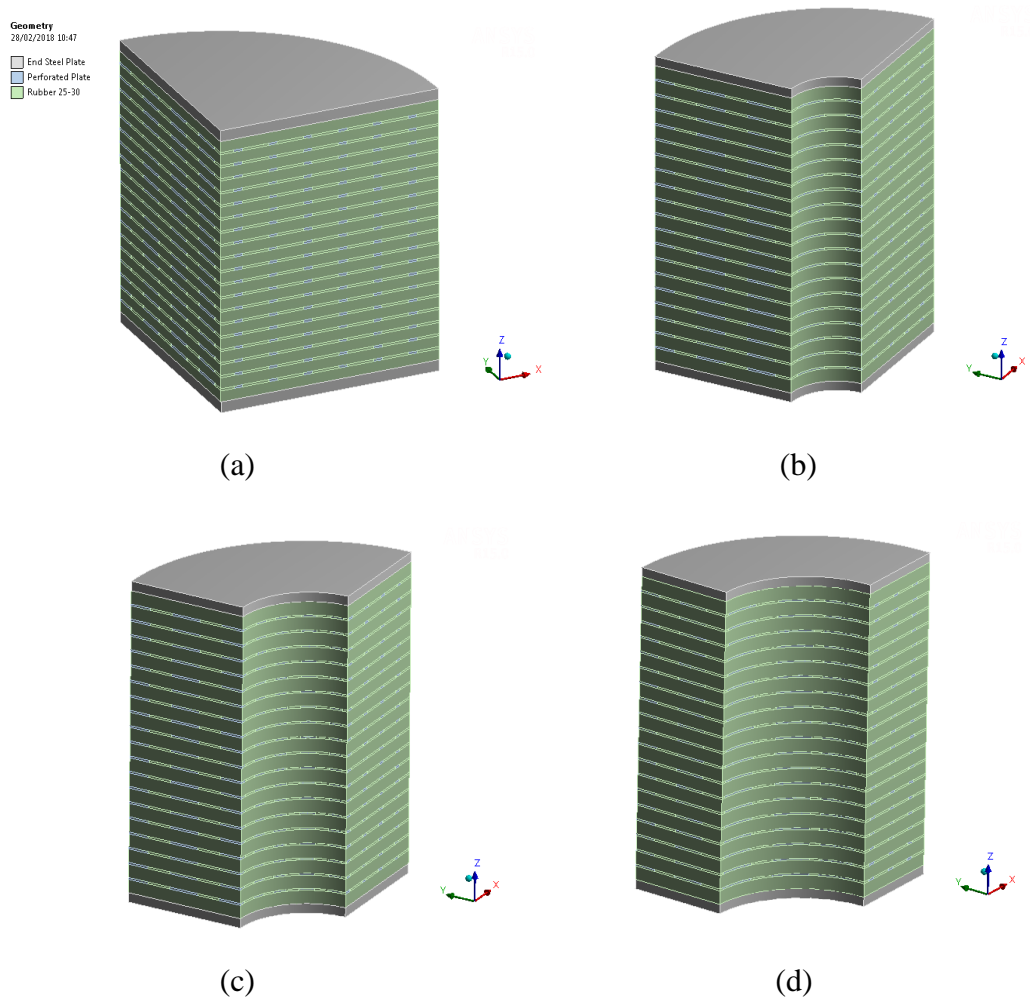


Figure 8.2. FE model of modified isolators in a quarter

(a). M0; (b). M1; (c).M2; and (d). M3.

8.3.2 Loading history of MC-PREIs for vertical analysis

The loading conditions for MC-PREIs analysis are similar with previous section as shown in Fig 7.13. The difference is only on the axial force subjected to the isolator. In this section, the axial force applied on the MC-PREIs model is approximately 40 kN (1.274 MPa). This value was taken to represent the lowest axial force of light structure designed in section 5.3. The loading rate was also similar with experimental test of 2.6 kN/sec. The FE result of vertical analysis only capture the backbone FE result. In addition, it was very effective in reducing time consuming in running process. The finite element program used employs the Newton-Raphson method to solve the nonlinear problem. The load is subdivided into a series of load increments that can be applied over several load steps.

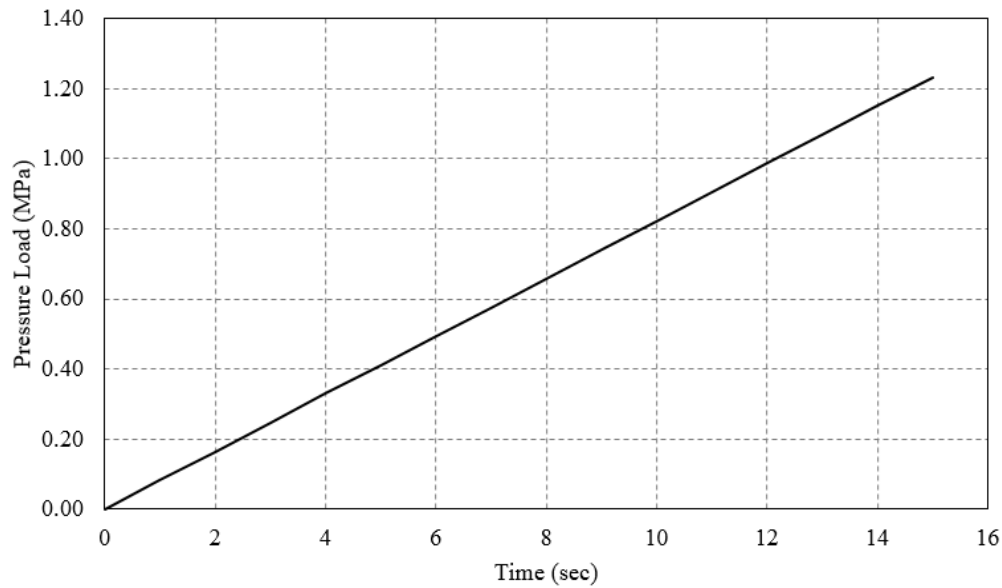


Figure 8.3. The loading condition of MC-PREIs on FE program.

8.3.3 Mesh condition of MC-PREIs for vertical analysis

In this section, mesh condition of MC-PREIs are presented. In general, the basic concept of mesh conditions were similar with unmodified model illustrated in chapter 7.4.2. The difference was only on the number of nodes and elements due to the modification geometry on the isolator. The skewness value was critical parameter to measure the quality of mesh condition for each model MC-PREIs. The detail setting of mesh conditions are presented in Fig 8.4

In Fig 8.4, mesh condition of each model are presented. The number of nodes, elements and skewness value are also described. Related to the mesh size of elements, the sizes were similar with initial setting in chapter 7.4.2. The mesh sizes were set 2, 5, and 10 mm for the perforated plates, rubber layers, and end-plates, respectively. The trend of number nodes and elements perform decrease significantly relative to reducing geometry area of isolator. As shown in Fig 8.4, M0 model has 491,064 nodes and 61,633 elements with skewness value of 0.208. Model M1 has 436,478 nodes and 53,371 elements with skewness value of 0.224. Model M2 has 415,149 nodes and 51,172 elements with skewness value of 0.211. Model M3 has 399,327 nodes and 45,124 elements with skewness value of 0.204. The skewness value for all models indicate below of 0.25. It means that the quality of mesh in ANSYS is categorized as excellent as show in Table 7.4.

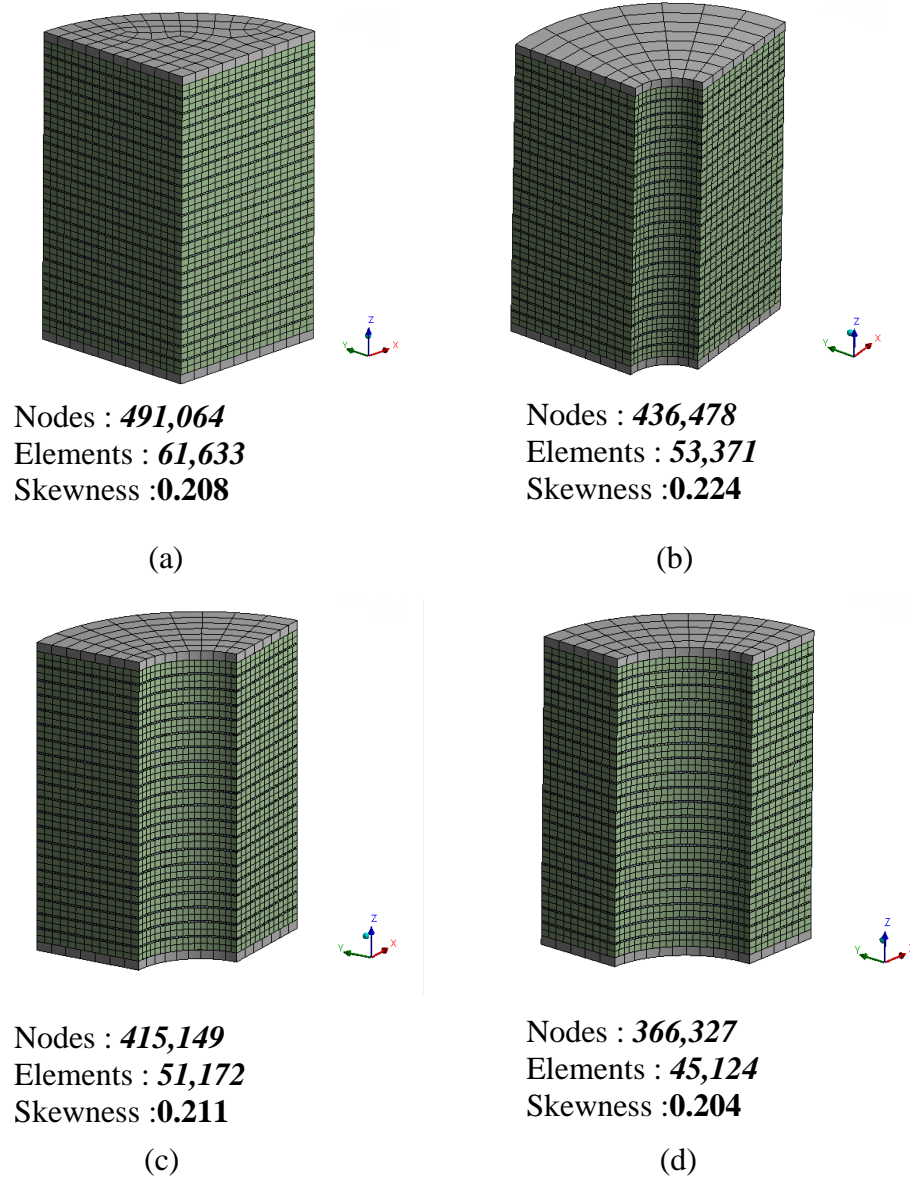


Figure 8.4. Mesh condition of MC-PREIs model

(a). M0; (b). M1; (c).M2; and (d). M3.

8.3.4 Parametric Study of MC-PREIs for vertical analysis

Further analysis was conducted using the FE model to investigate the vertical characteristics of elastomeric bearings due to geometric modification. Considering the low shear modulus of rubber (G), the isolator was intended to be applied on a light structure with a vertical pressure of 1.27 MPa. It was conducted to achieve the target of fundamental period of isolated structure approximately 2

sec. Therefore, the compression load subjected to the FE model was replaced as 1.27 MPa from the initial load of 2.548 MPa.

8.3.4.1 Vertical Stiffness

By using FE analysis, the vertical stiffness of the modified isolators are illustrated in Fig. 8.5. The stiffness, K_V , was normalized by the unmodified FE mode, denoted K_{V0} , with a function of d/D and S/S_0 , where S_0 is the unmodified shape factor. In Fig 8.5 (a), the characteristic of vertical stiffness as a function of d/D shows a significant decrease, while the area removed (P) also exhibits a similar decrease. It can be concluded by reducing the loaded area yields a large decrease in normalized stiffness. The modification to the interior geometry also shows a significant decrease of the vertical stiffness, even at low values of d/D . For instance, the value of K_V/K_{V0} at $d/D = 0.25$ is 0.38, compared to the proportional area normalized stiffness of $K_V/K_{V0} = 0.94$. The graph of interior (i) modification describes the concave upward and the contrasting condition is illustrated on the proportional area (P) that presents a concave downwards. The maximum difference between interior (i) and area removed (P) in normalized stiffness is 0.62 at $d/D = 0.38$, while the minimum difference in normalized stiffness is 0.56 at $d/D = 0.25$.

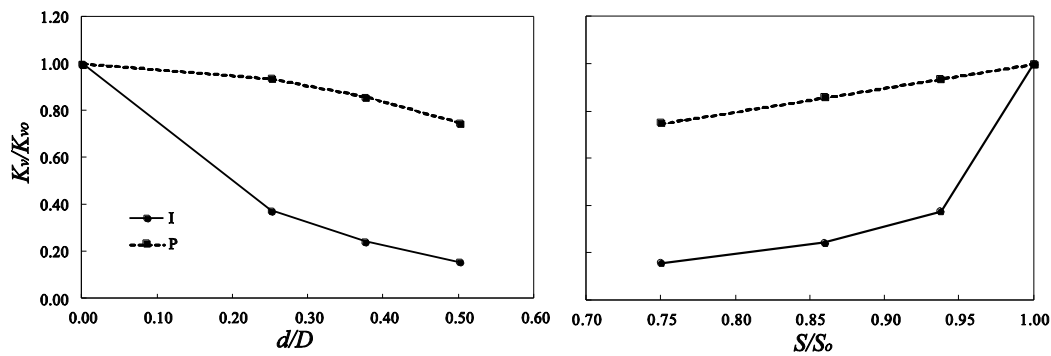


Figure 8.5 Normalized vertical stiffness as a function of (a) Normalized diameter and (b) normalized shape factor

A similar characteristic is also presented in Fig 8.5 (b), which shows K_V/K_{V0} as a function of S/S_0 . The change in S for interior modification is identical to the change in diameter (d). Reduction phenomena is also exhibited in normalized stiffness as a function of S/S_0 . Slight difference are shown in the area

removed curve (P), as the dashed line performs linearly. This means that the decreasing normalized stiffness is proportional to the function of S/S_0 for an isolator of a circular shape.

8.3.4.2 Compression Modulus

A similar condition with vertical stiffness is also shown in the compression modulus of modified isolators. A normalized compression modulus, denoted as E_c/E_{c0} , exhibited an abrupt decrease as illustrated in Fig 8.6, where E_{c0} is identified as the compression modulus of the unmodified model. It can be shown that the magnitude of E_c/E_{c0} was larger compared to the normalized stiffness of a similar diameter. In other words, the effect of interior modification on compression modulus of PREIs was less sensitive than the vertical stiffness. As shown in Fig 8.6, the minimum normalized compression modulus was approximately 0.21. The increase in diameter was followed by the decrease of compression modulus of modified isolators.

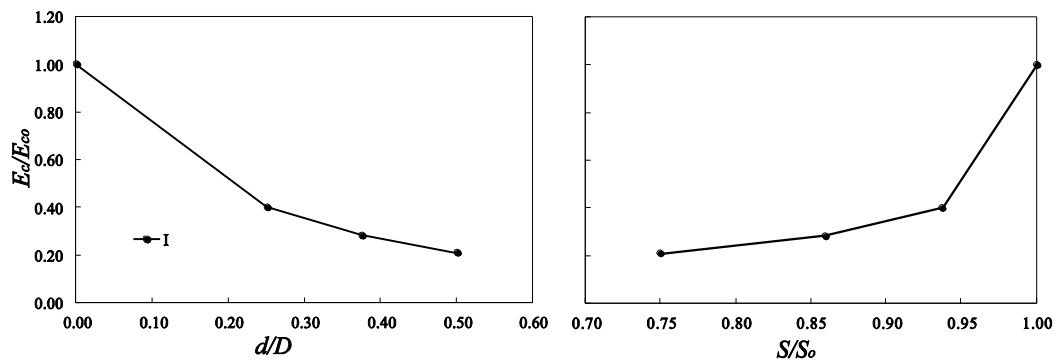


Figure 8.6 Normalized compression modulus as a function of (a) Normalized diameter and (b) normalized shape factor

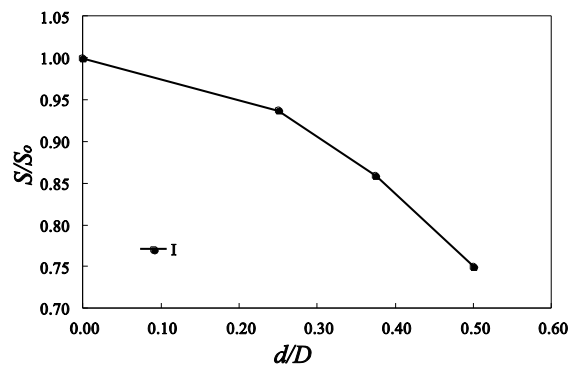


Figure 8.7 Normalized shape factor as a function of normalized diameter

Normalized shape factor as a function of d/D is illustrated in Fig 8.7. The shape factor for interior modifications is nearly inversely proportional to the change in diameter. Initially, the shape factor decreased at a larger rate for interior modification. The interior modification of the loaded area of the isolator resulted in a large change in the shape factor. The interior modification by reducing loaded area caused an increasing unloaded area by πdt .

The minimum normalized shape factor is 0.75 at $d/D = 0.5$. The higher the change in diameter (d) of the modification will influence the shape factor to decrease significantly. The decreasing shape factor on a modified isolator is more sensitive due to the larger unloaded area. The decreasing restraint of an elastomer to a perforated plate was illustrated by the lower shape factor. This phenomena is believed to be primary responsible for the high sensitivity of the interior modification.

8.3.4.3 Vertical Strain

Fig 8.8 (a) – (c) illustrate the FE results of the vertical strain, ε_{zz} , of the isolator at the top, mid-height and bottom of the elastomer layer, respectively. The X-axis represents a function of x/r where r is the radius of isolator and x is the distance from the center point. The value of zero represents the center of the isolator and the value of one represents the edge. As shown in Fig 8.8 for the unmodified isolator, denoted M0, the behavior was nearly constant for the vertical strain, with an exception at the edges where lateral bulging occurred along across segments AA. The phenomena reflected the basic assumption of the pressure solution, which was that the horizontal planes remain horizontal. At the top layer of the elastomer, M0, the vertical strain at the center is nearly zero and then increases proportional to the distance from the center. The bulging effect was shown in the edge of the elastomer by increasing the magnitude of the vertical strain under compression.

Contrary conditions can be seen on the modified isolator, denoted M1, M2, and M3. The bulging effect occurs at the inner and outer portions of the isolator. The increasing normalized vertical strain on the rubber was caused by the effect of interior modification on the isolators. The increased diameter increased

the vertical strain on the elastomer layer, particularly at the edges. The magnitude of vertical strain at the inner edges, exhibited a large difference in strain, while the outer edges were identical and much smaller than the inner side. The bulging effect was considerably sensitive at the inner edge of the isolator, due to proximity to the central point of the loading in compression. The larger the diameter of the interior modification, the bulging effect represented by vertical strain at inner edge also increases proportionally.

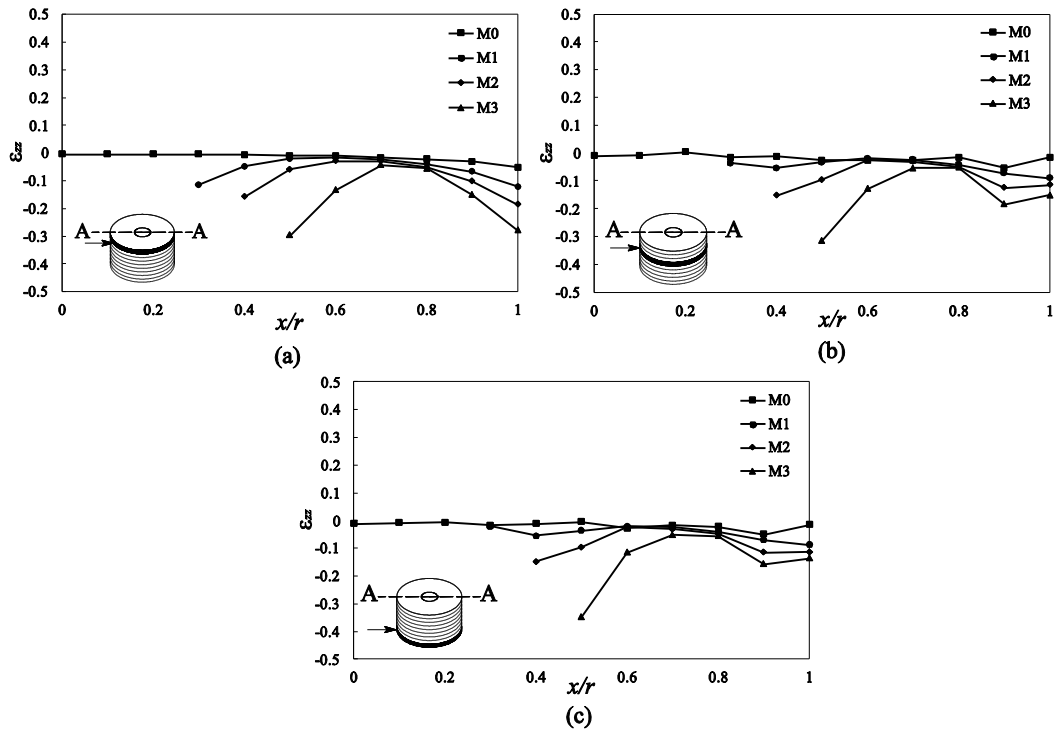


Figure 8.8 Vertical strain distribution of elastomer; (a). At the top layer ; (b). Mid-height layer; (c). Bottom layer of elastomer.

8.3.4.4 Vertical Stress

Figure 8.9 shows FE results of normalized vertical stress distribution, S_{zz}/\bar{P} , on the elastomer layer, where S_{zz} is the vertical stress at the surface of the elastomer layer. Figure 8.9 (a) – (c) show normalized vertical stress distributions on the top, mid-height and bottom layer of the elastomer, respectively. The vertical stress of the unmodified model, M0, illustrated that the highest magnitude is on the central region of isolator, but then decreases significantly to nearly zero at the edge. Furthermore, it can be shown that the vertical distribution on the unmodified isolator was identical at the top layer and

the bottom level. The results are proportional to the vertical strain, as in Fig 8.8, which shows that the lowest vertical strain yields the highest vertical stress distribution under compression.

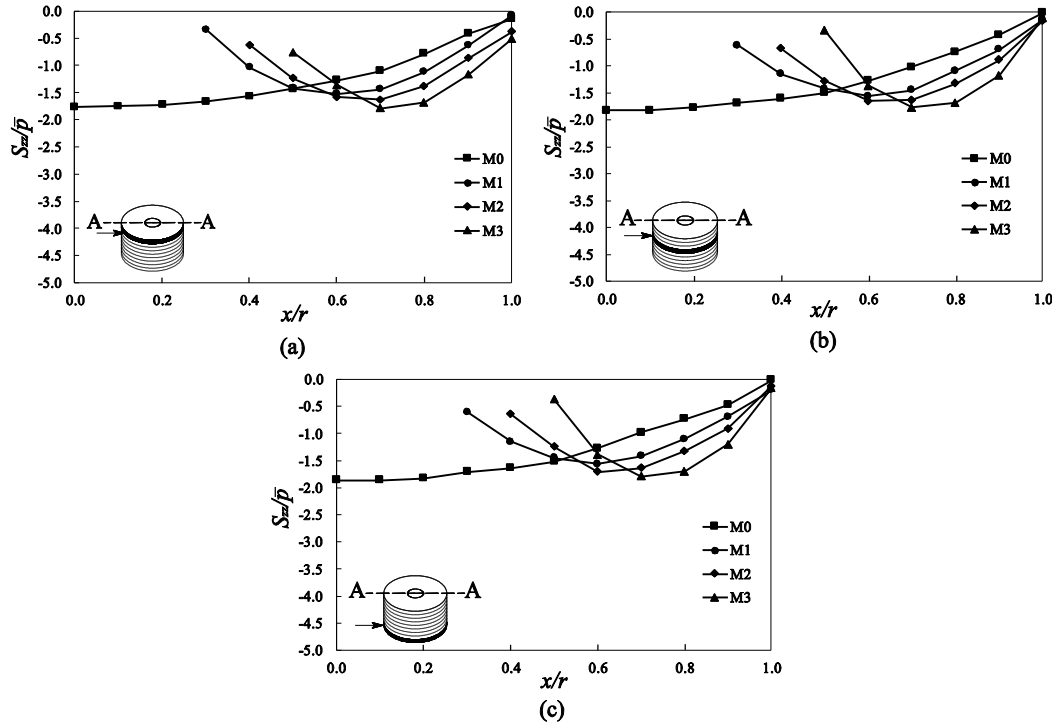


Figure 8.9 Normalized vertical stress distribution of elastomer; (a). At the top layer; (b). Mid-height layer; (c). Bottom layer of elastomer.

Introducing the interior modification of isolators alters the vertical stress distribution significantly along the segment AA. Similar to the unmodified model, the stress distribution for all modified models were similar between the top to the bottom level. The stress distribution trends were concave upwards with the highest stress magnitude nearly equal to the highest stress of the unmodified model. As the diameter increased, the stress distribution along the segment AA for all modified models altered significantly, however, the peak stress did not exceed the maximum stress of the unmodified model. The interior modification of the isolator was not affected by the peak vertical stress on the elastomer layer.

8.3.4.5 Shear Stress

The shear stress contour S_{xz} of the FE analysis normalized by p is described in Fig 8.10, and was located at the mid-height of the isolator for both

unmodified and modified models. A peak S_{xz} / \bar{p} value of 0.129 was studied in the unmodified model. The peak S_{xz} / \bar{p} value appeared at the edge of outer diameter of the unmodified model (M0). As illustrated earlier, the interior modification of the isolator caused the additional unloaded area in inner side of isolator thereby allowing additional lateral bulging and increasing the shear stress at the edges of the modification. For an interior modification, the peak S_{xz} / \bar{p} value occurred near the edge of the inner and the outer diameter, and was investigated to determine the effect of modification to the shear stress under compression. According to the modified model, denoted M1, the peak value increased by 113% from the initial geometry (M0). Similar trends were also shown in models M2 and M3, where the peak S_{xz} / \bar{p} value increased significantly by 138% and 189%, respectively.

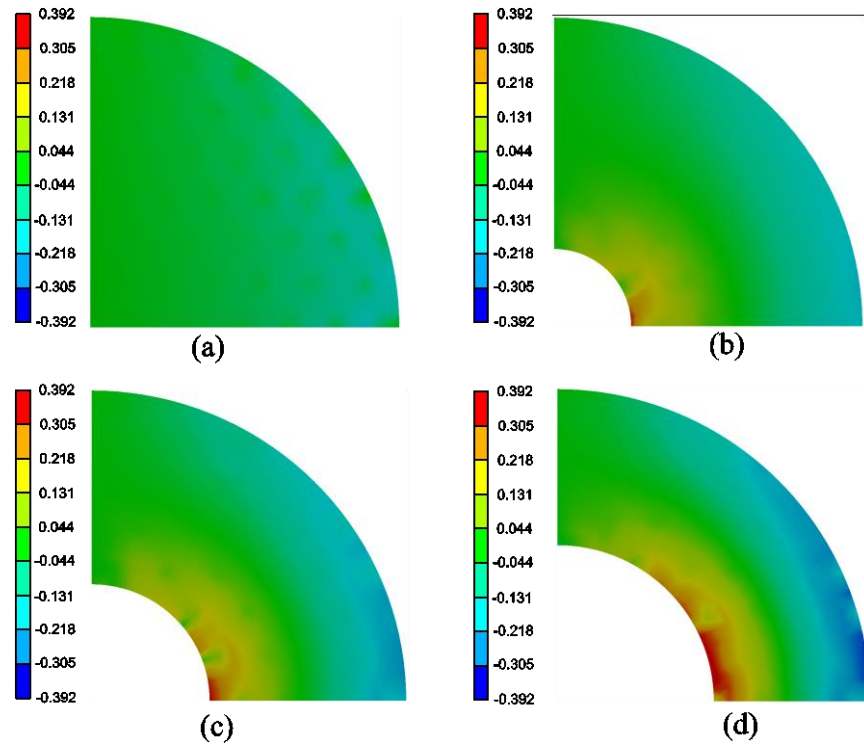


Figure 8.10 Normalized S_{xz} shear stress contour at the interface of the center elastomeric layer with interior modification d/D ;
(a). 0 ; (b). 0.25 ; (c). 0.38 ; (d). 0.5.

The normalized S_{yz} / \bar{p} shear stress contour is illustrated in Fig 8.11. Significant shear stress developed in the vicinity of the edges of isolator. A peak S_{yz} / \bar{p} value of 0.118 was seen in the unmodified model, M0. For the modified

isolator, the peak S_{yz}/\bar{p} value occurred near the inner and outer edges. The diameter modification alters the shear stress magnitude of elastomer layer significantly. The peak value of M1 increases by 103%. The models of M2 and M3 showed a similar increase in peak S_{yz}/\bar{p} value of 139% and 227% larger than S_{xz} , respectively. Although the geometry of the isolator was symmetric in all direction, the difference in shear stress values in S_{xz} and S_{yz} occurred, because the configuration of holes on the perforated plate were different in the x - and y -directions. The length of perforated plate is installed in the x -direction of FE model. However, the difference in magnitude was not significant for shear stress.

A series of analyses using FE method considered the effect of interior modifications to shear stress. The overall peak shear stress was studied in S_{xz} and S_{yz} for the modified model. The larger of diameter modification yields the increasing of shear stress distribution significantly on the isolators. Therefore, the FE results showed that the magnitude of peak shear stress was very sensitive to the interior modification of the isolator.

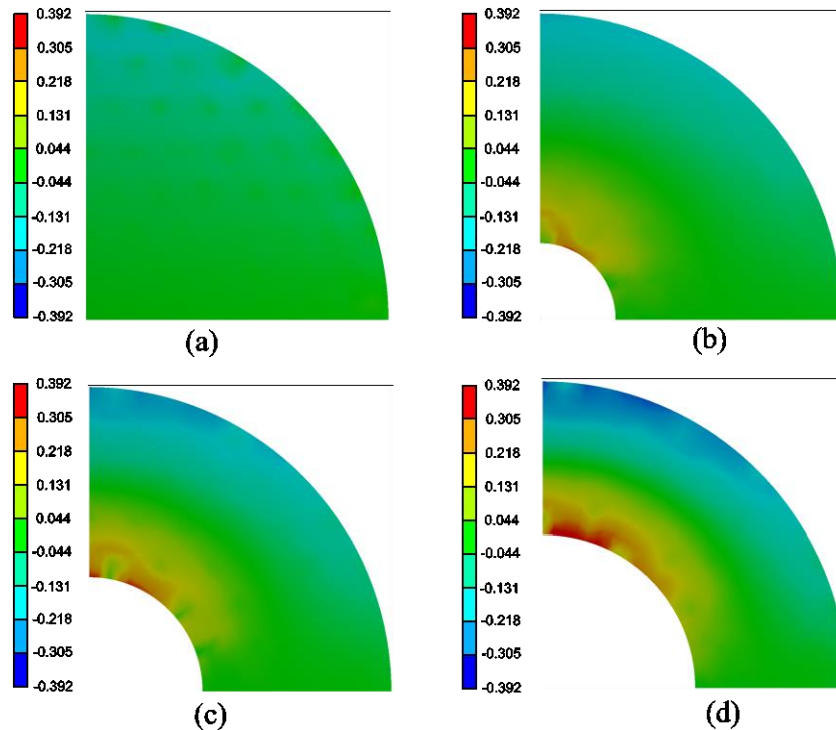


Figure 8.11. Normalized S_{yz} shear stress contour at the interface of the center elastomeric layer with interior modification d/D ;
(a). 0 ; (b). 0.25 ; (c). 0.38 ; (d). 0.5.

8.3.4.6 Perforated Reinforcement Stress

Fig 8.12 describes the Von Mises stress contour normalized by the vertical pressure, σ_v/\bar{p} , on the lowest layer of the perforated plate in the isolators with interior modification.

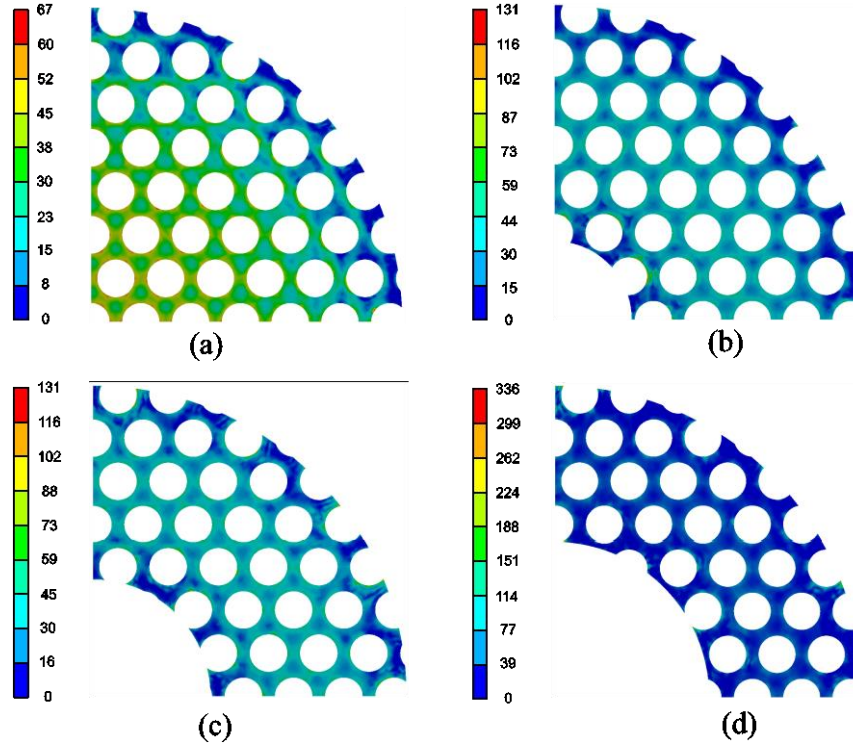


Figure 8.12 Normalized Von Mises stress contours in the lower perforated reinforcement layers for isolators with interior modification d/D ; (a). 0 ; (b). 0.25 ; (c). 0.38 ; (d). 0.5.

Introducing an interior modification on the inner side of an isolator caused a major increase in the stress on the perforated plate. The highest stress occurred on the periphery of the holes of perforated plate, and these stresses were neglected for the stress analysis. The main concern for stress is what occurs on the surface area of perforated plate. As the diameter of the modification increased, the peak value of σ_v/\bar{p} also increased, surpassing the peak value of the unmodified model. The model with $d/D = 0.25$ (denoted as M1) experienced a 25% increase in stress compared to the unmodified model. A similar condition occurred on the $d/D = 0.38$ and 0.5 (denoted M2 and M3), where the normalized stress increased significantly by 61% and 132%, respectively. The modification on interior of isolator provided more of an effect on the perforated plate. Although the stresses

on the reinforcement due to pressure are not considered important (Kelly and Shakhzod., 2001), particularly for modified circular perforated elastomer isolators (MC-PREIs), a stress analysis on the reinforcement must be considered to ensure the stress on the perforated plate does not exceed the yield stress of the reinforcement material.

8.4 Finite element study on lateral response of MC-PREIs.

This section presents the subsequent characteristics analysis of Modified Circular Perforated-Reinforced Elastomeric Isolators (MC-PREIs) under lateral load. The previous study (Lesmana and Sugihardjo, 2018) related to the vertical response of MC-PREIs has been conducted to understand how modification influence the performance of the isolators under compression. In the vertical analysis, MC-PREIs indicated a good performance under compression. The compression modulus and vertical stiffness were extremely sensitive to modification on the interior side of the isolator. In order to complete the understanding of MC-PREIs behavior, the horizontal characteristic of MC-PREIs is required to investigate. It is critical to understand how modifications on the loaded area of PREIs will influence the performance of the isolator under lateral load, including stress and strain demands in the elastomer and reinforcement layers.

A series of analyses were conducted to investigate the influence of interior modifications on the lateral characteristics of MC-PREIs. Finite element analysis was utilized to investigate the effect of modifications on the lateral behavior. The FE model was validated using the experimental test results and was subsequently employed to investigate a parametric study of interior modifications on the loaded area of an isolator. Further analysis using finite element method was also carried out to examine the horizontal stiffness, stress and strain distributions on both reinforcement and elastomeric layers. The series analysis are presented below:

8.4.1 FE model of MC-PREIs for lateral analysis

The FE analysis on lateral response of MC-PREIs is presented as a subsequent study of the modified isolator. Similar to previous analysis (section 7.5), the isolator was also presented as half of model shown in Fig 8.13. The

primary reason was to reduce time-consuming in running process. In the lateral analysis of MC-PREIs, the models were subjected to compression load in z -direction then continued to single shear laterally in x -direction. In this condition, the model was arranged symmetrically in z - x planes. The symmetries in z - x planes produced free translations of the model in x - and z -direction. With this condition, the half model of isolator was considered sufficient in representing the full model of MC-PREIs.

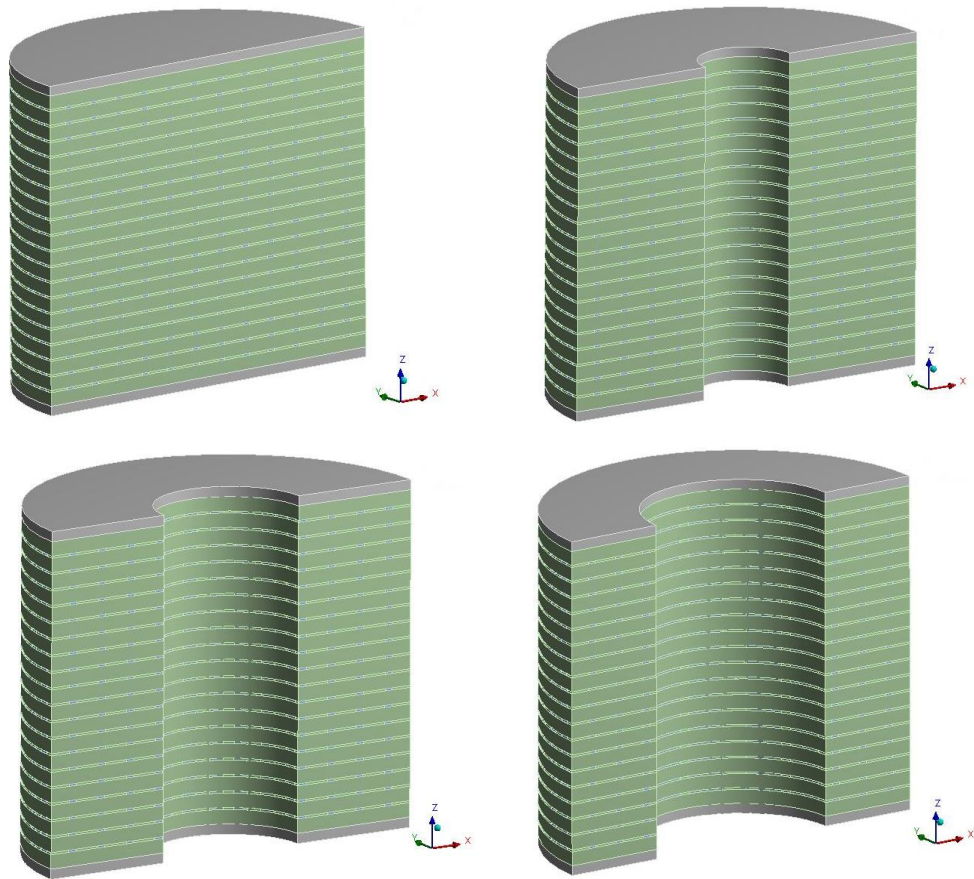


Figure 8.13. FE model of modified isolators for lateral analysis
(a). M0; (b). M1; (c).M2; and (d). M3.

In modeling perforated plate, a similar concept model was also used in modeling MC-PREIs by considering perforated plate as a full plate. The existence of holes on perforated plate required a small size in meshing process. It was conducted due to the restricted capability of computers to process highly nonlinear calculation of MC-PREIs. Therefore, to simplify the model and reduce

the number of elements and nodes, the idealization of using the full plate in modeling reinforcement in the lateral analysis was decided.

8.4.2 Loading history of MC-PREIs for lateral analysis

The loading conditions of lateral analysis of MC-PREIs analysis are similar with previous section as shown in Fig 7.10. The model was subjected to axial load of approximately 80 kN and continued to move freely in the lateral direction until 100 mm with a frequency of 0.5 Hz. The boundary conditions at the bottom side of isolator were arranged as the fixed base in all directions to simulate the real condition of isolator on the application that was bolted on the foundation. The top side of the end steel plate was only free in z- and x-direction and fixed in y-direction. The finite element program used employs the Newton-Raphson method to solve the nonlinear problem. The load is subdivided into a series of load increments that can be applied over several load steps.

8.4.3 Mesh condition of MC-PREIs for lateral analysis

In this section, mesh conditions of MC-PREIs for lateral analysis are presented. In general, the basic concept of mesh conditions were similar with unmodified model illustrated in chapter 7.4.2. The difference was only on the number of nodes and elements due to the modification geometry on the isolator. The skewness value was critical parameter to measure the quality of mesh condition for each model MC-PREIs. The detail setting of mesh conditions are presented in Fig 8.14

In Fig 8.14, mesh conditions of each model are presented. The number of nodes, elements and skewness value are also described. Related to the mesh size of elements, the sizes were similar with initial setting in chapter 7.4.2. The mesh sizes were set 2, 5, and 10 mm for the perforated plates, rubber layers, and end-plates, respectively. The trend of number nodes and elements perform decrease significantly relative to reducing geometry area of isolator. As shown in Fig 8.14, M0 model has 187,512 nodes and 25,427 elements with skewness value of 0.07. Model M1 has 120,666 nodes and 16,019 elements with skewness value of 0.04. Model M2 has 119,336 nodes and 15,744 elements with skewness value of 0.03. Model M3 has 116,803 nodes and 15,240 elements with skewness value of 0.02.

The skewness value for all models indicate below of 0.05. It means that the quality of mesh in ANSYS is categorized as excellent as show in Table 7.4.

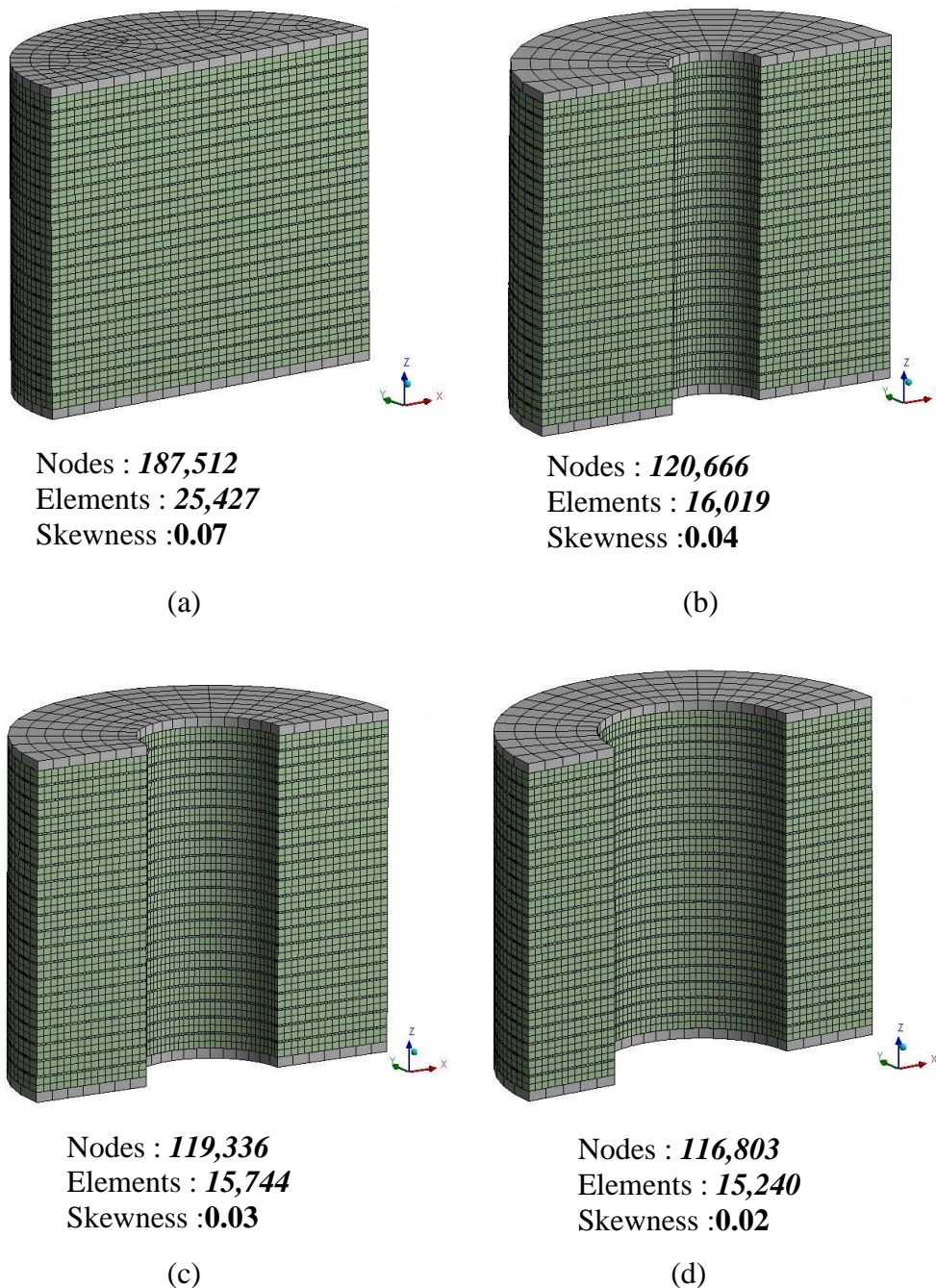


Figure 8.14. Mesh condition of MC-PREIs model for lateral analysis

(a). M0; (b). M1; (c).M2; and (d). M3.

8.4.4 Parametric Study of MC-PREIs for lateral analysis

A parametric study using FE analysis was performed in order to observe the lateral response of PREIs due to interior modification. The FE model of MC-PREIs was applied vertical pressure of 2.548 MPa similar to experimental test. In modeling MC-PREIs, the initial model was modified by removing the area in the center portion of the isolator, with a certain diameter (d). The unmodified model was denoted as M0, while the three modified model were denoted as M1, M2, and M3 with an interior diameter (d_i) of 50 mm, 75 mm and 100 mm, respectively.

8.4.4.1 Effective lateral stiffness

Fig 8.15 shows the lateral stiffness of FE model of MC-PREIs normalized by the lateral stiffness of the M0, K_0 , as a function of u/t_r where K is stiffness of modified model. The figure illustrates that the improvement of lateral response by modifying the interior area of isolators are followed by decreasing of normalized lateral stiffness, gradually. The curves perform similar pattern that as the modification diameter increase, the normalized lateral stiffness of the isolators decreases. The trend of curves increases depending on the lateral displacement. Commonly, the normalized lateral stiffness of the models are nearly constant at large displacement between $u/t_r = 0.6$ to $u/t_r = 1$. For M1 model, the normalized lateral stiffness, at $u/t_r = 1$, is approximately 0.68. It means that the interior modification with a diameter of 50 mm is able to reduce the lateral stiffness of PREIs about 32%.

Similar characteristics are described by model M2 that the curve increases significantly at $u/t_r = 0.1$ to $u/t_r = 0.6$ then nearly constant until $u/t_r = 1$ while the stiffness of PREIs reduces of 48%. In other word, by using M2, the objective to obtain the desired stiffness for the axial force of 40 kN on the isolated model (Hidayat et al., 2016) is achieved by providing a fundamental period of structure 2 sec. Somewhat differences are indicated by M3 model related to the trend of the curve and normalized lateral stiffness. The normalized lateral stiffness remains nearly constant for all displacement level. As shown at $u/t_r = 1$, the model of M3 is able to reduce the lateral stiffness of PREIs larger than other models, about 71%. It indicated that the larger the modification diameter of MC-PREIs highly influence the lateral stiffness of PREIs. However, further analysis related to stress

and strain relationship must be conducted to ensure that modified model satisfy for applying as base isolation and will be discussed later.

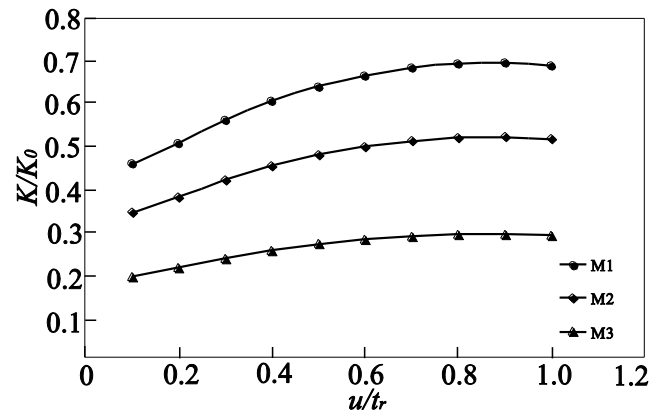


Figure 8.15 Stiffness of the modified isolator normalized by the stiffness of unmodified model.

8.4.4.2 Load-displacement relationship

Fig 8.16 presents the normalized lateral load-displacement relationship of MC-PREIs derived from FE results. The curves characteristic are similar to Fig 8.15 that lateral forces tend to decrease as the diameter of interior modification increase.

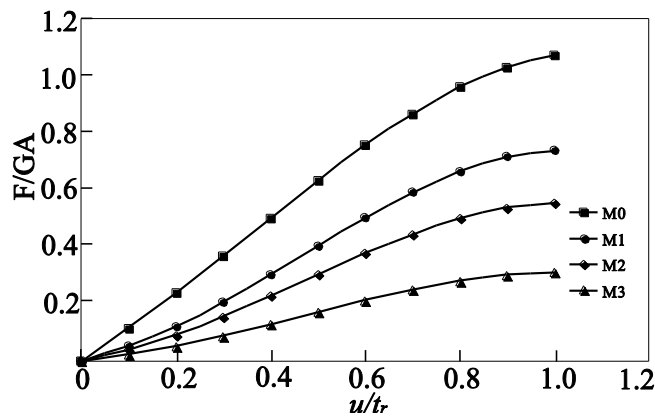


Figure 8.16. Comparison of lateral-displacement relationship of isolators derived from FE analysis.

The normalized lateral force at $u/t_r = 0$ to $u/t_r = 0.8$ performed stiffening behavior for all models except M3. The stiffening characteristic remains nearly constant for all models at $u/t_r = 0.9$ to $u/t_r = 1$. The magnitude of normalized lateral force for all models, at $u/t_r = 1$, illustrate similar trend with normalized lateral

stiffness on Fig 8.15 that is 0.739; 0.554; and 0.310 for M1, M2, and M3, respectively. It means that the increase of modification diameter was evident considerably influence the lateral force of PREIs.

8.4.4.3 Stress and strain in elastomer layers

Determining local coordinate of stresses and strains for PREIs that experience large displacement and rotation are considered the critical point in this section. Fig 8.17 illustrates the definition of local stress in elastomer element, before and after displacement of elastomer layer under lateral load. Generally, σ_{11} , σ_{22} dan σ_{33} are parallel to the global coordinate of x , y , and z . Under large lateral load, the local coordinate update with the displacement and rotation, as shown in Fig 8.17 (b). In this research, the stress values in elastomer and reinforcement are normalized with vertical pressure ($\bar{p} = 2.548$ MPa). Therefore, the following normalized stresses are determined : $S_{11} = \sigma_{11}/\bar{p}$, $S_{22} = \sigma_{22}/\bar{p}$ and $S_{33} = \sigma_{33}/\bar{p}$.

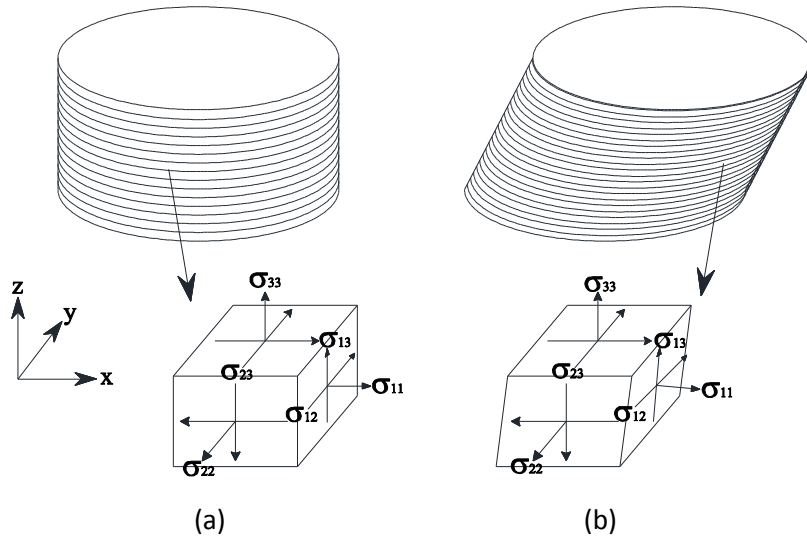


Figure 8.17. Local stress in the isolator ; (a). Undeformed shape, (b). Deformed configuration.

Fig 8.18 illustrates the contour of S_{11} in the center elastomer layers in the unmodified isolator, M0, and modified isolators (M1, M2, and M3), under compression without lateral displacement. The FE analysis indicates that the modification on the interior area of isolator decreases the stress, S_{11} , under compression. The unmodified model, M0, shows that the highest magnitudes of

S_{11} are on the central region of the isolator, furthermore it decreases significantly to nearly zero at the edge. As the diameter of interior modification increases, the distribution area of stress on the center decreases and expands to the inner and outer edges of the isolator. An extended discussion on the behavior of MC-PREIs under pure compression load is offered in (Lesmana et al., 2018).

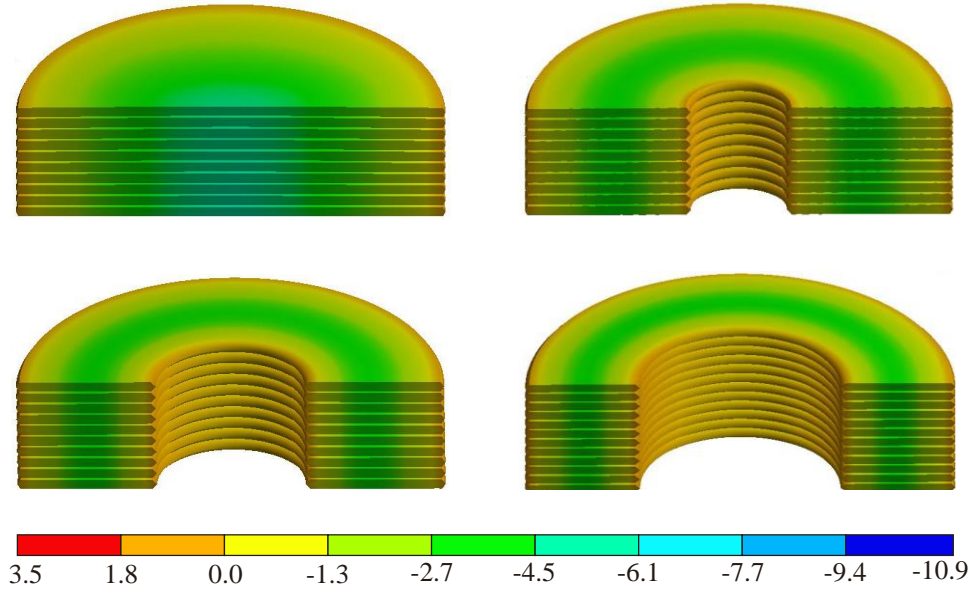


Figure 8.18 . Contours of S_{11} in the center elastomer layer under compression.

Fig. 8.19 and 8.20 illustrate the contour of S_{11} in the center elastomer layers in the same isolators at $u/t_r = 0.5$ and $u/t_r = 1.0$. The figures indicate that introducing an interior modification yields in a reduction in the peak value of S_{11} in the central region elastomer layer. The FE shows that interior modification on isolator alters the location of the peak stress of S_{11} as the lateral displacement increase. As the lateral displacement increase, the locations of the peak S_{11} gradually shift and at $u/t_r = 1.0$ (see Fig 8.20), the stresses are occurred to above and below the modification along the x -axis. Generally, the stress on the center elastomer layer increases significantly as the lateral displacement increase. However, by modifying the interior area of the isolator and increasing the diameter of the hole, the peak stress value on the isolator decreases significantly. In other word, the modification by cutting a hole in the center portion of isolator can reduce the stress of isolator under large lateral displacement.

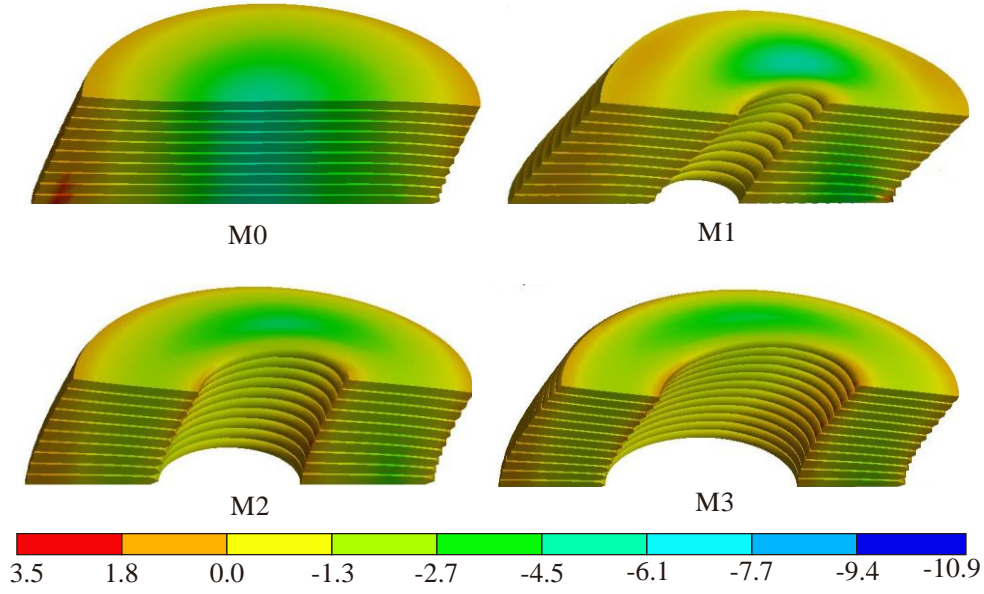


Figure 8.19. Contours of S_{11} in the center elastomer layer at $u/t_r = 0.50$.

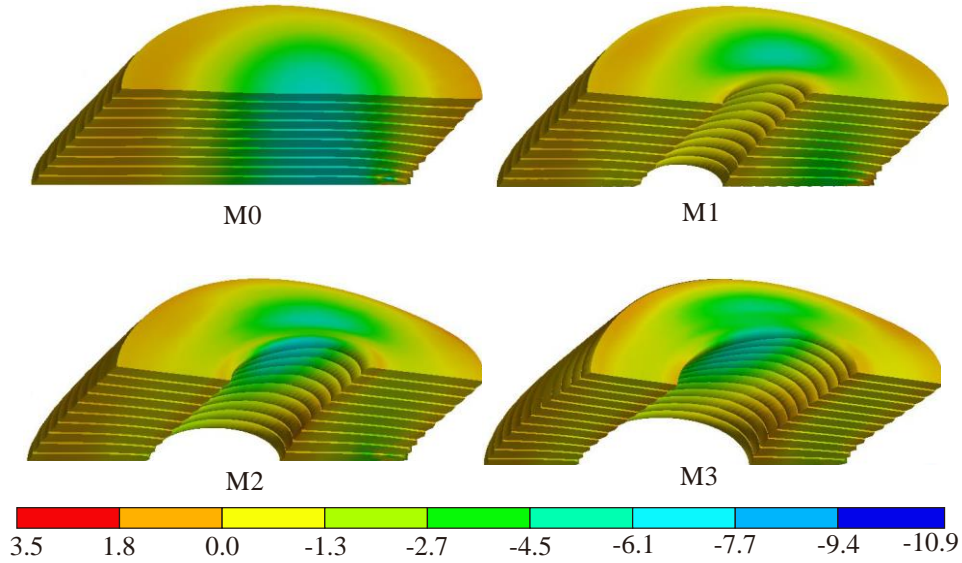


Figure 8.20. Contours of S_{11} in the center elastomer layer at $u/t_r = 1.00$.

Fig 8.21 compares the distribution of S_{11} , S_{22} , and S_{33} at the mid-height of middle rubber layer in the M0, M1, M2, and M3. Generally, the distributions and the values of S_{11} , S_{22} and S_{33} in each isolator are similar. In the unmodified model, M0, the stresses enhance significantly as lateral displacement increase. At $u/t_r = 0$ the normalized peak stress of all stresses are approximately -1.7 then increase

drastically, at $u/t_r = 1.0$ of about -3.0. Similar to Fig 8.18, 8.19 and 8.20, for the unmodified model (M0), the highest magnitude of stresses occur in the center of the isolator in all lateral displacement level ($u/t_r = 0$; 0.5 and 1.0). Contrary conditions are described on modified isolator, M1, M2, and M3. The distribution of normalized stresses performs decrease significantly in all lateral conditions. Even, the smallest stresses occur as the diameter of the hole and lateral displacement increase. It indicates that the interior modification on the PREIs is able to reduce the stresses on rubber layers at all lateral conditions ($u/t_r = 0, 0.5$ and 1.0).

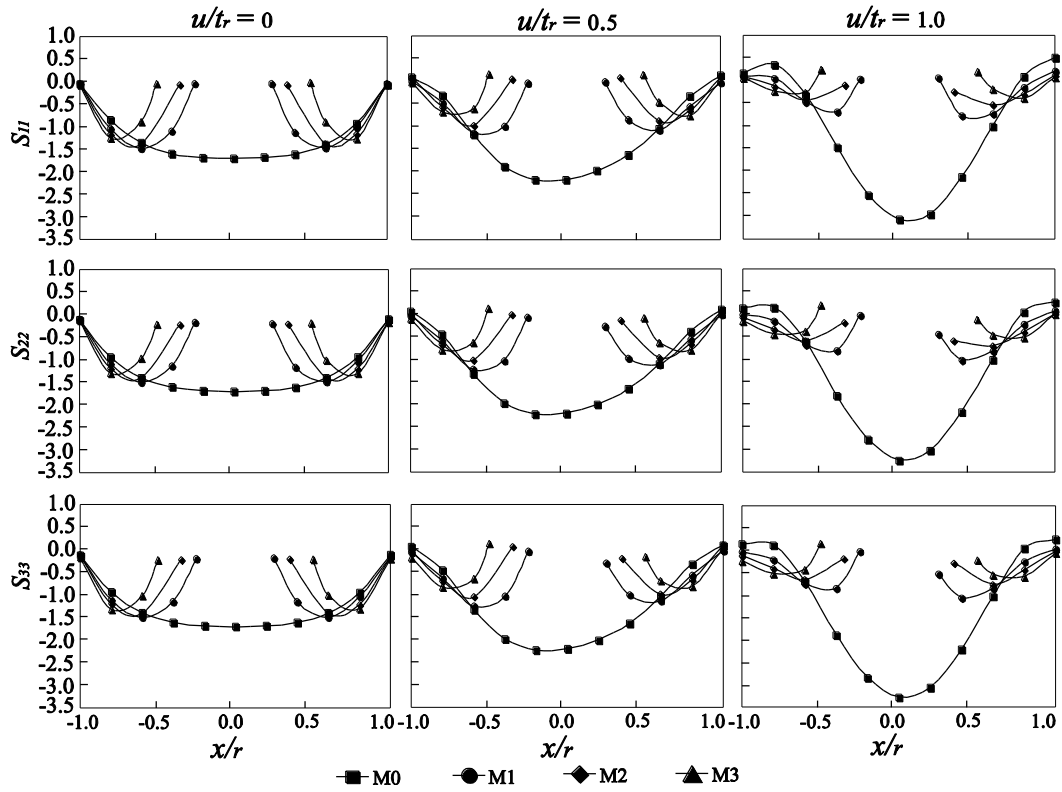


Figure 8.21 Variation of normalized stress profiles in the center elastomer layer in the M0, M1, M2 and M3.

The magnitude of stresses on the outer edges of isolators (M0, M1, M2, and M3) show similar characteristic related to stress value. The stresses are almost similar at $u/t_r = 0$ and $u/t = 0.5$. However, the difference among the models is clearly occurred as the isolator experience large horizontal displacement, at $u/t_r = 1.0$. The obvious differences between unmodified and modified models are in

the central region of the isolator. The existing of the hole in the center creates the inner edges on the isolator. On the unmodified model, M0, the highest stresses occur at the center point, typically at $u/t_r = 1.0$ while for modified isolators the stresses on the center are reduced due to the removing area on the center of the isolator. For modified model, the stresses occur in the inner edges that are identical with outer edges in all displacement conditions.

8.4.4.4 Deform shape

The deformed shape of isolator under different displacement condition is illustrated in Fig 8.22. Generally, the deformed shape between unmodified and modified isolator is similar due to the isolators are bonded with steel end plate and reinforced with rigid reinforcement. The FE analysis indicates that the peak shear strains in the elastomer layers increase when a modification is introduced.

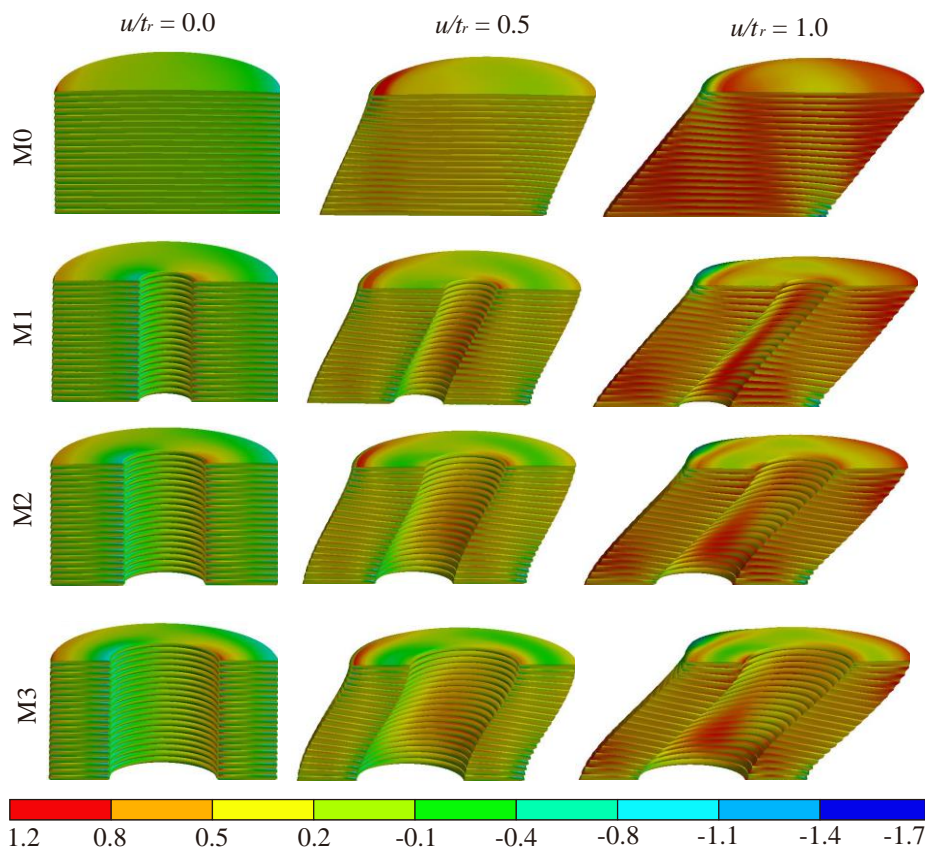


Figure 8.22. Contour of shear strain γ_{13} under different displacement condition.

Under pure compression, the peak shear stress, γ_{13} , in the unmodified (M0) model, is observed at the edge of the isolator $x = \pm r$ along x , with a value of approximately 0.4. As the diameter modification increase, the peak shear strain in the center of an isolator at $u/t_r = 0$ is nearly constant. The high shear strain occurs at the inner edges of the isolator and increases significantly as the diameter modification increase.

The opposite result is shown when the isolator experiences lateral displacement at $u/t_r = 0.5$, the peak shear strain at the edges of inner hole increase. The FE indicates that when the isolators undergo small lateral displacement at $u/t_r = 0.5$, the peak shear strain, γ_{13} , on the elastomers, increase proportionally as the diameter of modification increase. The contrary conditions are described when isolator experience large lateral displacement at $u/t_r = 1.0$ that the peak shear strain, γ_{13} , decrease significantly. The FE analysis illustrates that the large shear strain is occurred in the inner edges of the modification due to large localized deformation of the elastomer layers at those location.

8.4.4.5 Stress in reinforcement

The distribution of S_{11} of center reinforcement layers is presented in Fig. 8.23. Under pure compression, the peak normalized stress in the unmodified isolator is approximately 10.849. Introducing modification results the stress in modified isolator decrease at location $x/r = \pm 0.6$ with values of 7.146; 6.843; 4.912 for M1, M2 and M3, respectively. As loaded laterally under displacement $u/t_r = 0.5$, the high stress develops and increases at location $x/r = -0.8$ and $+0.8$ for compression and tension, respectively while the stress at inner edges of isolator nearly constant and similar to under compression condition. As lateral displacement increase ($u/t_r = 1.0$), the stress on modified isolator nearly constant as illustrated at $u/t_r = 0.5$. The contrary condition appears for unmodified isolator under large displacement ($u/t_r = 1.0$) that the distribution of stress changes significantly with two peak positive and negative stresses. The FE indicate that interior modification enables significantly to reduce the stress in the reinforcement at the different lateral magnitude.

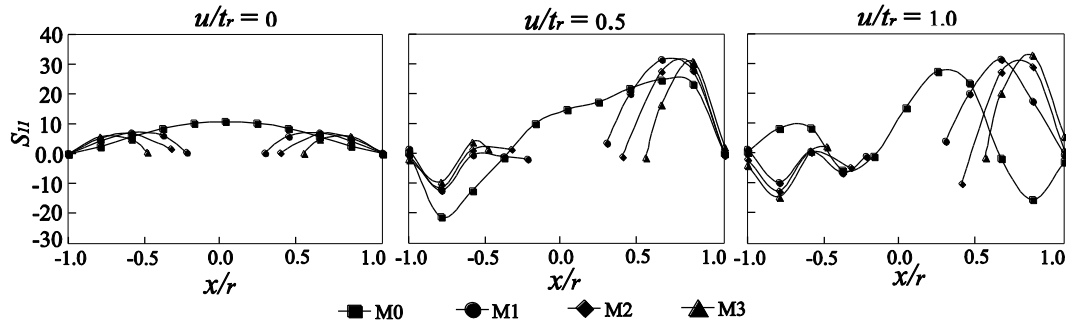


Figure 8.23 Distribution of S_{II} in the center of reinforcement layer in isolator M0, M1, M2 and M3.

8.5 Summary of finite element study of MC-PREIs.

The introduction of modified isolator is to obtain the lower horizontal stiffness of PREIs. It is conducted since the unmodified isolator is not able to provide the desired horizontal stiffness for achieving target of fundamental period. Furthermore, the limited of shear modulus of rubber material is to be the primary reason to modify the geometry of isolator. The detail of analysis results from modified isolator are presented in Table 8.2.

Table 8.2 Vertical and horizontal characteristic of MC-PREIs

Model	Vertical			Horizontal		
	Stiffness (kN/mm)	Modulus (MPa)	%	Stiffness (kN/mm)	Modulus (MPa)	%
M0	33.20	216	100	0.102	0.35	100
M1	12.50	87	38	0.070	0.35	68.8
M2	8.09	61	24	0.053	0.35	51.6
M3	5.21	45	16	0.029	0.35	28.9

As illustrated in section 5.3.7, join A1 (4.6 ton) located on one storey require lower horizontal stiffness of approximately 0.046 kN/mm to achieve fundamental period of 2 second. However, the isolator analyzed in this research provides the higher stiffness that is approximately 0.122 N/mm, as shown in Table 6.5. Therefore, the modification of isolator is introduced to derive the desired horizontal stiffness. According to Table 8.2, model of M3 is suitable to apply on the join A1 subjected to 4.6 ton. This method is considerably effective in reducing lateral stiffness of PREIs.

CHAPTER 9

CONCLUSIONS AND RECOMMENDATIONS

9.1 Introduction

A series of experimental test and FE analysis have been conducted to observe the characteristics of Perforated-Reinforced Elastomeric Isolators (PREIs) under compression and lateral load. The primary objective of this research is to develop low-cost base isolation for residential housing by replacing conventional steel plate with alternative material. The perforated plate is selected as a new reinforcement to reduce both the weight and cost of isolator. Both the analytical and experimental demonstrate that it is possible to replace the steel reinforcement with perforated plates for the seismic protection of residential building. The resulting isolator is certainly much lighter than the current base isolator.

The research results that the rough cost estimation for one unit PREIs is about USD \$70 to \$100/unit while the weight is approximately 130 N per unit. However, according to its performance, it is necessary to make sure that the isolator is applicable on a real structure. Therefore, further experimental tests and studies are required to observe the characteristics of an isolator in all conditions including loading and environmental effects. In this chapter, the conclusion related to experimental and analysis results are presented. The details of conclusion and recommendation are illustrated below.

9.2 General findings

After conducting a series of analysis and experimental testing, some general conclusions are obtained as follows:

1. The target of fundamental period of isolated structure for low-rise residential building is recommended of approximately 2 second to produce elastic behavior.
2. The rubber material used in this research project is categorized as low damping since the values of damping ratio of isolator are below of 10%. Therefore, additional device is required to enhance the damping ratio and lateral displacement capacity of isolator.

3. In this research project, Ogden model is the most appropriate constitutive model to represent the rubber material on ANSYS FE program.
4. The yield strength ratio between perforated plate (POA 51%) and solid plate is about 0.52. It means that the strength of material reduces 50% from the initial strength.
5. The basic concept of steel-reinforced elastomeric isolators (SREIs) is able to apply on perforated-reinforced elastomeric isolators (PREIs) by reducing the area of reinforcement depending on the percentage open area of perforated plate.
6. In order to enhance the lateral response of isolator to obtain lower horizontal stiffness, the modified isolators are required by removing interior area of isolator. The interior modification is one of the alternative methods for an engineer to optimize their seismic design of PREIs.
7. The bounded isolator using end steel plate is not sufficient to apply on the low-rise structure since the limited lateral capacity and damping ratio. Therefore, the development of unbounded isolator is recommended.

9.3 Vertical characteristic of PREIs under compression.

A series analysis and experimental test of isolator have been carried out to investigate the vertical characteristic of isolator under pure compression. The conclusions derived from FE analysis and experimental test are given below:

1. An initial assumption in regarding a perforated plate as rigid reinforcement is correct. It can be seen in analytical solution that the equation of rigid reinforcement is feasible to be employed in predicting characteristics of PREIs under compression and lateral load. The only difference is on the area of reinforcement that perforated plate area is reduced by the existing holes depending on the percentage open area (POA) of plate.
2. A seismic isolator must provide a very high vertical stiffness and a low horizontal stiffness. The characteristics of isolator satisfy for this condition since the vertical stiffness is approximately ± 300 times more than the horizontal stiffness.

3. The vertical stiffness of PREIs are highly influenced by POA of perforated plate. The reduction of vertical stiffness is inversely proportional to POA of perforated plate. As POA of perforated plates increase the vertical stiffness decrease significantly. The contrary conditions shown in compression modulus. The POA of perforated plate has no effect on the compression modulus of PREIs.
4. The larger area removed from the isolator is followed by decreasing of compression modulus and vertical stiffness. In other word, the compression modulus and vertical stiffness are extremely sensitive to modification on the interior side of an isolator.
5. The larger diameter of an interior modification increase the opportunity of bulging effect on the elastomer layer, typically in the inner side of isolator. It can be seen in the vertical strain of the elastomer with the largest diameter (d).
6. The interior modification of an isolator did not affect the peak vertical stress on the elastomer layer. The vertical stresses on the elastomer of the modified isolator were identical to those of the unmodified isolator.
7. The interior modification of the isolator affected the peak shear stress of the elastomer layers. The stresses generally occur in the vicinity of modification.
8. The interior modification increased the vertical stress and Von Mises stress distribution in the perforated plate.
9. As the diameter of the modification increased, the stress increased proportionally. Therefore, the stress on perforated plate must not surpass the yield strength of the material.

9.4 Horizontal characteristic of PREIs under lateral load.

A series analysis and experimental test of isolator have been carried out to investigate the lateral characteristic of isolator under combination load, compression and lateral displacement. The conclusions derived from FE analysis and experimental test are given below:

1. The most important parameter of isolator to derive lowest horizontal stiffness is shear modulus (G). In this research project, the shear modulus of rubber material are as expected to be in accordance with the design. The value of G

of isolator is 0.35 MPa. With this value, the rubber material is categorized as low-grade rubber material with low shear modulus (G). It is possible to apply the isolator on light structures such as housings or residential buildings.

2. The use of perforated plate on the isolator has an advantage for reducing quantity of steel material and the weight of isolator without decreasing the performance both in lateral and vertical.
3. The basic concept of SREIs can be employed in design process of PREIs, typically on lateral stiffness. The difference is only on the reinforcement area of perforated plate depending of POA.
4. The effect of POA of perforated plate has no influence on the lateral characteristic of PREIs under combination load. In other word, the lateral characteristics between PREIs and SREIs are similar.
5. The isolator tested in this research project is intended for axial force of 80 kN. It is determined to make sure the structure having fundamental period of 2 sec. In order to apply the isolator to the lower than 80 kN, the modification on the isolators are required. The alternative method proposed in this research project is interior modification on loaded area denoted as Modified Circular Perforated-Reinforced Elastomeric Isolators (MC-PREIs).
6. Introduction of interior modification on PREIs enhance the lateral response of isolator. The larger removing area in the central region of isolator was followed by decreasing gradually of lateral stiffness of isolator. Removing interior area of 6.25%, 14.06% and 25% caused decreasing lateral stiffness of 29%, 52%, 69%, respectively.
7. Comparing the lateral load-displacement relationships of the isolator illustrated that as the modification diameter increase, the lateral force decreased significantly.
8. Introduction a modification on PREIs described that the stress on the center elastomer layer increased as the lateral displacement increased. However, by modifying the interior area of the isolator and increase the diameter of the hole (d_i), the peak stress value on the isolator decreased. In other word, the modification by cutting a hole in the center portion of isolator can reduce the stress of isolator under different displacement magnitude.

9. The FE analysis indicated that when the isolators experienced small displacement at $u/t_r = 0.0$ and $u/t_r = 0.5$, the peak shear strain, γ_{13} , on the elastomers, increase proportionally as the diameter of modification increase. The contrary conditions are described when isolator experienced large displacement at $u/t_r = 1.0$ that the peak shear strain, γ_{13} , decrease significantly. The FE analysis illustrated that in the edges of the modification, large shear strain occurs due to large localized deformation of the elastomer layers at those location.
10. The FE indicated that interior modification significantly reduced the stress in the reinforcement at the different lateral magnitude. Therefore, the stress on the perforated plate must not surpass the yield strength of the material.

9.5 Recommendations

An analytical solution and experimental test of isolator have been carried out to develop low-cost base isolation system. This concept is very promising because currently it is difficult to produce isolators intended for small buildings in highly seismic environments where the isolators are lightly loaded. Some recommendations are presented as follow:

1. The number of specimens should be added to provide more experimental data test for vertical and horizontal test.
2. Generally, rubber material is classified as hyperelastic material that its stiffness depends on how fast the load is applied. Therefore, the loading condition in the experimental test is the critical point to derive the valuable result of the test. The dynamic loading is required to conduct experimental test of isolator since the loading condition is a function of time.
3. According to the experimental test results and FE analysis, the results do not perform a good agreement. The load applied on the specimen was static load that could not consider the loading rate during the test. Therefore, the test results under compression and lateral load, are not feasible to be employed.

4. The test apparatus that satisfy the requirement to perform dynamic load must be provided in experimental test process to obtain the feasible test result.
5. Further experimental studies are required to investigate the characteristics of isolator under large displacement. The parameter studies consist of horizontal stiffness, vertical stiffness, shear modulus, damping ratio and stability under large displacement.
6. In order to enhance the capacity of the lateral stiffness of isolator, the modified isolator by reducing loaded area is possible to carry out as alternative method in reducing lateral stiffness, significantly. Reducing 50% of loaded area is able to decrease the lateral stiffness of approximately 30%.
7. The experimental test are required to investigate the characteristics of MC-PREIs. The experimental test results are able to compare with FE analysis. The parameter studies of MC-PREIs consist of horizontal stiffness, vertical stiffness, shear modulus, damping ratio and stability under large displacement.
8. Further analysis related to unbounded of isolator is highly recommended to conduct since the limited of bounded isolator under large displacement.
9. A numerous rubber materials must be provided to derive various shear modulus.
10. Finite element analysis is a powerful method in predicting hyperelastic material, especially base isolation. However, high specification computer is required to solve highly nonlinear behavior of isolator.

REFERENCES

- Ali, A., Hosseini, M and Shari, B. B. (2010). A review of Constitutive Models for Rubber-Like Materials. *American J. of Engineering and Applied Sciences*, 3 (1), pp 232-239.
- American Society of Civil Engineers (ASCE). (2010). Minimum Design Loads for Buildings and other Structure, *American Society of Civil Engineers*, Reston, VA. ASCE/SEI 7-10.
- American Society for Testing and Material. (2017). Standard Test Methods for Vulcanized Rubber and Thermoplastic Elastomers—Tension. D412. American National Standard.
- Angeli, P., Russo, G and Paschini, A. (2013). Carbon fiber- reinforced rectangular isolators with compressible elastomer : Analytical solution for compression and bending. *International Journal of Solids and Structure*, 50, pp 3519-3527.
- ANSYS Mechanical APDL.(2012). Release 15, ANSYS Ltd.
- Ashkezari, G.D., Aghakouchak, A.A and Kokabi, M. (2008). Design, Manufacture and evaluation of the performance of steel like Fiber Reinforced Elastomeric Seismic Isolators. *Journal of Material Processing Technology*, 197: 140-150.
- Badan Standarisasi Nasional (BSN). (2012). Tata Cara Perencanaan Ketahanan Gempa Untuk Gedung dan Non Gedung (SNI 1726:2-12). Indonesian National Standard (in Indonesian).

- Badan Standarisasi Nasional (BSN). 2013. Persyaratan Beton Struktural untuk Bangunan Gedung (SNI 2847:2013), Indonesian National Standard (in Indonesian).
- Bogojavenskij, K., Neubauer and A., Ris, V. (1978). Technology of producing of lightweight profiles. VEB DeutscherVerlag fur Grundstoffindustrie, Leipzig, Germany. Pp 565. (in German).
- Bol, M and Reese, S. (2003). Finite element modelling of polymer networks based on chain statistics. *Constitutive Models for Rubber III*, edited by J Busfield & A Muhr (A A Balkema Publishers, UK), 203-211.
- British Standard. (2005). Structural bearings: elastomeric bearings. 1337-3. British Standard, UK.
- British Standard. (2009). Anti-seismic devices. 15129. British Standard, UK.
- Computer & Structures, Inc. (CSI), (2008). Linear and Nonlinear Static and Dynamic Analysis and Design of Three-Dimensional Structures, v.14.2.2, Berkeley: Computer & Structures, Inc.
- Cook, R. D. (1995). Finite Element Modeling for Stress Analysis. John Wiley&Sons, Inc, New York, United State.
- Designers, Specifiers and Buyers Handbook for Perforated Metals. (1993). Publications of the Industrial Perforators Associations (IPA).
- Dezfuli, F. H and Alam, M, S. (2013). Multi-criteria optimization and seismic performance assessment of carbon FRP- based elastomeric isolator. *Engineering Structure* , 49, pp 525-540.
- Engelen, N. C. V., Osgooei, P. M., Tait, J. M and Konstantinidis, D. (2014). Experimental and finite element study on the compression properties of

- Modified Rectangular Fiber-Reinforced Elastomeric Isolators (MR-PREIs). *Engineering Structure*, 74: 52-64.
- Forno, M., Martelli, A and Dusi, A. (1999). Implementation and validation of hyperelastic finite element models of high damping rubber bearings. in *Constitutive Models of Rubber*, edited by A Dorfmann & A Muhr (A A Balkema Publishers, UK), 237-247.
- Fung, Y. C. Biomechanics: Mechanical Properties of Living Tissues, Springer-Verlag, New York, N.Y., 1981.
- Gent, A. N. (2012). Engineering with Rubber: How to Design Rubber Components. *Hanser Publishers*, Munich, German.
- Ghosh, P., Saha, A and Mukhopadhyay, R. (2003). Prediction of tyre rolling resistance using FEA. in *Constitutive Models for Rubber III*, edited by J Busfield and A Muhr (A A Balkema Publishers, UK), 141-145.
- Herrmann, L. R. (1965). Elasticity Equations for Nearly Incompressible Materials by a Variational Theorem. *J. AIAA*, Vol. 3, pp. 1896-1900.
- Inel, M., Ozmen, H. B and Bilgin, H. (2007). Re-Evaluation of Building Damage During Recent Earthquake in Turkey. *Engineering Structure*, 30 : 412-427.
- Jakel, R. (2010). Analysis of Hyperelastic Materials with Mechanica (Theory and Application Examples). *Presentation for the 2nd SAXSIMIS*, Technische Universitat Chemnitz.
- Kalkan, E and Chopra, A. K. (2010). Practical Guidelines to Select and Scale Earthquake Records for Nonlinear Response History Analysis of Structure. U.S. Geological Survey Open-File Report 1068, pp: 124.

- Kelly, J. M and Konstantinidis, D. (2007). Low-cost seismic isolators for housing in highly seismic developing countries. ASSISI 10th World Conference on Seismic Isolation, Energy Dissipation and Active Vibrations Control of Structures, Istanbul, 28–31.
- Kelly, J. M. (1992). Analysis of fiber-reinforced elastomeric isolators. *J Seismol Earthquake*, 2(1):19–34.
- Kelly, J. M. (1999) Analysis of fiber-reinforced elastomeric isolators. *J Seismol Earthq Eng*, 2(1), 19–34.
- Kelly, J. M. (2002). Seismic isolation systems for developing countries. *Earthquake Spectra*, 18(3), pp: 385–406.
- Kelly, J. M. (1990). Base Isolations: Linier Theory and Design, *Earthquake Spectra*, Vol. 6 No. 2, pp: 223-244.
- Kelly, J. M. (1998). Base Isolations: Origins and Development, National Information Service for Earthquake Engineering (NISEE), University of California, Berkeley.
- Kelly, J. M and Calabrese, A. (2012). Mechanics of Fiber Reinforced Bearings. *Pacific Earthquake Engineering Research Center* : 101.
- Kelly, J. M. and Takhirov, S. M. (2001). Analytical and Experimental Study of Fiber-Reinforced Elastomeric Isolators. *Pacific Earthquake Engineering Research Center* : 11.
- Kelly, J. M and Andrea, C. (2012). Mechanics of Fiber-reinforced Bearings, Pacific Earthquake Engineering Research Center.

- Kelly, J. M and Shakhzod, M. T. (2001). Analytical and Experimental Study of Fiber-Reinforced Elastomeric Isolators, Pacific Earthquake Engineering Research Center.
- Kelly, J. M and Konstantinidis, D. (2009). Effect of friction on unbonded elastomeric bearings. *J Eng Mech*, 135(9), pp: 953–60.
- Kelly, J. M and Konstantinidis, D. (2011). Mechanics of rubber bearings for seismic and vibration isolation. Chichester: John Wiley & Sons.
- Kelly, J. M. (2008). Analysis of the run-in effect in fiber-reinforced isolators under vertical load. *J Mech Mater Struct*, 3(7), 1383–401.
- Kelly, T. E. (2001). Base isolation of structures: Design guidelines. New Zealand: Holmes consulting group Ltd.
- Kelly, T. E. (2001). Base Isolation of Structure : Design Guidelines. Holmes Consulting Group, Wellington, New Zealand.
- Kilar, V and Koren, D. (2009). Seismic Behavior of Asymmetric Base Isolated Structure with Various Distributions of Isolators. *Journal of Engineering Structures*, (31), pp: 910-921.
- Konstantinidis, D., Kelly, J. M and Makris, N. (2008). Experimental investigation of the seismic response of bridge bearings. Report EERC-2008/02. Earthquake Engineering Research Center, University of California, Berkeley.
- Korochkina, T. V, Claypole, T.C and Gethin, D. T. (2005). Choosing constitutive models for elastomers used in printing process, in *Constitutive Models for Rubber IV*. Edited by P E Austrell & L Kari (A A Balkema Publisher, UK), pp: 431-435.

- Lesmana, Y and Sugihardjo, H. (2018). Finite element study on a vertical characteristic of modified circular perforated-reinforced elastomeric isolators (MC-PREIs). *Asian journal of civil engineering*. pp :1-3. (Doi: 10.1007/s42107-018-0085-5).
- Lisicins, M., Mironovs, V., Boiko, I and Lapkovskis. (2015). Sandwich Wall Constructions Made of Perforated Metallic Material. *Argonomy Reserach*, 13 (3), pp: 662-670.
- Liu, C.H., Choudhry, S and Wertheimer, T. B. (1998). Low-Order Triangular Elements with Volume Constraints. *Modeling and Simulation-based Engineering*, Vol. I, Eds. S.N. Atturi and P.E. O'Donoghue, pp: 272-277.
- Liu, G. R and Quek, S.S. (2003). *The Finite Element Method: A Practical Course*. Butterworth-Heinemann, Jordan Hill, Oxford, England.
- Matsagar, V. A and Jangid, R. S. (2004). Influence of Isolator Characteristics on The Response of Base-Isolated Structures. *Engineering Structures*, Vol. 26, pp: 1735-1749.
- Melkumyan, M. G. (2008). Seismic Isolation Experience Accumulated in Armenia. The 14th World Conference on Earthquake Engineering (WCEE), Beijing, China.
- Miller, K. (2000). Testing Elastomer for Hyperelastic Material Models in Finite Element Analysis. Axel Products Testing and Analysis Report.
- Naem, F and Kelly, J. M. (1999). *Design of Seismic Isolated Structure: from Theory to Practice*. John Willey & Sons, Inc, United States of America.

- Osgooei, P. M., Tait, M.J and Konstantinidis, D. (2014). Finite Element Analysis of Unbonded Square Fiber-Reinforced Elastomeric Isolators (FREIs) under Lateral Loading in Different Directions. *Composite Structure*, Vol. 113, pp: 164-173.
- Osgooei, P. M., Engelen, N. C. V., Tait, M. J and Konstantinidis, D. (2015).m Experimental and finite element study on the lateral response of Modified Rectangular Fiber-Reinforced Elastomeric Isolators (MR-FREIs). *Engineering Structure* , 85, pp: 293-303.
- Park, Kyu-Sik., Jung, Hyung-Jo and Lee, In-Won. (2002). A Comparative Study on Aseismic Performance of Base Isolation Systems for Multi-Span Continuous Bridge. *Journal of Engineering Structure*, 24, pp: 1001-1013.
- Russo, G., Pauletta, M and Cortesia, A. (2013). A Study on Experimental Shear Behavior of Fiber-Reinforced Elastomeric Isolators with Various Fiber Layouts, Elastomers and Aging Conditions. *Engineering Structures*, Vol. 52, pp: 422-433.
- Santhosh, H. P., Manjunath K. S and Kumar, K. S. (2013). Seismic Analysis of Low to Medium Rise Building for Base Isolation. *Journal of Research in Engineering and Technology*, pp: 2319-1163.
- Seibert, D. J and Schoche, N. (2000). Direct comparison of some recent rubber elasticity models. *Rubber Chem Thecnol*, 73, pp: 366-384.
- Shahzad, M., Kamran, A., Siddiqui, M. Z and Farhan, M. (2005). Mechanical Characterization and FE Modeling of a Hyperelastic Material. *Material Research*, 18 (5), pp: 918-924.

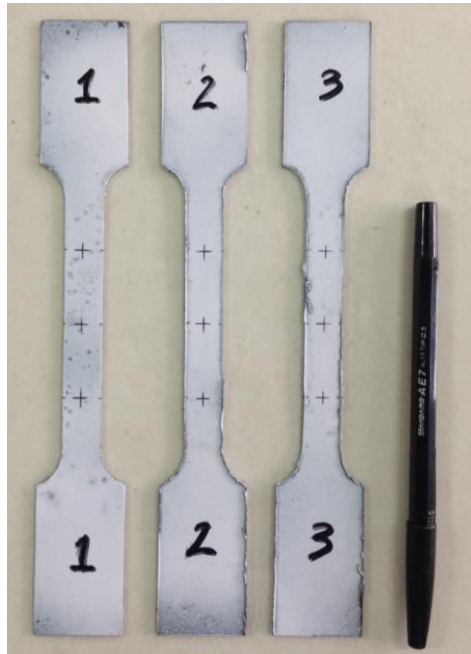
- Spizzuoco, M., Calabrese, A and Serino, G. (2014). Innovative low-cost recycled rubber-fiber reinforced isolator: Experimental tests and finite element analyses. *Engineering Structure*, 76, pp: 99-111.
- Sugihardjo, H., Tavio and Lesmana, Y. (2016). Behavior of a Base-Isolated Residential House in a Highly Seismic Region. *International Journal of Applied Engineering Research (IJAER)*, Research India Publications, 11 (14), pp: 8253-8258.
- Sugihardjo, H., Tavio and Lesmana, Y. (2018). FE Model of Low-Grade Rubber for Modeling Housing's Low-Cost Rubber Base Isolators, *Civil engineering Journal*, vol 4:1.
- Taniwangsa, W. (1996). Experimental and Analytical Studies of Base Isolation Applications for Low-Cost Housing, Ph.D. Thesis, University of California, Berkeley.
- Taniwangsa, W and Kelly, J. M. (1996). Studies on Seismic Isolation for Housing in Developing Regions, 11th World Conference on Earthquake Engineering (WCEE), Acapulco, Mexico, Paper No. 261.
- Timbrell, C., Wiehahn, M., Cook, G and Muhr, A. H. (2003). Simulation of crack propagation in rubber, in *Constitutive Models for Rubber III*. Edited by J Busfield and A Muhr (A A Balkema Publishers, UK), 11-20.
- Tsai, H. C and Kelly, J. M. (2002). Stiffness analysis of fiber-reinforced rectangular seismic isolators. *J Eng Mech*, 128(4), pp: 462–70.
- Tsai, H. C and Kelly, J. M. (2005). Buckling load of seismic isolators affected by flexibility of reinforcement. *Int J Solids Struct*, 42, pp: 255–69.

- Tsai, H. C. (2004). Compression stiffness of infinite-strip bearings of laminated elastic material interleaving with flexible reinforcements. *Int J Solids Struc*, 41(24), pp: 6647–60.
- Uniform Building Code. (1997). International conference of building officials. California: Whittier.
- Vulcano, A. (1998). Comparative Study of The Earthquake and Wind Dynamic Response of Base-Isolated Buildings. *Journal of Wind Engineering and Industrial Aerodynamics*, Vol. 74-76, pp: 751-764.
- Wadley, H. N. G., Fleck, N.A and Evans, A.G. (2003). Fabrication and structural performance of periodic cellular metal sandwich structures. *Composites Science and Technology*. 63, pp: 2331–2343.

”This page is intentionally left blank”

APPENDIX A.

Specimen of Perforated Tension Test

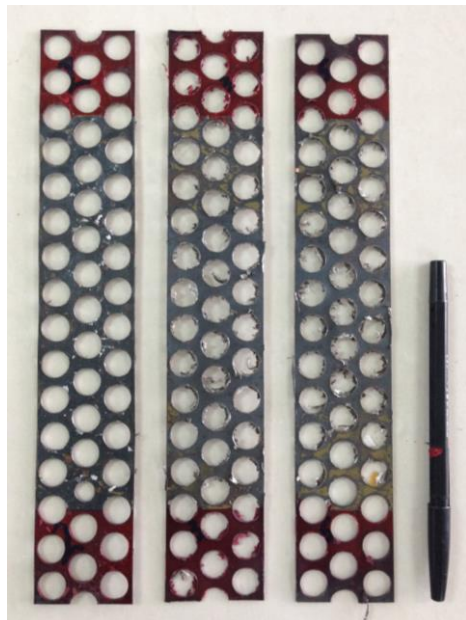


(a)

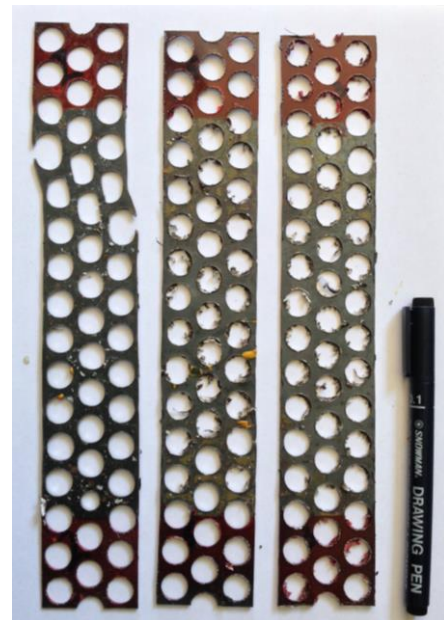


(b)

Figure A1. Specimens A; (a) Before test; (b). After test.

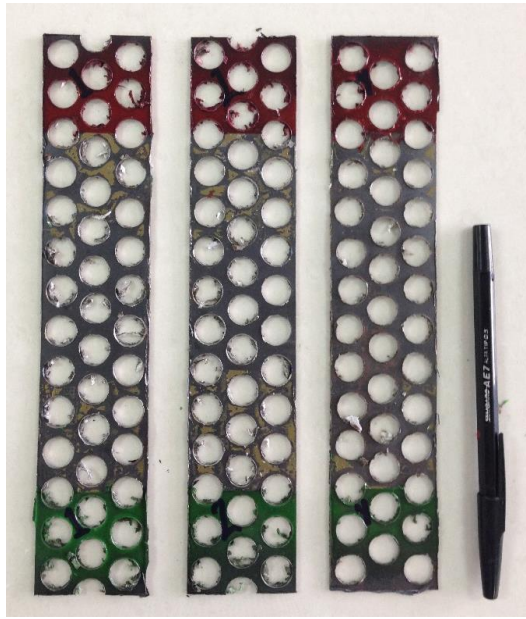


(a)

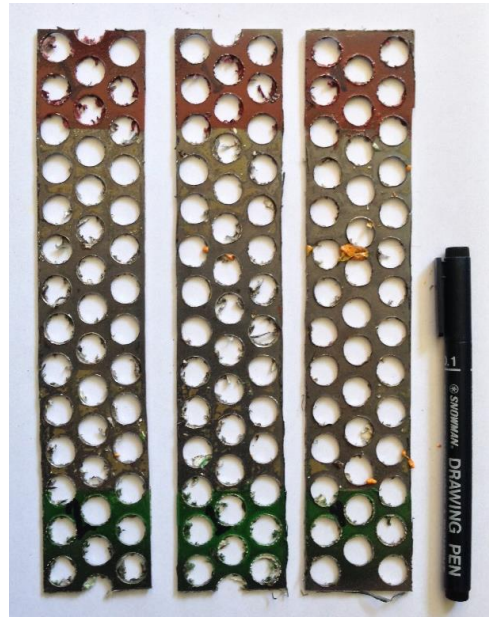


(b)

Figure A2. Specimens B1; (a) Before test; (b). After test.

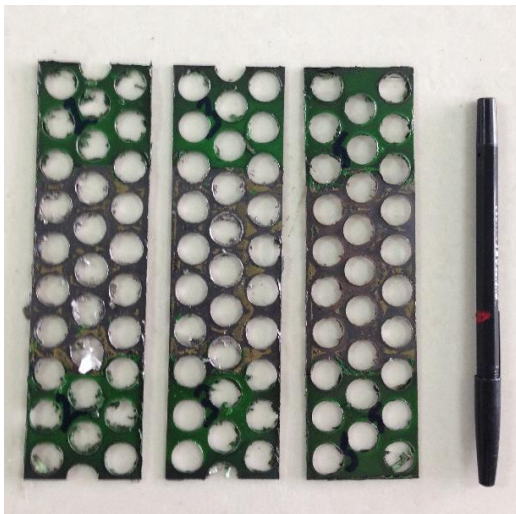


(a)

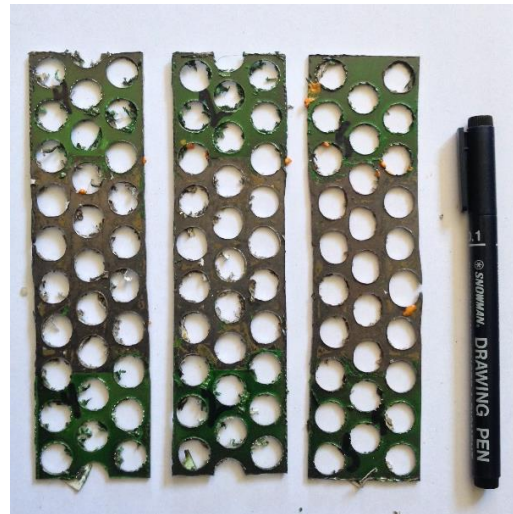


(b)

Figure A3. Specimens B2; (a) Before test; (b). After test.

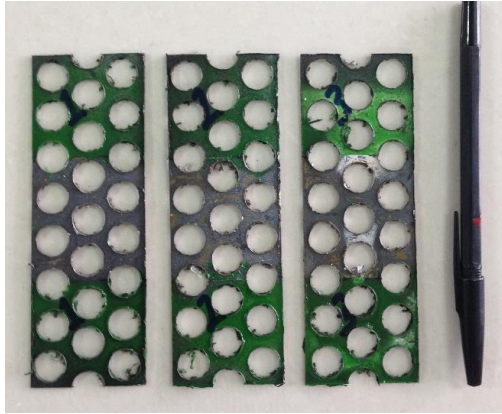


(a)

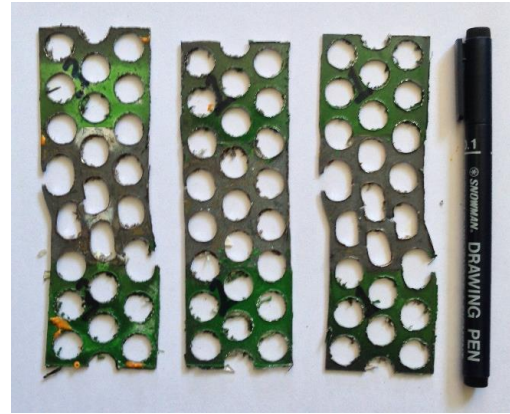


(b)

Figure A4. Specimens B3; (a) Before test; (b). After test.

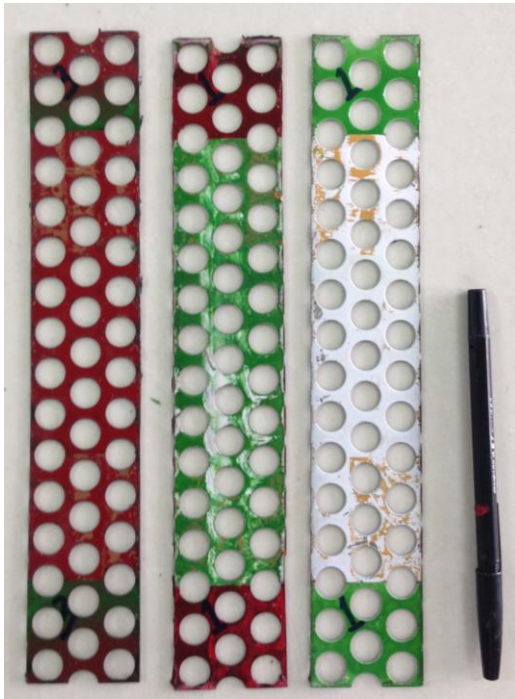


(a)

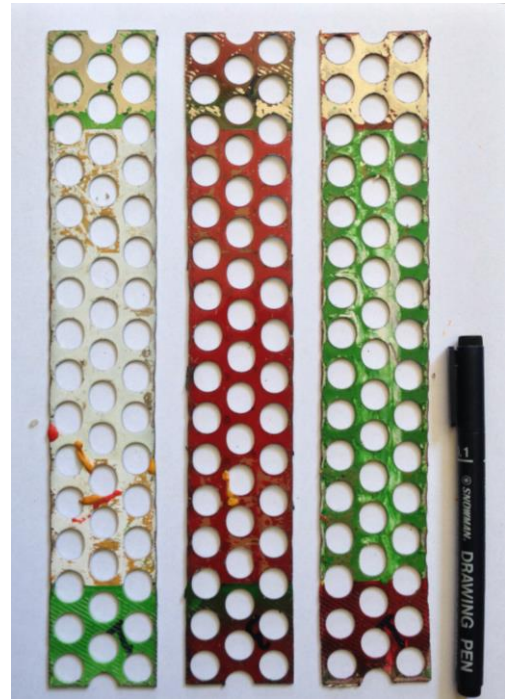


(b)

Figure A5. Specimens B4; (a) Before test; (b). After test.

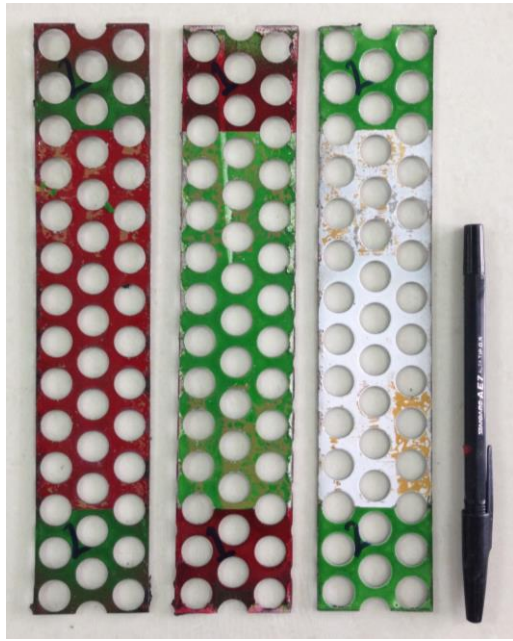


(a)

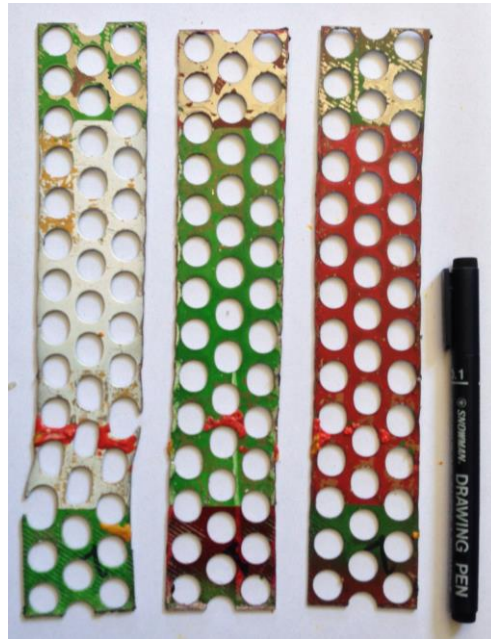


(b)

Figure A6. Specimens C1; (a) Before test; (b). After test.



(a)

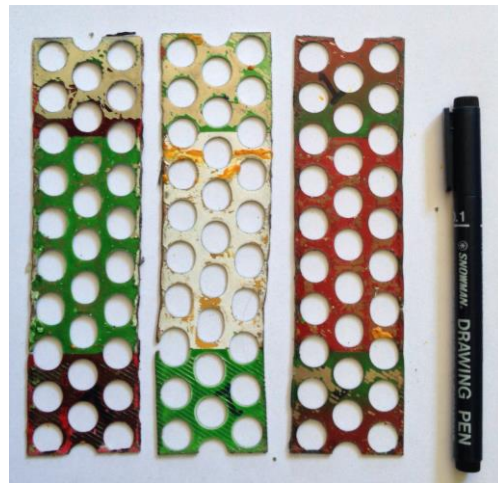


(b)

Figure A7. Specimens C2; (a) Before test; (b). After test.

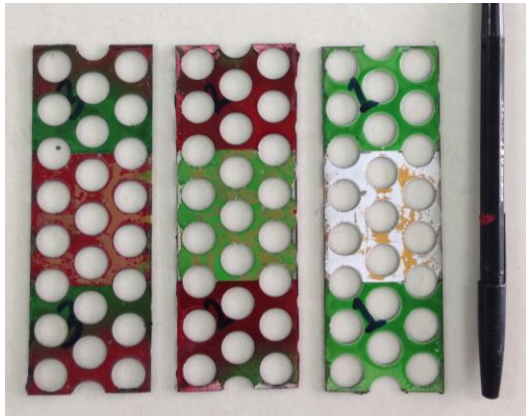


(a)

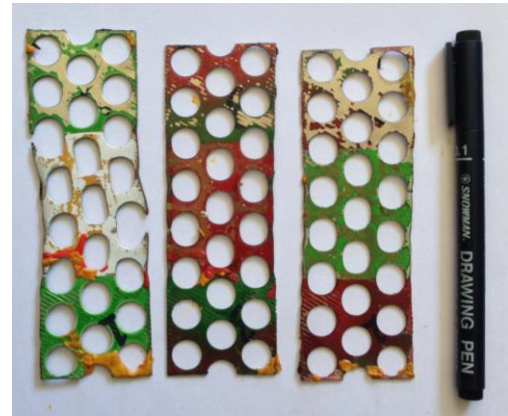


(b)

Figure A8. Specimens C3; (a) Before test; (b). After test.



(a)



(b)

Figure A9. Specimens C4; (a) Before test; (b). After test.

"This page is intentionally left blank"

BIOGRAPHY



Name : Yudha Lesmana

Place / Date of birth : Singkawang / July 4th 1988

Religion : Islam

E-Mail : yud4rk@gmail.com

Phone Number : +6281999333101

Home Address : Jl. Sukun 8/No.7 Perumnas Kamal, Bangkalan-East Java.

A. History of Education :

2006 – 2009 : Diploma 3 of Civil Engineering, Technology Institute of Sepuluh Nopember, Surabaya, Indonesia.

2009 – 2010 : Diploma 4 of Civil Engineering, Technology Institute of Sepuluh Nopember, Surabaya, Indonesia.

2011 – 2013 : Magister Program of Civil Engineering, Technology Institute of Sepuluh Nopember, Surabaya, Indonesia.

2013 – 2018 : Doctoral Program of Civil Engineering, Technology Institute of Sepuluh Nopember, Surabaya, Indonesia.

B. Scientific Paper :

1. Lesmana, Y.; Tavio; and Sugihardjo, H., 2016. Finite Element Analysis of Perforated – Reinforced Elastomeric Isolators (PREIs) under Pure Lateral Loading, The 3rd International Conference on Earthquake Engineering and Disaster Mitigation (ICEEDM-III 2016), 1-2 August, Nusa Dua, Bali, Indonesia.
2. Tavio; Sugihardjo, H.; and Lesmana, Y., 2016. Seismic Behavior of Base-Isolated Residential House with Various Soil Type in High Seismic Regions by Nonlinear Time-History Analysis, The 3rd International Conference on Earthquake Engineering and Disaster Mitigation (ICEEDM-III 2016), 1-2 August, Nusa Dua, Bali, Indonesia.
3. Sugihardjo, H.; Tavio; and Y. Lesmana. (2016). Behavior of a Base-Isolated Residential House in a Highly Seismic Region,” International Journal of Applied Engineering Research (IJAER), Research India Publications, V. 11, No. 14 pp. 8253-8258.
4. Tavio; H. Sugihardjo; A. Purniawan; and Y. Lesmana. (2017) “Behavior of Rubber Base Isolator with Various Shape Factors.” AIP Conference Proceedings : doi.org/10.1063/1.501151.
5. Sugihardjo, H., Tavio., Manalu, I and Lesmana, Y. (2018). Seismic study of lead-rubber bearing application in kutai kartanegara steel arch bridge. International journal on advanced science engineering information technology. Vol 8:2.
6. Sugihardjo, H., Tavio and Lesmana, Y. (2018). FE model of low grade rubber for modeling housing’s low-cost rubber base isolators. Civil engineering journal, Vol 4:1.
7. Lesmana, Yudha and Sugihardjo, H. (2018). Finite element study on the vertical characteristic of modified circular perforated-reinforced elastomeric isolators (MC-PREIs). Asian Journal of Civil Engineering, pp: 1-13. (Doi: 10.1007/s42107-018-0085-5).
8. Sugihardjo, H and Lesmana, Yudha. (2018). Finite element study on the horizontal characteristic of modified circular perforated-reinforced elastomeric isolators (MC-PREIs). Asian Journal of Civil Engineering (*Under review*).

9. Sugihardjo, H and Lesmana, Yudha. (2018). The Seismic Performance of Residential Housing under Strong Earthquake Shaking. Asian Journal of Civil Engineering (*Under review*).
10. Sugihardjo, H and Lesmana, Yudha. (2018). Perforated-reinforced Elastomeric Isolators (PREIs) Experiment. Asian Journal of Civil Engineering (*Under review*).

C. Scientific Meeting Attended :

1. Paper presenter with topic, “ *Behaviour Analysis of High Rise Building Used Base Isolation due to Earthquake Loads with Nonlinier Time History Analysis*”, The National Conference of Civil Engineering – IX 2013, On Technology Institute of Sepuluh Nopember, Surabaya, Indoensia.
2. Paper presenter with topic, “ *Finite Element Analysis of Perforated – Reinforced Elastomeric Isolators (PREIs) under Pure Lateral Loading*”, The 3rd International Conference on Earthquake Engineering and Disaster Mitigation (ICEEDM-III 2016), 1-2 August, Nusa Dua, Bali, Indonesia.
3. Paper presenter with topic, “ An Approach Method with Finite Element in Determining Strain Energy Function of Rubber Material”. - International Conference on Physics and Mechanics of New Materials and Their Applications” (PHENMA 2018) and Exhibition, August 9-11, 2018, Busan, South Korea.
4. Paper presenter with topic, “Behavior of Rubber Base Isolator with Various Shape Factors”, 3rd International Conference on Construction and Building Engineering (ICONBUILD) 2017, August 14-17, 2017, Palembang, Indonesia.
5. Participant of the International Joint Workshop, “ Advanced Technology in Seismic Protection for Buildings- Seismically Isolated Systems and Vibration Control Systems, August, 25, 2017, Bandung, Indonesia.
6. Participan of the International Joint Workshop, “ Structural Design of High-Rise Buildings with passive Control Devices, August 20-21, 2018, Bandung, Indonesia.

"This page is intentionally left blank"